A Study of the Non-linear Variation in the Temperature of the Water Density Anomaly as a Function of Solute Concentration

A thesis submitted for the degree of
Doctor of Philosophy

Presented by
Allan Stewart B.Sc.

Department of Experimental Physics,

National University of Ireland, Maynooth

Maynooth

Kildare

7th September 2010

Research Supervisor
Michael F. Cawley M. Sc., Ph. D.

Head of Department
J. Anthony Murphy M. Sc., M. S., Ph. D.

NUI MAYNOOTH

Ollscoil na hÉireann Má Nuad

Contents

Abstract

In this study an experimental technique which permits detailed study of the temperature of maximum density of pure water and aqueous solutions is presented. The density of water as a function of temperature passes through a maximum at 3.98°C. This temperature of maximum density (T_{md}) changes when solutes are added to the water. This investigation is carried out by cooling a rectangular chamber containing a test fluid. Throughout the tests a 4°C temperature gradient is maintained. As the test fluid is cooled through its density maximum the normal single cell convection that occurs in the presence of a temperature gradient is replaced by a double cell. Monitoring this double cell is the basis of all tests carried out in this study.

For solutes such as ionic salts and sugars, the temperature of maximum density decreases in a linear manner as the solute concentration increases ('Despretz law'). It had been noted, however, in previous work that for monohydric alcohols such as methanol and ethanol the behaviour of the temperature of maximum density is non-linear, showing an initial rise above 4°C as the solute concentration is increased, followed by a drop below 4°C as the concentration continues to rise. Results presented here from more detailed studies indicate that the behaviour of the temperature of maximum density in such cases is highly non-linear, moving through several local maxima in the low concentration region for both ethanol and 2-propanol. Macroscopic and microscopic are investigated in an attempt to understand and explain this unexpected behaviour.

Acknowledgements

There are many people who have helped me over the past three years of my research. Many people have gone beyond the call of duty on more then one occasion. I would like to thank all of these people.

The person, who I would like to thank most, is my supervisor, Michael Cawley. Firstly for giving me the opportunity to work as part of the fluids group in N.U.I., Maynooth, and secondly for his enthusiasm and encouragement, without which none of this would have been possible.

I thank Professor J. Anthony Murphy for the use of the facilities in the Experimental Physics Department, in N.U.I., Maynooth.

I would also like to thank Gerard Cotter who was present during the three years of my postgraduate course. Gerard helped make the fluids lab a friendly and pleasant environment in which to work. I would also like to thank David Watson for helping to design and construct the new components of the experimental apparatus, John Kelly for supplying computers as quickly as I could break them, and to all the other technical staff who helped with ordering components, printing needs and circuit board design and construction.

I would like to thank my parents, Aedìn and Ian, who have supported me in many ways on my long journey through university. My granddad, John your support over the years has been invaluable. I would also like to thank my brothers Karl and David for their support and encouragement. Finally, to Jennifer Minogue, thank you for all your support over the past three years, as always, you have been amazing.

Chapter One

Introduction

1.1 Properties of Water

Water is a very common substance. Our very existence depends on water. It occupies over two-thirds of the earth's surface; one-twentieth is covered in ice. Water is also present in the atmosphere, with air comprising of between 0% and 4% water vapour. It can be present in its solid form, liquid form and gaseous form at any one time on the surface of the earth. The human body is made up of between fifty-five and seventy-eight percent water by weight [1]. The human brain is over eighty percent water, blood, 83 percent water, and even bone contains 22 percent water. Waters importance extends to its status as being a possible precursor to the existence of life on other planets. No known life form can exist without water.

Despite water being so common, it is a very unusual substance, with many anomalous features [2]. Although it is apparently a very simple molecule (H_20) it exhibits a highly complex character due in part to its inter-molecular hydrogen bonding [2]. In a water molecule, two hydrogen atoms are covalently bonded to a single oxygen atom; the link between the atoms is formed by the sharing of an electron. Each water molecule consists of four electron pairs, two of which are associated with the hydrogen atom and two are lone pairs. When in a solid state, all four of the electron pairs participate in hydrogen bonding with successive water molecules. This results in a highly cohesive three-dimensional array. For ice to convert to water, the weaker hydrogen bonds need to be broken to allow for movement. For water to change to its gaseous state it is required that all the hydrogen bonds are broken. Both of these transitions require large amounts of energy.

Many of water's properties are very different when compared to molecules of similar composition and size. Water has both an unusually high melting point (0°C) and boiling point (100°C). Figures 1.1-1 (a) and (b) show the melting and boiling points of the other chalcogens when bonded with two hydrogen atoms. Extrapolating back from polonium, through tellurium, selenium and sulphur, oxygen

would, if it followed the trend have a melting point at approximately -100°C (173K) and a boiling point of -73°C (200K). These are considerably lower then the actual values of the melting and boiling points of water of 0°C (273K) and 100°C (373K) respectively. Water behaves differently to all the other molecules in the graph.

All the water molecules in ice are held relatively static, and participate in four hydrogen bonds, two as donor and two as acceptor. For melting of ice to occur, some of the weaker hydrogen bonds must be broken, this allows the molecules to move around. Large amounts of energy are required to break these bonds. Only a small amount of energy is reclaimed from the change in volume ($P\Delta V = -0.166$ J mol^{-1}) [2]. The change in the Gibbs free energy ΔG must be zero at the melting point.

$$\Delta G = \Delta H - T\Delta S$$

$$where\ \Delta H = \Delta U + P\Delta V$$

U is the internal energy, P is the pressure, V is the volume, T is the temperature, S is the entropy and H is the enthalpy. As the temperature is increased, the amount of hydrogen bonding in liquid water decreases and its entropy increases. Melting will only occur when there is sufficient enthalpy change to provide the energy required for the bond breaking. The low entropy (high organization) of liquid water causes this melting point to be high [2].

The boiling point of water is over 170°C higher then expected by extrapolation as seen in figure 1.1-1 (b). It is also much higher than O_2 (90 K) or H_2 (20 K). Liquid water is highly cohesive due to the considerable hydrogen bonding. This makes it difficult to remove water molecules from the surface, as a result of this, the vapour pressure is reduced. As boiling cannot occur until this vapour pressure equals the external pressure, a higher temperature is required [2].

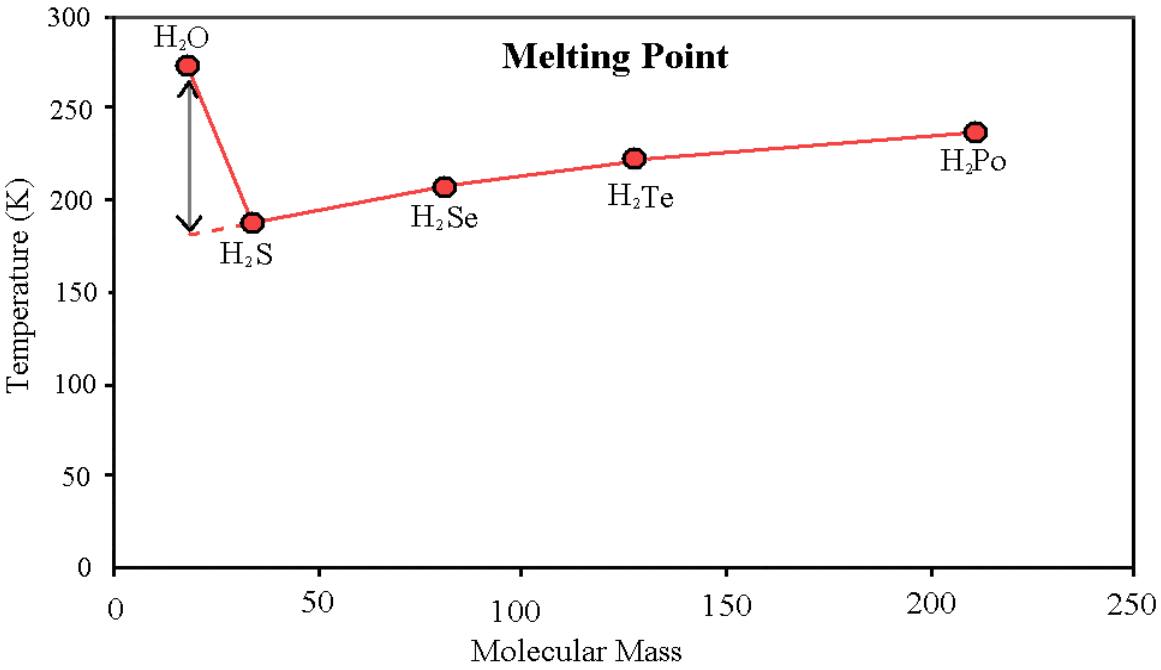

Figure 1.1-1 (a) *Melting point temperature versus Molecular mass for the chalcogens bonded with H_2.*

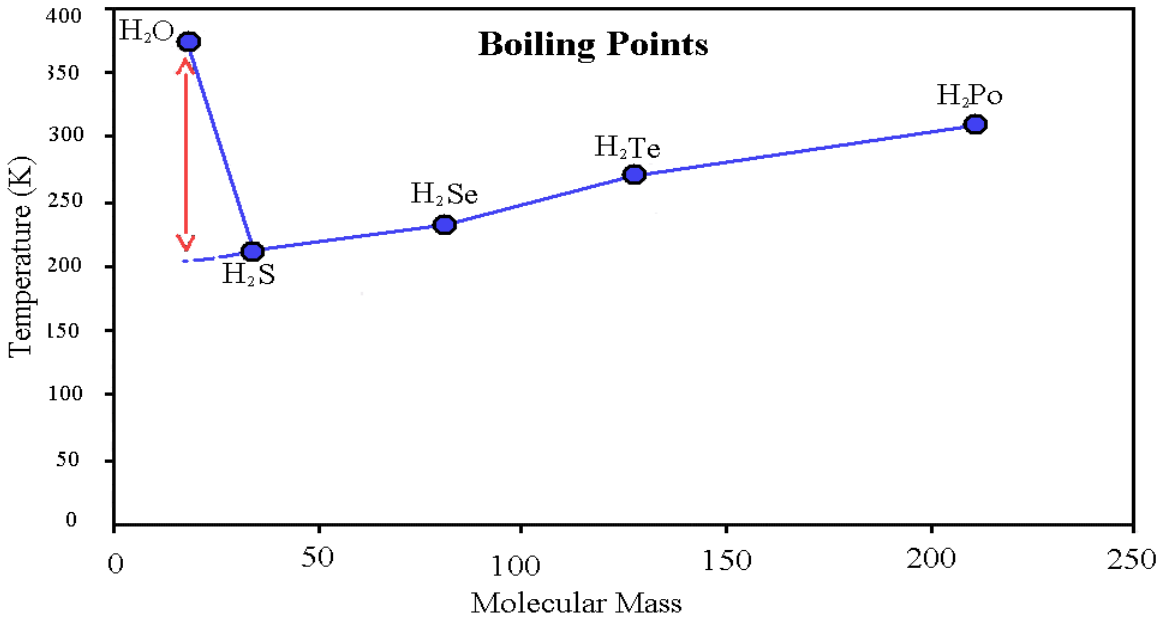

Figure 1.1-1 (b) *Boiling point temperature versus Molecular mass for the chalcogens bonded with H_2.*

Shown in figure 1.1-2 are some anomalies of water that are related to temperature. They include the presence of a minimum in the compressibility of water as a

function of temperature at 46.5°C; other anomalies indicated by the graph include the minima of the specific heat capacity at 36°C and the density maximum occurring at a temperature of 3.98°C [2].

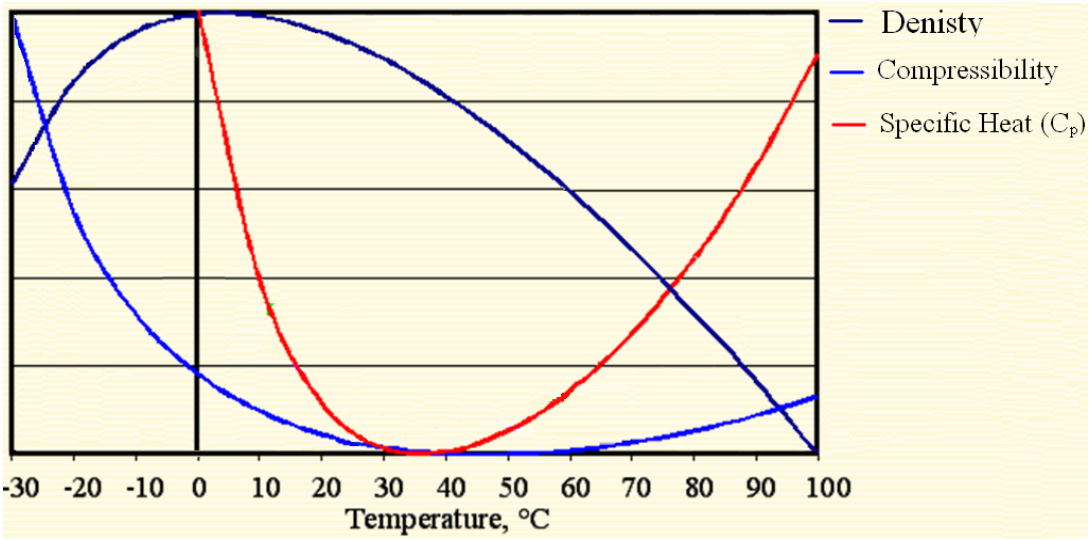

Figure1.1-2 *Some anomalous properties of liquid water that are related to temperature. The graph uses data that has been scaled between their maximum and minimum values.*

At 25°C, water has a specific heat capacity of 4179 $J.Kg^{-1}.K^{-1}$ [3]. Ethanol, a liquid substance with a similar density has a specific heat capacity of 2453 $J.Kg^{-1}K^{-1}$. The large specific heat capacity of water is as a result of the strong hydrogen bonds between the water molecules. The high specific heat capacity of water has some very significant effects on the weather of the entire planet. The oceans act as huge heat reservoirs for the planet. The North Atlantic Drift is a by-product of the high specific heat capacity of water. The North Atlantic Drift brings large amounts of heat from the Gulf of Mexico to the British Isles and keeps the waters surrounding the islands ice free year round. It has been estimated that the North Atlantic Drift brings twice as much heat in one day as would be produced by burning all the coal mined globally in one year [4].

As can been above in figure 1.1.2, water also has a maximum density. The temperature of this maximum density is 3.98°C. The work in this thesis is focused on this density anomaly.

1.2 The Density Maximum of Water.

Water, unlike most substances, exhibits a density maximum as a function of temperature. Water contracts on melting, the addition of further heat results in continued contraction, until a density maximum of 999.9720 kg m^{-3} is reached at 3.98°C [5]. Heating beyond 3.98°C causes the water to expand.

This density maximum has many profound consequences for aquatic life on earth. Life in fresh water lakes and rivers, as well as in low salinity seas can be kept alive by the presence of the density maximum as water freezes. Due to the convection currents caused by the presence of the density maximum, warmer water during the summer is always at the top of the body of water. When the temperature drops below 3.98°C, the convection currents reverse and as a result the colder water is at the top, also if it freezes, the ice will remain on top of the water, allowing for aquatic life to survive below.

Due to the importance of the density maximum of water, it has been the subject of many detailed studies on the density profile of water [5], [6], [7] and then on sea water [8], [9], [10]. Thiesen *et al* [6] in 1896 and Chappius [11] in 1904 carried out detailed studies of the density of water as a function of temperature. The International Critical Tables of Numerical Data, Physics, Chemistry and Technology [12] published in 1928 contains a table derived from the mean of the data obtained by Thiesen *et al* and Chappius. In 1975, Kell [5] published a table of density data over the range -30°C and 150°C. This data is published in the 65th edition of the CRC handbook of Chemistry and Physics [13]. Along with the data on density, there is a 5th order polynomial equation for the density of water. For any

computational fluid dynamics simulations carried out for this work, a 3rd order polynomial (Eqn 1.2.1) is used that accurately describes the density of water over a temperature range of 0°C and 10°C. Over the temperature range used as part of this study there is no noticeable difference between the 3rd order polynomial and the 5th order polynomial. This 3rd order polynomial is graphed in figure 1.2-1 and shows the presence of the density maximum at approximately 4°C.

$$\rho(T) = c_0 + c_1 T + c_2 T^2 \qquad \text{(Eqn 1.2.1)}$$

where c_0 = 999.84508 kg m^{-3}, c_1 = 0.06378 kg m^{-3} °C^{-1}, c2 = -0.00801 kg m^{-3} °C^{-2}.

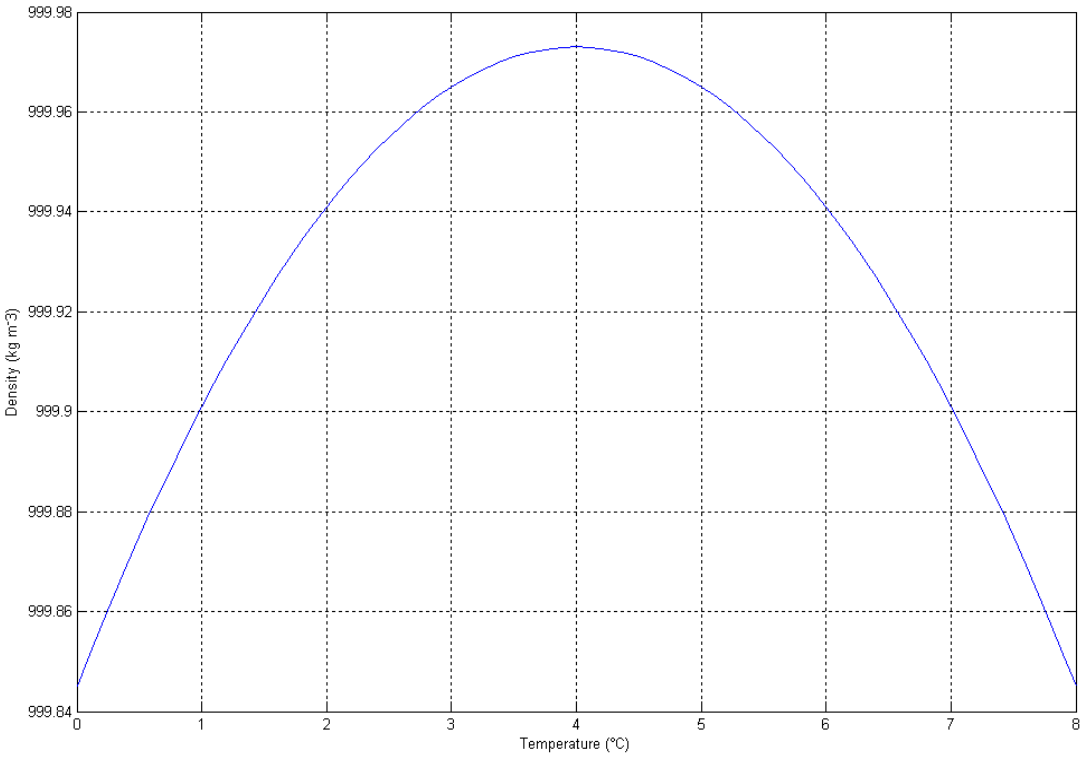

Figure 1.2-1 *Density of water as a function of temperature obtained from the 3rd order polynomial (Eqn: 1.2.1).*

1.3 The History of the Maximum Density of Water and Aqueous Solutions.

1.3.1 The Accademia del Cimento

The Accademia del Cimento was founded by Prince Leopold de'Medici and his brother Grand Duke of Tuscany Ferdinand II in 1657. It was the first scientific society in Europe. In 1667 the work of the Accademia came to an end with the publication of its *Essays on Natural Experiments* [14], illustrated and edited by the Secretary, Lorenzo Magalotti. Magalotti presented this publication to the Royal Society of London where it was translated into English to be published in 1684. Included in the publication are details of experimental work documenting the phase change of water; and its change in volume as a function of temperature. Many scientists regularly worked with the Accademia del Cimento. Some of the more illustrious participants include Christian Huygens, Robert Hooke and Henry Oldenburg. The first experiments of the Accademia concentrated on the barometer and on the thermometer, both of which were new fields of study at the time. From these initial experiments, new fields of research emerged.

Accademia del Cimento academicians conducted many experiments on liquids. These experiments included developing hydrometers to measure the specific weight of liquids, investigating the incompressibility of water, and investigating the freezing of liquids.

In the experiments on the freezing of liquids, a glass tube was used to verify the movement of liquids during the freezing process. It consisted of a bulb and a thin graduated tube 116cm long. It was effectively a water thermometer open at one end. A counting pendulum was used to accurately record the time. It was calibrated to complete 65 oscillations per minute.

Table of the Freezing Process		
Wonderful phenomena	**Degrees in vessel**	**Vibrations of the pendulum**
Natural state	142	0
Jump upon immersion	143 ½	23
Fall	120	255
Point of rest	120	330
Rise	130	462
Jump upon freezing	166	471

Table 1.3-1: *Table of results obtained by the Accademia del Cimento showing the density maximum of water and the expansion upon freezing.*

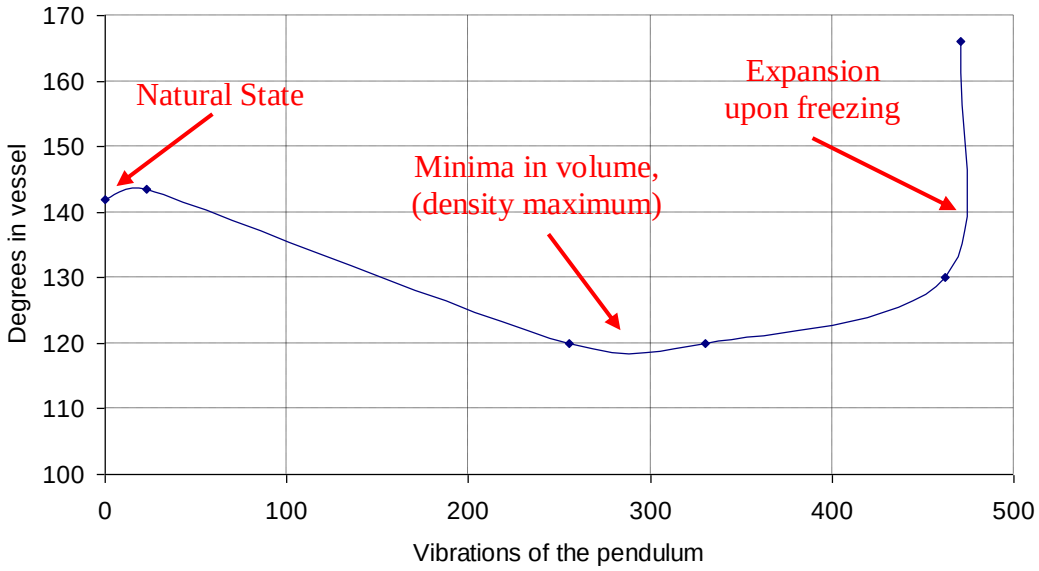

Figure 1.3-1: *Graph of the results obtained by the Accademia del Cimento showing the density maximum of water and the expansion upon freezing.*

To conduct the experiment, water was poured into the tube while in a table the degrees the water reached on the graduated scale was noted (table 1.3-1 and figure1.3-1); this was called the 'natural state'. When the container was surrounded in ice, a rise in the water level was observed; this phase was named 'the jump upon immersion'. It was known that this rise was due to a contraction of the glass as it was cooled and not an expansion of the water. To keep the temperature low, alcohol

and salt were sprayed on the ice surrounding the tube. Following this jump came the third phase, the 'fall' as the water in the tube descended slowly due to the cold. The next phase known as the 'point of rest' this was a time when the academicians did not notice any change in the volume of the water. After the 'point of rest' came a 'rise' in which the water rose slowly as the water approached freezing. The next state and final was unexpected, the 'jump upon freezing' as suggested marked a sudden jump in the volume of the water, which continued to rise until the water had frozen and broken the tube. This was one of the first recorded observations of the density maximum at a point just above freezing, and the expansion of water upon freezing.

1.3.2 Thomas Charles Hope

Towards the end of the 17th century Dr W. Croune [15], observed while investigating the expansion of water upon freezing that the water began to expand before it froze. This was observed by placing a glass ball containing water in to the snow. The level of the water was marked on the glass. Croune noticed that the "water rose very fast, about one-half inch". These results were announced to the Royal Society on the 6th of February 1683. The interpretation of these results was brought into question by many, in particular by Robert Hooke who attributed the rise of the water in the glass vessel to the contraction of the glass as it cooled. In an attempt to reduce these doubts, many experiments were carried out, including those by F. Slare in which the glass vessel was cooled prior to the insertion of the water. The water itself was brought near to the freezing point, and then added to the vessel. As before the level of the water rose while still remaining fluid. Hooke remained doubtful. Very little further investigation into this anomalous property of water occurred until 1772 by M. De Luc, however during this time, work carried out by Mairan (1749) and Du Crest (1757) showed that they were aware of the anomaly.

In 1772 Du Luc [15], while examining ways of improving thermometers, used a thermometer glass with water. Du Luc placed water near its freezing point into the

thermometer glass and began to heat it. It was observed that the water contracted until it reached 41°F (5°C), and from this point onwards the volume increased with temperature. The water was then allowed to cool again, and it began to contract, till it reached 41°F (5°C), and then began to expand as the temperature reached the freezing point. Du Luc concluded that water reached a density maximum at 41°F (5°C) and that the density decreased whether the temperature was increased or decreased from this point. Du Luc also observed that if the water was increased or decreased by the same amount from 41°F (5°C) that the change in density would be the same, for example water the density of water at 50°F (10°C) and at 32°F (0°C) are the same.

The presence of the density maximum was again called into question, this time by John Dalton [15]. Dalton used thermometers made of many materials, including earthenware, glass, brass and lead. He subjected water in each of these thermometers to a variety of temperatures. Dalton noted that the point of greatest density was found at different temperatures depending on the material the instrument was made of. For example, Dalton found that the temperature maximum for water in an apparatus made of earthen-ware to be 34°F (1.1°C), of glass to be 42°F (5.5°C), of brass to be 46°F (7.8°C) and of lead to be 50°F (10°C). Dalton concluded that water could not follow a different law depending on the nature of the material used to construct the instrument, and as a result the appearance of the anomaly in water was due entirely to the change in volume of the vessel containing the water. The next considerable contribution to the study of the density anomaly of water was by Thomas Charles Hope.

Thomas Charles Hope (1766-1844) was appointed professor of medicine in the University of Edinburgh in 1791, and later professor of Chemistry, again in the University of Edinburgh in 1795, initially as co-professor along with Joseph Black. From 1979 to 1843 Hope was the sole professor of chemistry in the University of Edinburgh. During Hope's time as professor he researched many things, one of

which was the first demonstration of the density maximum of water using convective techniques. Before Hope, all attempts to prove or disprove the presence of a density maximum had been based on the change in volume of the water contained in a vessel, and as a result of this there was always the doubt expressed by Hooke and Dalton that this change could be down to the contraction and expansion of the vessel itself.

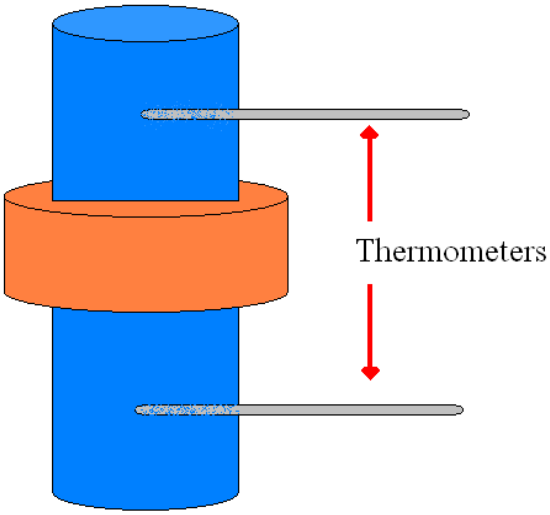

Figure 1.3-2 *Schematic diagram of Hope's apparatus.*

Hope devised experiments [15] where the change in volume of the holding vessel would be irrelevant. In Hope's experiments, he did not measure the change in volume; he instead measured the change in density of the water as it was heated and cooled. As a general rule, if a substance is heated, its density will decrease, and its volume will increase, whereas, cooling an object will result in an increase in the density and a decrease in the volume. So in Hope's experiments, if he heated or cooled the water, the less dense water would always rise to the top, and by keeping track of the temperature of the water at the top and the bottom, it was possible to detect if this water was hotter or colder than at the opposite end.

It was noted by Hope that the water, when heated accumulated at the top, water would follow other substances and expand when heated. Likewise, Hope indicated,

that if he found that the water, when cooled to its freezing point accumulated near the bottom of the vessel that the same conclusion would stand.

Figure 1.3-3 *A replica of Hope's apparatus in the National Science Museum, St. Patrick's College, Maynooth. The cork bungs show the holes through which the thermometers were placed.*

In Hope's "Experiments and Observations upon the Contraction of Water by Heat at Low Temperatures" [15] he describes a series of experiments along with the results he obtained. In one experiment, Hope placed water at 32°F (0°C) in a jar (see figure 1.3-2) with two thermometers. One of the thermometers was placed near to the top of the jar, and the other near to the bottom. After ten minutes had passed, and every twenty minutes after, Hope recorded the temperatures. Hope noticed that initially, the warmer water resided on the bottom, indicating that it was more dense, however, soon after the temperature passed 38°F (3.33°C), the water on the bottom stopped heating until the water on the top reached 38°F as well. Then the temperature gradient was reversed. Once the water reached 40°F, the warmer water was on the top, indicating that the water on top was now less dense. A graph of Hope's original

results can be seen in figure 1 of T. Greenslade's paper on Hope's experiments called "The maximum density of water" [16].

In another experiment, Hope cooled the water, instead of allowing it to heat up as he had done in the first experiment. He started with water at 53°F (11.67°C) in a jar, this time placed in a larger earthenware which contained ice-cold water. As soon as the ice water was placed in the jar and the thermometers adjusted, Hope recorded that the temperature on the bottom of the vessel had fallen to 49°F but the water on the top remained at 53°F (11.67°C). After this, readings were taken every nine to ten minutes. To speed up cooling, water was drained from the larger vessel, with ice-cold water returned in its place, agitation was provided to ensure an even temperature throughout. Hope's results indicated that initially the colder water sunk to the bottom, with the warmer water rising to the top, creating a temperature difference of 8°F. This stayed the same till the bottom reached 40°F (4.44°C) at which time, the colder water rose to the top creating at one instance a temperature difference of 4°F between the top and the bottom of the vessel. This experiment again indicated that water went through a density maximum at approximately 40°F (4.44°C).

1.3.3 César-Mansuéte Despretz and M. F. Rossetti

César-Mansuéte Despretz was born in 1791 at Hainaut, Belgium. Although not much is known of his early life, it is known that he was appointed master of studies in the *lyceum* of Bruges and later went to Paris to finish his studies. Despretz went on to lecture a course in chemistry in Paris. In 1837 Despretz was promoted to professor of physics at the College Henri IV. In 1847 he received the chair of physics at the Sorbonne. Despretz went on to become a naturalised Frenchman in 1838. During 1841, Despretz was elected to the *Académie des Sciences* in the field of general physics.

In the forty years that Despretz worked, he studied phenomena related to thermodynamics, heat transfer, sound, electricity, combustion and the properties of fluids. Within the field of thermodynamics, Despretz conducted experiments on the density of vapours, the compressibility of gases. He proved that the ideal gas law was not exact, that the compressibility of liquids decreases as the pressure increased, and that the density of water and saline solutions occurs at a maximum value, which for pure water was shown to occur at 4°C and that saline solutions decreased the temperature of maximum density (T_{md}). Despretz also showed that this decrease in T_{md} was more rapid then the decrease in the freezing point (or temperature of the phase change, T_{pc}) [17], [18], [19], [20].

The experimental procedure used by Despretz to locate the temperature of maximum density involved the simultaneous reading of a water and mercury thermometer. For the experiment, Despretz used six water thermometers and four mercury thermometers all equally graduated. All the thermometers were arranged in such a way that the diameter of the tubes varied alternatively in one or the other direction. In the first experiments carried out by Despretz, the thermometers were placed in a liquid bath, which was then cooled gradually. After exceeding the apparent maximum value, the liquid was left to heat by natural convection until the thermometers returned to their original readings. Thermal inertia was provided by inserting the thermometers in a copper vase, which was then submerged in a large earthenware vase. The experiments lasted for about ten hours, in which time eight to ten readings were taken.

As it was important to determine the exact absolute temperature of maximum density, Despretz needed knowledge of the expansion of the glass thermometers. To get around this problem, Despretz developed a new technique that was completely independent of the expansion of the glass. The new technique was based on the fact

that in a liquid mass in which the layers are at different temperatures, the molecules that are hottest tend to descend while the cooler molecules tend to rise. In his memoirs, Despretz includes a detailed description of the experimental procedure used to track the temperatures of the upper and lower layers as a function of time. This was done by locating the thermometers horizontally in the liquid. The intersection of the curves obtained gave the location of the temperature of maximum density [17]. After corrections were made to account for using the thermometers horizontally in the experiment as opposed to vertically as they were calibrated, Despretz came up with a result of 3.969°C for the temperature of maximum density of pure water [17]. Following these experiments, Despretz began testing solutions using the same technique. From his studies on the temperature maximum of saline solutions, Despretz came up with the 'Despretz Law' [18], [19]. The 'Despretz Law' states,

"the lowering of the temperature of the point of maximum density of water caused by the addition of a solute is directly proportional to the concentration of the latter".

M. F. Rossetti worked in the 1860's in this area. He attempted to link the temperature of the maximum density to the temperature of the phase change (T_{pc}) of water solutions. However the temperature of the phase change is a colligative property of solutions. Colligative properties are properties that depend on the number of molecules present, not the individual properties (e.g. size, mass) of the molecule. The temperature of the maximum density was found to depend on the nature of the solute as well as the concentration and is therefore non-colligative [21].

1.3.4 Goro Wada and Saburo Umeda

In 1961 while working in Department of Chemistry Faculty of Science Kobe University, G. Wada and S. Umeda published a paper entitled, *Effects of Nonelectrolytes on the Temperature of the Maximum Density of Water. I. Alcohols* [22]. The following year they published the second paper in the series, *Effects of Nonelectrolytes on the Temperature of the Maximum Density of Water. II. Organic Compounds with Polar Groups* [23]. In both these papers they test the effect of various nonelectrolytes on the temperature of maximum density of water.

At the time Wada and Umeda conducted this research, the effects of the electrolytes of the temperature of the density maximum was known. Electrolytes lower the temperature of maximum density at a rate that is almost proportional to the concentration of the solute added in dilute solution. Electrolytes follow the Despretz rule described earlier. Prior to this, only one solute had been shown to increase the temperature of maximum density of water above 3.98°C. Mitchell et al published a paper that indicated that ethanol caused the temperature of maximum density to rise at low concentrations [24].

Wada and Umeda used a dilatometer to measure the volume change of the solution being tested. The dilatometer used was a twisted-W shape. The capacity of the dilatometer was 0.3 litres (see figure 1.3-4); at either end a vertical capillary 0.6mm in diameter was attached. The smallest detectable change in volume was $3x10^{-5}$%. To detect the volume change, the level of the liquid in the capillary tubes was observed as the temperature varied. During the experiments, Wada and Umeda regulated the temperature of the thermostat to within 0.005°C. The experiments were carried out in a region ±2°C of the temperature of maximum density. Due to the thermal expansion of the dilatometer, the solution did not show a minimum

volume at its true temperature of maximum density. However, the changes in height of the liquid surface as a function of temperature near their respective temperatures of maximum density were very similar for both pure water and aqueous solutions. This similarity allowed for the true temperature of maximum density to be determined by graphing the apparent volume of pure water and that of the sample. Wada and Umeda state an absolute accuracy of ±0.02°C for this method [22].

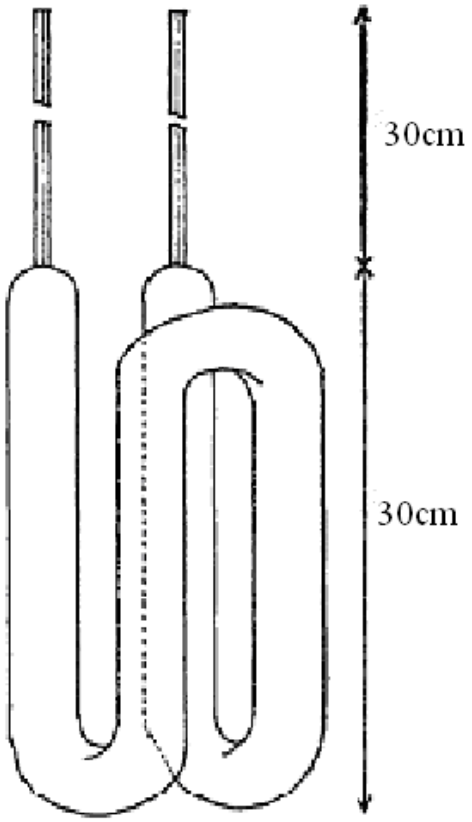

Figure 1.3-4 *Diagram of the dilatometer used by Wada and Umeda.*

1.3.5 **The temperature of maximum density and the Experimental Physics Department at N.U.I., Maynooth.**

The Experimental Physics Department in N.U.I., Maynooth has been involved in researching the temperature of maximum density of water since 2001. In 2004 M. F.

Cawley and P. McBride published a paper in this area entitled, *Flow visualization of free convection in a vertical cylinder of water in the vicinity of the density maximum* [25]. Further work, and the first solutions work was carried out by D. McGlynn who submitted his M.Sc. thesis in 2005 [26]. The convective flow technique used in this study is a modified version of the approach described in detail in Cawley et al (2006) [27]. Other work carried out on the temperature of maximum density of water has included work by P. O'Connor on the influence of the density maximum on the rate of heat transfer [28], and work by P. Mooney on heat transfer and heat flow asymmetry through water in the presence of the density maximum [29].

Current work being carried out by Gerard Cotter involved the development of a new technique that allowed for the determination of the temperature of maximum density of pure water and aqueous solutions under pressure [44]. This work carries on from work carried out previously to develop an equation of state for seawater obtained from many detailed studies of the liquid density anomaly as functions of pressure and salinity [8], [30], [31], [32] . Cotter found that for all the solutes tested, there was a linear decrease in the T_{md} as the pressure was increased. Cotter also found that different solutes, at different concentrations, give rise to different slope values for T_{md} versus pressure. To date it appears that there are at least two different types of trends, ionic salt solutions all lead to more negative slopes whereas the monohydric alcohols give rise to less negative slopes as solute concentration increases when compared to pure water. Figure 1.3-5 shows the main results obtained by Cotter.

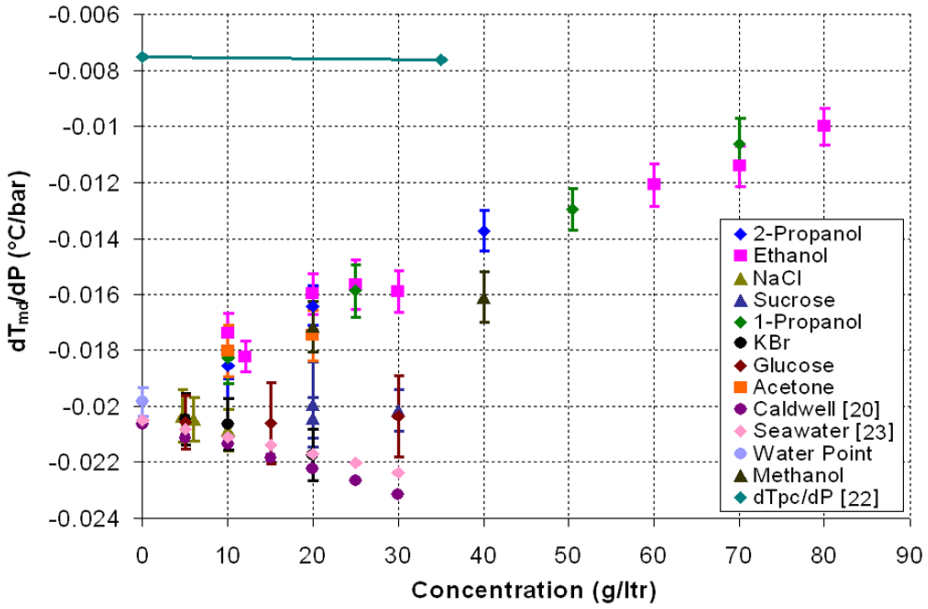

Figure 1.3-5 *Results obtained by Cotter for the rate of change of temperature of maximum density with respect to the rate of change of pressure at various concentrations* [44].

1.4 History of Monte Carlo Simulations

The origins of the Monte Carlo method can be traced back to World War II. Work was ongoing at a United States Department of Energy national laboratory known as the Los Alamos National Laboratory. It was here that the US government was undertaking the *Manhattan Project*, a secret project to build the world's first nuclear weapon. Physicists working at the laboratory were investigating radiation shielding. Even though the physicists had most of the required data regarding the average distance a neutron would travel in a substance before it collided with an atomic nucleus or how much energy the neutron was likely to give off following a collision, the system was too complicated and could not be solved analytically. John von Neumann and Stanislaw Ulam proposed that a solution to the problem could be found by modelling it on a computer using chance [33]. The name Monte Carlo

came from von Neumann, and is in reference to Ulam's uncle who borrowed money from relatives to go to a casino in Monte Carlo to gamble.

Monte Carlo methods were very important to the simulations being carried for the Manhattan Project. These first simulations were limited by the lack of computer processing power available at that time. The first electronic computer was developed in 1945, this resulted in an expansion of the areas in which the Monte Carlo method was employed. For example, the Monte Carlo method was used in the 1950's to help develop the world's first hydrogen bomb at the Los Alamos National Laboratory. Over time the method became popular in the areas of physics, physical chemistry and operations research. Monte Carlo methods are now used in a wide variety of fields, for example, telecommunications, computer gaming, finance and business, computational physics, aerodynamics and as used in this work, Monte Carlo molecular modelling (as an alternative to molecular dynamics).

The Monte Carlo method can be described as any method which solves a problem by generating suitable random numbers and observing the fraction of the numbers obeying some property or properties. The method is useful for obtaining numerical solutions to problems which are too complicated to solve analytically. It is a class of computer algorithm that uses repeated random sampling to compute its results. Details of how the Monte Carlo method works, and how it was employed for the purpose of this study are presented in chapter 5.

1.5 Review of Molecular Models

Water is a very complex substance and has many anomalous properties as a result of this complexity. The water molecule is comprised of two hydrogen atoms

covalently bonded to one oxygen atom. A covalent bond is one in which the electrons share an electron. Each water molecule consists of four electron pairs. A lone electron pair is a valence electron pair that is not engaged in bonding or sharing with other atoms. Two of the electron pairs are associated with the hydrogen atoms and two are lone pairs. When in a solid state, all four of the electron pairs participate in hydrogen bonding with successive water molecules. The electrons associated with the hydrogen atoms are closer to the nucleus of the oxygen than to the hydrogen nuclei. This is a as a result of the high electronegativity of oxygen compared to the electronegativity of hydrogen. This causes water to be a polar molecule, comprising of a relatively strong negative charge at the oxygen atom and a relatively strong positive charge at the hydrogen atoms. The strong hydrogen bonds that occur in water are as a result of water being a polar molecule.

Many of waters anomalous properties including the density maximum are thought to be as a result of the strong hydrogen bonding that occurs in water. It has been suggested that an understanding of the anomalous feature of the density maximum of water will reveal the origins of all the other anomalous properties of water, and will allow for a complete molecular-level description of water [34]. Many different approaches have been taken to model the temperature of maximum density of water at a microscopic level. A few of the approaches that are not used as part of this investigation are discussed in this section. The microscopic models that are used in this investigation are described in chapter five.

One explanation for the presence of the temperature of maximum density of water relies on finding the balance between packing efficiency (high density mode) and bonding optimisation (low density mode). In most substances, the optimisation of the packing density occurs as the temperature is lowered. This optimisation occurs because the lower temperature reduces the kinetic energy which permits the

molecules to move closer together, which in turn reduces the energy of the system. It has been speculated that in water as the temperature is lowered, it becomes more favourable for the water molecules to move further apart in order to optimise the energy of the hydrogen bonding.

An analytical model was developed by Cho et al. [34] to explain the presence of the density maximum. This model assumes the nearest neighbour in the hydrogen structure of water can be ignored, and that only the next nearest neighbours need to be considered. To support this idea, Cho et al. cite experimental evidence which shows the presence of two second neighbour peaks in the radial distribution, one at 3.4Å, which grows with the increase in temperature and another at 4.5Å which decreases with temperature. It appears that more second order neighbours are created at 3.4 Å at the expense of ordinary nearest neighbours of the open second order tetrahedral network. The analytical model developed by Cho et al. is based on this idea. The results obtained by Cho et al. agree with the results obtained experimentally.

Jedlovszky et al. [35] developed a computational model in an attempt to explain the presence of the density maximum of water. Jedlovszky et al. studied the differences in the structures of water using Monte Carlo simulations and a polarisable water model at temperatures above and below the temperature of maximum density. The model showed that with increasing temperature, an increasing number of molecules leave the tetrahedral hydrogen-bonded network. These molecules form closely packed structural units with their neighbours. This increase in the number of these closely packed patches on the density of the system can compensate the increasing thermal motion of the molecules up to a certain point. Jedlovszky believes these two opposite effects are responsible for the appearance of the temperature of maximum density of liquid water.

Tanaka [36] attempts to explain the unusual thermodynamic behaviour of water by using a simple two-order-parameter Landau-type theory without considering the effects of the liquid-liquid critical point. To describe the hydrogen-bonding effects on the phase behaviour they introduced a bond order parameter S, as well as a density order parameter ρ. Tanaka argues that in a usual liquid the crystallisation is primarily a result of the ordering of ρ, while in water it is due to the ordering of S at ambient pressure. The author states that the model described in the letter was also used to explain the behaviour of silica (SiO_2) in the supercooled state. Silica shows a density maximum in this region [37].

The density maximum of water has been studied extensively at a molecular level, despite this there is no agreement on a molecular model that accurately explains its occurrence. One aspect agreed upon by Cho, Jedlovszky and Tanaka is the importance of the hydrogen bonding in accounting for the density maximum of water and other anomalous features of water. However, solid-liquid phase change anomalies have been reported in other substances, including Gallium (Ga) and Bismuth (Bi) [38]. It is not known if either of these exhibits a density maximum in their liquid state, but is has been reported that gallium does show a density maximum under negative pressures [38].

1.6 The aim of this work

Prior to starting this work, there were many unanswered questions about how solutes affect the temperature of maximum density of water. The areas of uncertainty that I aimed to work on in this study were the effect of monohydric alcohols on the temperature of maximum density. This firstly involved the construction of a heat

exchange system and the design, development and construction of a syringe system that allowed for an automatic change in the concentration of an aqueous solution. Details of both systems are given in chapter two. The heat exchange system, when used with the syringe system allowed for a highly detailed scan of temperature of maximum density as a function of solute concentration to be carried out. The aim of this work was to employ this system on some of the lower order monohydric alcohols: methanol, ethanol, 1-propanol, 2-propanol and tert-butanol.

Once experimental results had been obtained, the aim was to try and interpret them. To do this, both macroscopic and microscopic models were developed to try and emulate the experimental results. The macroscopic models involved combining the state functions of various solutes and that of water. The microscopic studies involved employing Monte Carlo molecular modelling methods.

1.7 The Monohydric Alcohols.

The concentration scanning system developed as part of this work has been used to test the effects of various solutes on the temperature of maximum density as a function of solute concentration. The monohydric alcohols that were used as solutes are described here.

Methanol: Methanol (CH_3OH) is the simplest alcohol. It is colourless, light and very flammable. It has a distinctive odour that is similar to, but slightly sweeter then ethanol. Methanol is used as a solvent, fuel and as anti-freeze.

Ethanol: Ethanol ($CH_3–CH_2–OH$) is best known as the alcohol that is used in alcoholic beverages and alcohol thermometers. Other uses of ethanol include as an

antiseptic, fuel, deodorants, as well as an antidote for poisoning by other, more toxic alcohols, in particular methanol and ethylene glycol.

Propanol: Propanol is the simplest monohydric alcohol compounds with the same molecular formula but different molecular structures. Compounds with the same molecular formula but different molecular structures are known as isomers. There are two propanol isomers, 1-propanol ($CH_3CH_2CH_2OH$) and 2-propanol ($(CH_3)_2CHOH$) as shown in figure 1.7.1.

Butanol: A monohydric alcohol with four carbon atoms. There are four butanol isomers, n-Butanol, isobutanol, sec-Butanol and tert-butanol. The only butanol tested in this study was tert-butanol. Tert-butanol $(CH_3)_3COH$ is unique among the monohydric alcohols tested, and indeed among the butanols in that it is solid at room temperature. It has a melting point of 25°C.

	Viscosity (mPa s) @ 25°C	Heat Capacity ($J\ g^{-1}\ °C^{-1}$)	Density ($Kg\ m^{-3}$) @ 20°C	Melting Point (°C)	Boiling Point (°C)	Molar Mass
Methanol	0.793	2.53	791.4	-98	65	32.04
Ethanol	1.074	2.44	789.3	-114	78	46.07
1-Propanol	1.946	2.39	803.5	-126	97	60.10
2-Propanol	2.038	2.58	785.5	-90	82	60.10
n-Butanol	2.544	2.39	809.8	-90	118	74.12
Isobutanol	3.096	2.66	806.3	-114.7	99.5	74.12
sec-Butanol	-	2.44	801.8	-108	108	74.12
tert-Butanol	4.312	2.97	788.7	26	82	74.12

Table 1.7-1 *Properties of the lower order monohydric alcohols taken from [3]*

Methanol

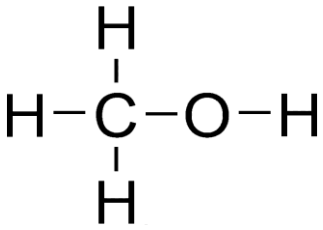

CH_3OH

Ethanol

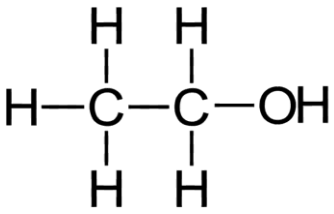

$CH_3–CH_2–OH$

1-Propanol

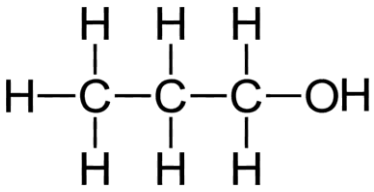

$CH_3CH_2CH_2OH$

2-Propanol

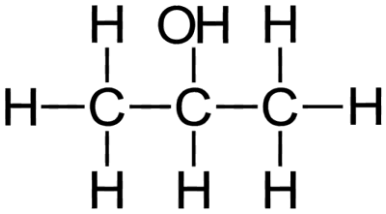

$(CH_3)_2CHOH$

n-butanol

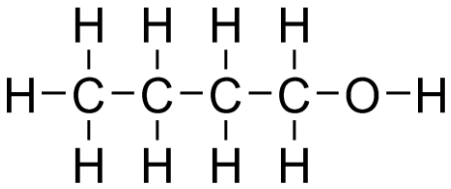

$CH_3(CH_2)_3OH$

iso-butanol

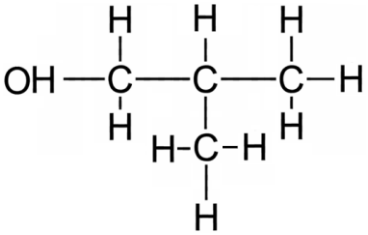

$(CH_3)_2CHCH_2OH$

sec-butanol

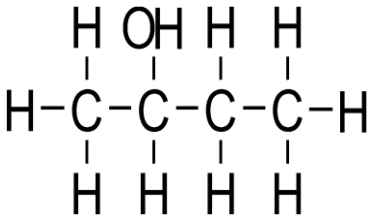

$CH_3CH(OH)CH_2CH_3$

tert-butanol

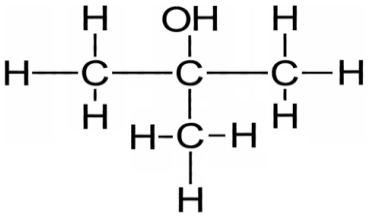

$(CH_3)_3COH$

Figure 1.7-1 *Molecular structures of the monohydric alcohols.*

1.8 Chapter outline

The following is an outline of the overall content of this thesis and summarises the topics covered in each chapter.

Chapter 2 describes the apparatus used to conduct the experimental work. It includes details of the heat exchange system, thermometry, the data acquisition software, syringe system and the test chamber.

Chapter 3 details the results obtained from the experimental work on the temperature of maximum density of water and aqueous solution. The solutions include NaCl, various monohydric alcohols and other solutes.

Chapter 4 presents details of the macroscopic modelling work carried out as part of this study. It comprises of macroscopic modelling of the temperature of maximum density if the solutions were ideal (without appreciable interaction between the solute and the water). Also in this chapter is an investigation of how the temperature of the phase change varies as a function of solute concentration, and how this variation compares with the expected value if the solutions were ideal.

Chapter 5 presents details of the microscopic modelling work carried out as part of this study. The differences between Monte Carlo and Molecular Dynamics methods are discussed. Various water models are introduced, as well as algorithms involving Metropolis Importance sampling and a Wang-Landau approach to Monte Carlo simulations.

Chapter 6 details the conclusions that are drawn based on the results obtained. A comparison is made between the experimental results and the modelling results. The questions that remain unanswered are detailed here as well as possible future work.

1.8.1 Author's direct contribution in this thesis.

The work carried out to complete this thesis has only been possible due to the contribution of fellow researchers working in the fluid dynamics group at N.U.I., Maynooth. The author's direct contribution to each chapter is listed here.

Chapter 2

- Improved the heat exchange system.
- Improved the efficiency of the control software.
- Designed, implemented and tested the concentration scanning system.
- Developed models that allowed for tests to be carried out into the effects of the change in the fluid volume within the test chamber on the observed temperature of maximum density.

Chapter 3

- Observation and analysis of the occurrence of the temperature of maximum density of water by tracking the convective flow within a sample of water, across which a constant temperature gradient is being applied.

- Detailed analysis of the behaviour of the temperature of maximum density of sodium chloride solutions.
- Detailed analysis of the behaviour of the temperature of maximum density of various monohydric alcohol solutions.
- Developed and tested an area integration technique to allow for the extraction of the temperature of maximum density from the data obtained from an experiment.
- Used root mean squared deviations to estimate the uncertainty in the temperature of maximum density and in the concentration.

Chapter 4

- Used macroscopic modelling techniques to compare the expected temperature of maximum density of a solution to the experimentally obtained temperature of maximum density as a function of solute concentration.
- Carried out a similar analysis to compare the expected temperature of maximum density of a solution to known temperatures of phase change as a function of solute concentration.

Chapter 5

- Comparison of Metropolis Importance sampling algorithm and Wang-Landau algorithm using lattice models (Ising and Potts).
- Developed and tested an off-lattice water model using a Mercedes-Benz water molecule and a Metropolis Importance sampling algorithm.

- Developed and tested a modified version of the Buzano et al [55]. gas-lattice model using the Wang-Landau algorithm. Used this model to study the influence of added molecules with strengthened or weakened potential interactions.

Chapter Two

Experimental Apparatus and Procedures

2.1 Introduction

In this section the apparatus used in the experiment is described. The goal of the experiment is to accurately measure the temperature of the density maximum of pure water and water solutions. The experiment consists of a test chamber filled with a test solution. Located either side of the test chambers are temperature-controlled reservoirs. These reservoirs are used to regulate the temperature of both sidewalls of the test chamber. In a typical experimental run, the sidewalls of the test chamber are given a starting temperature, with a 4°C gradient from one sidewall to the other. The temperatures of the sidewalls are then over time ramped (either up or down) in temperature, maintaining the 4°C gradient. In this section, the heat exchange system, thermometry and calibration, syringe system (used for concentration scans), the test chamber, and the data acquisition software are described.

2.2 Thermometry

For the purpose of this experiment, temperature sensitive resistors are used, commonly known as thermistors. The thermistors used in this study were Betatherm 5K3A373I NTC. The resistance of NTC or negative temperature coefficient thermistors varies inversely with temperature, and were chosen due to their predictability and large resistance change per degree. In the temperature region 0°C to 10°C in which the tests are primarily carried out, there is on average a change in resistance of 637.3Ω/°C [39]. A schematic diagram of the Betatherm thermistor used in these experiments is shown in figure 2.2-1.

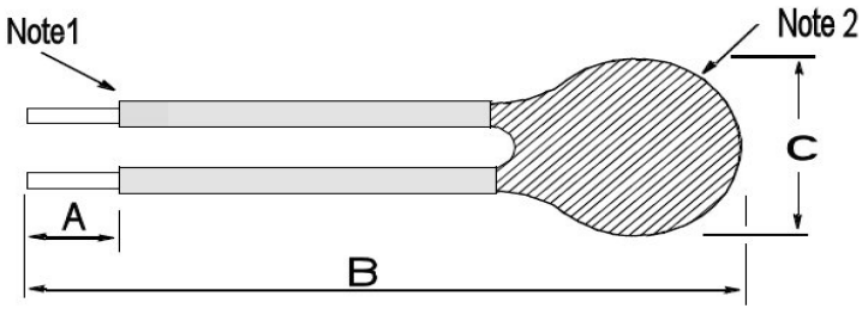

	Dimensions		
	A	B	C
	10 ± 2mm	200 ± 10mm	2.4mm Maximum
Note 1	30AWG Solid Silver Plated Copper with White Kynar Insulation		
Note 2	Black Stycast Epoxy		

Figure 2.2-1 *Diagram and details of the insulation and size of the Betatherm 5K3A373I NTC.*

The thermistors Betatherm thermistors used in this study have an operational range of -55°C to +150°C. The thermistors are bought in pre-insulated; however this insulation is not sufficient to protect the thermistors in the test chamber, as these thermistors are submerged in water and water solutions for long periods of time. To provide extra protection the thermistors that come into contact with fluids are coated in heat shrink. To do this, the thermistors are placed in a thin plastic tube to make them more rigid; they are then covered in the heat shrink. A heat gun is used to create a watertight seal around the thermistors. Loctite is added to the opening to ensure no water reaches the thermistor head. Tests have been carried out to test the response times of the thermistors that receive this extra coating, these tests involved placing two thermistors in a fluid bath, one with the extra coating, the other without. The conclusion from the tests was that the extra coating had a small effect on the response time of the thermistors. However, since the readings are taken every 2-3 seconds, a very fast response time is not necessary.

In this system, to obtain the temperature from the thermistors the voltage through a constant current circuit is read. This is done with a Measurement Computing 1208LS-USB card. From Ohm's law, once we know the current (in this case a

constant) and the voltage, we can calculate the resistance and therefore the temperature.

The circuit used for the constant current circuit is shown in figure 2.2-2. It provides a constant current of 200μA to the thermistor. The circuit consists of a voltage regulator, a non-inverting amplifier, a voltage follower and a 25kΩ resistor. The voltage regulator is there to provide a +5V constant output voltage. Its purpose is to provide a constant current through the thermistors. The 25kΩ resistor limits the amount of current flowing from the current regulator to the thermistor. The final operational amplifier (the 2nd 741 op-amp) is set up in a non-inverting configuration. As R_f and R_i are both 2kΩ, by equation 2.2-1 it can be seen that the circuit has a gain of 2, i.e. all output voltages are amplified by a factor of two. This circuit allows for the use of one thermistor.

$$Gain = 1 + \frac{R_f}{R_i} \qquad (2.2\text{-}1)$$

A total of eight thermistors are used in the system. They are located as following:

Fridge ambient	1
Inside test chamber	5
Main chamber sidewalls	2
Total	8

A bank of eight constant current circuits was set up on an electronic circuit board. The output from each of the constant current circuits is sent to a Measurement Computing 1208LS-USB card. An 11-bit analogue to digital converter (ADC) digitises the voltages. These ADC values are then saved to file by the LabWindows program. More details of the LabWindows program can be found in section 2.3 on data acquisition software. A photograph of a circuit board containing eight constant current circuits can be seen in figure 2.2-6.

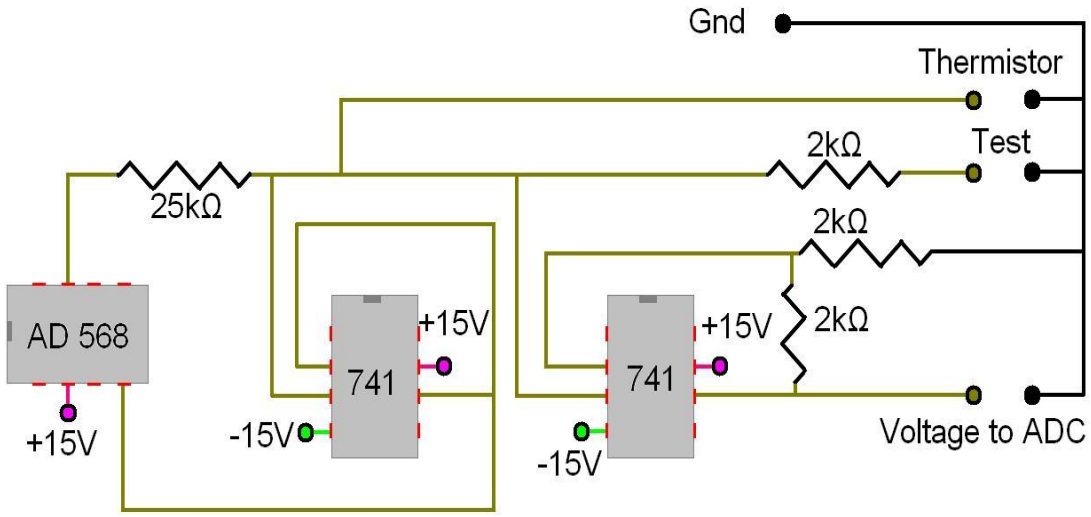

Figure 2.2-2 *Constant current circuit for a single thermistor. The test position is used to check if the circuit is functioning correctly. If it is, a voltage of 0.8V should be read between the terminals.*

Before using the thermistors in the system, they have to be calibrated. To do this, a calibrated mercury thermometer is used. The mercury thermometer is accurate to 0.1°C and is certified by the National Institute of Standards and Technology, USA.

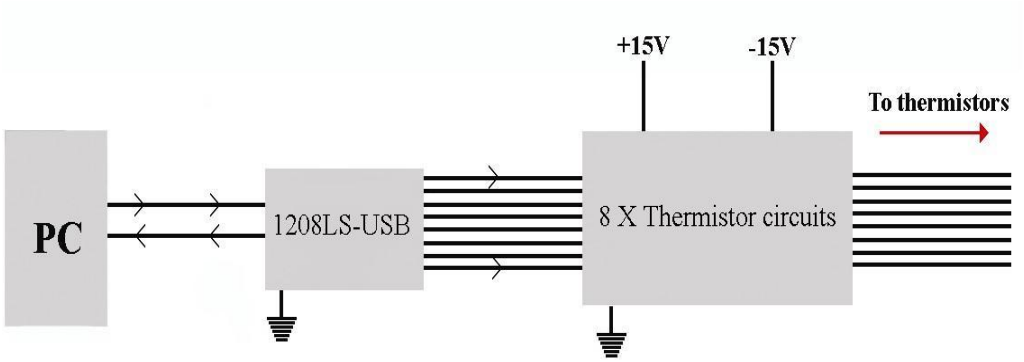

Figure 2.2-3 *Diagram showing how the thermistors are connected to the PC.*

It can be shown (see below) that the natural logarithm of the resistance of a thermistor (NTC) is directly proportional to the reciprocal of the absolute temperature. In this set up, the ADC number is a direct measurement of the thermistors resistance, so the natural logarithm of the ADC number was plotted against the reciprocal of the absolutes temperature. This gives a straight-line graph,

from which an equation is obtained. The slope and intercept from this straight-line graph allowed for the temperature to be calculated from a given voltage.

The natural logarithm of the resistance of a thermistor is directly proportional to the reciprocal of the absolute temperature, i.e.

$$Log_e \propto \frac{1}{T} \tag{2.2-2}$$

The resistance of a semiconductor is given by:

$$R = Ae^{\frac{E_g}{2k_BT}} \tag{2.2-3}$$

where R is the material's resistance, A is a constant dependent on the physical composition of the semiconductor, E_g is the semiconductor band gap, k_B is the Boltzmann's constant, T is the temperature in Kelvin.

By taking the natural logarithm of both sides, the following equation is obtained:

$$\ln R = \ln A + \frac{E_g}{2k_bT} \tag{2.2-4}$$

Since the ADC number is directly proportional to the voltage across the thermistor, and as a result directly proportional to the resistance of the thermistor, the slope obtained from the calibration is $E_g/2k_b$ and the intercept is ln(A). A typical graph of ln*(ADC number)* versus *1/T* can be seen in figure 2.2-4, along with the equation describing the line. This equation can be rearranged so that the temperature experienced by the thermistor can be obtained from the ADC number as shown in equation 2.2-5.

$$T = \frac{slope}{Ln(ADC\ number) - intercept} \tag{2.2-5}$$

Each thermistor has a slope and intercept that is unique. This slope and intercept is found from the calibration process described below. Once the slope and intercept has been found for each thermistor, it is written to a file that is read in at the start of each experimental run.

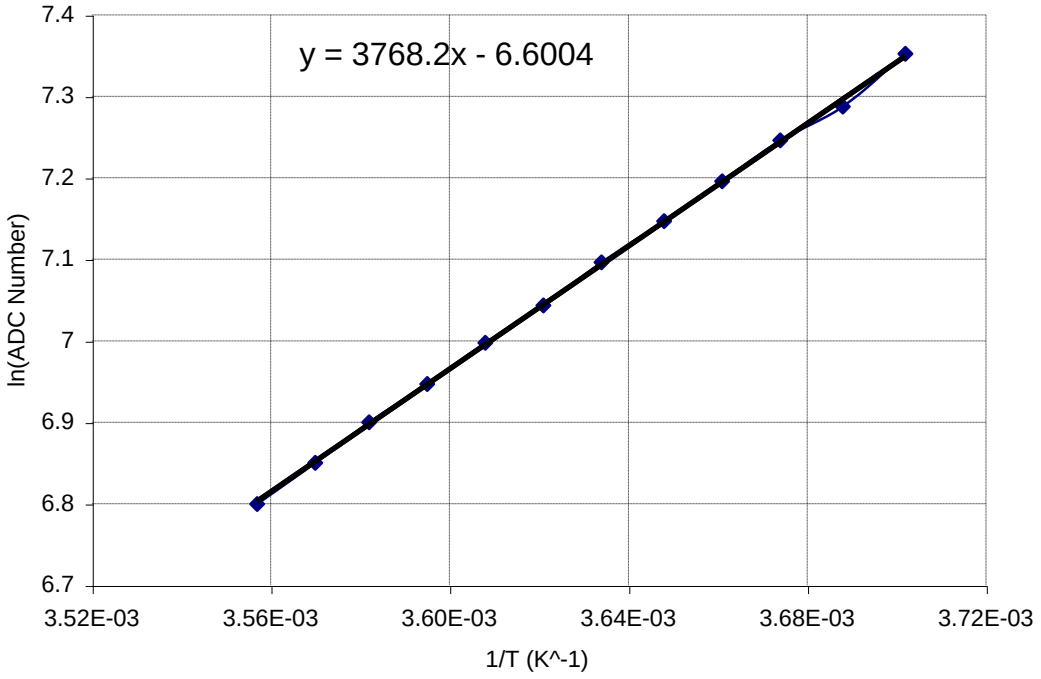

Figure 2.2-4: *Graph of ln(ADC number) versus 1/T for a 5kΩ Betatherm 5K3A373I NTC thermistor.*

Another equation that characterises the relationship between the voltage and resistance of a thermistor is the Steinhart-Hart equation, which is given by:

$$R = A\ln(T) + B\ln(T^3) \tag{2.2-6}$$

where R and T are the resistance and temperature as before, and A and B are constants characterising the thermistor. This equation is of use over large

temperature ranges, and as the temperature range in these experiments is less then 18°C, equation (2.2-4) is used.

To calibrate the thermistors, they are all placed in a container with ethylene glycol, which had been cooled below –2°C. The container of ethylene glycol is placed on a magnetic stirrer and heater to allow for heating and to maintain a uniform temperature. All the thermistors are gathered together in a tight bunch with the calibrated mercury thermometer and dipped into the ethylene glycol. A LabWindows program called 'Calibration.c' is run. This program, using the same analogue side of the Measurement computing USB card as before, reads in voltages and converts them to digital ADC numbers. These readings are taken every time the user clicks a button. The user graphical user interface (GUI) with is a graphical display created in LabWindows for each program, displayed a temperature, when the mercury thermometer reached this temperature, the user pressed the button, and the ADC numbers were recorded to file. This procedure is carried out over a range of temperatures from –2°C to 12°C, in one degree steps. A screen shot of the graphical user interface developed in LabWindows can be seen in figure 2.2-5.

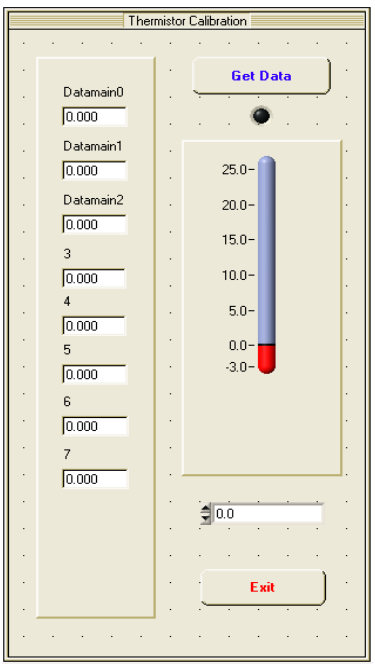

Figure 2.2-5 *Screen shot of the thermistor calibration GUI.*

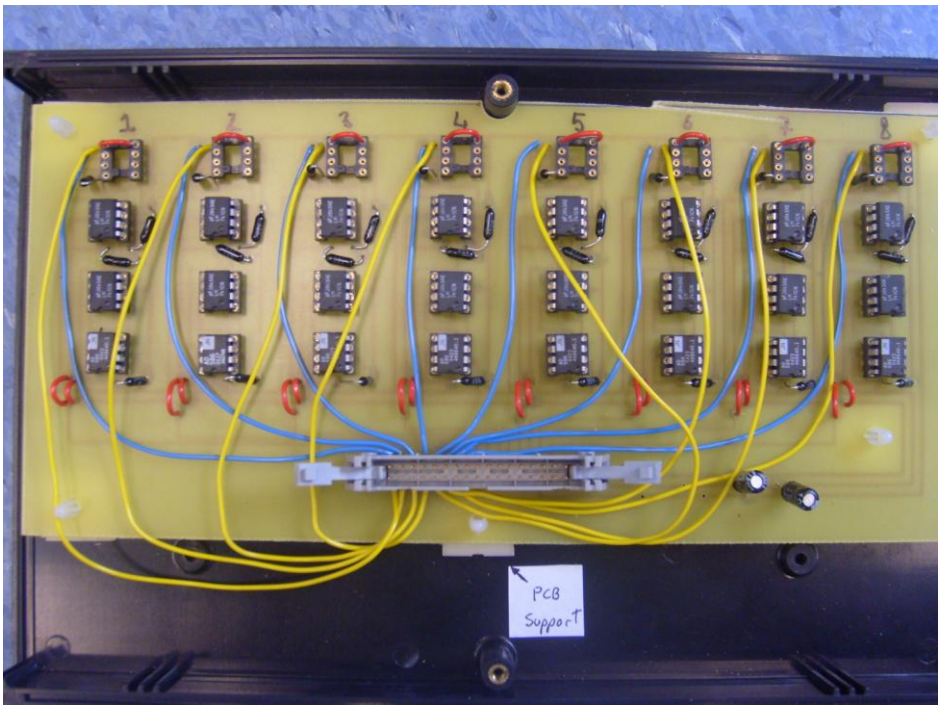

Figure 2.2-6 *A thermistor circuit board, containing 8 individual thermistor circuits, numbered 1 to 8.*

2.3 Data acquisition and Control Software

A Dell Optiplex Gx1 with an Intel Pentium II 333MHz PC running Microsoft Windows 2000 is used as the PC to run the calibration software and the software controlling the experiments. With the PC, two Measurement Computing USB-1208LS data acquisition cards (DAQ) are used as seen in figure 2.3-1. The USB-1208LS is a low speed USB 1.1 device. The USB-1208LS features eight analog inputs, two 10-bit analog outputs, 16 digital I/O connections, and one 32-bit external event counter. The +5 volt USB supply from the computer powers the USB-1208LS. No external power is required. The USB-1208LS analog inputs are software configurable for either eight 11-bit single-ended inputs, or four 12-bit differential inputs. An on-board industry standard 82C55 programmable peripheral interface chip provides the 16 digital I/O lines in two 8-bit ports. The USB-1208LS was set up as shown in figure 2.3-1, with eight single ended inputs.

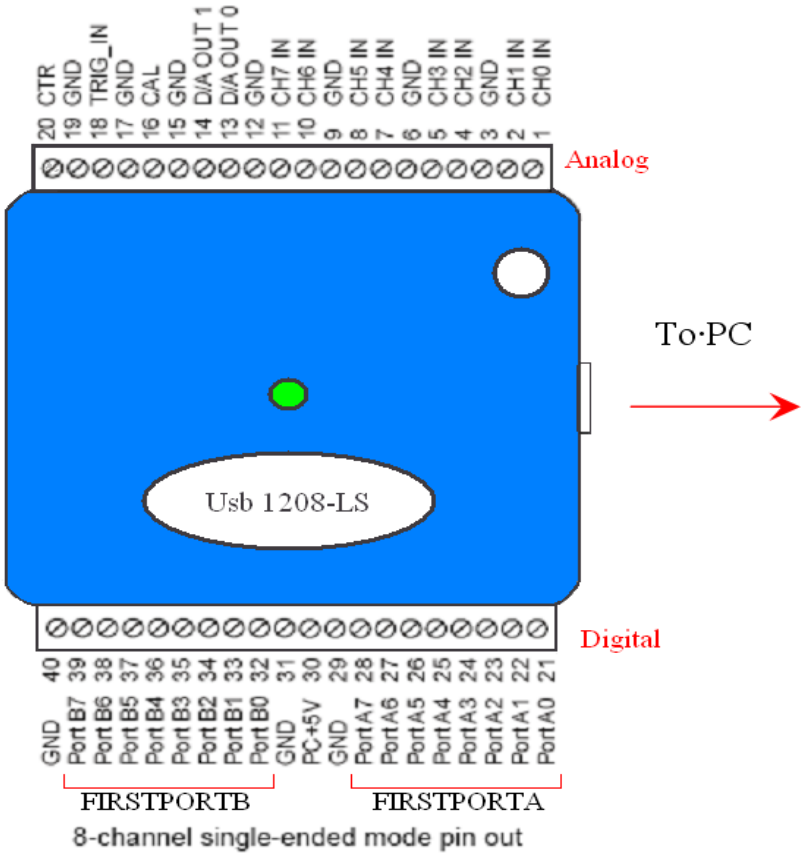

Figure 2.3-1 *Measurement Computing USB-1208LS channel layout, in 8-channel single ended mode, with port numbers.*

The software was written in structured C++. The software was compiled and executed using LabWindows. LabWindows was used as it allowed for a graphical user interface (GUI) to be created simply. The benefit of having the GUI is it graphs the temperatures measured by the thermistors in real time, which allowed for any problems that may occur during the experiment to be easily identified. A picture of the GUI used can be seen in figure 2.3-2. The red and blue lines on the graph shown on the GUI are the hot (T_h) and cold (T_c) side walls. The lime green line is the fridge ambient temperature. The other lines are three of the five thermistors within the test chamber. It was decided not to graph the remaining two thermistors from the test chamber purely for reasons of clarity. As the GUI is there to monitor the system, it was not deemed necessary to graph all five test chamber thermistors, this in turn makes the graph clearer, and easier to read.

The GUI allows the user to select one of four types of operation. The first operation is to start a ramp run. This begins with the left chamber and right chamber set at 8°C and 4°C respectively. It then steps down the temperature of each chamber by 0.1°C every 540 seconds, until the chambers reach 4°C and 0°C. This takes 21600 seconds (6 hours) to complete. The second operation is a 'hold run'. In this mode, the software sets the two side chambers to two temperatures specified by the user and continues to hold them steady till the user stops the program. This mode of operation is used to prepare the system for a ramp run. The third operation is a 'fridge run', which is used to hold the refrigerator at a set temperature. It is used to cool the refrigerator and freezer prior to beginning a hold run. The final operation choice is to conduct a 'concentration scan'. This mode operates in a similar manner to the ramp run, except it performs a down ramp followed by an up ramp, after which the concentration of the solute is changed. More information on the concentration scan is given in section 2.6.

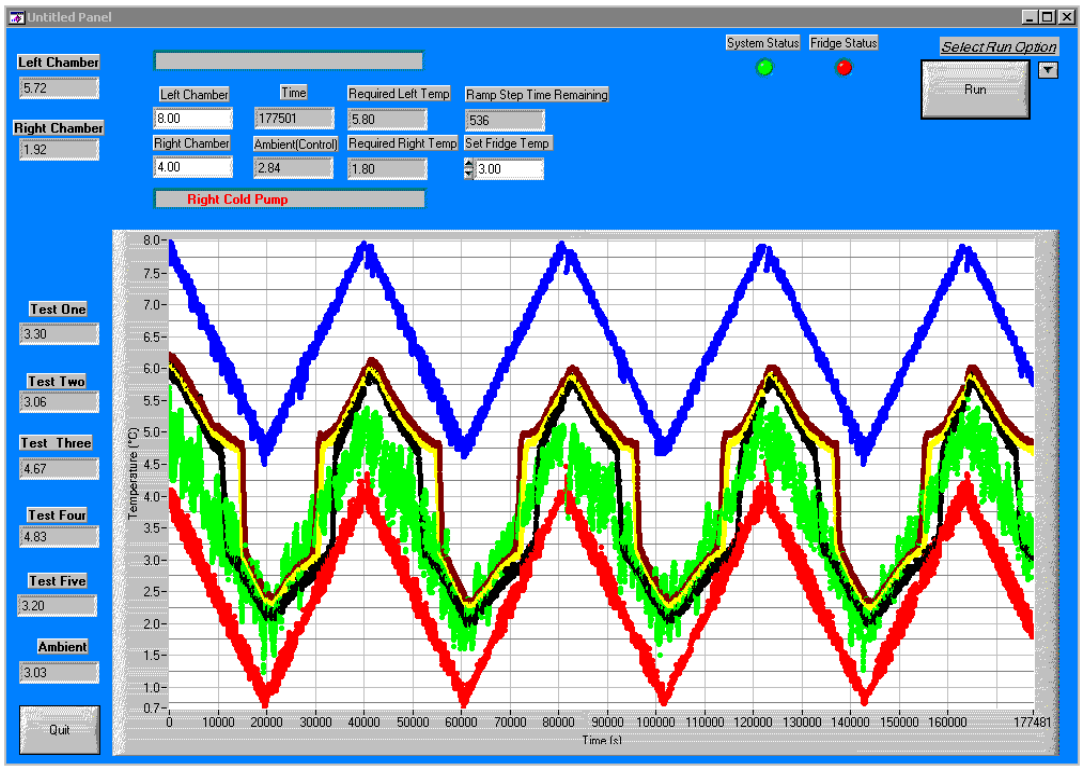

Figure 2.3-2 *LabWindows user interface of the control program.*

The GUI also displays the last temperature recorded by the thermistors. The software takes in ten readings from the thermistors and averages them for smoothing purposes. This average value is then converted to a temperature using the calibration data. This temperature is then printed to screen and saved to file along with the time. A graph of the thermistor values is also printed to screen. On the GUI a clock is displayed that shows the time till the next temperature stepping, along with the total number of steps taken. LED's are included to indicate if the system and fridge are on.

The C-code has seven primary functions that it uses to operate the system, excluding the main method. The flow chart in figure 2.3-3 indicates the sequence in which the methods are called.

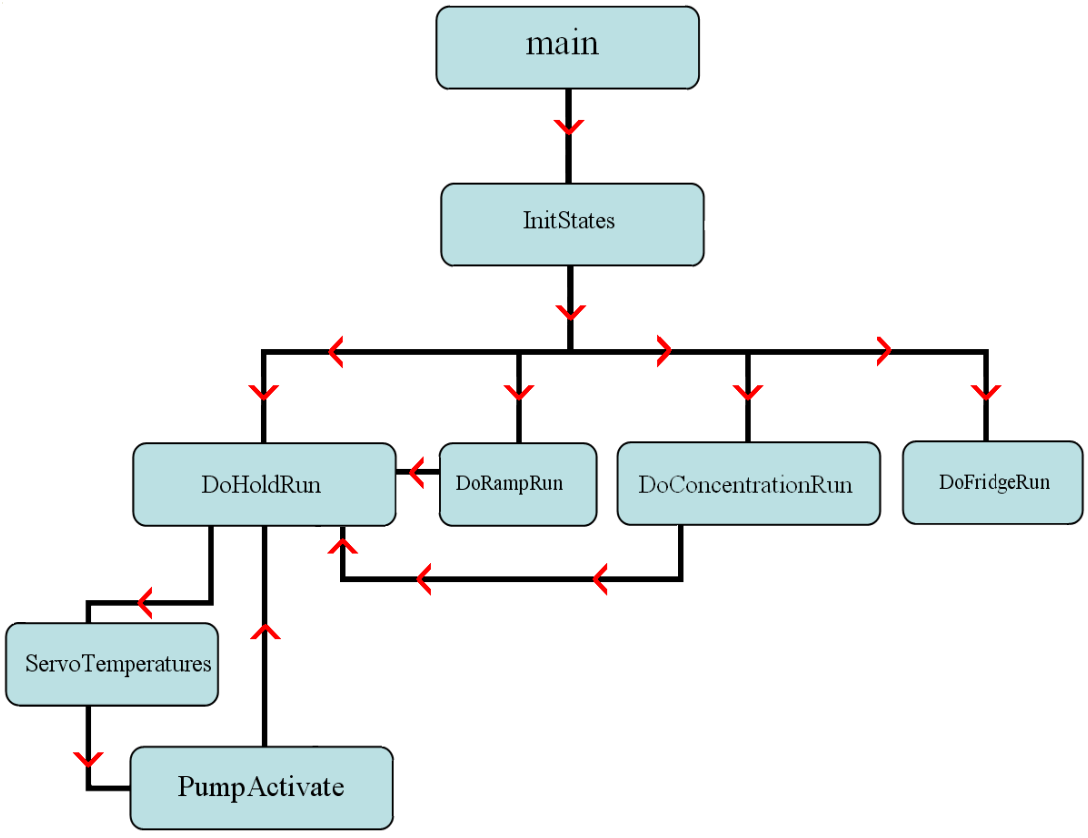

Figure 2.3-3 *Flow chart indicating the sequence in which methods are called.*

A brief description of the function of each method is also included.

InitialStates: This function initializes the two USB 1208LS cards, and sets the digital ports associated with each card as input or output as required. It also opens files for reading and writing to, as well as setting the pump values.

DoHoldRun: This is the function that gets called and run if the user selects 'Hold' on the GUI. Its function is to hold the left and right side chambers at values input by the user. It also reads the temperatures of the 8 thermistors and stores them.

DoRampRun: This user-selected function performs the ramp run. It starts with the two side chambers at pre-selected temperatures, and ramps their temperatures in 0.1°C steps every 540 seconds over 21600 seconds. The ramp run can be performed either with increasing temperature or decreasing temperature. This method re-uses the DoHoldRun method while holding a temperature for 540s.

DoConcentrationRun: This is the third option for run type selectable from the GUI. In this setting the system performs a down ramp followed by an up ramp, after which the concentration of the solute is changed. It calls the DoRampRun to ramp the side walls as in a standard ramp run.

DoFridgeRun: The final run type selectable from the GUI. It is a function that servos the fridge at a fixed a fixed temperature. Usually the system is left in this mode when not in use.

PumpActivate: This function receives values from ServoTemperatures. The values correspond to pumps. The function turns on the pumps as directed to by ServoTemperatures for five seconds, then turns them back off.

ServoTemperatures: Uses the thermistor values stored by the DoHoldRun function associated with the side chambers to decide if they are too hot or too cold. If they

are, the pump value of the pump that can correct the temperature is sent to PumpActivate.

RelayCheck: This is a function that was introduced for safety reasons. It controls the second USB 1208LS card. It is used to record the pumps that the software activates, and then monitors the pump power lines to see if the pump is correctly activated. If a pump fails to turn on or off, this function turns off a mains relay which supplies power to the pumps. This prevents the pumps overheating due to continued operation. This method also stops too much cold fluid being pumped through either side chamber which could freeze the test fluid and damage the test chamber.

To control the system, the Measurement Computing USB 1208LS card is used, this time it's the two 8-channel digital I/O ports that are used. The channels are called FIRSTPORTA and FIRSTPORTB. FIRSTPORTA is used to control the four Totton pumps by means of a four miniature relays. FIRSTPORTB is used to control the main pump power supply (as a cut-off for safety, see the method RelayCheck described above), the agitators and the fridge-freezer. Built into the system is safety cut-off similar to that used for the Totton pumps. All the power supplies, stepper motors, agitators, the controlling computer and the fridge-freezer are attached to a mains relay that is turned off in the event that something goes wrong. Further details are included in the next section on the heat exchange system.

2.4 Heat exchange system

The cooling system employed to conduct these experiments consists of a fridge-freezer, four small magnetic pumps, four expansion chambers, two side chambers and two sumps. The pumps used in this experiment are Totton DC15/5 magnetically coupled centrifugal pumps. Each pump requires 25 watts of power at 12 volts direct current. As the pumps have an internal resistance of 5.76Ω the power supply must be rated at over 2.1A. The maximum output of the pumps is 6.4litres per minute,

which is more then sufficient for this experiment. A photograph and a schematic overview of the system can be seen in figures 2.4-1 and 2.4-2. As can be seen in the diagram the test chamber is located between the two side chambers. Each side chamber has two miniature copper coils. One coil in each side chamber is connected to a cold sump and the other coil to the hot sump. Each circuit has one pump and one expansion chamber. The expansion chambers serve two purposes: they act as an opening in the circuit to allow for air bubbles to escape, and they are also reservoirs holding a large volume of fluid. The fluid contained within the expansion chambers in the freezer remains below -18°C, while the fluid in the expansion chambers outside the fridge-freezer unit are at room temperature (typically above 20°C).

All four circuits contain an ethylene glycol and water mixture, as does the cold sump in the freezer compartment. Both the cold sump and the cold expansion chambers are located in the same freezer compartment. The hot sump is located, along with the hot expansion chambers outside the refrigerator.

Mains relays are used to control the fridge-freezer and the agitators located in each of the side chamber. The fridge-freezer has had its internal thermostat removed. This allows the system to control the fridge temperature with the aid of a thermistor. This is a modification introduced by Mooney [29]. This reduces the amount of work the pumps have to do to maintain the temperature required in each of the side chambers. The fridge temperature is set to be the average of the two side wall temperatures. The effect of this can be seen by the lime-green line in the graph located on the GUI is figure 2.3-2.

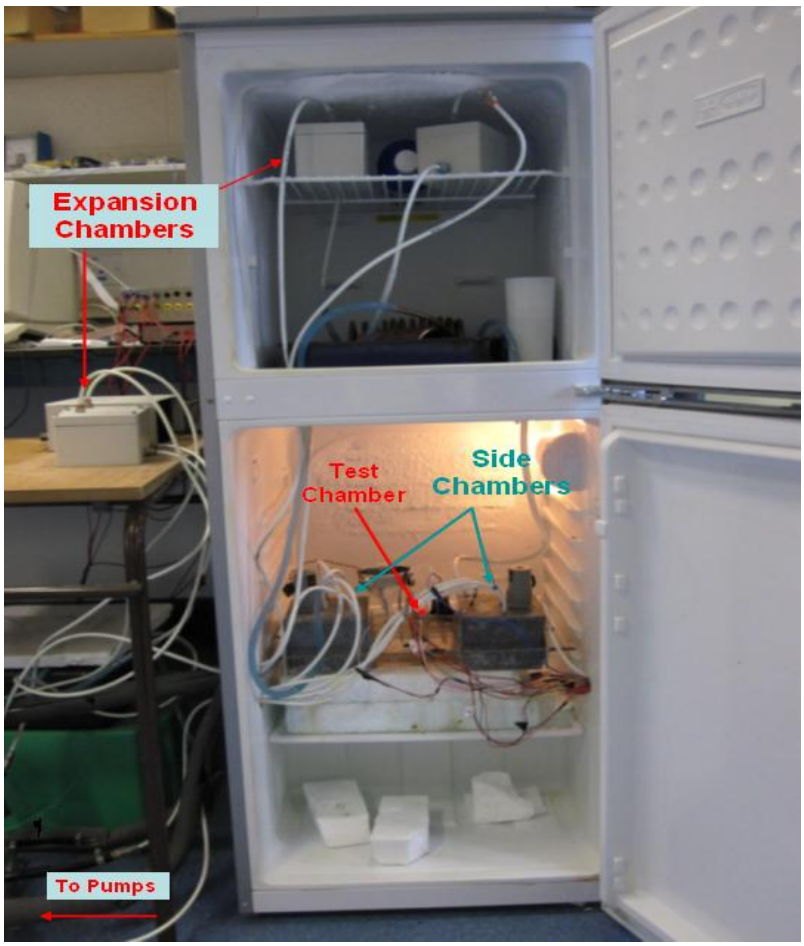

Figure 2.4-1 *Heat exchange system.*

The operation of the system is as follows:

1. The temperature of the T_h side chamber is read.
2. If this temperature is too hot or too cold, the heating or cooling pump associated with that side is turned on for a set time.
3. The temperature of the T_c side chamber is read.
4. If this temperature is too hot or too cold, the heating or cooling pump associated with that side is turned on for a set time.
5. The test chamber thermistors are read.
6. Repeat steps 1-5.

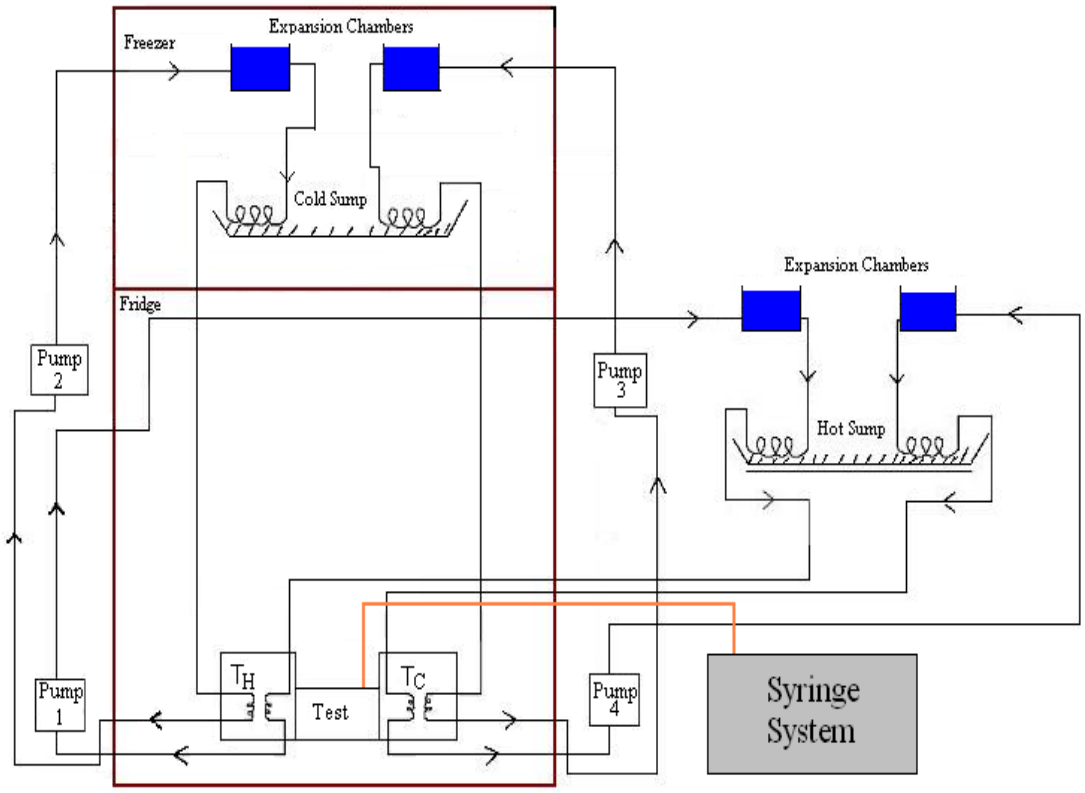

Figure 2.4-2: *Heat exchange system Diagram.*

To operate the system it is necessary to have individual control of all four pumps, agitators and the fridge. The operation of the four pumps is controlled using 12V miniature relays, one for each pump. A control line is sent from the USB-1208LS through a current buffer to ensure enough current is supplied, to the miniature relay. As can be seen in figure 2.4-3, the second USB-1208LS is used to check if the pumps have in fact turned on. This is done with the aid of four voltage dividers. The +12V line that comes from the miniature relay goes in to a voltage divider as well as the pump; the voltage is reduced to +5V and fed into the digital I/O of the second USB. This allows for easy diagnostics of pump and relay problems. This system was introduced to help solve a problem of relays sticking intermittently. To further aid this diagnostics procedure a full log of pump activation is kept. This can be used to identify whether a particular pump is not functioning properly. The concentration scanning system is not included in figure 2.4-3. It will be discussed in section 2.6.

The system used by McBride [40] and Mooney [29] required the use of two fridge-freezer units. These systems were more complicated. They had large reservoirs in each of the fridge-freezers, one for heating and one for cooling. The reservoir used for heating was located inside the fridge compartment, yet still contained a 60W heater. The system used in this experiment removed the need for the reservoirs, heater and the second fridge-freezer. As the volume of fluid within the system is less, the time taken to ready the system for an experimental run is shorter. Placing the sump associated with the heating coils outside the fridge compartment removed any need for heaters.

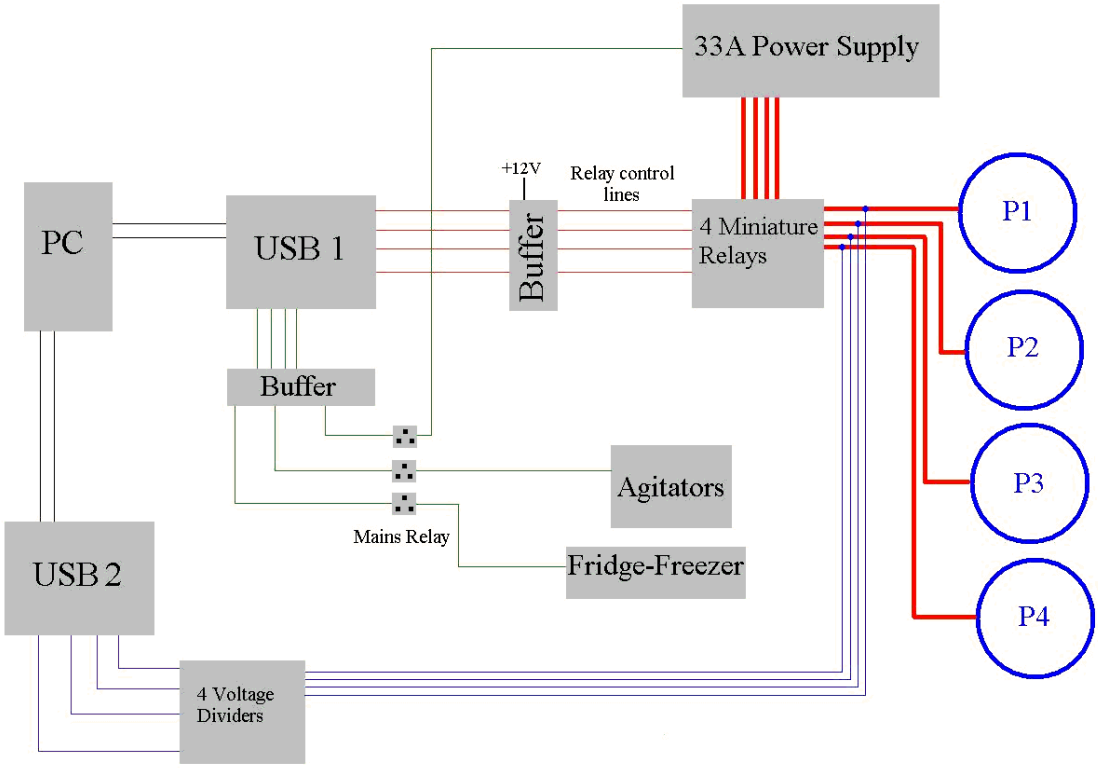

Figure 2.4-3 *Electronic Circuits used to control cooling system.*

2.5 The Test Chamber

For the experiments, the fluid is kept in a test chamber measuring 0.12m x 0.06m x 0.06m. The four sides not in contact with the side chambers are made of Perspex. The two side walls are made of aluminium and have a hole drilled into them to allow

for a thermistor to be placed there in. The thermistors within the chamber are centred on the y-axis and z-axis, and spread equidistant along the x-axis as seen in two-dimensions in figure 2.5-1.

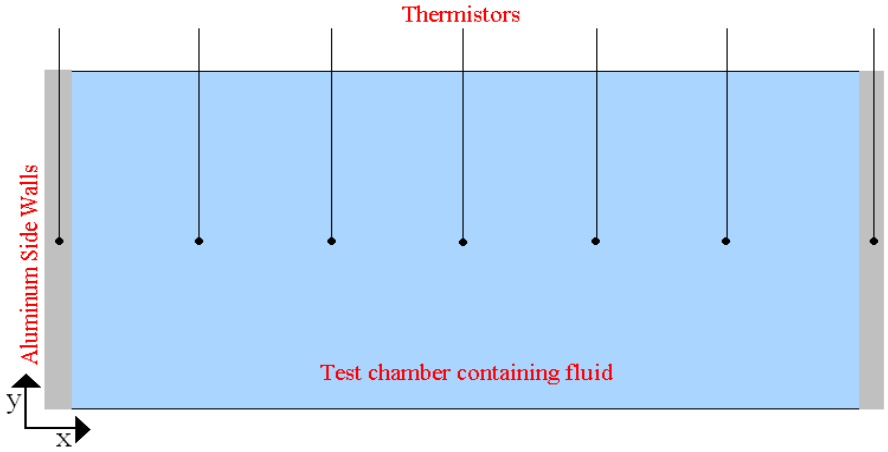

Figure 2.5-1 *Test Chamber.*

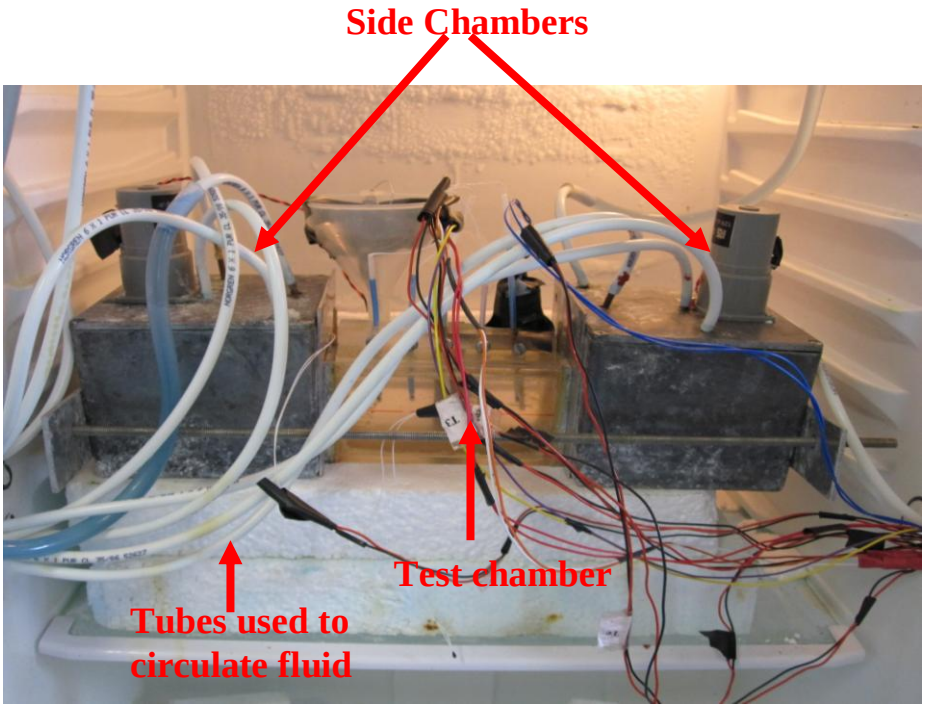

Figure 2.5-2 *Photograph of the test chamber between the two side walls.*

An agitator has been added to the test chamber to ensure proper mixing after a concentration change to ensure the solution is mixed properly. The agitator was custom made. It consists of a 5V D.C. motor which is fixed in place on the lip of the chamber. Extending into the chamber is a plastic rod with four steel pins to perform the agitation. A schematic diagram of the agitator can be seen in figure 2.5-3. The

agitator is located as far back towards the sidewalls in the corner of the test chamber. This is done to minimise the effects it has on the convection flows within the fluid.

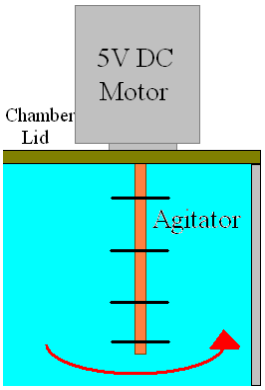

Figure 2.5-3 *Agitator used in the test chamber.*

2.6 Concentration Scans

In previous work on the effects of solutions on the temperature of the maximum density of water, linear or parabolic trends were deduced from four or five points. In this study the aim was to look at these trends in a lot more detail. To allow for this, while using the same convective heat flow technique as developed by Cawley at al (2004), modifications would have to be made. The biggest draw back of the technique used by Cawley et al (2004) was the time it took to conduct a scan on one solution. The tests carried out in these previous studies, and initially in this work, involved starting the system with the side walls at 10°C and 6°C and reducing them to 2°C and -2°C over 43200 seconds (12 hours). After each test, the chamber had to be removed, cleaned and the new test solution placed inside. This solution then had to be cooled, and the system brought back to its holding temperature with the side walls at 10°C and 6°C. This never allowed for more then five solutions to be tested in a week. One other downside to this technique was that it required that the thermistors be moved. This is not that significant an issue, but for comparing the temperature of maximum density from one solution to the next of higher concentration, it would be better if this movement could be avoided.

For example, the results presented on the effects of ethanol on the temperature of maximum density in chapter 3, I took over 150 readings, each consisting of a separate down and up ramp. To conduct this quantity of readings using the old system would have taken 60 weeks of continuous testing, assuming no interruptions due to break downs.

What was needed was a method of conducting an automatic concentration scan. The system that was developed allowed for up to 30 concentrations to be tested automatically. For each concentration a down ramp and an up ramp is conducted. This allows for an average result to be obtained for each concentration.

The system uses a linear actuator to control a syringe. The syringe can be filled with the liquid solutes at any concentration level, usually 100% or 25% by volume. In the case of solid solutes such as sodium chloride, a very high concentration solution is made up and used to fill the syringe. The linear actuator used in this experiment is a Nanotec L5609X2008-M6x0.5. It has a rated thrust of 85N and a resolution of 0.00125mm/step, this means that to move the treaded rod by 1mm, 800 clock steps are required. It has four separate coils, each requiring 2A of current. The resistance per coil is 1.37Ω. After each ramp run, the stepper moves a predefined distance causing a measured amount of the solute to be deposited into the test chamber. The test chamber is then agitated and allowed to settle before another ramp run is conducted.

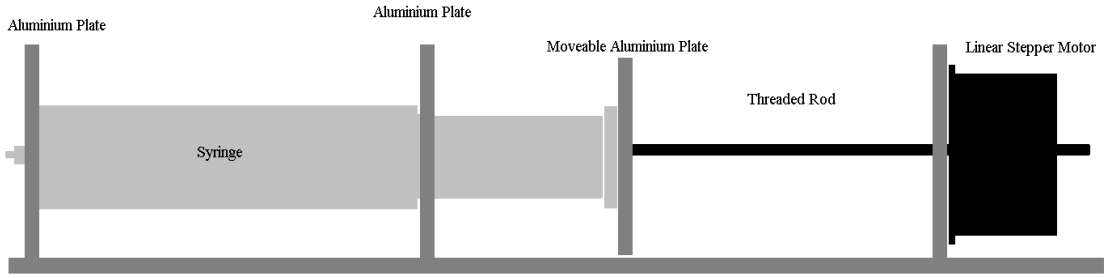

Figure 2.6-1 *Schematic diagram of the stepper motor and syringe apparatus.*

The software used to control this system is the same as before with the addition of one function called stepper. This method simply turns on a switches a control line in a NAND gate to allow clock pulses from a 555 chip through to the stepper motor driver. The circuit diagram is shown below in figure 2.6.4. Each of the four coils of the linear actuator has two cables associated with it. This makes it a unipolar stepper motor. It was converted to a bipolar motor by connecting two coils on each side together. This left two coils and four cables in total. This set up is shown in figure 2.6-2

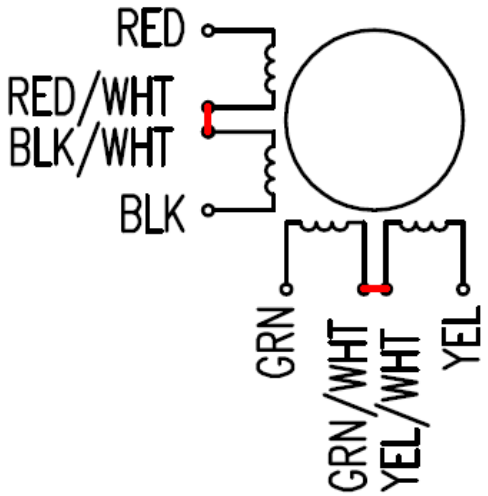

Figure2.6-2 *Linear actuator wiring diagram.*

An L298 dual full bridge driver is used in the control circuit for the linear actuator. The L298 is an integrated monolithic circuit that is designed for both high voltages and high currents and is used to control relays, solenoids and stepper motors. The stepper motor controller used in the circuit is the L297. The L297 can be used to drive bipolar and four phase unipolar stepper motors in either full step or half step modes. An advantage of the L297 over other controllers that were investigated is that it only required a clock, direction and mode (half or full step) input signals. This makes it an easy controller to integrate into a circuit. The clock in this circuit was provided by a KA555 single timer chip. The frequency of this chip is given by (Horowitz and Hill) [41].

$$f = \frac{1}{0.693(R_A + 2R_B)C} \qquad (2.6\text{-}1)$$

The apparatus used to hold the linear stepper motor and syringe was made up within the Experimental Physics Department. Similar units are available commercially and are used by chemists and in the field of medicine. These systems would not have given the flexibility that the custom systems unit does. Another advantage of building the system in the Experimental Physics Department is that it can be repaired on site both quickly and cheaply which may not be the case if the system was bought in. A schematic diagram of the apparatus can be seen in figure 2.6-1, and a photograph can be seen in figure 2.6-3.

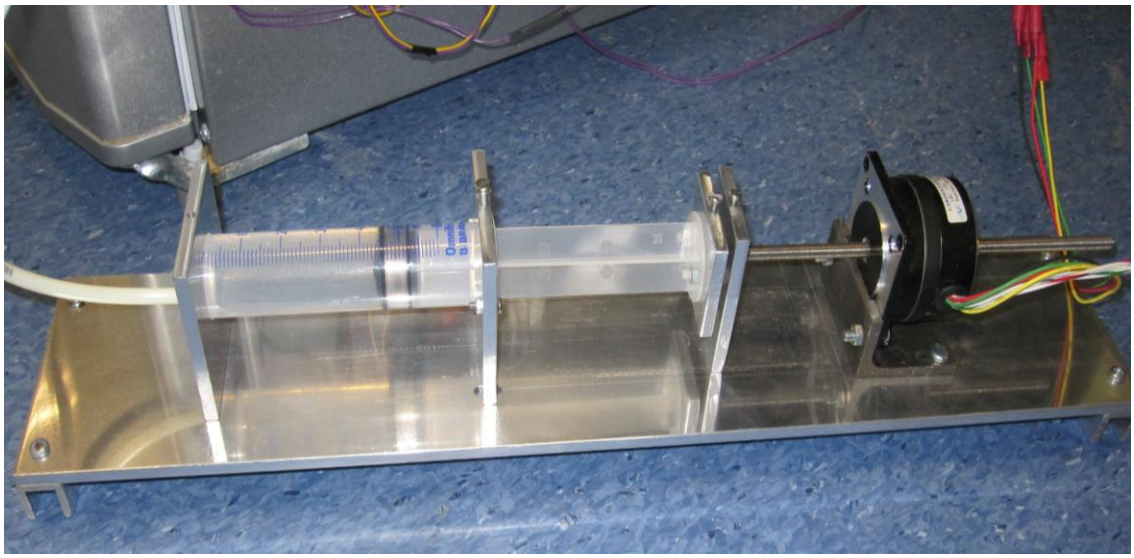

Figure 2.6-3 *Photograph of the stepper motor and syringe apparatus*.

The syringe system allowed the 150 down and up ramps to be completed in less than 80 days of testing, which is a significant improvement on the 420 days that would have been required otherwise. These improvements in time were achieved by being able to run the system 24 hours a day, 7 days a week while conducting a scan. Also the scan size was reduced from spanning 8°C to spanning 4°C.

In all the tests carried out in this work, the solvent has been pure water. The water that is used in the tests is passed through a distillation process to remove any

impurities that may effect the results. All the solutes are high in purity. The minimum purity as quoted by the manufacturer is 99.5%. A typical experimental run begins with 0.36 litres of distilled water in the test chamber. This volume of water is measured out using a medical syringe for high accuracy. The same procedure is followed when making a solution for the concentration scanning system. During a concentration scan, each injection is typically 2.5ml of a 25% solution.

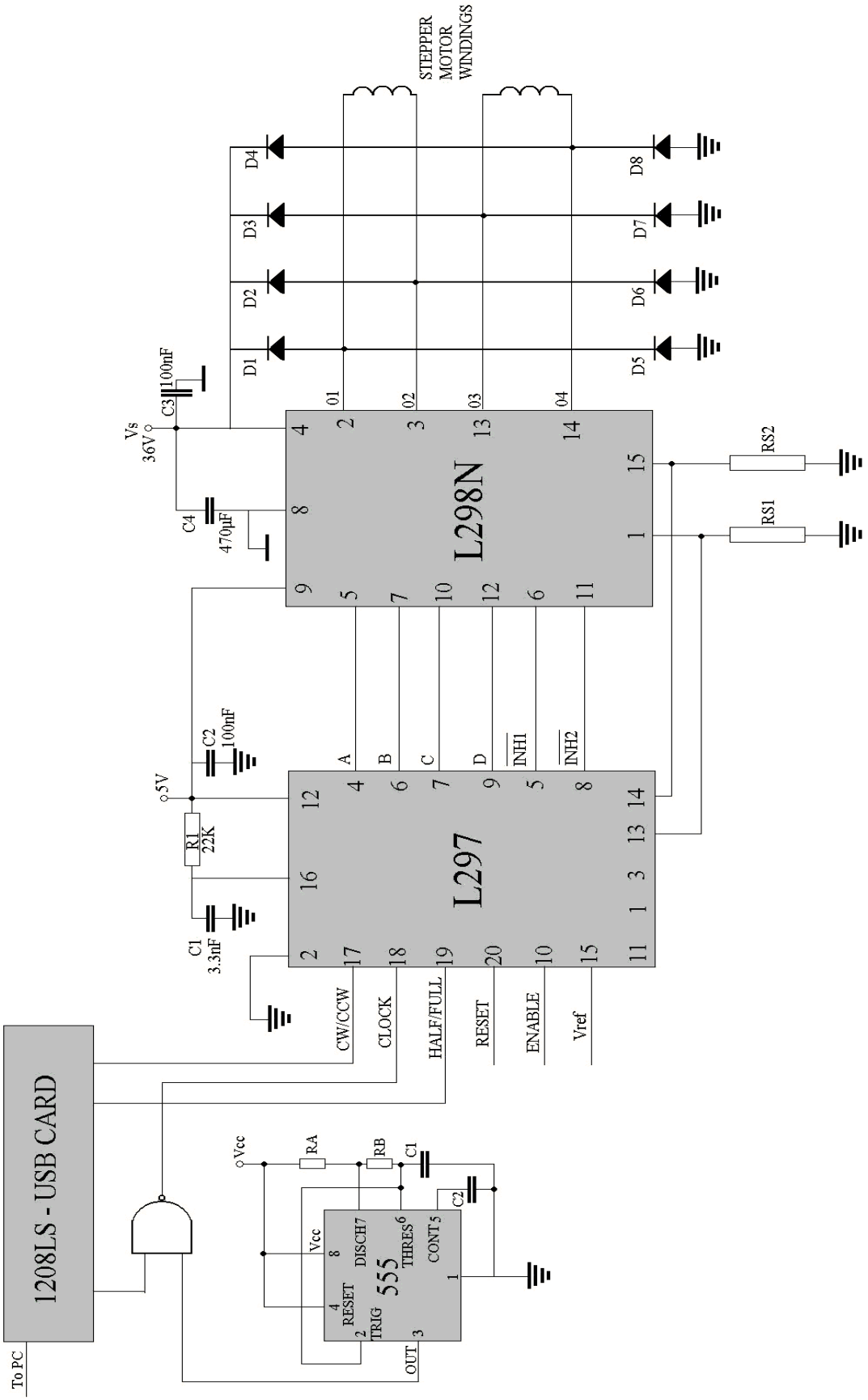

Figure 2.6-4 *Stepper Motor Circuit Diagram.*

2.7 Variation in the Fluid Volume in the Test Chamber.

The convective flow technique developed by Cawley et al (2006) always had the thermistors located in the centre of the test chamber, which was always completely filled. However in the tests carried out in this study, the level of the fluid changes from one run to the next. This change in volume is due to the injection of fluid after each up ramp in order to change the concentration on the solute. This causes the relative height of the thermistors to change. The test chamber is 0.06m in height, and the thermistors are located at a height of 0.03m. At the beginning of each run there is 360 millilitres of fluid in the test chamber which corresponds to a height of 0.05m.

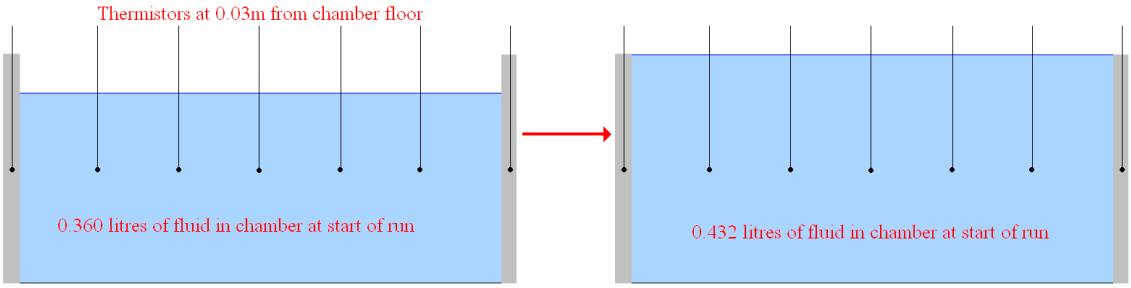

Figure 2.7-1 *The fluid level changing as the concentration scan progresses.*

To test what effect this would have on the value obtained for the temperature of maximum density, simulations were carried out in COMSOL Multiphysics™. COMSOL Multiphysics is a finite element analysis and solver software package that can be used for various physics problems and applications. Its benefit in the application required for this study is that COMSOL Multiphysics allows for the solving of 'multiphysics' problems. A multiphysics problem is defined as being a problem that requires more then one branch of physics to solve. In the simulations used for this investigation, two branches of physics are required. The simultaneous solving of both 'Convection and Conduction' and 'Incompressible Navier-Stokes' physics models are necessary. Another advantage of using COMSOL Multiphysics is it provides an extensive and well-managed interface to MATLAB.

It is recognised that the Comsol model used for test and optimisation purposes in this study is not a replica of the experimental arrangement. In particular, the model is 2-dimensional, and uses non-slip boundary conditions for the Navier-Stokes equations for all of the four boundaries of the 2-dimensional test region, whereas in reality there is a free surface at the top of the test liquid in the experiment. This is analogous to the difference between Benard convection (taking place between two horizontal parallel plates) and Marangoni convection (heated plate below, free surface at the top) [42]. Despite such differences, it has been found that the model successfully reproduces the relevant features of the experiment, with the anomaly shifting by the correct amount when the state equation of the fluid is modified to incorporate varying levels of salinity. It is proposed that the free surface feature be incorporated into the modelling in the future, but the considerable additional complexity introduced by the necessity of continual remeshing to account for a moving boundary was not deemed to be warranted at this stage.

2.7.1 The Governing Equations

When describing the behaviour of fluids mathematically, the conservation equations can be used. The conservation equations used are those describing the conservation of mass, energy and momentum. The Navier-Stokes equations describe the conservation of momentum, the name is generally used as a term to describe the complete set of equations used to solve computational fluid dynamics. In this study, the conservation of mass and momentum will be referred to as the Navier-Stokes equations and the conservation of energy equation will be referred to as the heat equation. The four equations are listed below (2.7-1 – 2.7-4).

$$\rho(T)\frac{\partial \bar{v}}{\partial t} + \rho(T)(\bar{v}.\nabla)\bar{v} = -\nabla p + \rho(T)\bar{g} + \mu(T)\nabla^2\bar{v} \qquad (2.7\text{-}1)$$

$$\nabla \cdot \bar{v} = 0 \qquad (2.7\text{-}2)$$

$$\frac{\partial T}{\partial t} + \bar{v} \cdot \nabla T = \alpha(T)\nabla^2 T \tag{2.7-3}$$

$$\text{where } \alpha(T) = \frac{k(T)}{\rho(T)C_p(T)}$$

$$\rho(T) = c_0 + c_1 T + c_2 T^2 \tag{2.7-4}$$

where $\bar{v}$ is the velocity (m.s^{-1}), T is the temperature (Kelvin), ρ is the density of the fluid (kg.m^{-3}), p is the pressure (Pa), $\bar{g}$ is gravity (m.s^{-1}), μ is the viscosity (Pa.s), α is the thermal diffusivity (m^2.s^{-1}), k is the thermal conductivity (W.K^{-1}.m^{-1}) and C_p is the specific heat capacity. The values of the specific heat capacities for various temperatures were found in reference [13].

It is worth noting that unlike other software packages, (NaSt2D for example), COMSOL does not use the Boussinesq approximations which assumes that the density of the liquid is constant except in the body force term of the Navier-Stokes equations.

Using the density state function a density profile curve can be obtained as in figure 1.2-1. For pure water the constants c_0, c_1 and c_2 are c_0 = 999.84508 kg m^{-3}, c_1 = 0.06378 kg m^{-3} °C^{-1}, c2 = -0.00801 kg m^{-3} °C^{-2}. This shows a density maximum at 3.98°C (277.13K). The temperature of maximum density is obtained by letting the derivative of $\rho(T)$ (equation 2.7-4) equal zero, i.e.

$$\frac{\partial \rho}{\partial T} = 0 = T_{\rho_{MAX}} \tag{2.7-5}$$

$$T_{\rho_{MAX}} = \frac{-c_1}{2c_2} = 3.98°C \qquad (2.7\text{-}6)$$

All the equations are solved in two dimensions, this is done to reduce the processing time required to carry out each simulation and it is assumed that the numerical investigations carried out in 2-D adequately represent the experimental results taken from the three dimensional chamber. This has been confirmed by carrying out a small number of tests using 3-D models.

These equations were used to simulate the experimental system. Once the simulation was finished, the results were analysed in the same way that the experimental runs are analysed (see section 3.2). The positions of the thermistors in the simulated test chamber were then varied to determine what effect, if any, this had on the temperature of maximum density obtained.

2.7-2 How the Variation in height effects the temperature of maximum density.

The model was developed to run for a simulated time of 43200 seconds. It started with the side walls at 8°C and 4°C and was ramped down to 4°C and 0°C and back to 8°C and 4°C, as in the experimental runs. The output was then examined with the thermistors placed in the centre of the chamber. The result of this simulation is shown in figure 2.7-2(a). The data corresponding to this simulation was extracted. The code described in chapter 3 for extracting the temperature of maximum density from an experimental run called do_int was applied to both the down ramp and the up ramp. The average temperature of maximum density for the down ramp and up ramp was 3.989°C. The same simulation was run with the thermistors moved to a height of 0.033m. The output from this simulation can be seen in figure 2.7-2(b). The shape of the anomaly has changed slightly in this graph. However after extracting the data and applying the do_int code, an average temperature of maximum density for the up and down ramp was found to be 3.981°C. The thermistors were moved to 0.036m and 0.04m in height figures 2.7-2(c) and (d), and the same procedure was applied. In these cases, the average temperature of maximum density for a down and up ramp was 3.977°C and 3.979°C respectively. Details of how these figures were obtained appear later in this section.

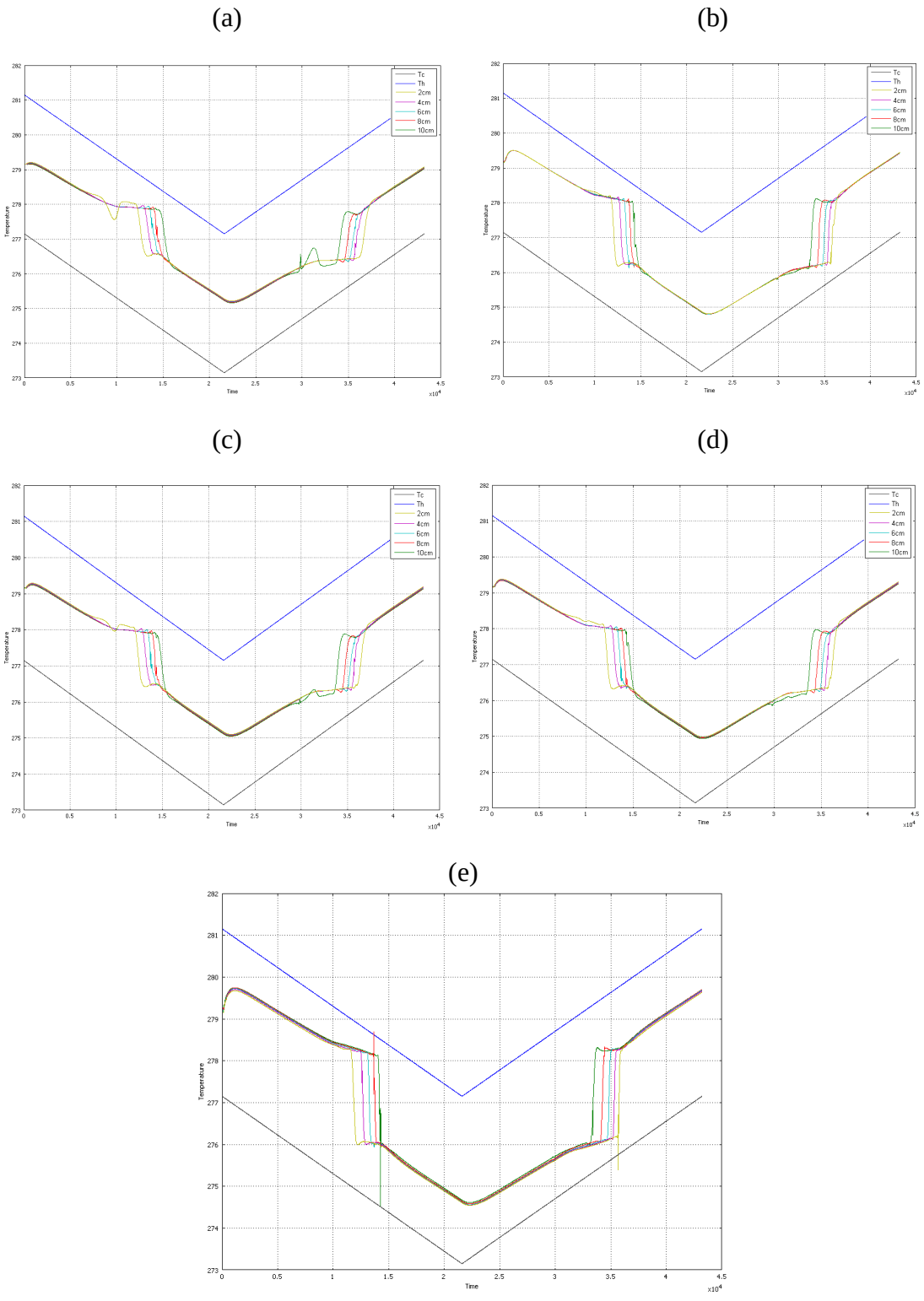

Figure 2.7-2 *Temperature in Kelvin versus time in seconds for a simulated pure water run, with the thermistors located at a height of (a) 0.030m (centre), (b) 0.033m, (c) 0.036m, (d) 0.040m and (e) 0.045m*

The concentration scanning experiments start with the thermistors placed at a height of 0.03m in 0.36 litres of fluid. The length and breath of the chamber are 0.12m x 0.06m, this means that the height of the fluid at the start of the run is 0.05m, as seen in figure 2.7-3. Consequently the thermistors are located at a height that is 60% that of the height of the fluid. This is the same as positioning the temperature monitoring points at 0.036m in the simulations. The simulations show that this does not effect the results obtained from the temperature of maximum density extraction code, do_int. Even when the temperature monitoring points are moved to a height of 0.04m within the chamber, there is a negligible change in the average temperature of maximum density obtained. It was not until the temperature monitoring points were placed at a height of 0.045m that the temperature of maximum density became significantly different from what was expected. When the temperature monitoring points were placed this high the temperature of maximum density was returned as 3.942°C.

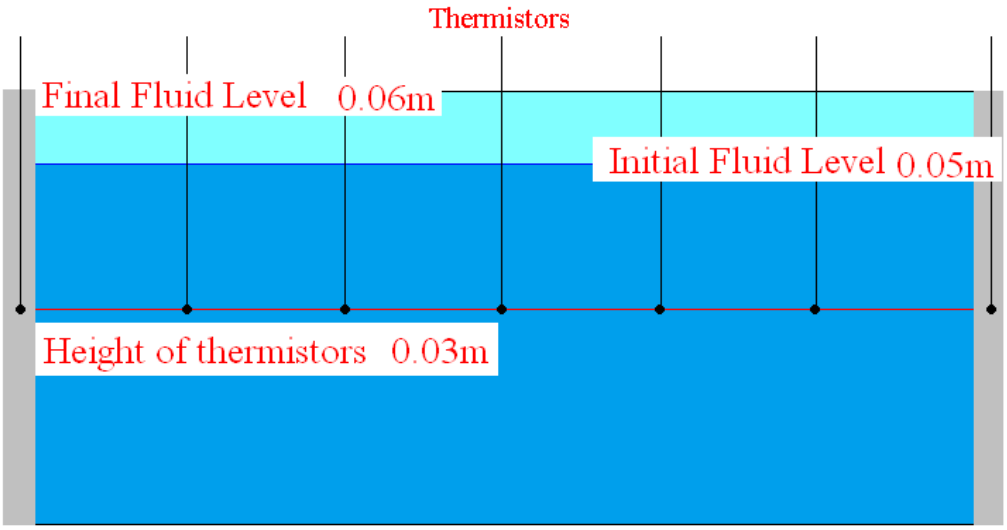

Figure 2.7-3 *The change in the fluid height within the test chamber as the experimental run progresses.*

This came about when the temperature monitoring points were placed at a height 75% of that of the water. This would equate to starting the experimental simulations with only 0.288 litres of fluid in the test chamber. No tests were ever started with

less then 0.36 litres of fluid in the test chamber. Table 2.7-1 summarises the results obtained from this investigation.

Level (m)	**T_{md} Down (°C)**	**T_{md} Up (°C)**	**T_{md} Average (°C)**	**Fluid Height (Litre)***
0.03	4.018	3.960	3.989	0.432
0.033	4.024	3.937	3.981	0.392
0.036	3.997	3.957	3.977	0.360
0.04	3.981	3.976	3.979	0.324
0.045	3.981	3.903	3.942	0.288

Table 2.7-1 *Summary of the investigation into the effects of the variation in the fluid height in the test chamber on the temperature of maximum density. *Corresponding experimental fluid height required to have the same relative shift in thermistor height.*

Over the range 0.03 – 0.04m, the average temperature of maximum density was 3.9815 ±0.0198°C, which encompasses the known temperature of maximum density of 3.98°C.

The experimental results obtained for NaCl solutions also confirms that the variation in the volume of fluid in the chamber has a negligible effect on the temperature of maximum density. These results are presented in section 3.3.

Chapter Three

Data Analysis Procedures and Results

3.1 Introduction

In this chapter the experimental results that were obtained during the course of this work are presented. The investigation involved measuring the temperature of maximum density for various aqueous solutions. It is known that the melting point and the boiling points are both colligative properties of water; as a consequence of this, the addition of solutes to water causes both the melting point and the boiling point to change in a linear fashion. Previous studies have indicated that the temperature of maximum density is not a colligative property.

A detailed study of the behaviour of the temperature of maximum density of various solutions was carried out. The method used to carry out this study is described in chapter 2. The technique relies on the anomalous feature that occurs in the temperature profile of five thermistors positioned equidistantly along the x axis, and centred on both the y and z axis of the test chamber. The method that is used to extract the temperature of maximum density for a given concentration is also presented in this chapter. The results presented here include tests carried out on pure water, sodium chloride, methanol, ethanol, 1-propanol and 2-propanol.

3.2 Extracting the Temperature of Maximum Density.

Once an experimental run has been completed, a data file contains the temperatures recorded from the eight thermistors within the refrigerator, along with the time is created. This data is inspected in graphical form to check for the presence of the anomaly. If an experimental run is completed on a substance that exhibits no density maximum such as pure ethylene glycol a graph like that obtained from COMSOL Multiphysics (figure 3.2-1) would result. This simulated run starts with the side walls at 10°C and 6°C, and they are ramped down to 2°C and -2°C. The five thermistors within the test chamber all read the same value. This is due to them being positioned centrally along the y and z axis out of the convective flow. As the ethylene glycol is heated close to the T_h side wall, it becomes less dense and rises;

conversely the ethylene glycol close to the T_c side wall gets cooled and becomes more dense. This increase in density causes it to sink. Together these two actions create a convective flow. This can be seen in figure 3.2-2. In this case, the convective flow moves in a clockwise direction. The colours represent the temperature (red being hotter, blue colder). The arrows represent the direction of the movement of the fluid. The small red dots indicate the location of the thermistors.

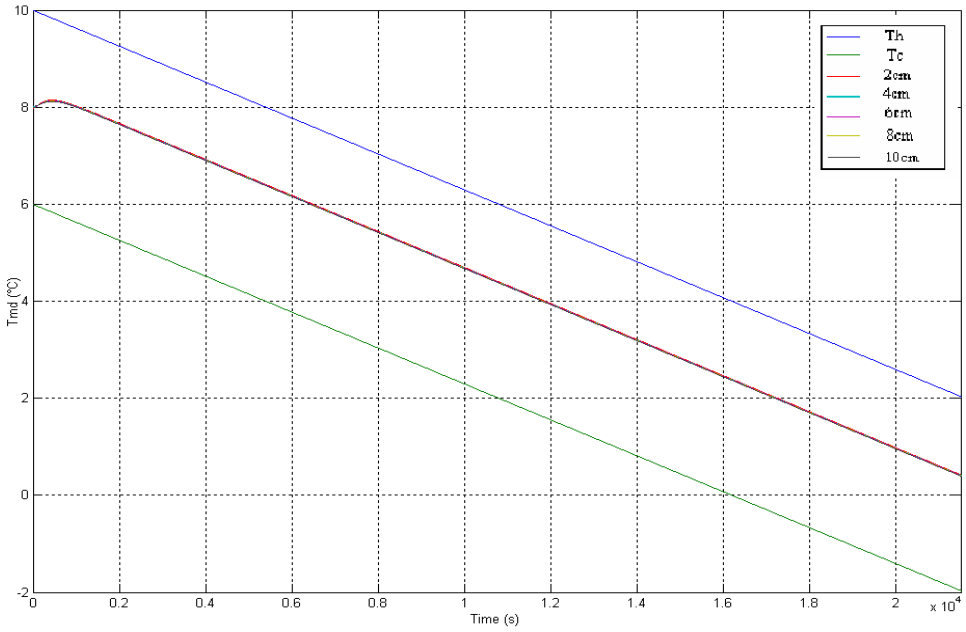

Figure 3.2-1 *Simulated pure Ethylene Glycol run.*

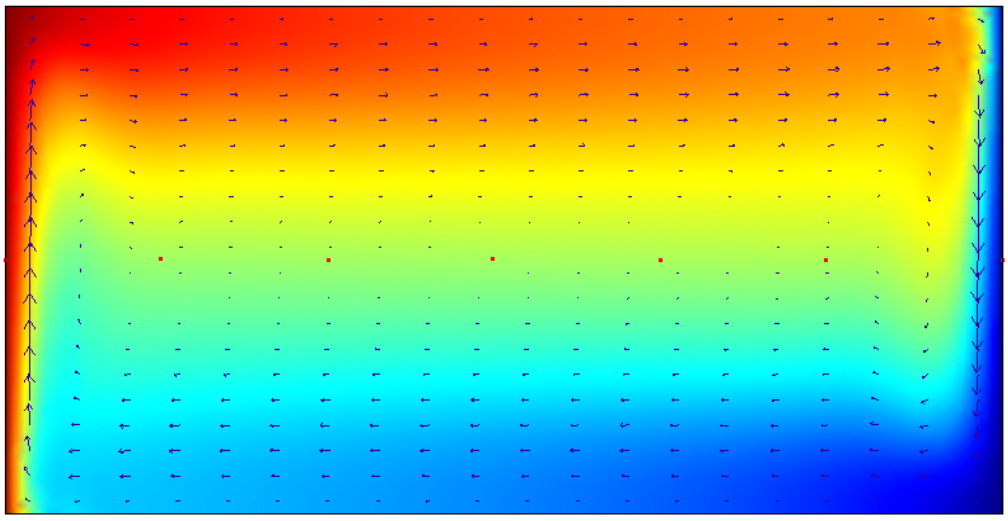

Figure 3.2-2 *Simulated visualization of the convective flow within the test chamber of a fluid without a density maximum.*

The picture for pure water is more complicated. When water is above its temperature of maximum density, it behaves in the same way as most other fluids, in that the warmer fluid rises as it is less dense, and the colder fluid sinks as it is more dense. However below the temperature of maxim density the converse happens. The colder water is less dense and rises, and the hotter water sinks as it is denser. This causes the convective flow to reverse.

This reversal of the convective flow is easily visible when the temperature of the thermistors versus time is plotted. To show exactly what is happening within the chamber, the results from a COMSOL Multiphysics simulation graph is shown along with various convective flow diagrams.

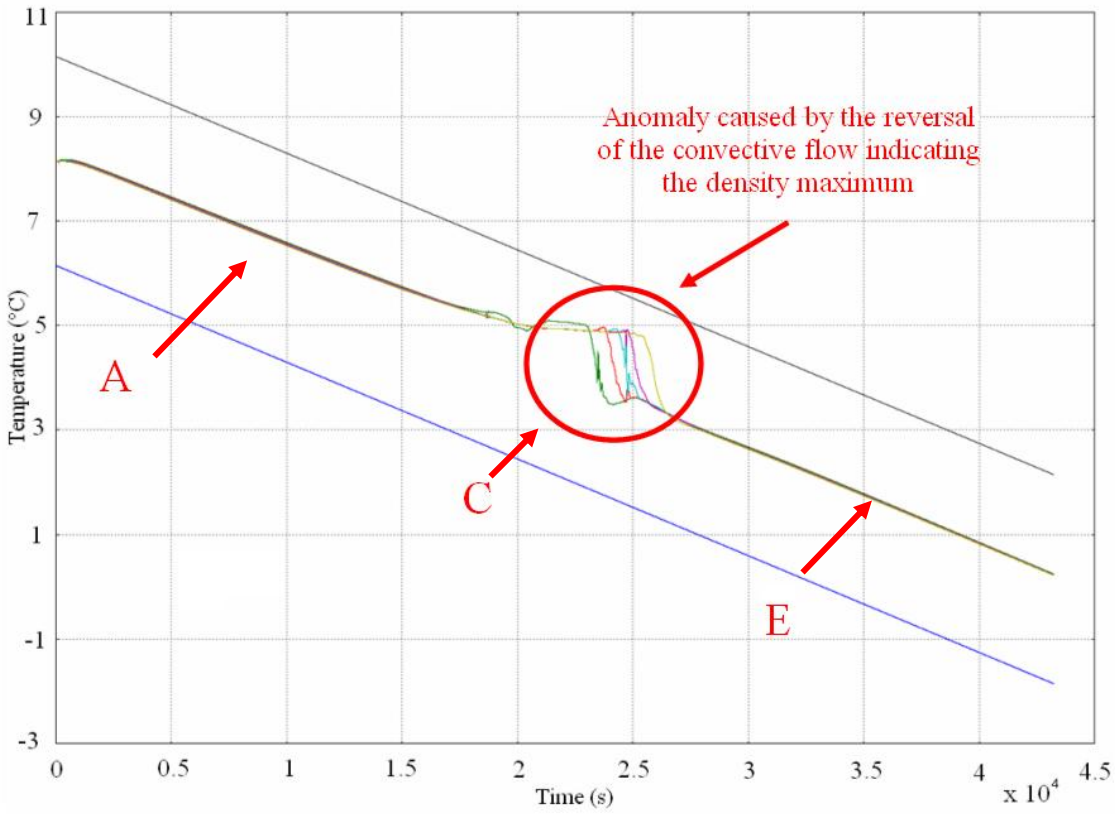

Figure 3.2-3 *Simulated pure water run.*

As can be seen from the figure 3.2-3 the presence of the density anomaly is very visible. The centre of the anomaly is the temperature of maximum density. Two methods are used to extract this value. Figure 3.2-4 shows the convective flow at locations A, C and E as indicated on figure 3.2-3. They show the direction of fluid flow before, during and after the density maximum.

(a)

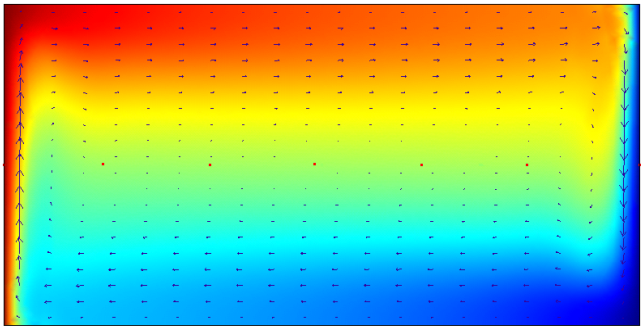

(b)

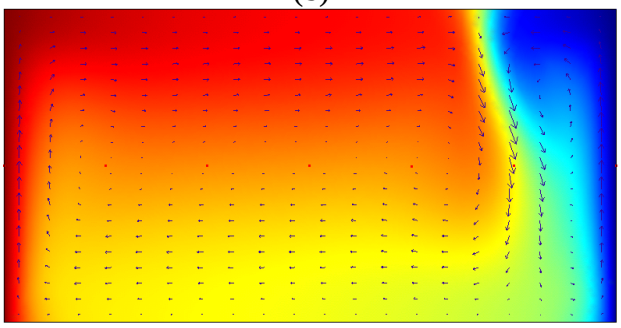

(c)

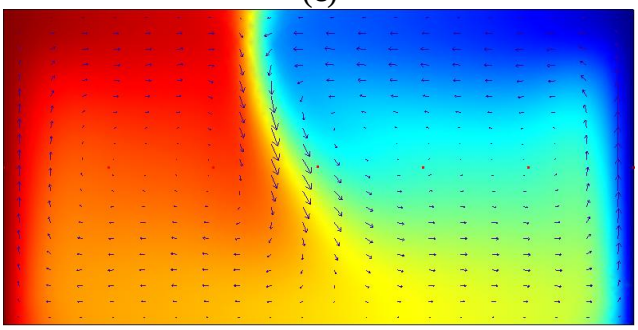

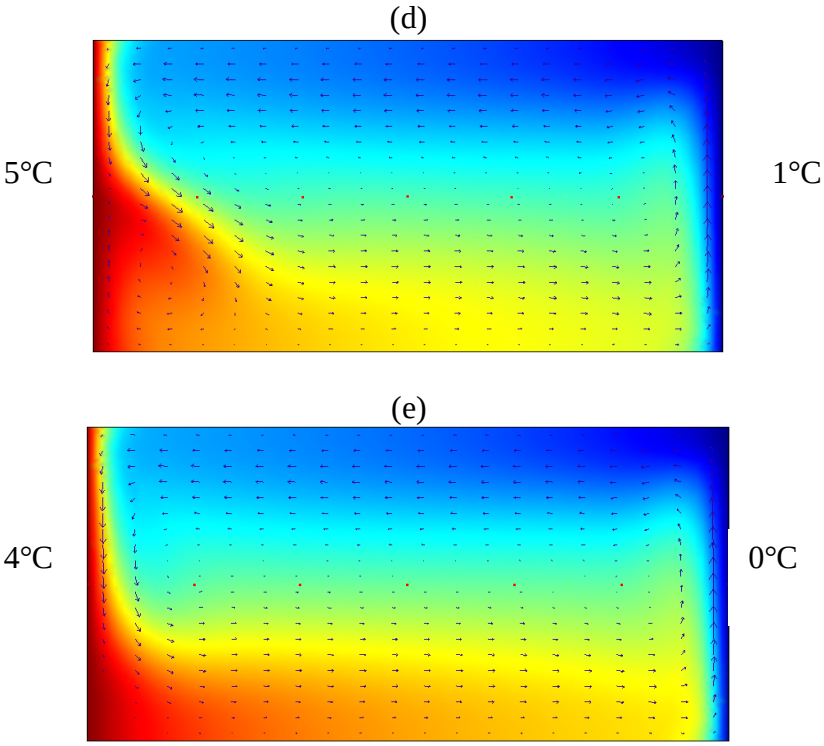

Figure 3.2-4 *The change in the convective flow as water passes through the density maximum.*

The first method involves printing out the graph and doing a 'fit-by-eye' using a ruler to measure its location. The fit-by-eye is used purely as a rough guide and to compare with the results obtained from the second method. The second method employed to extract the temperature of maximum density is based on an area-integration over the anomaly region. The data corresponding to the outer two thermistors located at 2cm and 10cm from the cold side wall are extracted from the data file. The area under the graph from each of the two thermistors is obtained using an area-integration as shown in figure 3.2-5. The grey section is the area under one thermistor, the grey and pink section is the area under the other thermistor. The difference of these two areas (grey shading only) is the area of the anomaly. The area corresponding to the anomaly is halved.

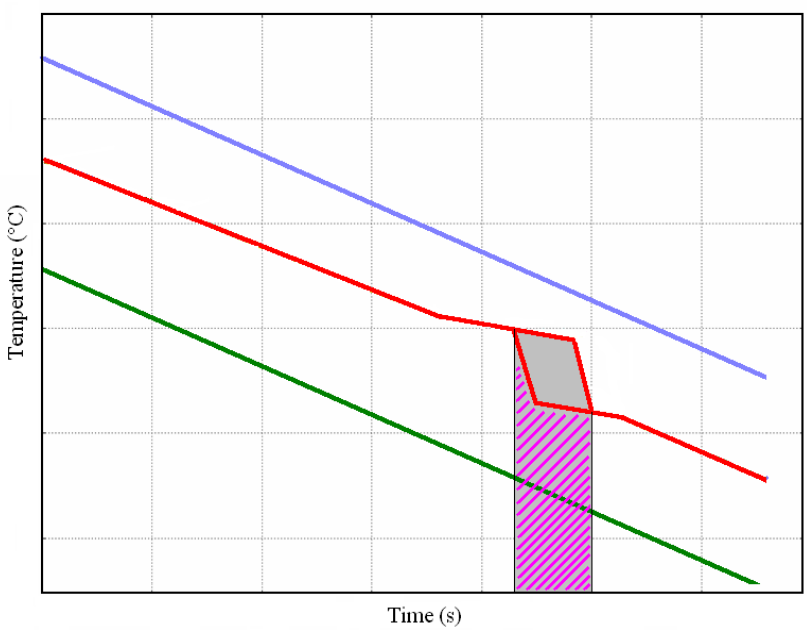

Figure 3.2-5 *The first integration carried out by do_int.*

A second integration is conducted. This second integration is a vertical scan of the two thermistors carried out in small steps to calculate the difference in area under each thermistor. When the difference in area is found to be equal to half the total difference in area, the corresponding temperature is saved to a file as shown in figure 3.2-6.

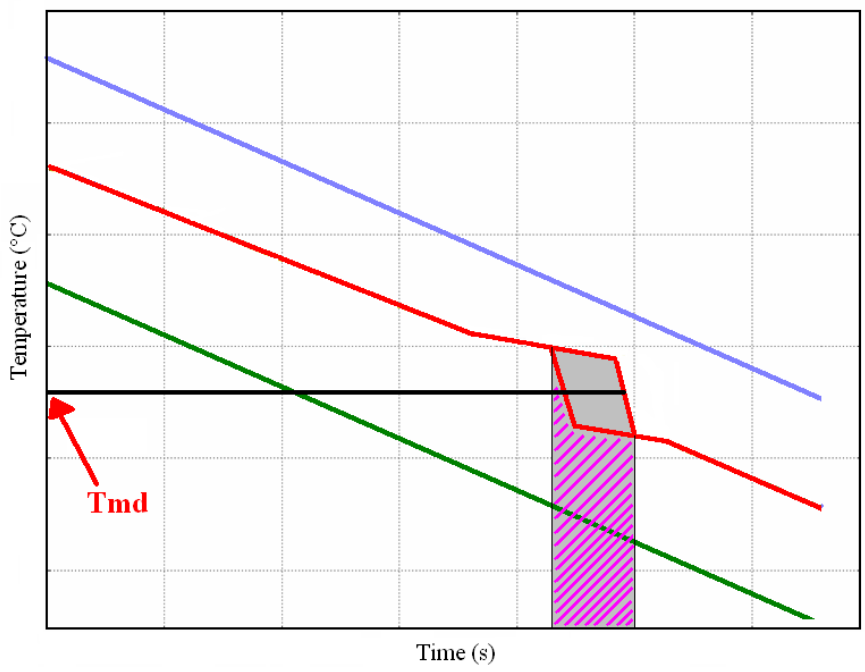

Figure 3.2-6 Extracting the temperature of maximum density using do_int.

This method works for both down and up ramps. COMSOL Multiphysics was used to verify this technique. Simulations were carried out using state functions with known temperatures of maximum density. The required data was extracted from the output file created by COMSOL. The area-integration technique was then applied to this data to verify that it worked. Simulations were run with various different, but known temperatures of maximum density and each time the correct value was obtained from the area-integration method. All the results presented in this section are obtained using this area-integration method. The procedure used to calculate the uncertainty in the values of temperature of maximum density are discussed in section 3.6.

In conjunction with the heat exchange system, the concentration scanning system described in section 2.6 was used for most of the tests. Figure 3.2-7 shows the output of the first three down and up ramps for an NaCl concentration scan. Figure 3.2-8 is included to show the importance of agitation in the test chamber. In this instance, the agitator failed to activate after the concentration had been changed. This results in the convective flows being permanently disrupted, and in turn the density anomaly is not visible. This allows for a simple way of checking that the agitators are working and mixing the solution correctly. Figure 3.2-9 shows the results of a complete ethanol scan. This scan consists of 21 separate up and down ramps and took 1.095×10^6 seconds to complete.

The ambient temperature surrounding the test compartment within the refrigerator was continually monitored throughout the experiments, and the refrigerator unit was controlled to maintain this ambient temperature at a level within the bounds of the temperatures of the hot and cold walls of the test chamber. Frequent control runs carried out on distilled water showed that slight variations of the ambient temperature within this range did not have a measurable influence on the value of the recorded temperature of maximum density.

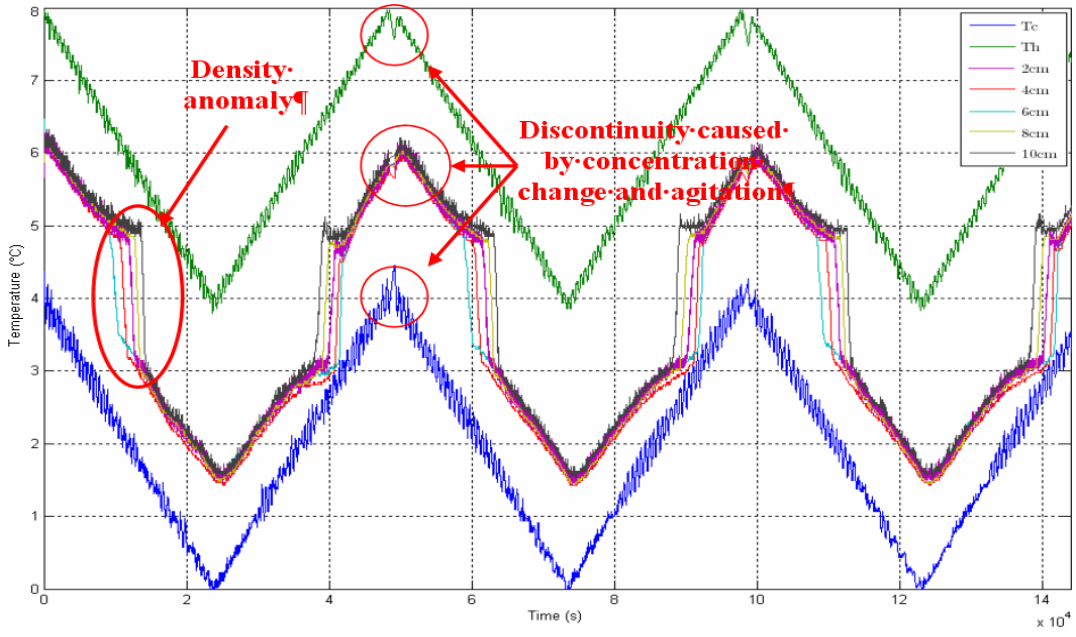

Figure 3.2-7 *Three down and up ramps obtained using the concentration scanning system.*

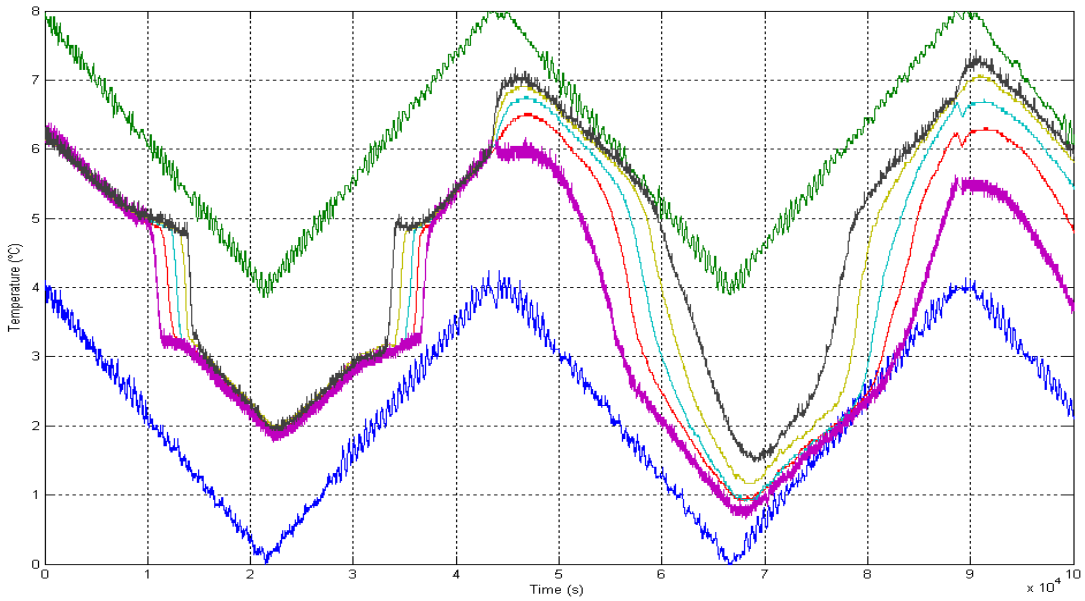

Figure 3.2-8 *Agitators failing to activate after a concentration change.*

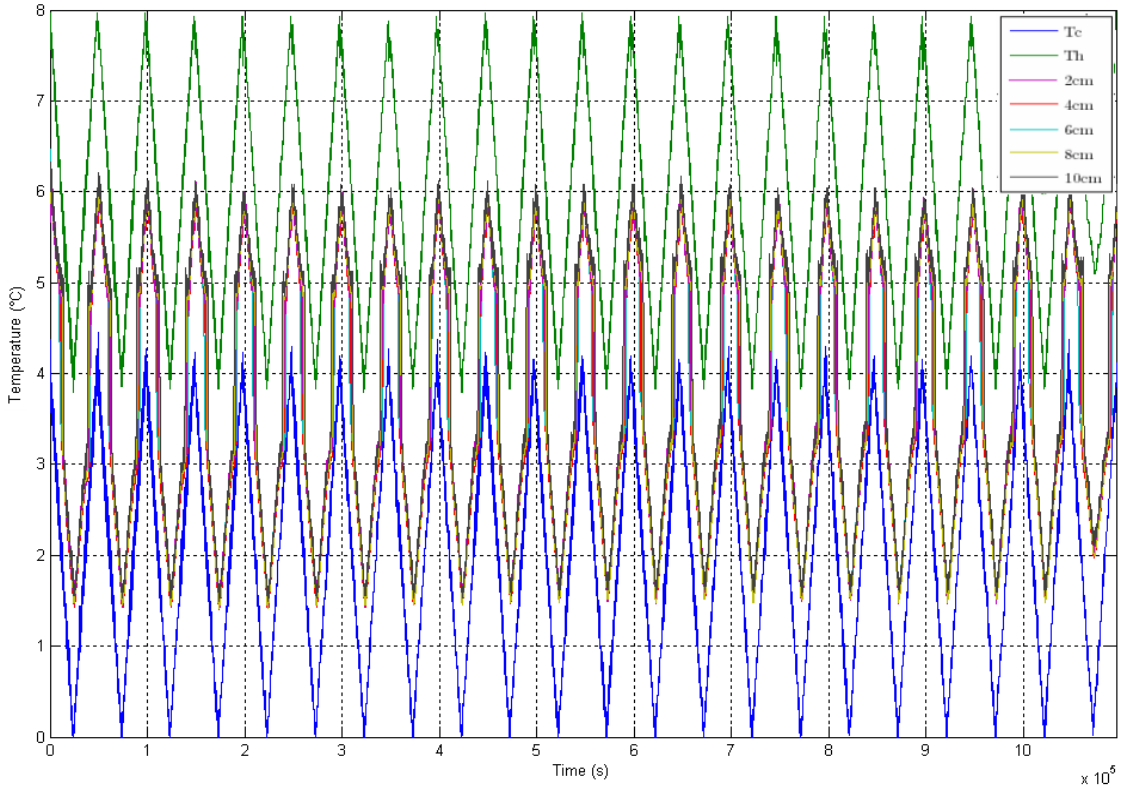

Figure 3.2-9 *A complete ethanol scan, consisting of 21 separate up and down ramps at different concentrations. This scan took 1.095x10^6 seconds (~12.5 days) to complete.*

3.3 The temperature of maximum density of saline solutions

To ensure the new concentration scanning system was functioning correctly, tests were carried out on the effects of NaCl on the temperature of maximum density of water. These tests started off with 360 millilitres of distilled water in the test chamber. A down ramp and an up ramp were carried out for each concentration, after which 1.8 millilitres of an 80g/litre NaCl solution was added to the chamber. This process was repeated 18 times. The results were graphed in figure 3.3-1, along with results taken from Caldwell [43]. Down and up ramps for pure water as well as for a 6.74g/litre saline solution are shown in figures 3.3-2 and 3.3-3. There is good agreement between the results taken with the concentration scanning system, and

those obtained by Caldwell. Table 3.3-1includes the average result of the down ramp and up ramp carried out at each concentration.

SODIUM CHLORIDE NACL		
Concentration (g/litre)	**Concentration (moles/litre)**	**T_{md} (°C)**
0.000	0.000	3.979
0.387	0.007	3.865
0.769	0.013	3.764
1.148	0.020	3.674
1.524	0.026	3.611
1.895	0.032	3.534
2.263	0.039	3.473
2.628	0.045	3.362
2.988	0.051	3.311
3.346	0.057	3.259
3.700	0.063	3.166
4.051	0.069	3.012
4.398	0.075	2.980
4.742	0.081	2.867
5.083	0.087	2.802
5.421	0.093	2.784
5.756	0.098	2.686
6.087	0.104	2.630
6.741	0.115	2.465

Table 3.3-1 *The variation of the temperature of maximum density (T_{md}) as a function of sodium chloride (NaCl) concentration.*

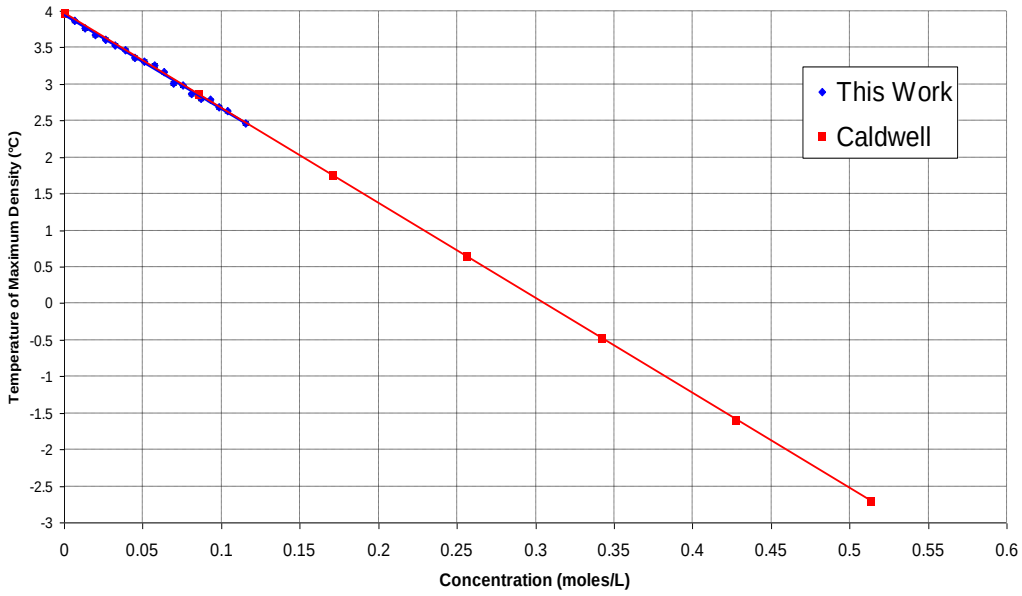

Figure 3.3-1 *Graph of temperature of maximum density versus concentration for an NaCl aqueous solution.*

The good agreement of the results obtained using the concentration scanning system with those obtained by Caldwell indicated that the system worked effectively. This allowed for the testing of other solutes whose effects on the temperature of maximum density were less certain.

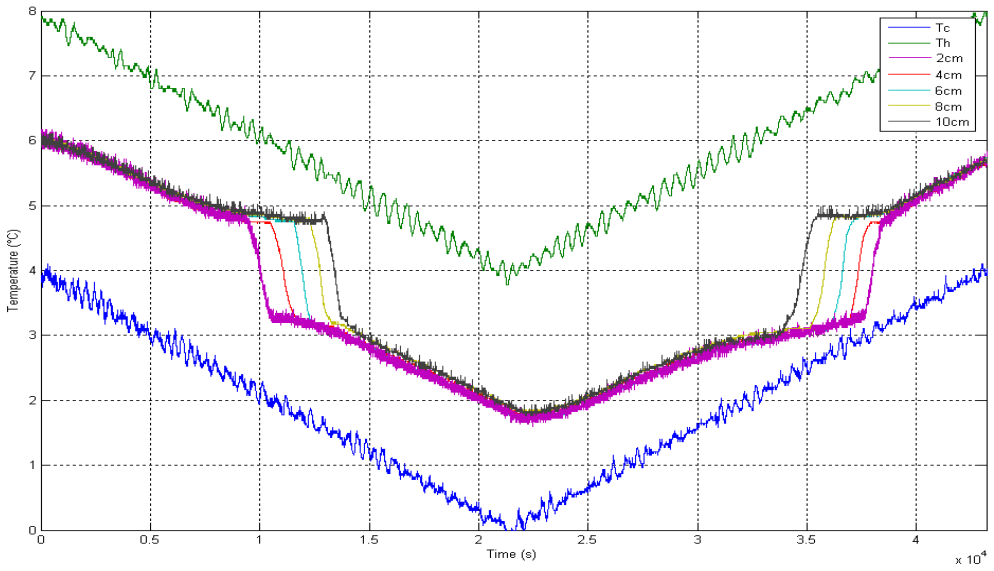

Figure 3.3-2 *Pure water ramp down and ramp up indicating a temperature of maximum density of 3.98°C.*

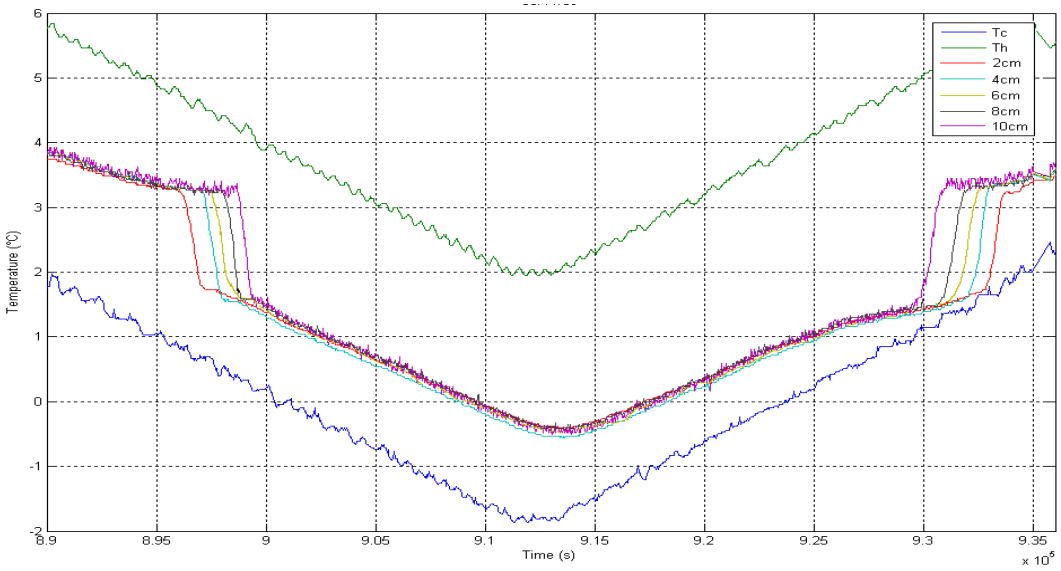

Figure 3.3-3 *6.74g/l saline solution ramp down and ramp up indicating a temperature of maximum density of 2.47°C.*

3.4 The temperature of maximum density of alcohol solutions

A total of four monohydric alcohols have been tested. The five alcohols tested are methanol, ethanol, 1-propanol, 2-propanol and tert-butanol. Each of these solutes was tested for their effects on the temperature of maximum density of water as a function of concentration. The distinguishing feature of the tests carried out in this study compared to previous work [22, 23] is the high resolution of the scans, typically an order of magnitude greater then previously reported. This high resolution in concentration has revealed structural detail which was not evident previously [44]. Each result is an average of at least one up ramp and one down ramp. The results of these concentration scans are presented in tables 3.4-1 -3.4-5.

Methanol CH_3OH		
Concentration (g/litre)	**Concentration (moles/litre)**	**T_{md} (°C)**
0.000	0.000	3.980
2.179	0.068	3.974
3.453	0.108	3.943
5.587	0.174	3.916
6.859	0.214	3.916
8.942	0.279	3.920
10.219	0.319	3.934
12.246	0.382	3.924
13.534	0.422	3.923
15.499	0.484	3.920
16.805	0.524	3.941
18.702	0.584	3.914
20.032	0.625	3.909
21.857	0.682	3.887
23.218	0.725	3.906
24.965	0.779	3.917
26.362	0.823	3.932
28.027	0.875	3.916
29.465	0.920	3.901
31.043	0.969	3.898
32.528	1.015	3.877
34.015	1.062	3.897
35.552	1.110	3.886
36.944	1.153	3.892
38.537	1.203	3.892
39.831	1.243	3.868
41.485	1.295	3.879
42.676	1.332	3.863
44.396	1.386	3.839
47.271	1.475	3.746
50.110	1.564	3.701
52.914	1.651	3.665
55.683	1.738	3.633

Methanol (continued)		
Concentration (g/litre)	**Concentration (moles/litre)**	**T_{md} (°C)**
58.419	1.823	3.571
61.122	1.908	3.536
63.793	1.991	3.495

Table 3.4-1 *The variation of the temperature of maximum density (T_{md}) as a function of methanol (CH_3OH) concentration.*

Ethanol CH_3CH_2OH		
Concentration (g/litre)	**Concentration (moles/litre)**	**T_{md} (°C)**
0.000	0.000	3.980
1.206	0.026	3.933
2.397	0.052	3.977
3.574	0.078	3.995
4.736	0.103	4.043
5.885	0.128	4.071
7.020	0.152	4.110
8.142	0.177	4.104
9.251	0.201	4.123
10.347	0.225	4.145
11.000	0.239	4.170
11.430	0.248	4.162
11.454	0.249	4.171
11.905	0.258	4.201
12.353	0.268	4.217
12.500	0.271	4.223
12.798	0.278	4.240
13.239	0.287	4.203
13.558	0.294	4.178
14.604	0.317	4.174
15.639	0.339	4.178
16.662	0.362	4.188
17.040	0.370	4.185
17.673	0.384	4.185
18.000	0.391	4.177

Ethanol (continued)		
Concentration (g/litre)	**Concentration (moles/litre)**	**T_{md} (°C)**
18.404	0.400	4.176
18.673	0.405	4.158
19.187	0.416	4.154
19.752	0.429	4.151
20.359	0.442	4.153
21.083	0.458	4.159
21.515	0.467	4.167
22.398	0.486	4.158
22.656	0.492	4.153
23.696	0.514	4.115
23.782	0.516	4.119
24.894	0.540	4.094
25.992	0.564	4.082
27.076	0.588	4.094
28.146	0.611	4.105
29.203	0.634	4.124
30.247	0.657	4.096
31.278	0.679	4.092
32.296	0.701	4.068
33.302	0.723	4.048
34.295	0.744	4.055
35.277	0.766	3.999
36.247	0.787	3.961
37.205	0.808	3.936
38.152	0.828	3.955
39.088	0.848	3.891
40.013	0.869	3.860

Table 3.4-2 *The variation of the temperature of maximum density (T_{md}) as a function of ethanol (CH_3CH_2OH) concentration.*

1-Propanoll $CH_3CH_2CH_2OH$		
Concentration (g/litre)	**Concentration (moles/litre)**	**T_{md} (°C)**
0.000	0.000	3.980
1.615	0.027	3.991
3.209	0.053	3.993
4.781	0.080	4.000
6.333	0.105	4.023
7.864	0.131	3.981
9.376	0.156	3.973
10.868	0.181	3.967
12.341	0.205	3.969
13.796	0.230	3.961
15.232	0.253	3.924
16.650	0.277	3.883
18.050	0.300	3.841
19.433	0.323	3.845
20.040	0.333	3.807
20.799	0.346	3.801
21.806	0.363	3.702
23.189	0.386	3.690
24.555	0.409	3.651
25.903	0.431	3.643
27.235	0.453	3.581
28.550	0.475	3.567
29.850	0.497	3.476
31.133	0.518	3.428
32.401	0.539	3.441

Table 3.4-3 *The variation of the temperature of maximum density (T_{md}) as a function of 1-propanol ($CH_3CH_2CH_2OH$) concentration.*

2-Propanol $(CH_3)_2CHOH$		
Concentration (g/litre)	**Concentration (moles/litre)**	**T_{md} (°C)**
0.000	0.000	3.985
1.252	0.021	4.032

2-Propanol (continued)		
Concentration (g/litre)	**Concentration (moles/litre)**	**T_{md} (°C)**
2.487	0.041	4.076
3.708	0.062	4.070
4.913	0.082	4.117
6.102	0.102	4.115
7.278	0.121	4.151
8.439	0.140	4.188
9.585	0.159	4.178
10.718	0.178	4.211
11.837	0.197	4.187
15.040	0.250	4.255
16.174	0.269	4.273
17.294	0.288	4.308
18.399	0.306	4.253
19.492	0.324	4.250
20.571	0.342	4.276
21.637	0.360	4.258
22.690	0.378	4.247
23.621	0.393	4.234
23.730	0.395	4.234
24.040	0.400	4.159
24.756	0.412	4.149
25.246	0.420	4.147
25.775	0.429	4.158
27.404	0.456	4.092
29.052	0.483	4.076
30.679	0.510	3.991
32.284	0.537	3.989
33.868	0.564	3.958

Table 3.4-4 *The variation of the temperature of maximum density (T_{md}) as a function of 2-propanol ($(CH_3)_2CHOH$) concentration.*

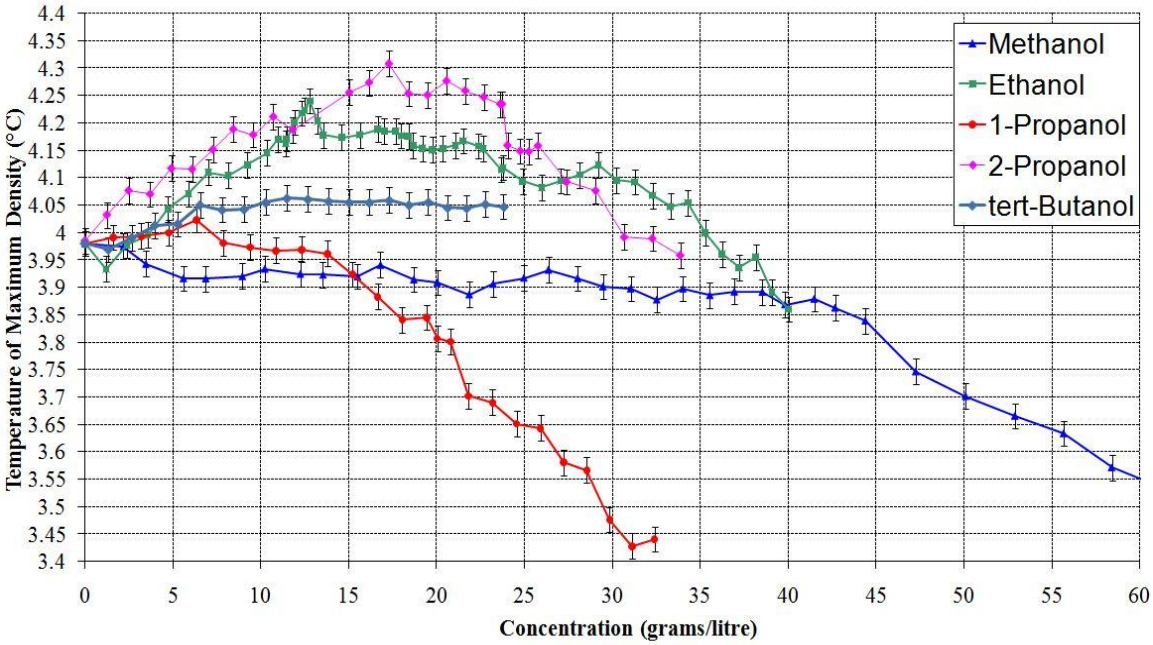

Figure 3.4-1 *The behaviour of the temperature of maximum density as a function of mass concentration (grams per litre) for a range of monohydric alcohols.*

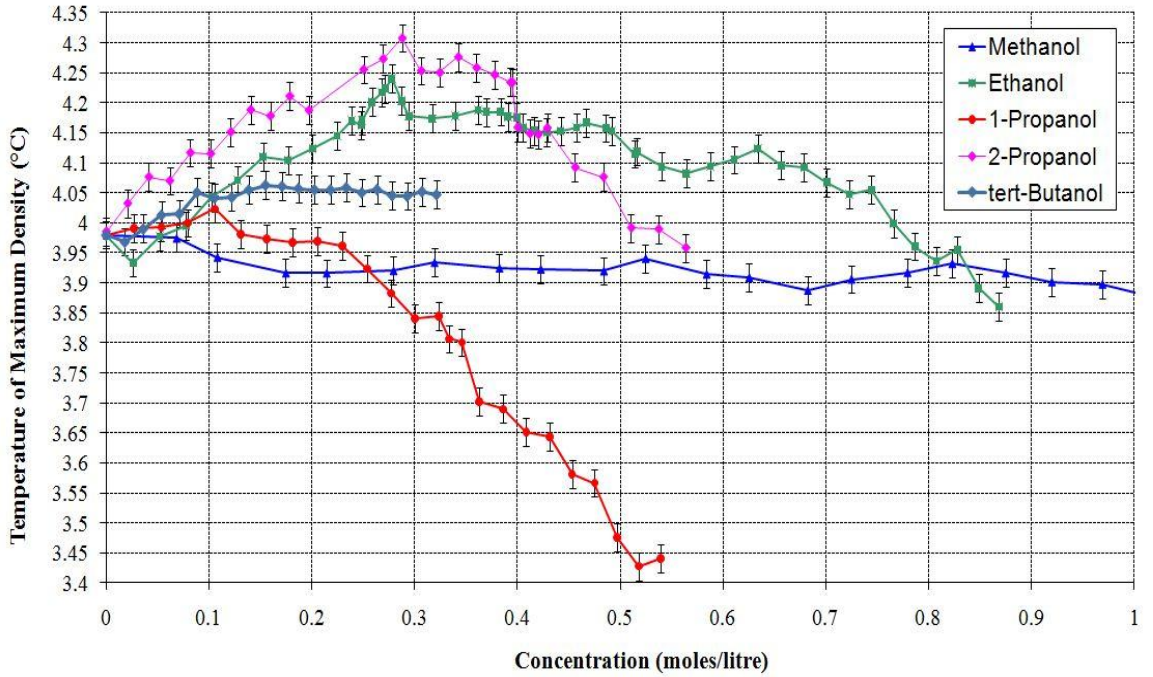

Figure 3.4-2 *The behaviour of the temperature of maximum density as a function of mass concentration (moles per litre) for a range of monohydric alcohols.*

In order to ensure the reproducibility of the results, numerous scans were conducted. These scans began with different initial concentrations, and at different times of the year. An example of this can be seen in figure 3.4-3 below. This graph shows the results of 5 separate ethanol scans carried out over a 6 month period. All the major features are reproduced successfully.

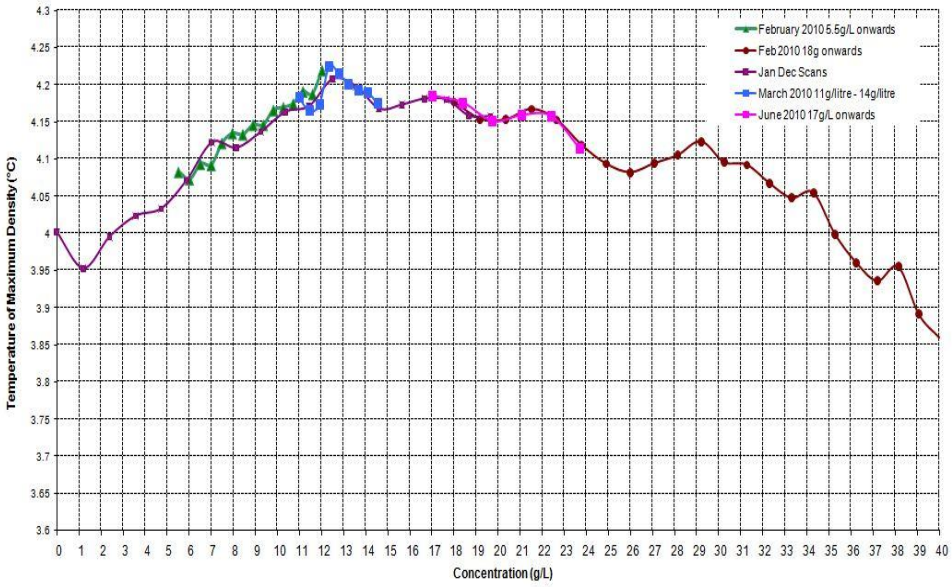

Figure 3.4-3 *Five separate ethanol scans conducted over a six month period.*

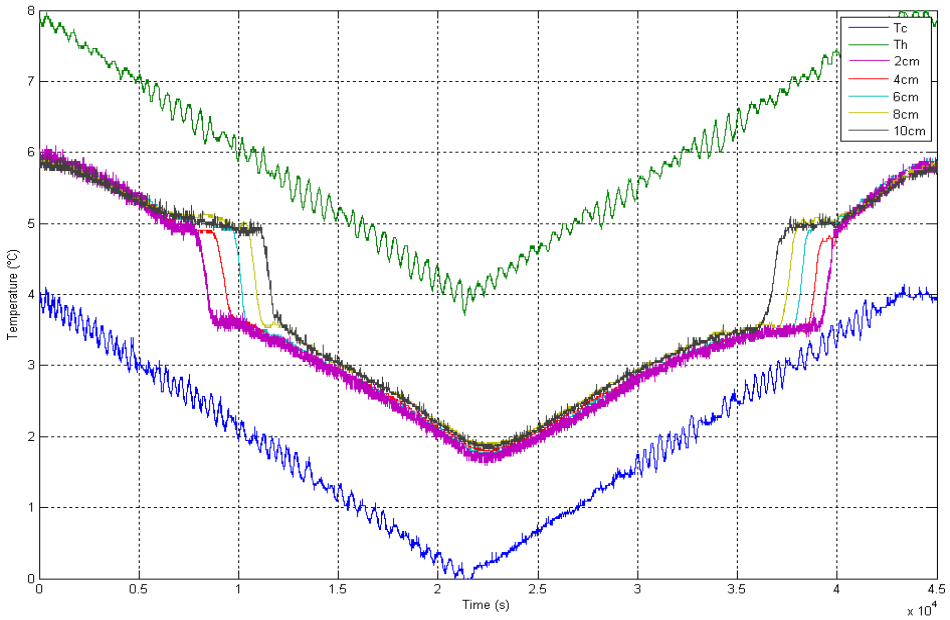

Figure 3.4-4 *12.8g/l ethanol solution ramp down and ramp up indicating a temperature of maximum density of 4.24°C.*

As expected from work carried out by Wade and Umeda [22] the monohydric alcohols do not show a linear depression of the temperature of maximum density as the concentration increased. Previous studies by Wade and Umeda [22] and Mooney [29] indicated that the temperature of maximum density could in fact rise above 3.98°C when certain monohydric alcohols are added in low concentrations. Both of these studies presented smooth curves for the graphs of temperature of maximum density versus concentration for methanol, ethanol, and the two isomers of propanol. The previous studies were carried out at a much lower concentration resolution then used in this investigation. This increased resolution indicates the presence of a lot more detail then previously recorded for both of the solutes that cause significant rises in the temperature of maximum density. Both the ethanol and 2-propanol scans reveal detailed structure with multiple local maxima and minima over the concentration range. Ethanol shows a maximum T_{md} of 4.24°C at 12.8g/litre (0.27moles/litre) as seen in figure 3.4-4. Following this local maximum, there is a sharp drop in the T_{md} as the concentration increases. This maximum is located on the first of two peaks. The second, smaller peak appears at ~30grams/litre (0.64moles/litre). The T_{md} versus concentration for 2-propanol also contains structure and moves through several local maxima in the low concentration region. 2-Propanol shows a higher temperature of maximum density of 4.31°C at 17.29g/litre (0.29moles/litre). It is worth noting that the highest temperature of maximum density for ethanol and 2-propanol occur at very similar molar concentrations (0.28moles/litre and 0.29moles/litre respectively). The results obtained from the 1-Propanol tests show, a small increase in the temperature of maximum density before dropping off. The graph of temperature of maximum density versus concentration for 1-propanol is smoother then that of ethanol and 2-propanol. The same is seen in the graph for methanol. Methanol does not indicate any rise in the temperature of maximum density. These results clearly disprove any notion of the temperature of maximum density being a colligative properly of water, as well as disproving the Despretz rule, that there is a linear relationship between the

T_{md} and the solute concentration. It is evident from the results that a simple non-linear model, such as a parabolic fit, cannot be used to characterise the behaviour of the T_{md} variation in the cases studied. A monohydric alcohol is an alcohol that contains one hydroxyl group (OH) on its molecule. The OH group has a net charge that makes it polar. This polarity allows it to form hydrogen bonds with the water molecules. As shown in the next section, the monohydric alcohols behave differently to other solutes as well as each other.

A notable result obtained is the difference between the effects that the two isomers of propanol have on the temperature of maximum density. The first isomer of propanol, 1-propanol is a primary alcohol with only one carbon atom attached to the C-OH group, 1-propanol shows a very slight elevation of the temperature of maximum density and shows a non-linear depression. The second isomer, 2-propanol is the lowest order secondary alcohol, it has two carbon atoms attached to the C-OH group, 2-propanol initially elevates the temperature of maximum density before depressing it in a non-linear fashion. This shows differences between the isomers and suggests that the change in the temperature of maximum density is dependent on the molecular arrangement of the molecule. Methanol and ethanol are both primary alcohols. It is intriguing that it is one primary alcohol and one secondary alcohol that show the most significant elevations in the temperature of maximum density. It would be desirable to extend these high resolution studies to include the four isomers of butanol (the next monohydric alcohol in the series).

The increased resolution of this study has shown structure not seen before. The results presented by Wada and Umeda [22] for the monohydric alcohols can be represented by a parabolic curve, this is due to the sparsely populated graph. The results presented in this report are in good agreement with the results presented by Wada and Umeda. Some of these results can be seen in figures 3.4-5 and 3.4-6. Figure 3.4-5 shows the results obtained for ethanol solutions in this work along with

those obtained by Wada and Umeda, in figure 3.4-6 the same comparison is shown for 1-propanol.

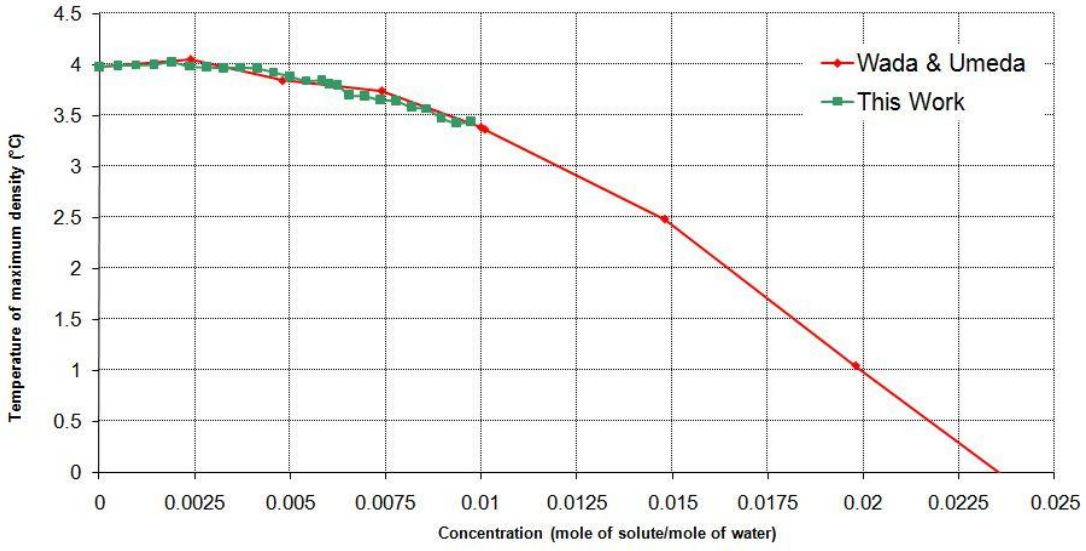

Figure 3.4-5 *Results for ethanol solutions obtained in this work compared to those obtained by Wada and Umeda.*

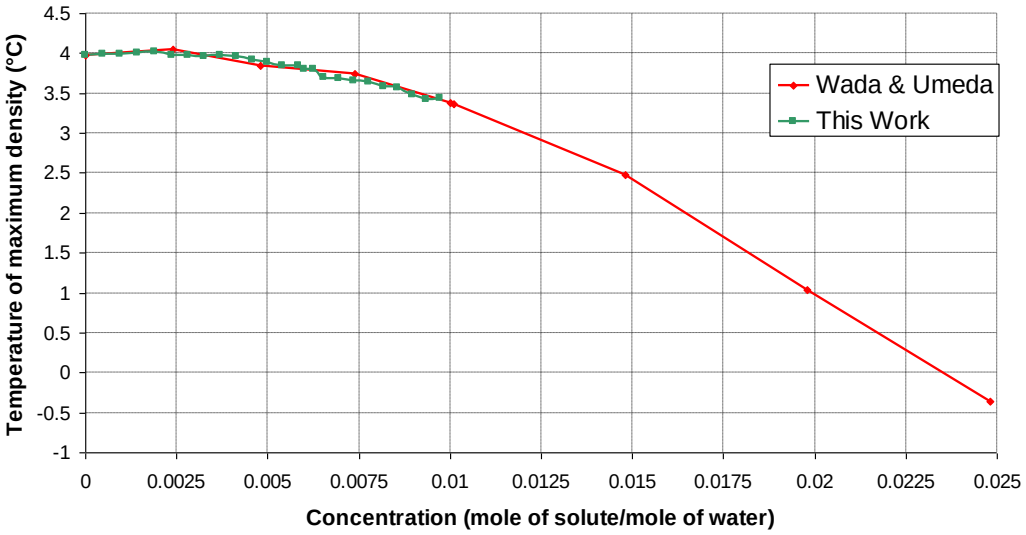

Figure 3.4-6 *Results for 1-propanol solutions obtained in this work compared to those obtained by Wada and Umeda.*

Tests were also carried out on *tert*-butanol. A concentration scan, starting with pure water, up to a concentration of 23.8 g/l was conducted. It was expected that *tert*-

butanol would cause the temperature of maximum density to rise above that observed by the addition of 2-propanol. This expectation came about after studying the results obtained by Wada and Umeda [22] for *tert*-butanol. In their paper, they quote a maximum temperature of maximum density of 4.41°C. The results obtained from this work are presented in table 3.4-6 and graphed in figure 3.4-7.

tert-Butanol $(CH_3)_3COH$		
Concentration (g/litre)	**Concentration (moles/litre)**	**T_{md} (°C)**
0.000	0.000	3.980
1.346	0.018	3.969
2.674	0.036	3.990
3.984	0.054	4.013
5.276	0.071	4.015
6.551	0.088	4.051
7.809	0.105	4.041
9.050	0.122	4.043
10.275	0.139	4.055
11.484	0.155	4.063
12.677	0.171	4.061
13.855	0.187	4.057
15.017	0.203	4.055
16.165	0.218	4.055
17.298	0.233	4.059
18.417	0.248	4.050
19.523	0.263	4.056
20.614	0.278	4.045
21.692	0.293	4.044
22.756	0.307	4.052
23.808	0.321	4.047

Table 3.4-6 *The variation of the temperature of maximum density (T_{md}) as a function of tert-Butanol ($(CH_3)_3COH$) concentration.*

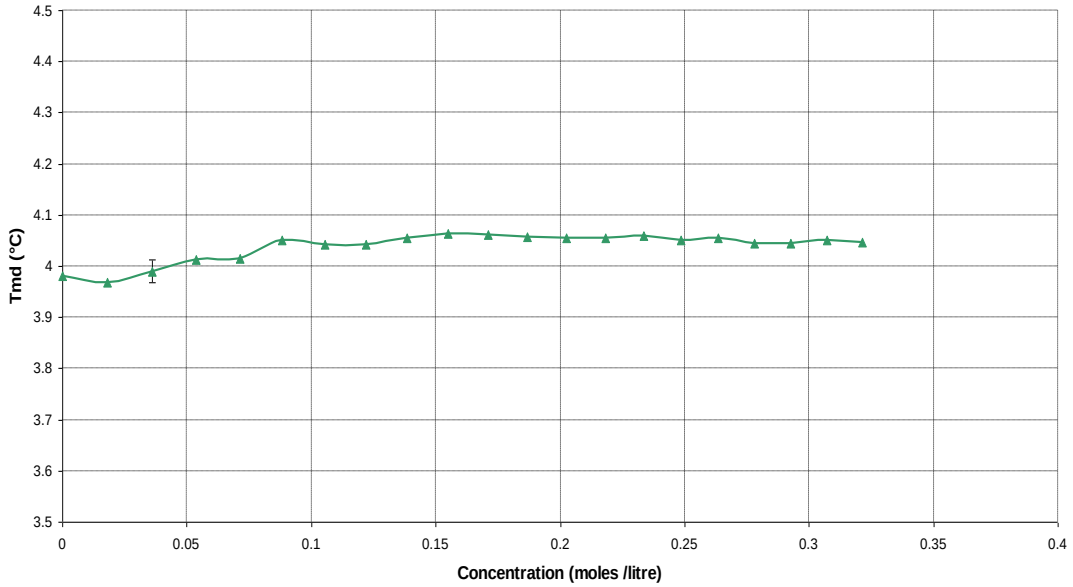

Figure 3.4-7 *The behaviour of the temperature of maximum density as a function of mass concentration (moles per litre) for tert-Butanol.*

The results obtained for tert-Butanol as part of this work, do not agree with those obtained by Wada and Umeda. This fact is illustrated in figure 3.4-8, which shows both sets of results graphed together.

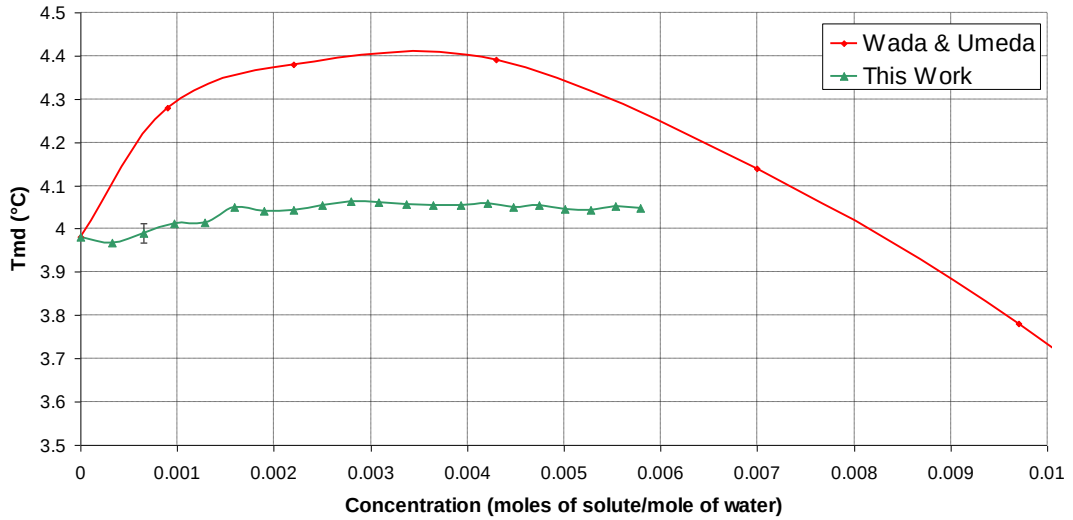

Figure 3.4-8 *Graph comparing results obtained as part of this work and those presented by Wada and Umeda for tert-Butanol.*

The reason for the difference in the tert-Butanol results is unclear, it is worth nothing that the results obtained by Wada and Umeda for *tert*-Butanol have been called in to question previously in a paper by Kaulgud [45]. Kaulgud states that the tert-Butanol results at low concentration must be in error.

3.5 The temperature of maximum density of other solutions

As part of this study, the effect on the temperature of maximum density of three non-monohydric alcohols was also investigated (ethylene glycol is a dihydric alcohol due to the presence of two hydroxyl groups). Sodium chloride, sucrose and ethylene glycol were tested. The tests on ethylene glycol and sucrose were carried out before the concentration scanning system was developed. The sodium chloride results are shown in table 3.3-1.

Sucrose $C_{12}H_{22}O_{11}$		
Concentration (g/litre)	**Concentration (moles/litre)**	**T_{md} (°C)**
0	0	3.98
20	0.058	3.16
40	0.117	2.22
60	0.175	1.23

Table 3.5-1 *The variation of the temperature of maximum density (T_{md}) as a function of sucrose ($C_{12}H_{22}O_{11}$) concentration.*

Ethylene Glycol $C_2H_6O_2$		
Concentration (g/litre)	**Concentration (moles/litre)**	**T_{md} (°C)**
0	0	3.98
5	0.081	3.70
7.5	0.121	3.54
10	0.161	3.41
15	0.242	3.20

Ethylene Glycol (continued)		
Concentration (g/litre)	**Concentration (moles/litre)**	**T_{md} (°C)**
20	0.322	2.89
22	0.354	2.79
31	0.499	2.18
40	0.644	1.70
45	0.725	1.38
55	0.886	0.71

Table 3.5-2 *The variation of the temperature of maximum density (T_{md}) as a function of ethylene glycol ($C_2H_6O_2$) concentration.*

The three non-monohydric alcohol solutes all depress the temperature of maximum density linearly. The rate at which they depress the temperature of maximum density differs from solute to solute. When the concentration is expressed in grams per litre, sodium chloride has the steepest slope of the three solutes that cause a linear suppression on the temperature of maximum density. When the concentration is expressed in moles per litre, sucrose has the steepest slope. This change is due to the relative molar masses of sodium chloride and sucrose, sodium chloride has a molar mass of 58.44grams per mole, compared with 342.3grams per mole for sucrose.

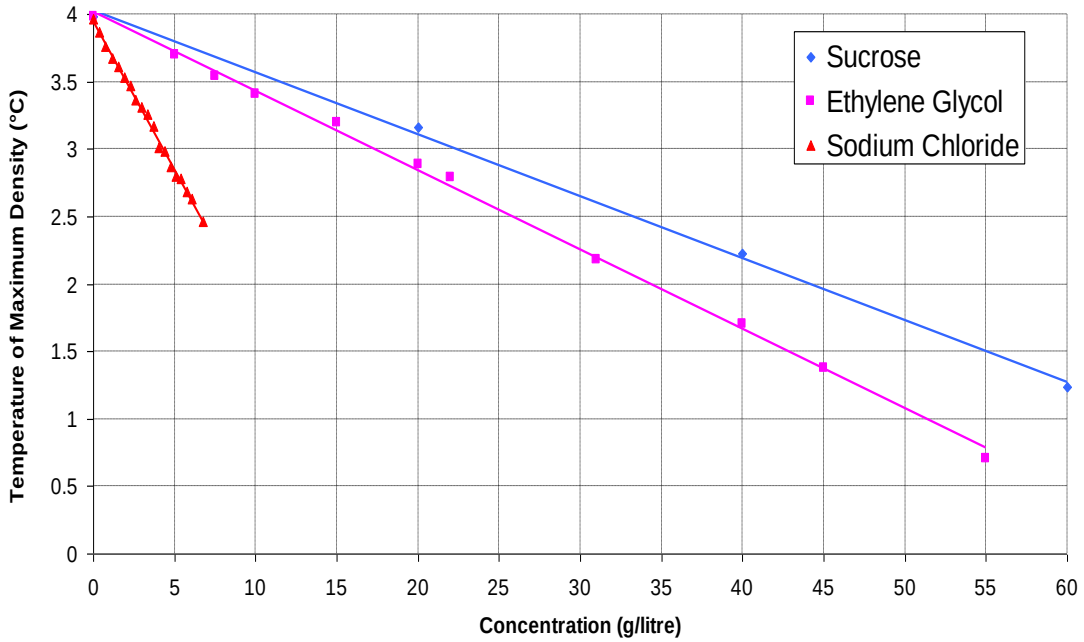

Figure 3.5-1 *The behaviour of the temperature of maximum density as a function of mass concentration (grams per litre).*

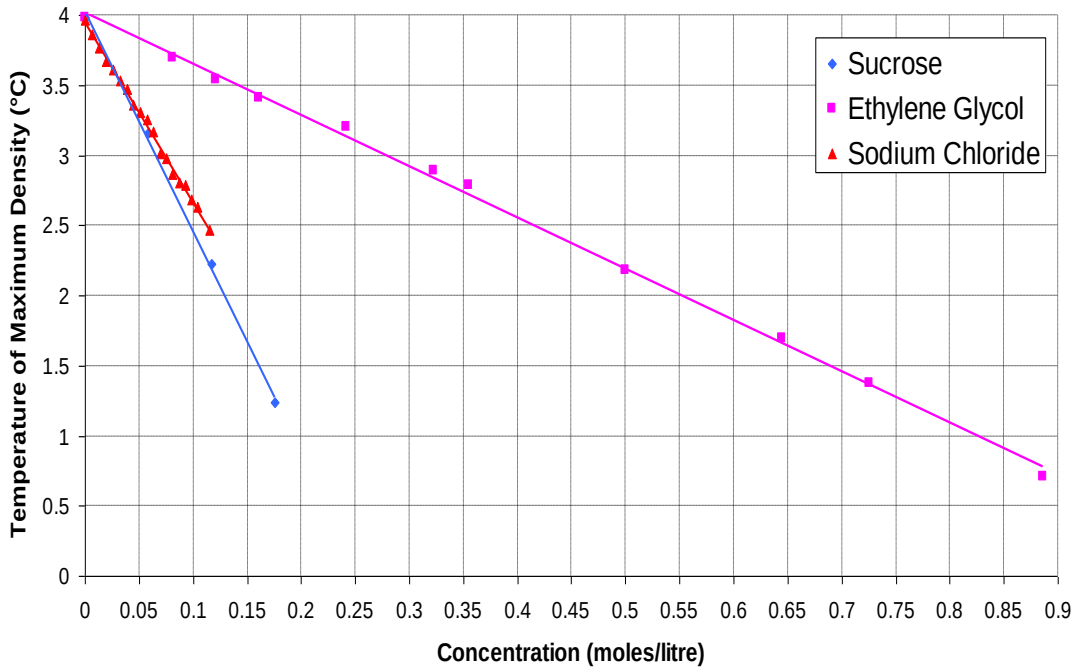

Figure 3.5-2 *The behaviour of the temperature of maximum density as a function of mass concentration (moles per litre).*

The results obtained as part of this work for ethylene glycol are compared to those presented by Wada and Umeda [22] in figure 3.5-3.

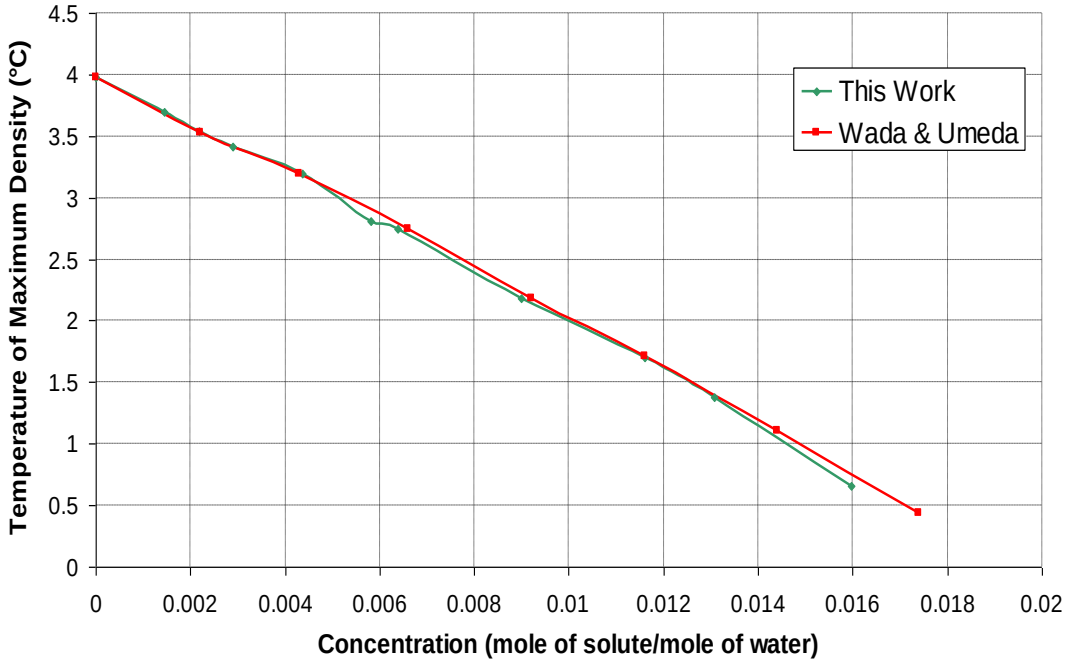

Figure 3.5-3 *Results for ethylene glycol solutions obtained in this work compared to those obtained by Wada and Umeda.*

3.6 Error analysis

There are two types of errors to be calculated as part of this study. Firstly there is the error in the temperature of maximum density as calculated by the do_int extraction code, and the second error is associated with the amount of injected solute in the concentration scanning system. Both errors are quantified in this section. In addition, for the ethanol and 2-propanol results, a chi-squared analysis is carried out to compare these results to a best fit parabolic curve. This analysis is carried out to find out the probability that the obtained results fit a parabolic curve.

3.6.1 Errors on the temperature of maximum density

To calculate the errors associated with the temperature of maximum density, a root mean squared deviation analysis was carried out. A best fit line was generated for the sodium chloride results obtained by Caldwell [43]. An equation that described this best fit line was obtained. The decision to use Caldwell's results was based on the near perfect agreement between his results and the seawater equation presented by Chen and Millero [8]. The equation was of the form given in 3.6-1.

$$T'_{md} = mx + c \tag{3.6-1}$$

where T'_{md} is the temperature of maximum density predicted by Caldwell for a given concentration x, and c is the temperature of maximum density of pure water. The best fit line for Caldwell's data gave the equation 3.6-2.

$$T'_{md} = -13.018x + 3.9804 \tag{3.6-2}$$

Once this equation had been obtained, the T'_{md} for each concentration tested as part of this work was calculated. This T'_{md} was then compared to the $(T_{md})_{average}$ obtained experimentally for the same concentration.

$$(T_{md})_{average} = \frac{(T_{md})_{up} + (T_{md})_{down}}{2} \tag{3.6-3}$$

A root mean squared deviation (RMSD) was calculated following the equation 3.6-4. The $\sigma^2_{Caldwell}$ term is to account for the uncertainty in the Caldwell points.

$$RMSD = \sqrt{\left(\sqrt{\frac{\sum (T'_{md} - (T_{md})_{average})^2}{n}}\right)^2 + \sigma^2_{Caldwell}} \tag{3.6-4}$$

The result of this analysis was that the RMSD = 0.0232°C. The graph in figure 3.6-1 shows how this error appears on the concentration scan performed on NaCl, and how it compares to the results obtained by Caldwell. It is clear from the graph that the results are in very good agreement. All the values of temperature of maximum density presented in the work are assumed to have uncertainties of ±0.0232°C.

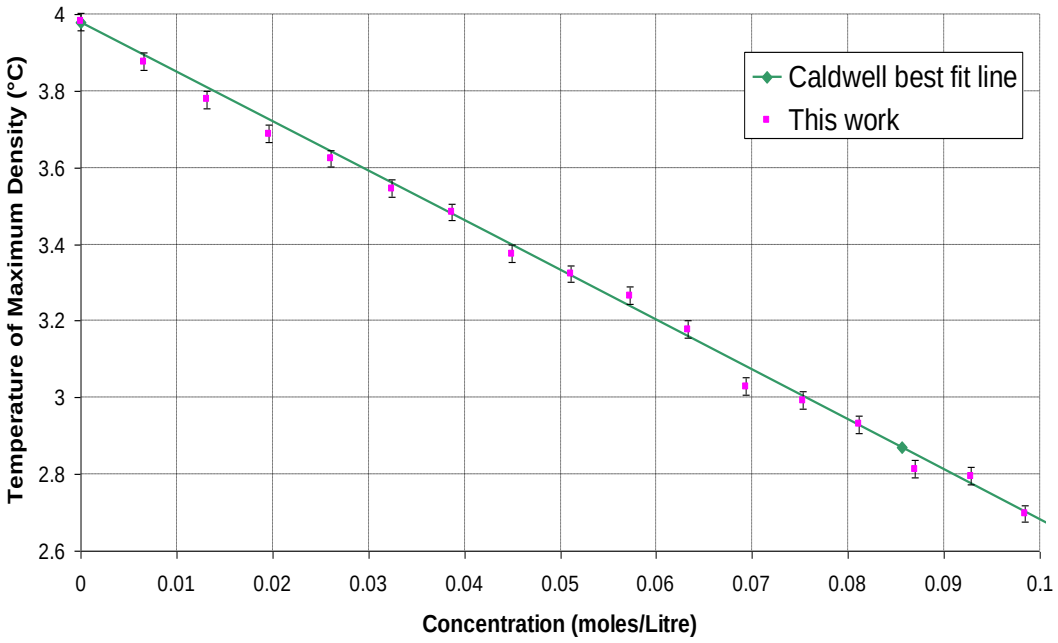

Figure 3.6-1 *Sodium chloride concentration scan including error bars.*

3.6.2 Errors on the solute concentration

In this section an error is put on the concentration readings. In the experiments, the concentration of the solution is changed after every up ramp. Tests needed to be carried out to calculate the variation in the volume of fluid injected each time. It was expected that this variation would be small due to the mechanical and electronic set up of the concentration scanning system. The electronics are set up in a way that the oscillator that controls the clock signal for the stepper motor is on all the time,

and is controlled by a NAND gate. The NAND gate is operated by the Measurement Computing USB-1208LS device. The signal sent to the USB-1208LS device is controlled by a delay which is calculated by the computers clock speed which was 333MHz. The oscillator chip was operated at a frequency of 1.1 kHz, combined with the fact that it takes 800 clock steps to move the syringe a distance of 1mm, it is reasonable to assume that the variation in the time for which the stepper motor is operated is negligible.

It is possible that a variation in the volume of fluid injected might result from relaxation in the syringe. Many steps have been taken to reduce this risk, including the use of a linear stepper motor and threaded rod. This design does not require the motor to be kept on for the duration of the run, as the threaded rod cannot slip back, reducing the change of air being pulled back into the syringe. Another feature of the mechanical design that reduces the chance of a variation on the volume of fluid being injected include the use of a narrow gauge, medical needle at the end of the tube connecting the syringe and the test chamber. Tests were carried out to test the effectiveness of these measures employed to reduce the variation in the volume of fluid being injected into the test chamber.

To test how accurately the system injected a fixed amount of fluid, the concentration scanning system was set up to inject fluid in to a beaker that was placed on an electronic weighing scale accurate to 0.01g. A series of 10 injections were carried out and the mass was recorded each time. The results are presented in table 3.6-1, and graphed in figure 3.6-2. A root mean squared deviation was carried out on the results. The equation 3.6-5 was used for this analysis.

$$RMSD = \sqrt{\sum_{\forall i} \frac{(m_{average} - m_i)^2}{n}} \qquad (3.6\text{-}5)$$

where $m_{average}$ is the average mass of all n injections, and m_i is the mass of the *ith* injection.

Injection	Mass (grams)	$m_i - m_{i-1}$
0	0	
1	2.22	2.22
2	4.39	2.17
3	6.59	2.2
4	8.76	2.17
5	10.98	2.22
6	13.22	2.24
7	15.39	2.17
8	17.61	2.22
9	19.82	2.21
10	22.02	2.2

Table 3.6-1 *Results table for error analysis on concentration changes.*

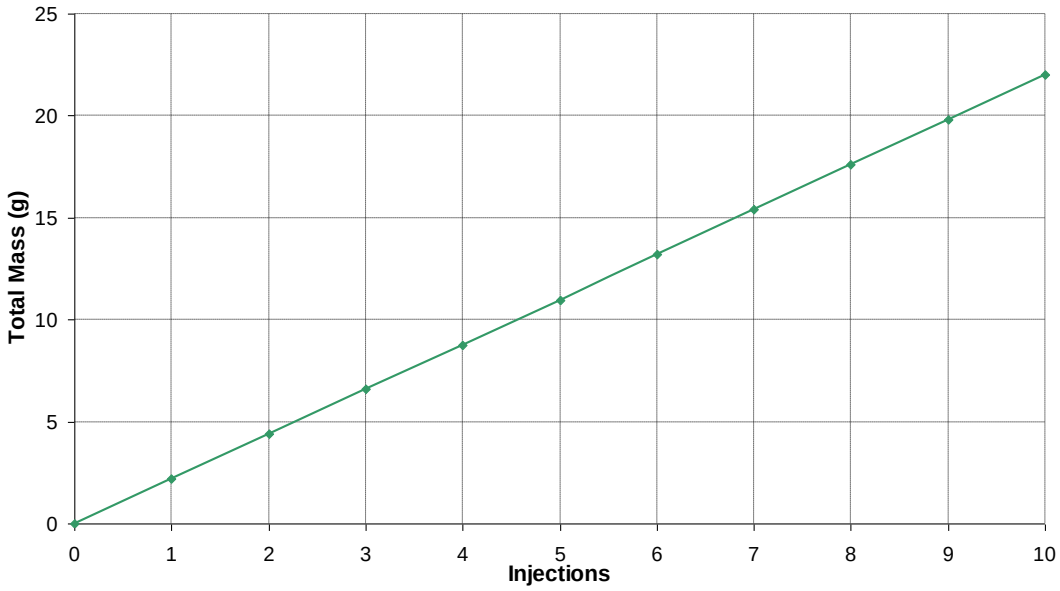

Figure 3.6-2 *Graph of injections versus total mass.*

The average volume of mass of the fluid injected was 2.202 grams and the root mean squared deviation was 0.025 grams. This corresponds to an uncertainty in the mass of the injected fluid of 1.1%. As a result of this very small uncertainty, no

error bars for concentration are included on temperature of maximum density versus concentration scans.

3.6.3 Chi-squared analysis

Previous works [22, 45] have assumed that the temperature of maximum density profiles for the monohydric alcohols follow a parabolic trend. In this section, details of a chi-squared test are presented which tests the measurements presented in figure 3.4-1 against a parabolic fit. The chi-squared test was used to find the probability of the results obtained in the course of this work follow a parabolic curve. The parabolic curve has to pass through 3.98°C at a concentration of 0g/l (pure water). The first step in this procedure is to obtain a 2nd order polynomial of the form $T_{md} = a_2 x^2 + a_1 x + a_0$ that includes the constraints and fits the data obtained experimentally. For ethanol, the best-fit curve is $T_{md} = -1.40x^2 + 1.10x + 3.98$, and for 2-propanol it is $T_{md} = -3.98x^2 + 2.11x + 3.98$. Once the best fit curves were obtained, a Chi-squared sum was carried out. The form of the Chi-squared sum χ^2 is shown in equation 3.6-6.

$$\chi^2 = \sum_i \left[\frac{y_i - T_{md_i}}{\sigma_{yi}} \right]^2 \qquad (3.6\text{-}6)$$

where y_i is *ith* experimental result, T_{md_i} is the temperature of maximum density obtained using the best-fit equation for the same concentration of the *ith* experimental result, σ_{yi} is the uncertainty on each experimental data point as described in section 3.6-1.

In total there are 52 ethanol results quoted in this work, the T_{md_i} has 3 constraints, a_2, a_1 and a_0, therefore the chi-squared sum has 49 degrees of freedom. The result for the chi-squared sum for ethanol was χ^2 = 123.9967 for 49 degrees of freedom. This gives a probability of P = 2 x 10^{-8}. For 2-propanol there are 30 results presented in this work and the best-fit curve has the same the same 3 constraints. The result for the chi-squared sum for 2-propanol was χ^2 = 49.9704 for 27 degrees of freedom. This means that the probability of the 2-propanol results following a 2nd order polynomial is P = 0.0046. These results are summarised in table 3.6-2.

	Ethanol	**2-Propanol**
Number of Results	52	30
Constraints	3	3
Degrees of freedom	49	27
Error on each result, σ_{yi}	0.022	0.022
Chi-squared sum χ^2	123.9967	49.9704
Probability, P	2 x 10^{-8}	0.0046

Table 3.6-2 *Summary table of chi-squared analysis.*

The probability that either ethanol or 2-propanol follow a 2nd order parabolic curve is very small and as a result, it has been concluded that the relationship between the temperature of maximum density and concentration can not be accurately described by a 2nd order polynomial.

Chapter 4

Macroscopic Modelling.

4.1 Introduction

This chapter discusses investigations carried out by means of macroscopic models into the effects of the addition of solutes on the temperature of maximum density and the temperature of phase change. The macroscopic modelling involved combining the state functions of the solute and solvent. The results from this combined state function are compared against the experimentally obtained results and the temperature of phase change (T_{pc}). A second approach involved developing a model that used a Monte Carlo method to simulate the interactions between individual molecules and is described in chapter five.

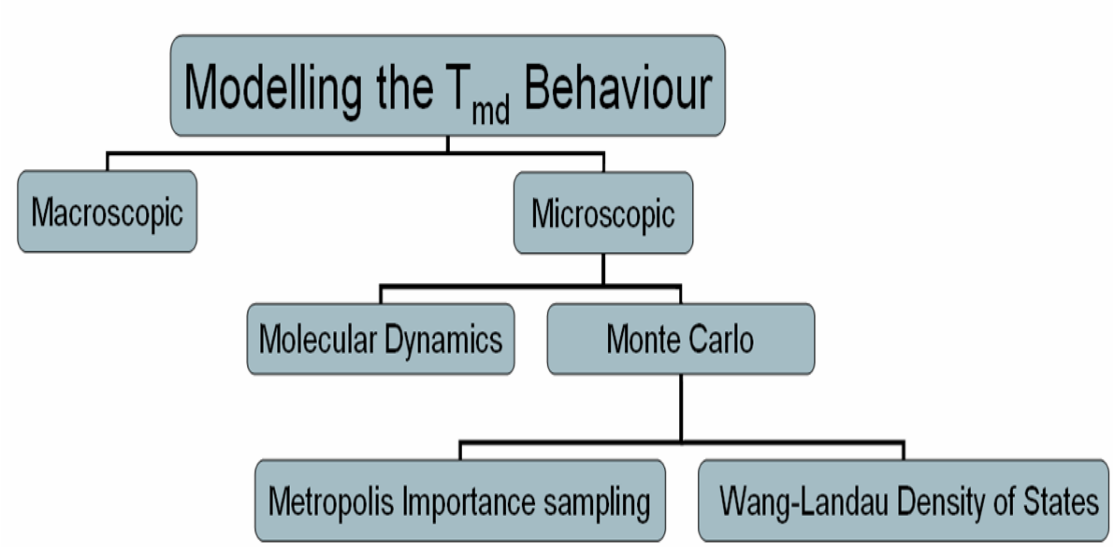

Figure 4.1-1 *Chart indicting the approach taken to modelling the behaviour of the temperature of maximum density in this study.*

4.2 Combining the state functions of the solute and solvent.

The macroscopic modelling used in this study involves making predictions of the temperature of maximum density of an aqueous solution if it were an ideal solution. An ideal solution is described as being one in which there is no appreciable interaction between the solute and the water. The difference between the temperature of maximum density of the ideal mixture and the experimentally found

temperature of maximum density gives an indication as to the mutual interaction between the solute and the solvent [22]. For the purpose of this study, two classes of solutes are used, ethylene glycol in one class, and the monohydric alcohols in the other. Ethylene glycol is used as experimentally it has been found to decrease the temperature of maximum density of water linearly as the concentration is increased. The monohydric alcohols are used as they were investigated in the experimental section of this study and their effect on the temperature of maximum density of water is highly non-linear.

To obtain the predicted temperature of maximum density T'_{md} of a solution an assumption is made that the volume V of an aqueous solution is equal to the volume of the water plus the volume of the solute added. This assumption is only used at small concentrations. This gives a total volume at θ °C of

$$V = xV_s(\theta) + (1-x)V_w(\theta) \tag{4.2-1}$$

where V_s is the molar volume of the solute at θ °C, V_w is the molar volume of water at θ °C and x is the solute concentration in moles of solute per mole of water. In the temperature range 0-5°C, it is reasonable to assume that V_s will increase linearly, while V_w can be expressed by the parabolic equation 4.2-3. These assumptions are based on observations. Most solutes expand at a linear rate over small temperature ranges. The equation 4.2-3 agrees very well with equation 2.7-4 over the temperature ranges being examined.

$$V_s = V_{s_0}(1+\alpha\theta) \text{ [22]} \tag{4.2-2}$$

$$V_w = V_{w_m}\{1+\beta(\theta-3.98)^2\} \text{ [22]} \tag{4.2-3}$$

where V_{s_0} is the volume of the solute at 0°C and V_{w_m} is the volume of water at its temperature of maximum density. α is a coefficient relating to the thermal

expansion of the solute, β is a coefficient relating to the thermal expansion of water. Substituting equations 4.2-2 and 4.2-3 into equation 4.2-1 gives

$$V = V_{s_O}(x + \alpha x\theta) + V_{w_M}(1-x)\{1 + \beta(\theta - 3.98)^2\}$$

At the temperature of maximum density the rate of change of the volume with respect to temperature must equal zero, i.e.

$$T`_{md} = \frac{dV}{d\theta} = 0 = \alpha x V_{s_O} + 2\beta\theta V_{w_M}(1-x) - 7.96\beta V_{w_M}(1-x) \qquad (4.2\text{-}4)$$

$$\Rightarrow \theta = \frac{7.96\beta V_{w_M}(1-x) - \alpha x V_{s_O}}{2\beta V_{w_M}(1-x)}$$

This condition allows the temperature of maximum density of an ideal solution, T'_{md} to be given as

$$T'_{md} = -\frac{x}{1-x} \cdot \frac{\alpha}{2\beta} \cdot \frac{V_{s_0}}{V_{w_m}} + 3.98 \qquad (4.2\text{-}5)$$

In this study β, the coefficient of thermal expansion of water has a value $7.8 \times 10^{-6} deg^{-1}$, V_{w_m} has a value of 18.016cc mol^{-1}.

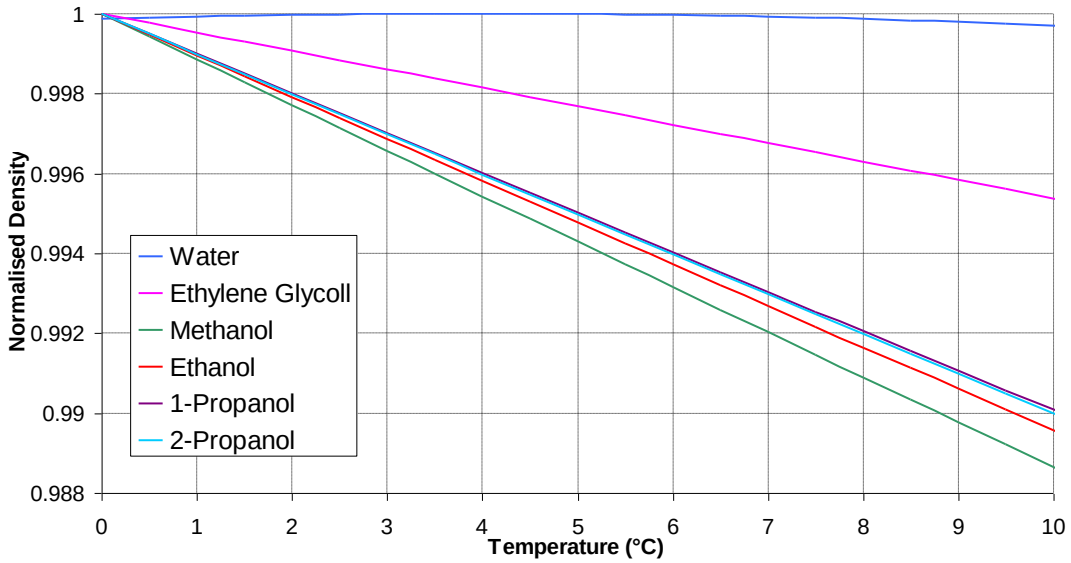

Figure 4.2-1 *Normalised density profiles of water, ethylene glycol and four monohydric alcohols.*

The simulated results are in effect combining one of the alcohol density curves seen in figure 4.2-1 with that for water (the curves in figure 4.2-1 are normalised, this is not done in the models).

The water curve in figure 4.2-1 comes from equation 2.7-4. The curves for ethylene glycol were obtained by rearranging equation 4.2-2 in to a form that gives the density in kg m^{-3} and is shown in equation 4.2-6.

$$\rho(T) = \frac{1000 * molar\ mass}{V_{s_o}(1+\alpha T)} \tag{4.2-6}$$

In this macroscopic study, ethylene glycol, methanol, ethanol, 1-propanol and 2-propanol are investigated. The table 4.2-1 shows the coefficients of thermal expansion and molar volumes of each solute.

Substance	α **x10^{3} deg^{-1}**	V_{s_0} **cc mol^{-1}**
Ethylene Glycol	0.464	55.139
Methanol	1.148	39.556
Ethanol	1.053	57.141
1-propanol	1.002	73.283
2-propanol	1.01	74.993

Table 4.2-1 *Coefficients of thermal expansion α and molar volumes V_{s_0} of each solute [22].*

Figure 4.2-2 shows the results obtained from the macroscopic study. Each graph shows the expected temperature of maximum density as a function of solute concentration as well as the experimentally obtained results.

(a) Ethylene Glycol

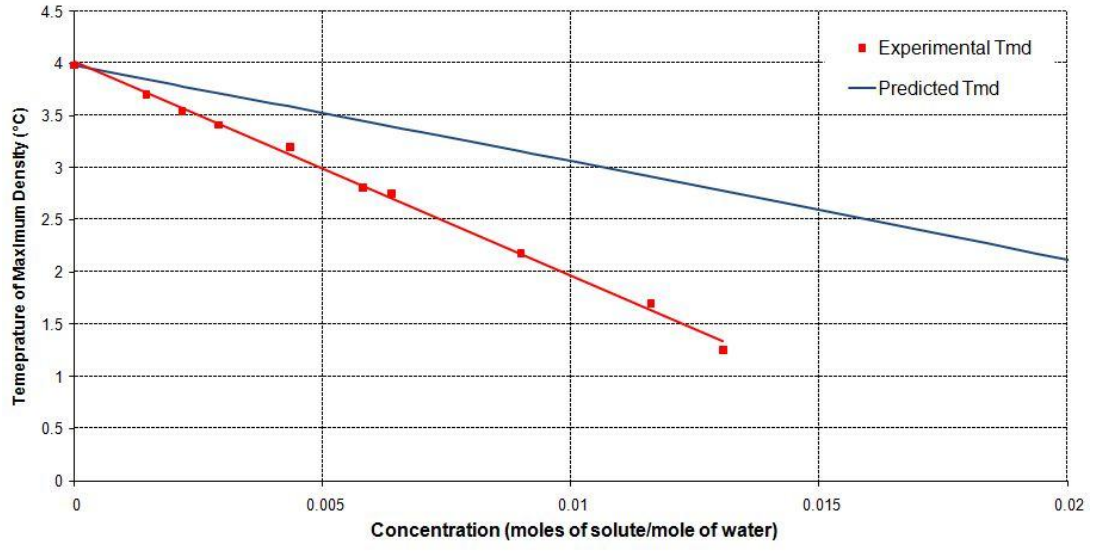

(b) Methanol

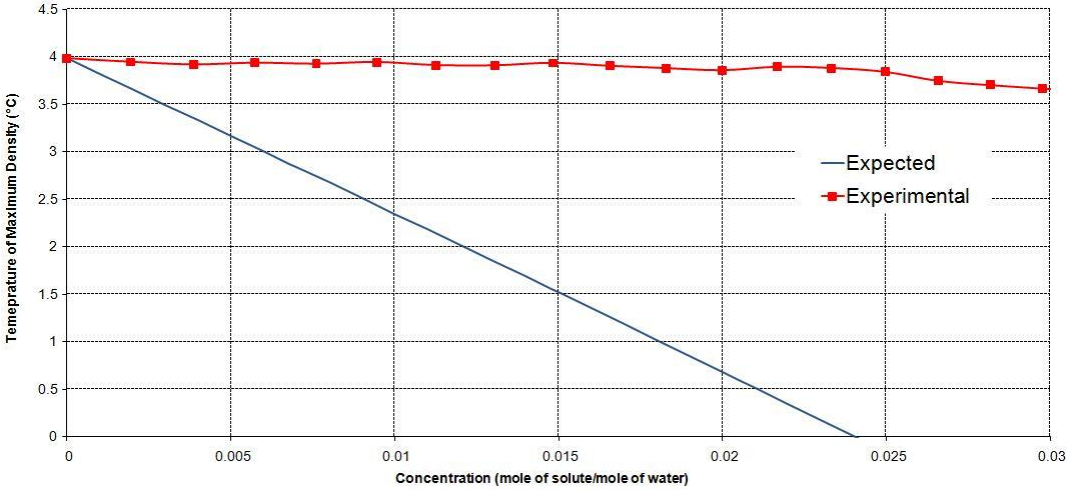

(c) Ethanol

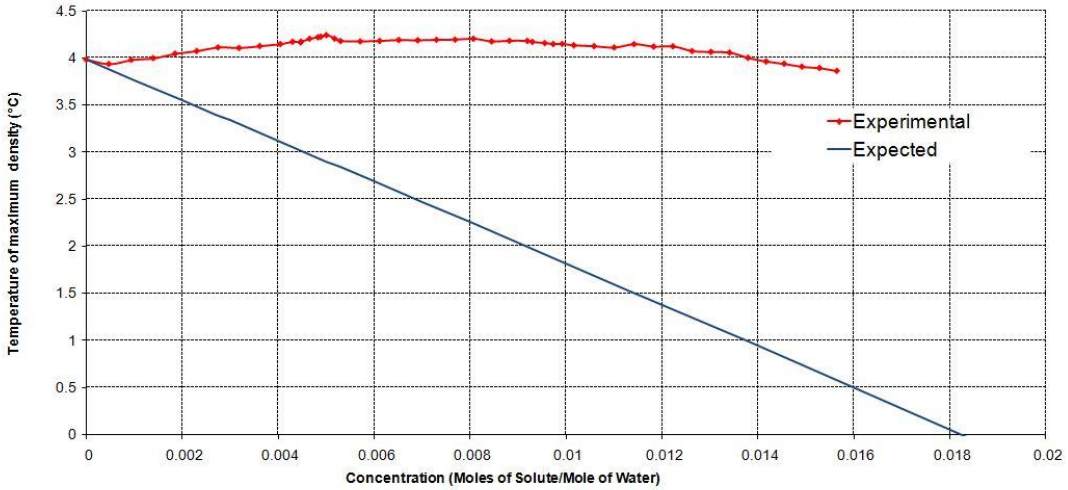

(d) 1-Propanol

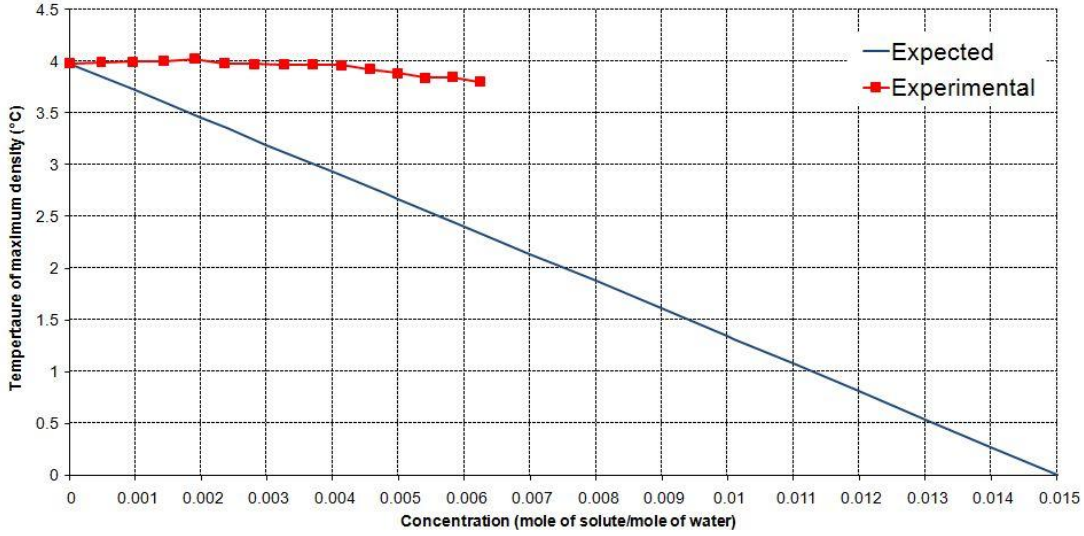

(e) 2-Propanol

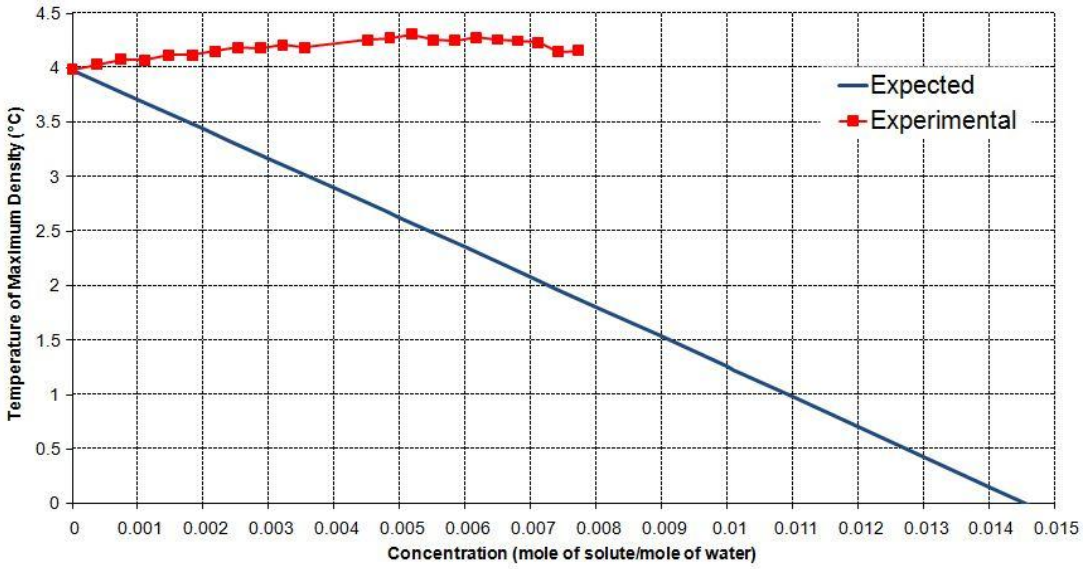

Figure 4.2-2 *Experimental temperature of maximum density and predicted temperature of maximum density as a function of solute concentration for (a) Ethylene Glycol, (b) Methanol, (c) Ethanol, (d) 1-propanol and (e) 2-propanol.*

The expected temperature of maximum density changes from solute to solute. The rate at which the expected temperature of maximum density decreases is regulated by the coefficient of thermal expansion and the molar volume of the solute. As can be seen in equation 4.2-5, the expected temperature of maximum depends on the coefficient of thermal expansion and the molar volume. Figure 4.2-3 compares the expected temperature of maximum density of each of the solutes studied. From figure 4.2-3 it can be seen that the isomers of propanol are predicted to have very similar effects on the temperature of maximum density of water as a function of concentration as their values of α and V_{s_0} are very similar (see table 4.2-1). It has been shown however in chapter 3 that this is not the case in practice. Experimentally 1-propanol and 2-propanol have been found to effect the temperature of maximum density in a different way.

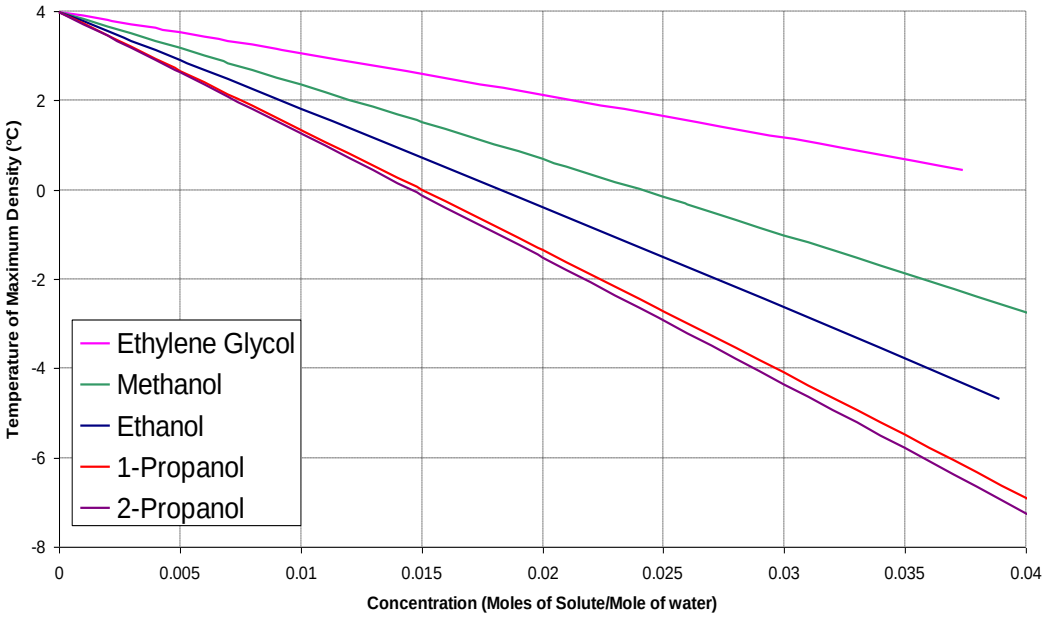

Figure 4.2-3 *Summary of the macroscopic investigation into the effects of various solutes on the temperature of maximum density of water.*

4.3 Experimental Phase Change versus Expected Phase Change

An investigation was carried out on the temperature of phase change of the solutes used in the temperature of maximum density investigations. Phase change temperatures as a function of concentration were obtained from the CRC Handbook of Chemistry and Physics [3], these values were compared to an expected temperature of phase change obtained from using the phase change temperature of both water and the solute in question. From both these values, an equation for the expected phase change temperature ($T`_{pc}$) was developed.

$$T`_{pc} = T_{pc_S}.x + (1-x)T_{pc_W}$$

where T_{pc_S} is the temperature of phase change of the solute, T_{pc_W} is the phase change of water, and x is the concentration in moles of solute per mole of water.

Substance	Temperature of Phase Change (°C)
Water	0.0
Methanol	-97.7
Ethanol	-114.3
1-Propanol	-126.5
2-Propanol	-89.5
Ethylene Glycol	-12.9

Table 4.3-1 *Temperature of phase change for various substances.*

From table 4.3-1 and the values obtained from the CRC Handbook of Chemistry and Physics, graphs of expected temperature of phase change were compared to the experimentally obtained results.

(a) Ethylene Glycol

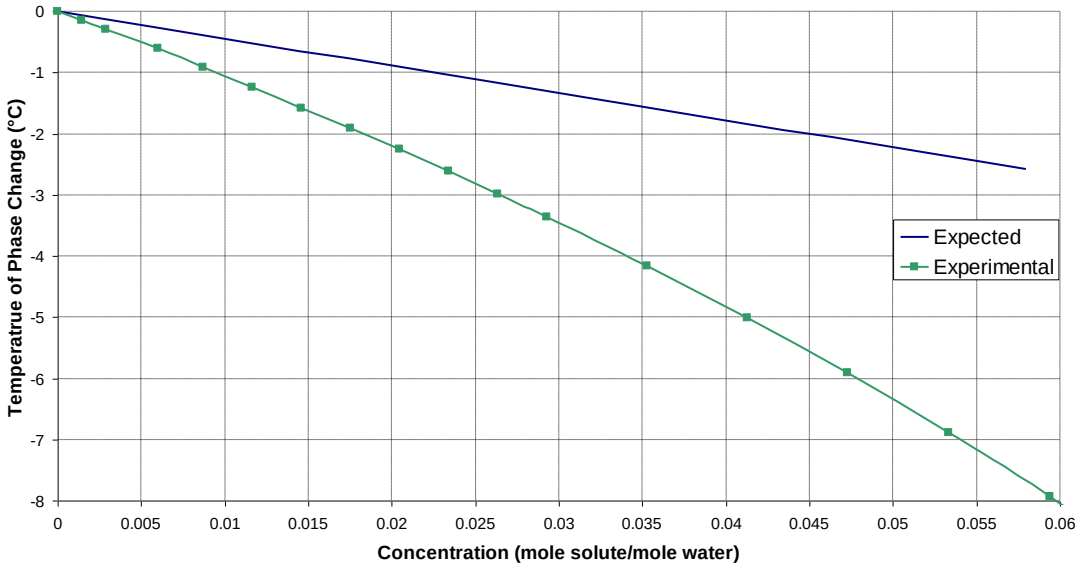

(b) Methanol

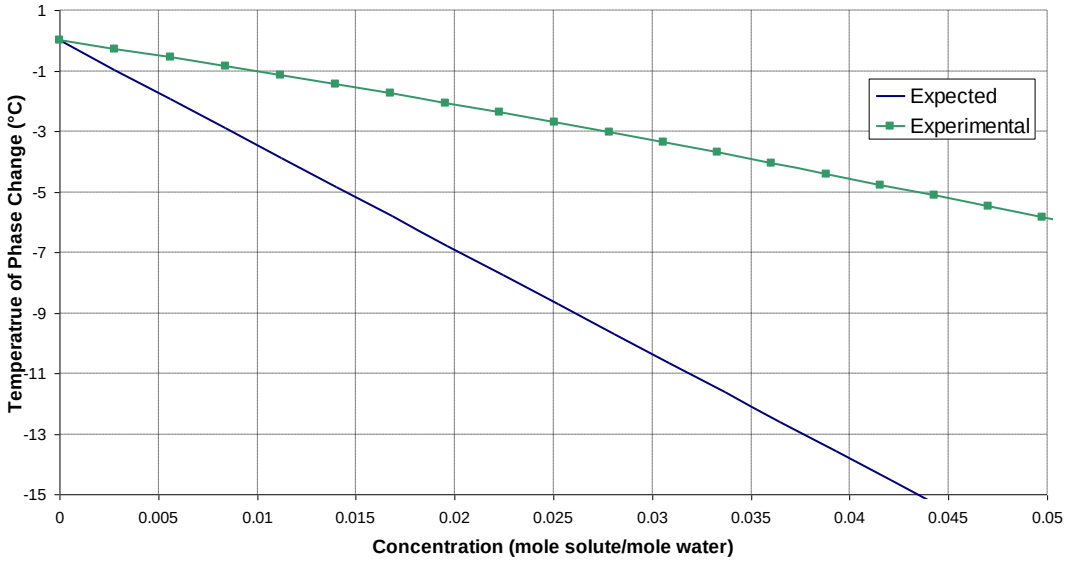

(c) Ethanol

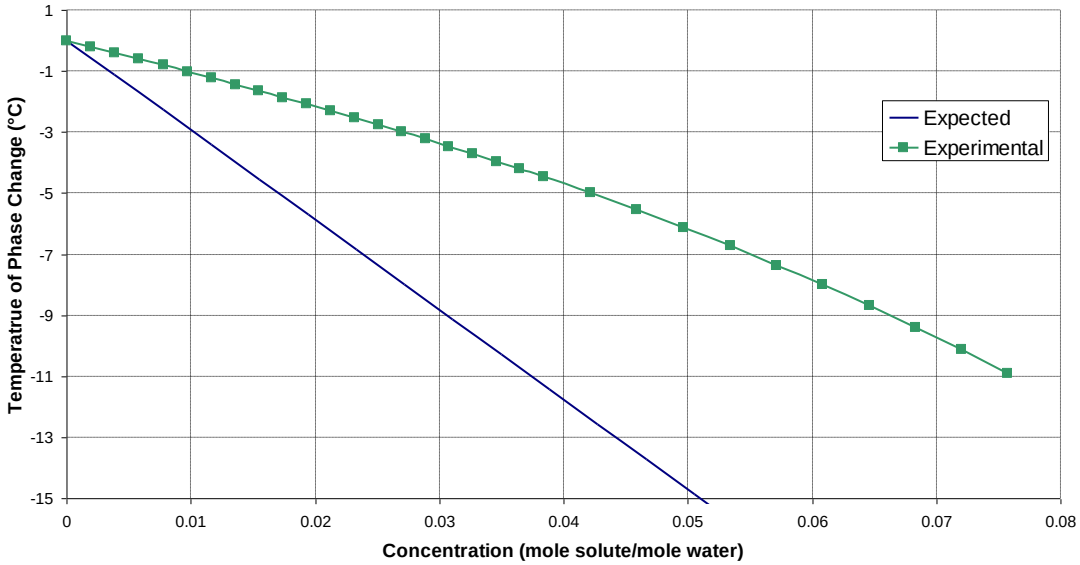

(d) 1-Propanol

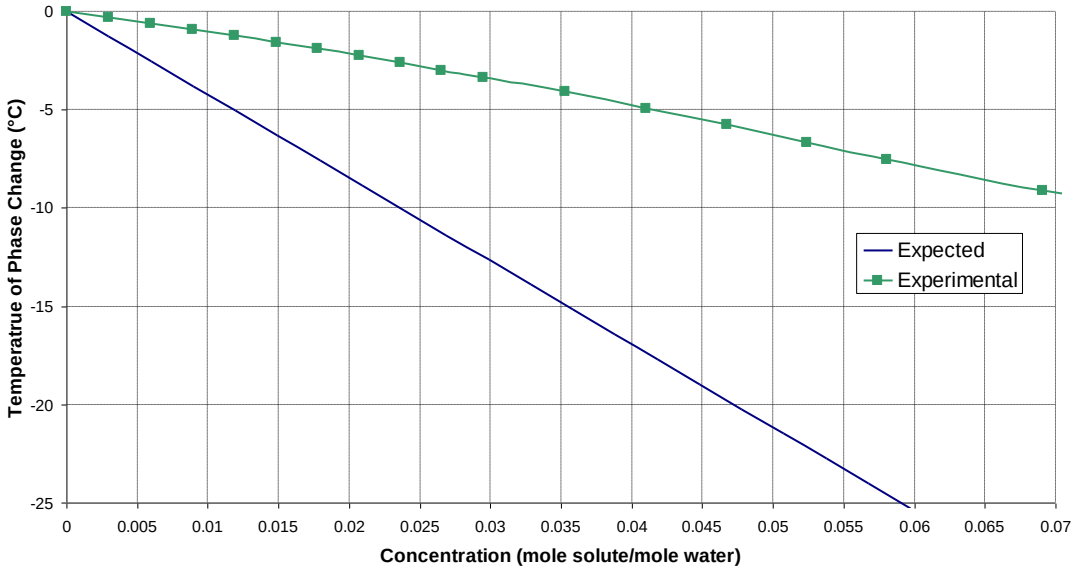

(e) 2-Propanol

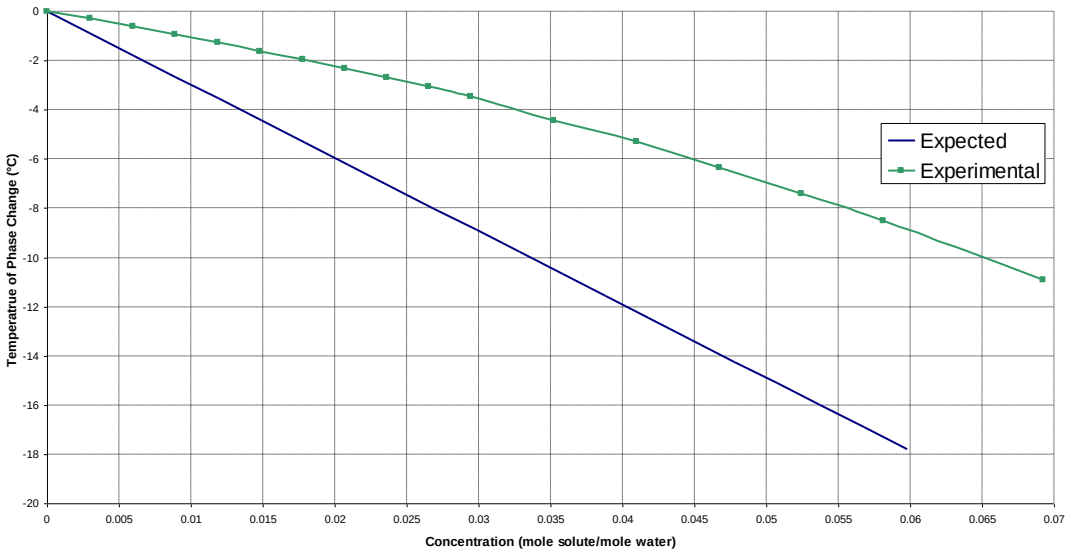

Figure 4.3-1 *Experimental temperature of phase change and predicted temperature of phase change as a function of solute concentration for (a) Ethylene Glycol, (b) Methanol, (c) Ethanol, (d) 1-propanol and (e) 2-propanol.*

The graphs in figure 4.3-1 show the expected temperature of phase change as a function of solute concentration as well as the experimentally obtained values. The expected value is based on the solution being an ideal solution, meaning there is no appreciable interaction between the solute and the water. In each case the expected

temperature of phase change is linear. Experimentally it is found that the temperature of phase change is non-linear at high concentrations. At low concentrations it is linear for all test solutes. The level of agreement between the expected and experimental temperature of phase change varies from solute to solute. Ethylene glycol and 2-propanol do not show any agreement between the expected and experimental temperature of phase change, while ethanol and 1-propanol do.

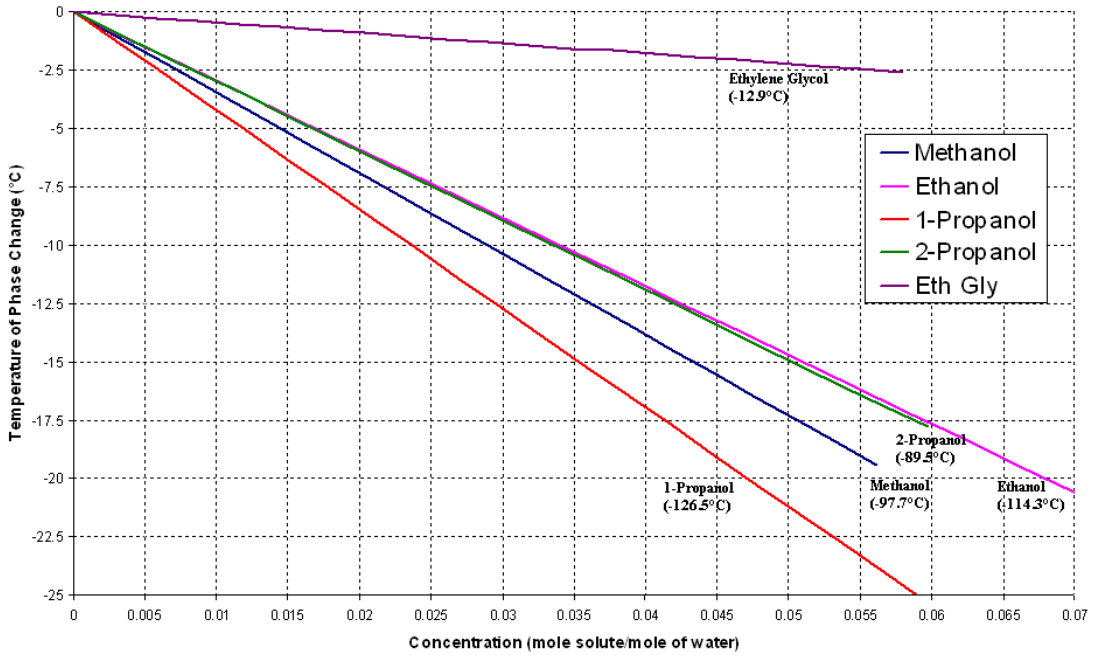

Figure 4.3-2 *Summary of the macroscopic investigation into the effects of various solutes on the temperature of phase change of water.*

4.4 Temperature of maximum density versus Temperature of Phase Change.

In 1867 Rossetti compared the temperature of maximum density to the temperature of phase change for a range of solutes [21]. Rossetti tried to show that the temperature of maximum density of water was a colligative property, just like the phase change is at low concentrations as seen in table 4.4-1.

Solute	T_{pc} at 0.02 mole solute/mole of water (°C)
Ethylene Glycol	-2.2
Methanol	-2.13
Ethanol	-2.115
1-Propanol	-2.115
2-Propanol	-2.23

Table 4.4-1 *Illustrating the colligative nature of the temperature of phase change at low concentrations.*

As seen from the results presented in this work and previously by Wada and Umeda [22], [23] the temperature of maximum density is not a colligative property. In this section, the differences between the temperature of maximum density and the temperature of phase change are investigated as a function of solute concentration. Both the experimental and expected values for each are presented.

(a) Ethylene Glycol

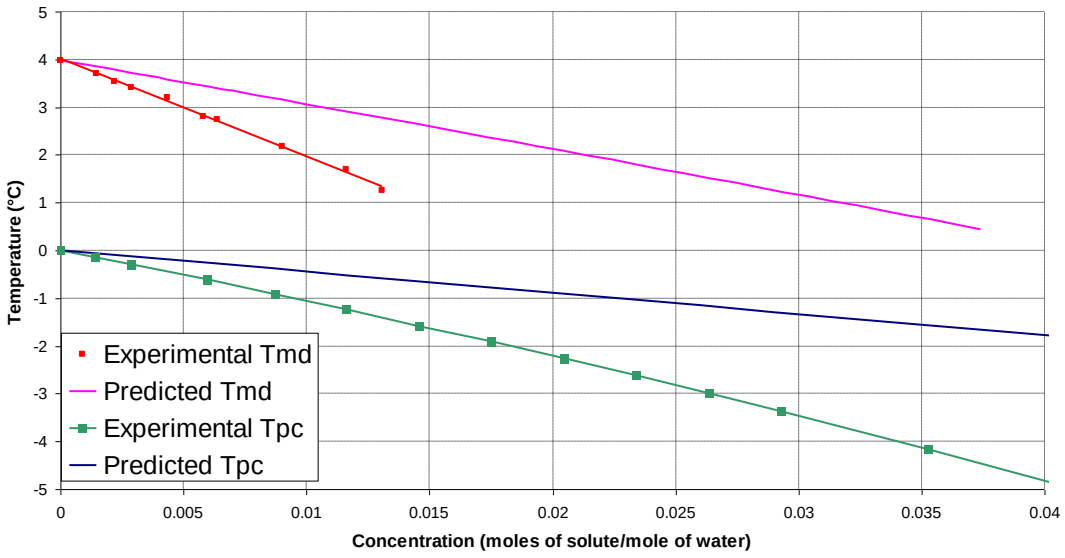

(b) Methanol

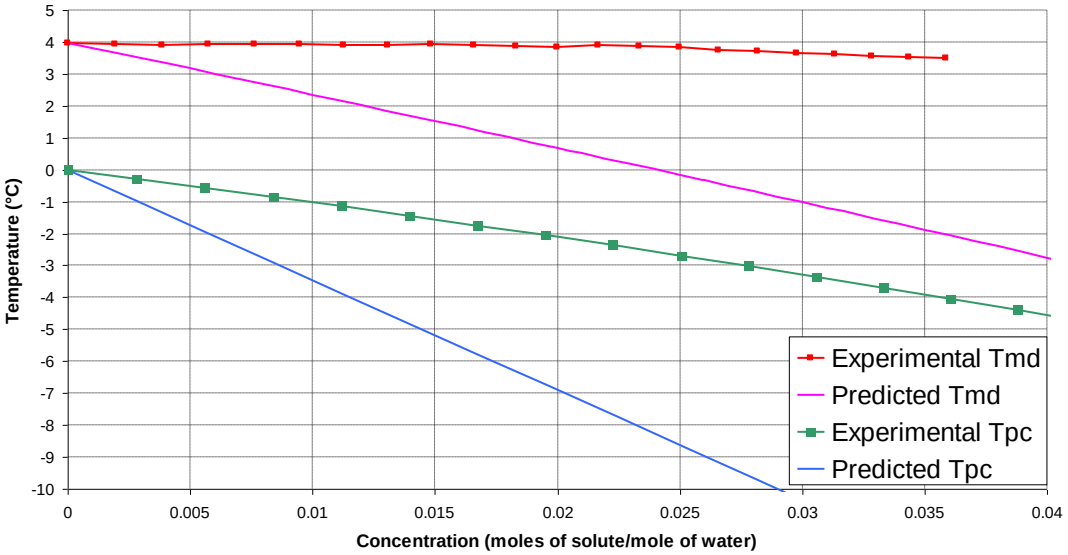

(c) Ethanol

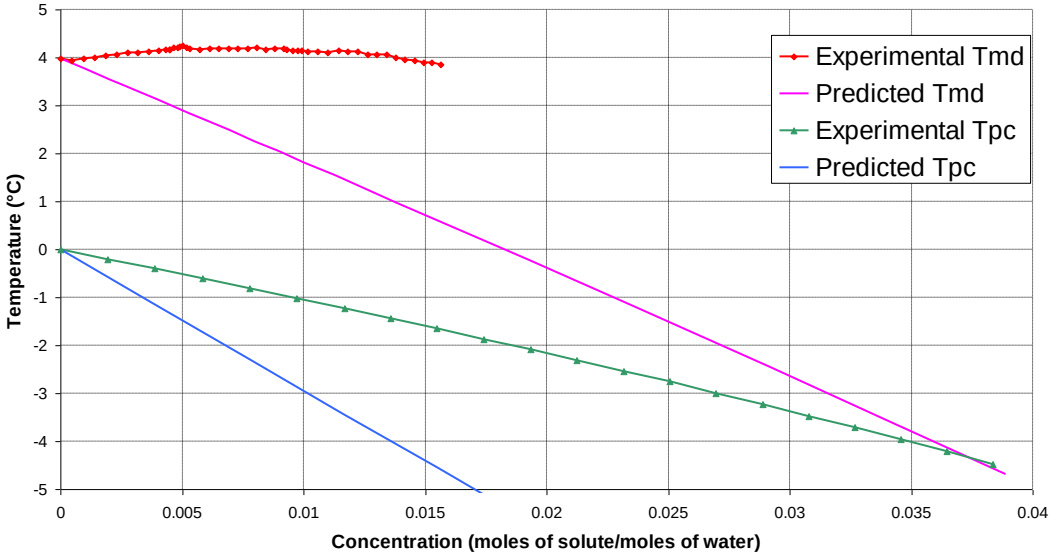

(d) 1-Propanol

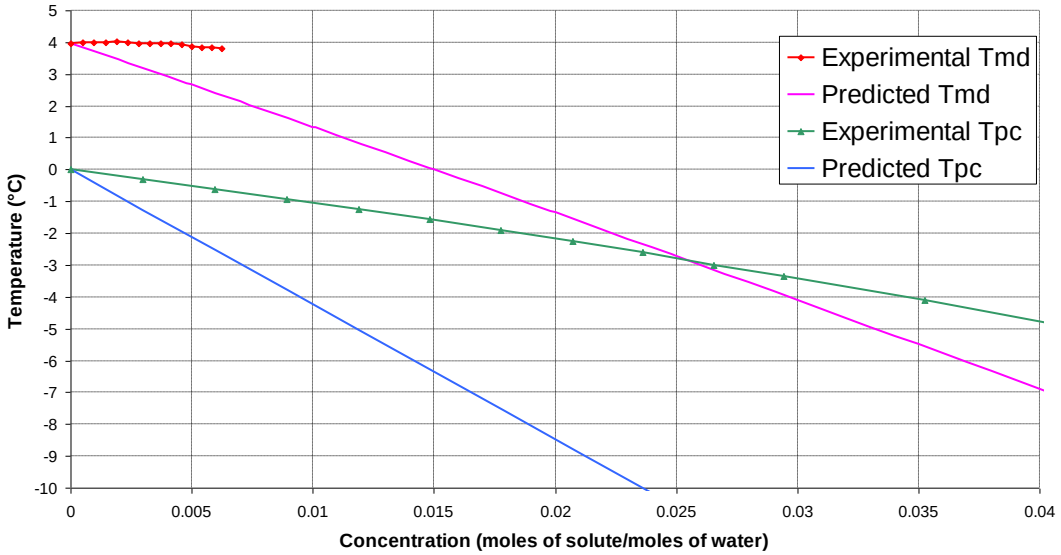

(2) 2-Propanol

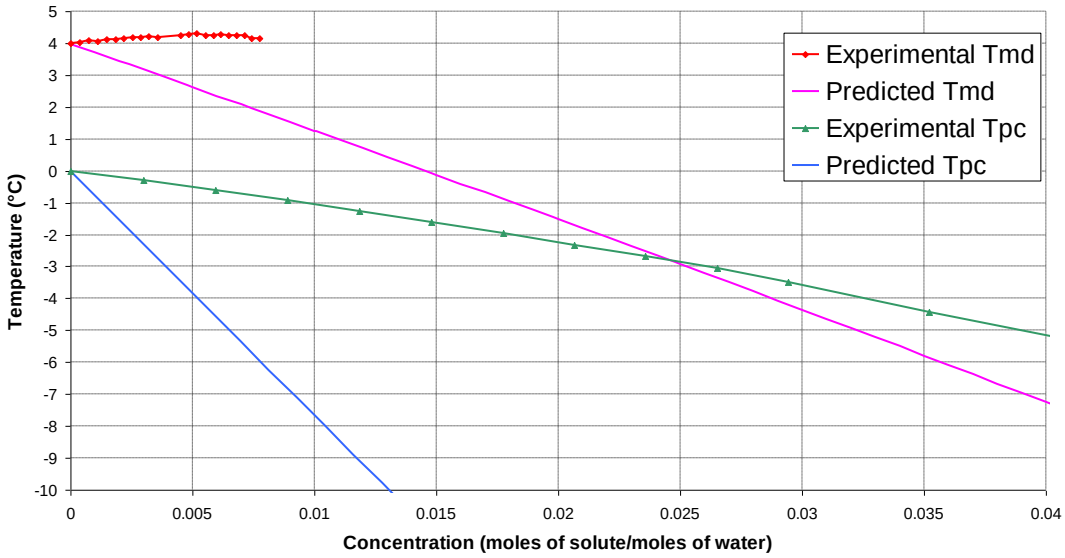

Figure 4.4-1 *Graphs comparing the temperature of maximum density with the temperature of phase change for (a) Ethylene Glycol, (b) Methanol, (c) Ethanol, (d) 1-propanol and (e) 2-propanol.*

The graphs in figure 4.4-1 show how the temperature of maximum density and temperature of phase change are affected by changes in concentration for each of the solutes investigated. It is clear that the temperature of maximum density is not a colligative property and as can be seen in figure 4.4-2, that at low concentrations the temperature of phase change is colligative.

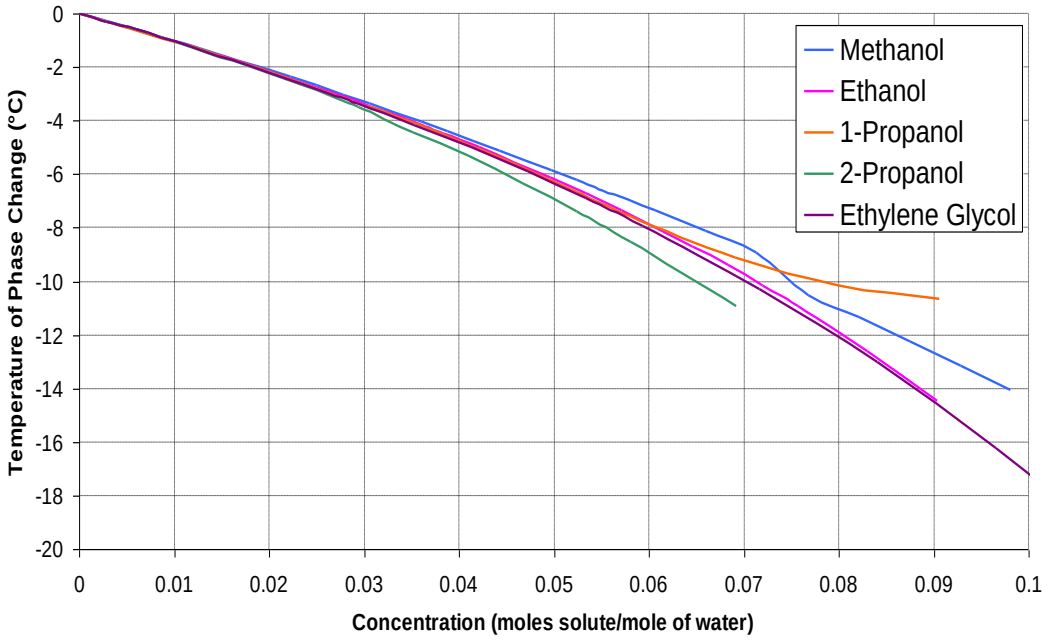

Figure 4.4-2 *Graph comparing the experimentally obtained temperature of phase change of various solutes in water obtained from [13]. At low concentrations they overlap indicating that the temperature of phase change is a colligative property.*

4.5 Summary

In this chapter an investigation was carried out to predict how the temperature of maximum density and temperature of phase change would change as a function of solute concentration for a variety of solutes. These predictions were based on the solution being ideal. An ideal solute being described as one in which the solute and solvent have negligible interaction with each other. When the experimental temperature of maximum density is compared to the expected temperature of maximum density of the solutions investigated it is clear that there are two very different trends. Ethylene glycols experimentally obtained temperature of maximum density is depressed linearly just as the predicted temperature of maximum density, but the experimentally obtained temperature of maximum density is suppressed at a quicker rate. All the alcohols tested follow a different trend. The experimentally

obtained temperature of maximum density is always higher then the predicted value. For the alcohols, experimentally some of them show a rise in the temperature of maximum density, and none of them show a linear relationship of temperature of maximum density versus solute concentration, while the predicted temperature of maximum density indicates a linear suppression.

Solute	**T_{md} Observed v Model**	**T_{pc} Observed v Model**
Ethylene Glycol	L	L
Methanol	H	H
Ethanol	H	H
1-Propanol	H	H
2-Propanol	H	H

Table 4.5-1 *Summary of how the observed temperature of maximum density and temperature of phase change compared the values obtained from the model. H indicates that the observed temperature is higher then the expected temperature and L indicates that the observed temperature is lower then the expected temperature.*

In all cases except for ethylene glycol, the experimentally obtained temperature of phase change is lower then that of the predicted value. These results are summarised in table 4.5-1.

Chapter 5

Microscopic Modelling.

5.1 Introduction to Microscopic Modelling

The macroscopic modelling discussed in chapter four has many limitations as it does not take into account any interactions that occur between the solute and the solution. The microscopic modelling looks at the same problem at a more fundamental level. Figure 5.1-1 indicates some of the possible approaches that can be taken to model the anomalous behaviour of water.

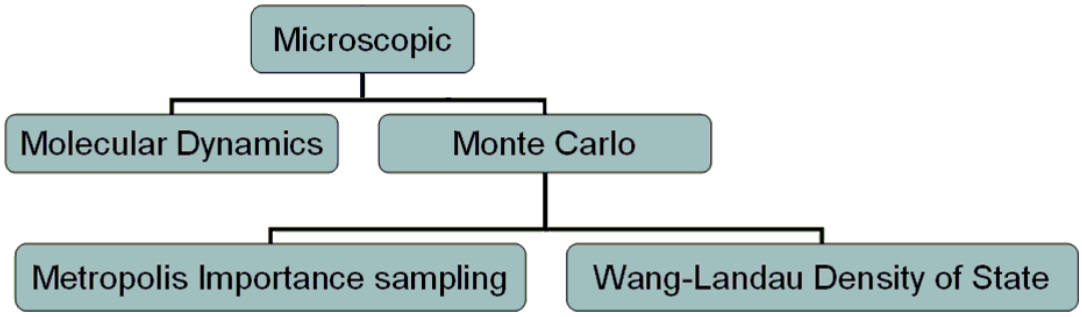

Figure 5.1-1 *Chart indicating the possible microscopic approaches to modelling water.*

Within the microscopic studies there are two approaches that were examined as part of this study. Molecular dynamics models were investigated, which is a deterministic approach. Various Monte Carlo models were developed for the reasons explained in section 5.2, this is a stochastic approach. In section 5.2, both approaches are described and compared. In computer science, a 'deterministic' algorithm is informally described as one which behaves predictably. From an initial state, its future states can be predicted to a high degree of accuracy. The use of the term 'stochastic' effectively means that the algorithm relies on probability.

The section below indicates how this chapter is presented.

5.2 Explains the main principles of both Molecular Dynamics and Monte Carlo simulations. Outlining the benefits of Monte Carlo for the purpose of the models developed as part of this work.

5.3 Introduces Metropolis Importance sampling and the Wang and Landau algorithm, both of which use a Monte Carlo method.

5.4 Explains the Lennard-Jones potential.

5.5 Describes various possible water models in brief followed by a detailed description of the Mercedes-Benz model of the molecule.

5.6 Introduces the Buzano model.

5.7 Describes how the off-lattice model worked as well as the results obtained from it.

5.8 Describes how the Metropolis Importance sampling algorithm and the Wang-Landau algorithm were applied to a modified Buzano, gas lattice model using a Mercedes-Benz water molecule, as well as presenting the results obtained from each algorithm.

5.9 Describes the effects of introducing molecules to the lattice of the temperature of maximum density.

5.10 Details how the introduction of molecules with different hydrogen bond strengths affects the temperature of maximum density.

5.2 Methods used to conduct Molecular Simulations

5.2.1 Molecular Dynamics.

Molecular dynamics (MD) is a form of computer simulation that allows for atoms and molecules to interact with each other for a set period of time. These interactions give a view of the motion of the atoms and are based on approximations of known physics. Molecular dynamics has a theoretical basis in the analytical mechanics of Euler, Hamilton, Lagrange and Newton equations that govern mechanical dynamics, fluid mechanics and classical mechanics [46]. The simplest possible molecular

dynamics model consists of a collection of structureless particles that only require Newton's second law to describe their motion. At the next level of complexity, there are rigid molecules that require the Euler equations as well as Newton's second law. Molecules that have internal degrees of freedom while still being subjected to structural constraints will involve Lagrange methods for incorporating geometric constraints into the dynamic equations.

In MD the equations of motion are only solvable numerically. This is because of the nature of the interatomic interaction, exemplified by the Lennard-Jones potential with a strongly repulsive core, as a result of which, atomic trajectories are unstable in the sense that an infinitesimal perturbation will grow at an exponential rate.

5.2.2 Monte Carlo

Monte Carlo (MC) methods are a class of computational algorithms that use repeated random sampling to compute results. It is a stochastic method that relies on probabilities. We are using it to simulate fluids. To do this a random trial configuration consisting of molecule positions and orientations is generated, which is compared to an evaluated 'acceptance criterion' by calculating the change in energy and other properties in the trial [47]. In simple terms, we use the Monte Carlo method to generate random configurations, and if the new configuration has less energy than the previous configuration it is accepted. If the new energy is greater, a Boltzmann factor is compared against a randomly generated number to see if the new energy is accepted or rejected. How the Monte Carlo method is used in this work is detailed in section 5.3.1.

Monte Carlo simulations take 'snap shots' of the system, not caring how it moves from one configuration to the next once it is energetically feasible.

5.2.3 Monte Carlo Methods versus Molecular Dynamics

The Monte Carlo algorithm is based on exploring the energy surface by randomly probing the geometry of the molecular system, whereas MD actually simulates the time evolution of the molecular system, providing the actual trajectory of the system. A stochastic simulation (using a Monte Carlo algorithm) results in a large number of configurations being accumulated, and the potential energy function is calculated for each of them. This data is used in turn to calculate the thermodynamic properties of the system.

As the Monte Carlo method is not deterministic, and therefore does not offer time evolution of the system in a form suitable for viewing [48]. This does not mean that MD is better for deriving the thermodynamic properties of a system. In many cases MC is a lot more efficient then the MD approach. Currently Monte Carlo simulations have a strong hold in the area of simulations of liquids and solvation processes in chemistry [48].

A decision had to be made as to what approach should be taken for the purpose of this study. Initially molecular dynamic simulations were investigated; however, molecular dynamics for larger molecules or systems is a computationally difficult task for even the most powerful supercomputers. As a result of this a stochastic approach was investigated and now makes up all of the work carried out in the area of molecular simulations carried out for this report.

5.3 Monte Carlo Studies

As part of the Monte Carlo studies undertaken in this work, two separate algorithms are used. A Metropolis Importance Sampling method and a Wang-Landau Density of States method are used. In this section, both methods are described, with their advantages and disadvantages.

5.3.1 Metropolis Importance Sampling.

The Metropolis sampling algorithm is the most popular realisation of the Monte Carlo Method. The Monte Carlo method begins with the molecules being assigned random positions and orientations. A random molecule is selected and changed. The change is either accepted or rejected based on the Boltzmann factor. After the completion of a set number of changes the algorithm ends. In general it works as follows [48]:

1. The initial atom/molecule coordinates are specified.
2. Select at random, an atom *i* and move it by random displacement ΔX_i, ΔY_i, ΔZ_i.
3. Calculate the change in potential energy ΔU corresponding to this displacement.
4. If $\Delta U < 0$ accept the new coordinates and go to step 2.
5. Otherwise, if $\Delta U \geq 0$, select a random number R in the range [0, 1] and if
   A. $e^{\frac{-\Delta U}{kT}} > R$ accept the new coordinates and go to step 2.
   B. $e^{\frac{-\Delta U}{kT}} \leq R$ keep the original coordinates and go to step 2.

Step 5 shows that if the change in energy ΔU, is large and positive, the change is unlikely to be accepted. Two types of models were studied using the Metropolis sampling algorithm, an 'off-lattice' model, and a 'gas-lattice' model. The off lattice model allows for the molecules to undergo a change in position as well as orientation, where as in the gas-lattice model, there are a fixed number of sites that a molecule can occupy. These sites are fixed in location. A site can be either occupied or vacant, signifying that it is a gas-lattice model, and a molecule in such a site can have one of a fixed number of orientations.

The lattice Monte Carlo simulations have been built up in complexity from a simple 'Ising' model, which is a statistical mechanics model named after Ernst Ising. The

Ising model is a discrete collection of variables (or spins), which can take the value –1 or 1. Spins that are beside each other interact. If they have the same sign, the energy is incremented by one; otherwise the energy is decreased by one. After the total energy of the system is calculated, one spin is flipped. Metropolis sampling using the Boltzmann distribution is then used to decide if the new configuration is accepted or rejected. A generalised variation of the Ising model was then developed. This model is known as the Potts model after Renfrey B. Potts. The model can be used to study the behaviour of ferromagnets and other systems in solid-state physics. Whereas in the Ising model there are two possible states, the Potts model allows for q states, where q is a positive integer. Setting q = 2 in the Potts model, simulates the Ising model.

The code that was used to simulate the Ising models was a simple Monte Carlo rejection method based on a Boltzmann distribution. The code began by setting up a lattice of randomly placed 1's and –1's. Then depending on the temperature, they would begin to align as seen in the tables below.

Unaligned Spins (Ising Model)

1	-1	-1	-1	1	-1	1	-1	-1	1
-1	-1	-1	-1	1	1	-1	-1	-1	1
1	-1	1	-1	1	1	1	-1	-1	1
-1	-1	-1	1	1	1	-1	-1	-1	1
-1	1	1	1	-1	1	-1	1	-1	1
-1	-1	1	1	-1	1	1	1	-1	1
1	-1	-1	-1	-1	-1	-1	-1	1	-1
-1	-1	-1	1	1	-1	-1	-1	-1	1
1	-1	-1	-1	1	1	-1	1	1	-1
-1	1	1	1	-1	-1	1	1	1	1

Aligned Spins (Ising model)

1	1	1	1	1	1	1	1	1	1
1	1	1	1	1	1	1	1	1	1
1	1	1	1	1	1	1	1	1	1
1	1	1	1	1	1	1	1	1	1
1	1	1	1	1	1	1	1	1	1
1	1	1	1	1	1	1	1	1	1
1	1	1	1	1	1	1	1	1	1
1	1	1	1	1	1	1	1	1	1
1	1	1	1	1	1	1	1	1	1
1	1	1	1	1	1	1	1	1	1

The same code was then adapted to the more general Potts model and ran in the same way. For the simulation results shown below, q = 6.

Unaligned Spins (Potts Model)

1	5	4	6	3	4	1	5	5	3
4	6	4	4	2	2	5	5	6	1
2	6	2	4	3	2	3	6	5	1
6	5	5	1	3	3	6	6	6	2
5	1	3	2	6	2	4	1	5	3
6	5	2	1	4	3	1	3	4	3
2	6	5	4	4	4	5	6	2	6
5	4	4	1	2	5	4	6	5	2
1	6	4	5	1	1	5	1	2	4
4	3	3	3	5	4	1	2	1	2

Aligned Spins (Potts model)

6	6	6	6	6	6	6	6	6	6
6	6	6	6	6	6	6	6	6	6
6	6	6	6	6	6	6	6	6	6
6	6	6	6	6	6	6	6	6	6
6	6	6	6	6	6	6	6	6	6
6	6	6	6	6	6	6	6	6	6
6	6	6	6	6	6	6	6	6	6
6	6	6	6	6	6	6	6	6	6
6	6	6	6	6	6	6	6	6	6
6	6	6	6	6	6	6	6	6	6

These models were originally run using a Metropolis sampling method. Temperature scans were also carried out in using the Metropolis sampling approach for the Ising and Potts models. Figure 5.3-1 shows a graph of energy versus temperature for the Ising model.

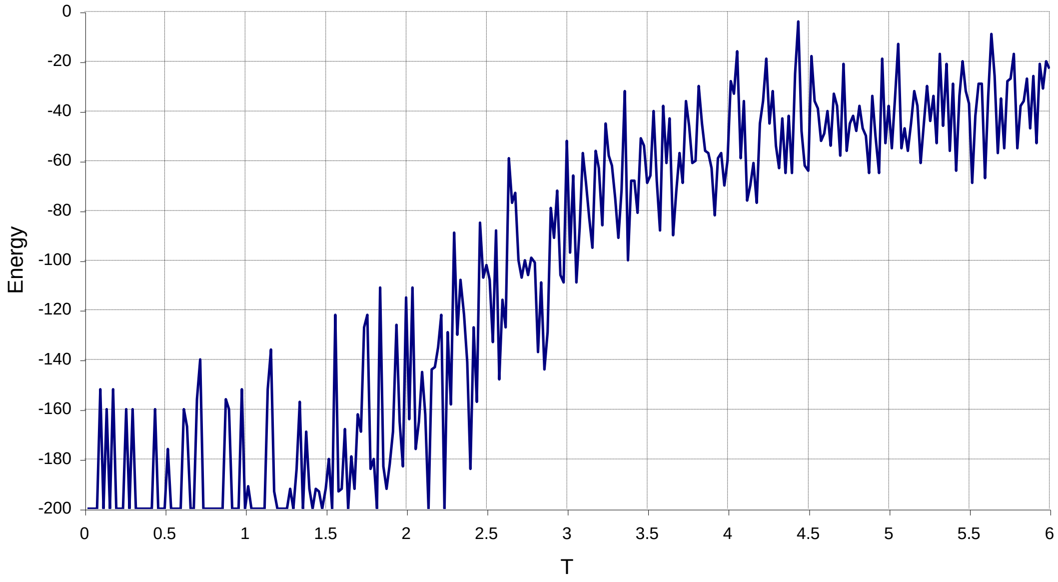

Figure 5.3-1 *Graph of energy versus reduced temperature T for the Ising model, using Metropolis sampling.*

There is a clear trend in the graph; the minimum energy is –200 (-2 for each of the 100 lattice sites), then there is a second-order phase change. The minimum energy

of –2 per lattice site is as expected, as each site interacts with 4 neighbours, and if they are aligned an energy of –1 is added. To allow for double counting the total energy is divided by 2. The problem with the graph above is clear: it is very noisy. This is a problem with Metropolis sampling. However, Metropolis sampling does have an advantage over the Wang and Landau method described in the next section; it allows for the state of the system to be visually inspected for any given temperature.

5.3.2 Wang and Landau Method

The Wang-Landau method works differently to the Metropolis method. Instead of sampling the probability distribution at a fixed temperature as is done in the Metropolis method, a random walk is performed in energy space to extract an estimate for the density of states function. The density of states (dos) function is the number of states at each energy level that are available to be occupied [44]. As the systems in this study all have discrete energy levels, the density of states gives the number of states for a given energy level, not the actual density. Once the density of states function has been obtained, subsequent calculations can be performed to compute the state probability at any temperature by weighting the dos function by an appropriate Boltzmann factor and normalising by the partition function. The partition function Z_n as seen in equation 5.3-1 encodes the statistical properties of a system.

A practical method that allowed for the extraction of the density of states function would be very beneficial. Wang and Landau [49] first used this method. In essence the Wang - Landau method allows for the calculation of the density of states of a given system *g(E),* the number of all possible states (configurations) for an energy E of the system. The partition function Z_n can be expressed in terms of the density of states *g(E)*. Direct measurement of the density of states is not the goal of the experiment. The goal of the simulations carried out as part of this study is to investigate density and energy as a function of temperature. As *g(E)* does not

depend on the temperature, a distribution can be constructed at any temperature if *g(E)* can be estimated to a high degree of accuracy for all energies. This allows the partition function to be calculated once *g(E)* is known.

$$Z_n = \sum_{\{configurations\}} e^{\left(\frac{-E}{k_\beta T}\right)} = \sum_E g(E) e^{\left(\frac{-E}{k_\beta T}\right)} \qquad (5.3\text{-}1)$$

Most thermodynamic properties can be calculated from Z_n, and of importance to this study, the density and energy as a function of temperature are obtainable from Z_n.

From the simplest lattice model investigated here, the Ising model, the density of states function *g(E)* could be obtained in theory by performing an unbiased random walk in energy space, changing at random the spins and accepting all the new energy configurations. The histogram that results of the energy distribution should converge to the density of states. This however is not a practical approach due to the very large number of possible configurations for even the simplest of systems. For example, an Ising model of a 10 x 10 square lattice has 2^{100} (approximately 1.27×10^{30}) spin configurations. As the possible numbers of spin orientations and lattice size increases, the numbers of spin configurations increases exponentially. Computationally, these models would take far too long to run.

The Wang-Landau algorithm works differently to conventional Monte Carlo methods, which generate a distribution $g(E)e^{\frac{-E}{k_B T}}$ at a given temperature T. A simple example of the Wang-Landau algorithm is presented at the end of this section. The Wang-Landau algorithm estimates *g(E)* directly by performing a random walk that produces a flat histogram in energy space called 'ghist'. For all the systems modelled in this study, the random walk has been carried out by changing the orientation of a randomly chosen site, but the energy E of each configuration is only accepted with a probability that is proportional to the reciprocal of the density of states. During the random walk, an energy histogram 'ehist' is also accumulated. This histogram keeps track of the number of times a

given energy level is visited. For each visit, the corresponding level in 'ehist' is incremented by 1. During each random walk, the algorithm modifies the estimate for the density of states by a controlled modification factor f. By the end of each walk there should be a flat histogram for 'ehist', and 'ghist' gives the density of states. The modification factor f is carefully controlled, and by the end of the simulations should be very close to 1. The Wang-Landau algorithm has been used in the study of many complex systems, including, but not limited to studies of a Potts antiferromagnet [50], fluids [51] and atomic clusters [52]. The systems modelled in this study are based on classic spin systems with discrete energy levels. This means that references to the density of states g(E) means the number of states for a given energy level E, not the actual density.

To study this algorithm, a code called WL_dice was developed. It uses a Wang-Landau algorithm to simulate the rolling of two dice. The output of each random walk is written to a file, which allows for the study of the progression of the density of states. This model was chosen as the output result is known. The energy in this model is the sum of the values, which in this case is the sum of the uppermost faces. There are 36 possible configurations (6^2), with the following density of states:

E (sum of faces)	g(E)
2	1
3	2
4	3
5	4
6	5
7	6
8	5
9	4
10	3
11	2
12	1

After the first random walk as shown in figure 5.3-2, it can be seen that the density of states does not correspond to the known density of states.

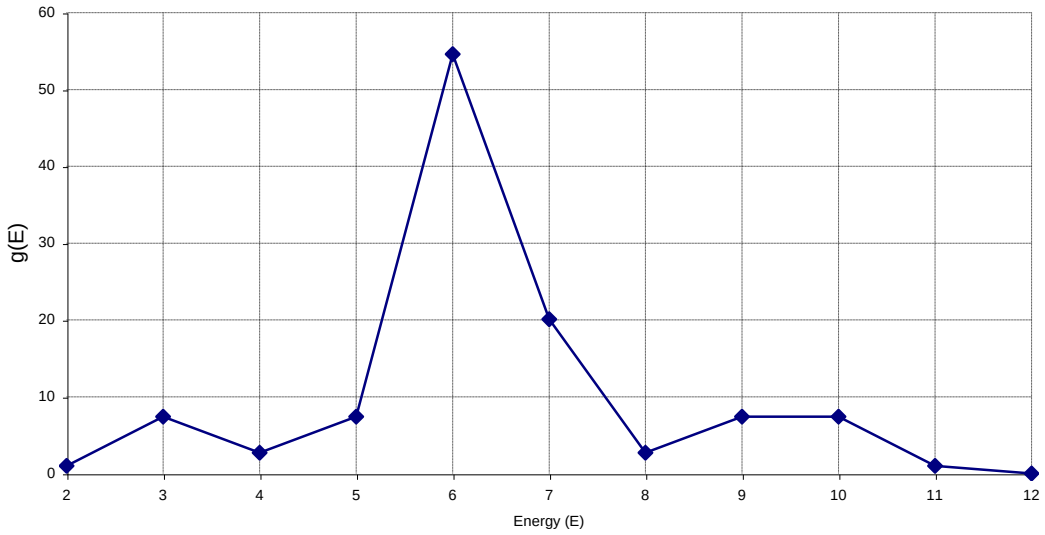

Figure 5.3-2 *Density of states as calculated after the first random walk.*

After 15 random walks through energy space the modification factor f reached 1.000001, which was the pre-decided value to terminate the algorithm. The resulting density of states can be seen in figure 5.3-3. The values match the table above perfectly.

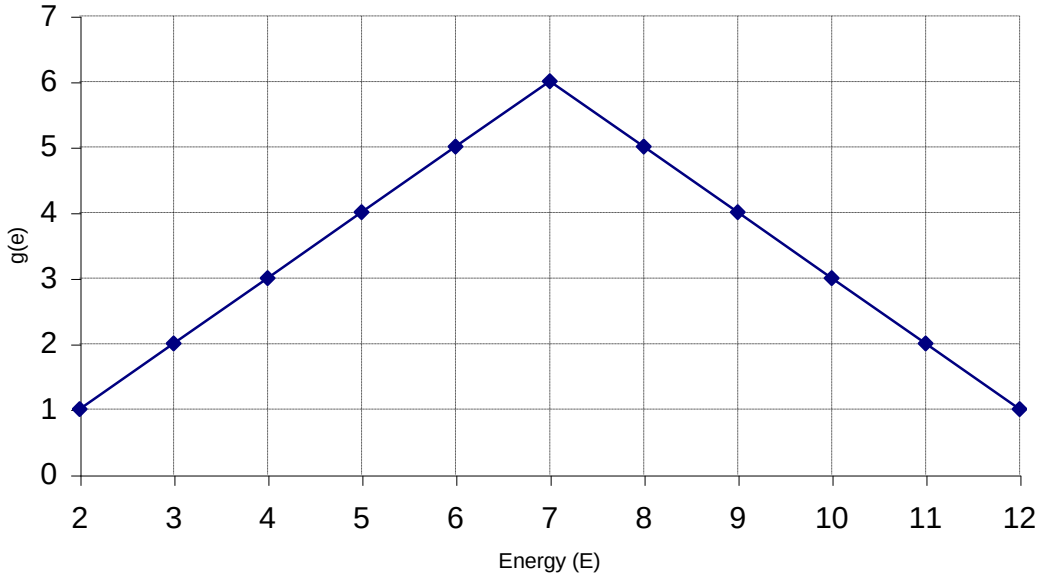

Figure 5.3-3 *Density of states as calculated after the last random walk.*

For comparison, the Ising model was adapted to use the Wang-Landau algorithm. The graph shown in figure 5.7.4 is very smooth and is not subject to noise unlike the

same gragh produced using the Metropolis sampling method shown in figure 5.3-1. This is one clear advantage of the Wang–Landau algorithm. The other being the amount of information available, including the specific heat capacity as a function of T, Helmholtz function as a function of T and entropy as a function of T.

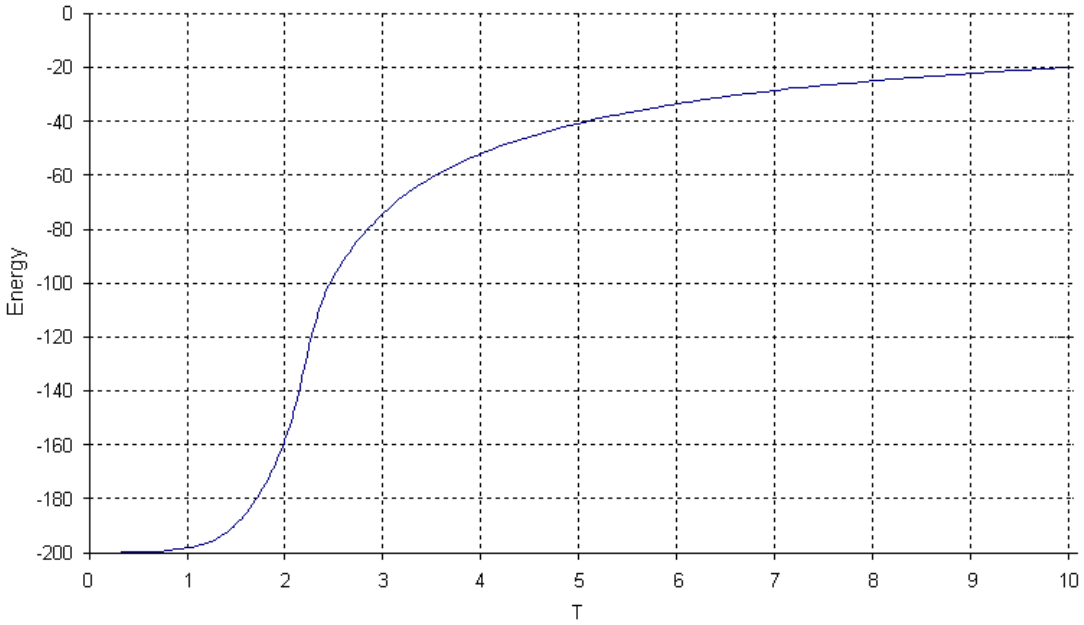

Figure 5.3-4 *Energy versus T for the Ising model, using the Wang-Landau algorithm.*

More complicated models may require a random walk to be carried out in more then one dimension. For example Landau carried out a random walk in energy and order parameter space in order to study the effect of an applied magnetic field on the Ising and Potts model [49]. In the study conducted by Landau, the parameter space was magnetisation. This resulting estimate of the dos function was of the form g(E, M). As will be shown in section 5.8.2 this study requires the estimation of a 2-D density of state function g(E, N), where E is the energy, and N is the number of occupied sites (this relates to the density of the system due to it being a gas lattice model). From this the partition function is obtained as shown in equation 5.3-2.

$$Z = \sum g(E,N) \exp\left(\frac{-\Delta E}{k_B T}\right) \exp\left(\frac{\mu N}{k_B T}\right) \qquad (5.3\text{-}2)$$

where μ is the chemical potential (pressure variable), k_B is the Boltzmann constant, T is temperature. The picture gets more complex in section 5.10 when a third dimension is required to allow for a random walk to take place in energy, density and concentration space. This requires the estimation of the density of states function to be of the form g(E, d, c). This third dimension is described in section 5.10.

5.4 Lennard-Jones Potential

To develop a model of the system it is important to know how the individual molecules and atoms interact with each other, and the forces they exert on each other. The simplest model of such a system consists of spherical particles that interact with each other. There are two principle features of such interatomic particles. They resist compression and as a result repel reach other at close ranges. At longer ranges they attract each other in an effort to bind the particles in the solid and liquid states [46]. There are many forms of potential functions that exhibit these features. One of the most well known is the Lennard-Jones (LJ) potential. John Lennard-Jones originally proposed the LJ potential for liquid argon in 1924. The Lennard-Jones potential for a pair of atoms i and j located at r_i and r_j is given as:

$$u(r_{ij}) = \begin{cases} 4\varepsilon\left[\left(\dfrac{\sigma}{r_{ij}}\right)^{12} - \left(\dfrac{\sigma}{r_{ij}}\right)^{6}\right] & r_{ij} < r_c \\ 0 & r_{ij} \geq r_c \end{cases} \qquad (5.4\text{-}1)$$

where $\mathbf{r}_{ij} = \mathbf{r}_i - \mathbf{r}_j$ and $r_{ij} \equiv |r_{ij}|$. The parameter ε is the depth of the potential well and σ is the (finite) distance at which the interparticle potential is zero. The term r_c is known as the cut-off distance. It denotes the region beyond which the potential is

assumed to be zero. This is done to reduce computational time. The $\left(\frac{\sigma}{r_{ij}}\right)^{12}$ term is the repulsion term and the $\left(\frac{\sigma}{r_{ij}}\right)^{6}$ term describes the attraction term.

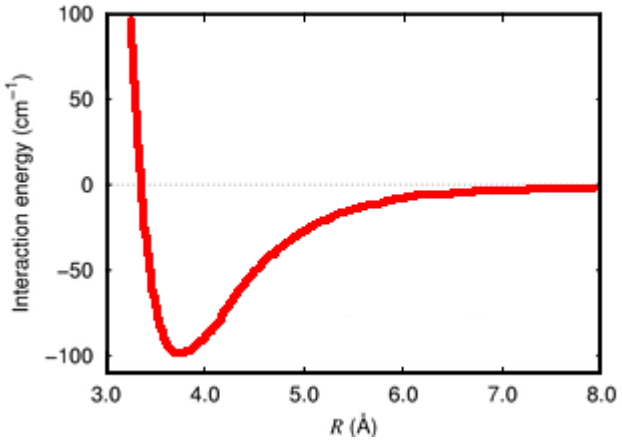

Figure 5.4-1 *Lennard-Jones potential curve.*

5.5 Water Models

When beginning to construct a simulation, a model of the water molecule has to be selected. As with any computational simulation there exists the usual trade off between accuracy and computation time. The more detailed the model, the more accurate one can expect the results to be but the time taken will also be significantly longer.

There are many models of water of various levels of detail. The simplest is that of a small spherical disk. However this provides little understanding and gives no worthwhile information as a model consisting of a small spherical disk will not involve any hydrogen bonds. More advanced models can be categorised by the number of 'sites' they contain. Common models contain 3, 4, or five sites.

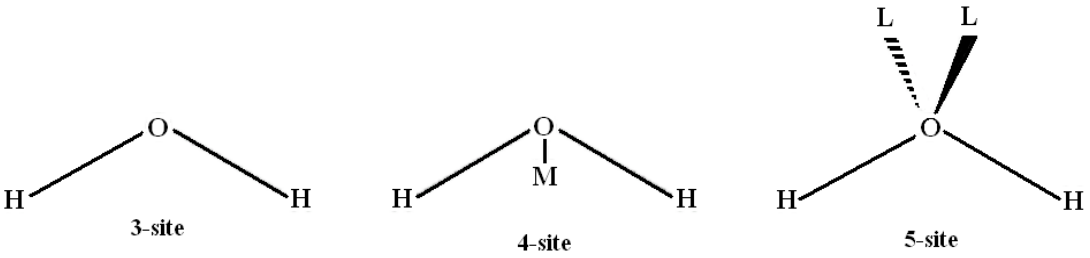

Figure 5.5-1 *Examples of water models.*

In the diagram 5.5-1, the H represents a hydrogen atom, the O represents an oxygen atom, M represents a 'dummy' negatively charged atom used to improve electrostatic distribution around the water atom. The L represents a lone pair of electrons. The molecule chosen for this work is 4-site, 3-arm model known as the Mercedes-Benz (MB) molecule. The 3 arms in the MB molecule are separated by 120°. It acquired this name due to its resemblance to the car manufactures Mercedes-Benz logo. Figure 5.5-2 shows the MB model.

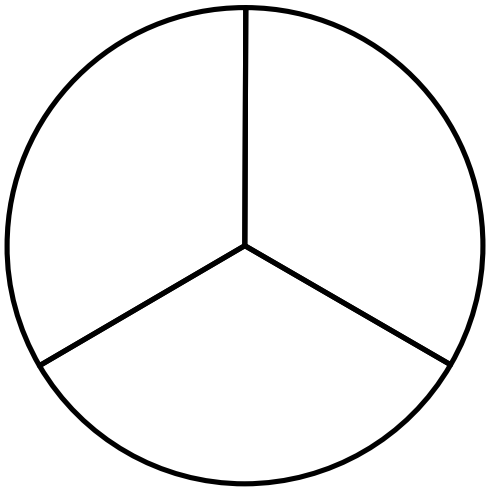

Figure 5.5-2 *Mercedes-Benz water molecule.*

The MB molecule was chosen as it has been shown to identify the main features of water including some of the anomalous features such as the density anomaly. A paper by Silverstein et al [53] shows that the MB molecule can be used to identify the density maximum amongst other properties. Within the simulations, the MB

molecule involves two types of interactions. There are Lennard-Jones interactions as described above in section 5.4 and there is an explicit hydrogen-bonding (HB) term. This gives a total potential energy of molecule i with molecule j as being

$$U(X_i X_j) = U_{LJ}(r_{ij}) + U_{HB}(X_i X_j) \qquad (5.5\text{-}1)$$

This equation uses a system developed by Ben-Naim [54] and summarized in figure 5.5-3. X_i denotes a vector representing both the coordinates and the orientation of the i^{th} particle r_{ij} is the centre to centre distance of the i^{th} and j^{th} particles. U_{LJ} is defined as in (5.4-1)

$$U_{HB}(X_i X_j) = \varepsilon_{HB} G(r_{ij} - r_{HB}) \sum_{k,l=1}^{3} G(\hat{i}_k \cdot \hat{u}_{ij} - 1) G(\hat{j}_l \cdot \hat{u}_{ij} + 1) \text{ [54]} \qquad (5.5\text{-}2)$$

where G(x) is an un-normalised Gaussian function,

$$G(x) = e^{\left[\frac{-x^2}{2\sigma^2}\right]} \qquad (5.5\text{-}3)$$

the unit vector $\hat{i}_k$ represents the k^{th} arm of the i^{th} particle, and $\hat{u}_{ij}$ is the unit vector joining the centre of the molecule i to the centre of molecule j. The parameters ε_{HB} = -1 and r_{HB} = 1 define the optimal hydrogen bond energy and bond length.

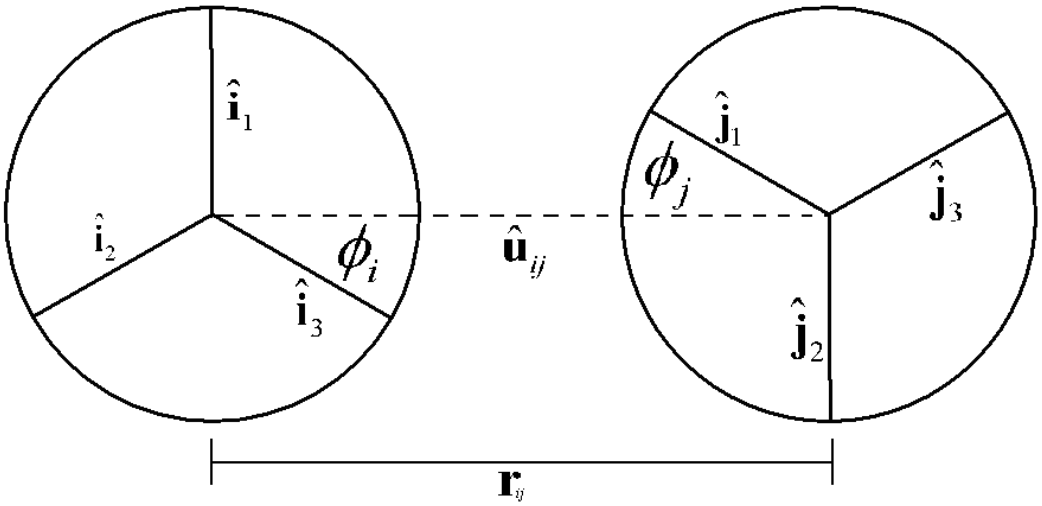

Figure 5.5-3 *Two MB water molecules, separated by a distance r_{ij}.*

5.6 Buzano Model

The Buzano model is a model that uses the Mercedes-Benz logo as seen in figure 5.5-2 to represent water [55]. The model used is a two-dimensional triangular lattice. Each lattice site can be occupied or empty. There are two energy terms in action in this system, a van der Waals potential and energy due to hydrogen bonding. Two nearest neighbour water molecules exert an attractive force $-\varepsilon < 0$ to represent the van der Waals potential. The arms can form hydrogen bonds with each other. Whenever two arms from nearest neighbours point towards each other, hydrogen bonds are formed. When a hydrogen bond is formed, the resulting energy is increased by $-\eta < 0$.

Due to the lattice structure of the model, each water molecule can form at most three hydrogen bonds, and has only two bonding orientations. In the Buzano model there are 22 possible orientations.

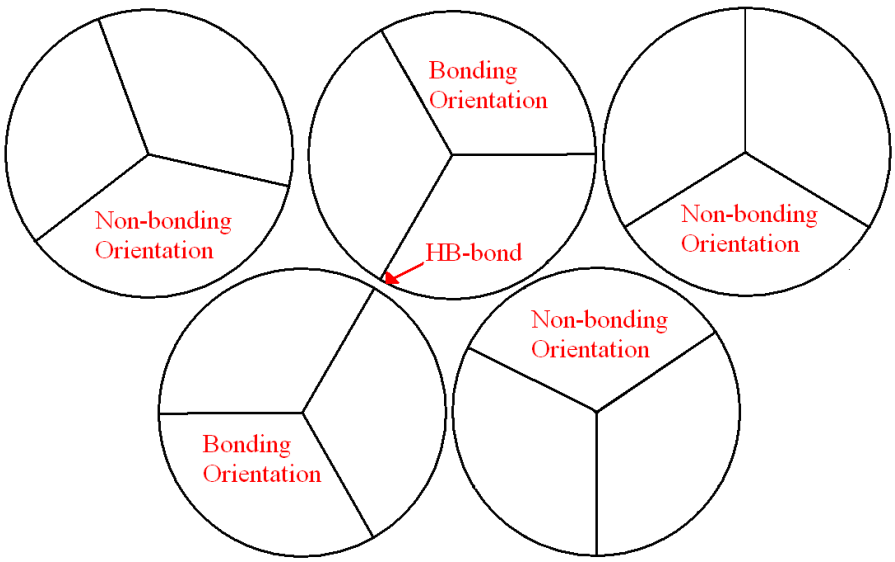

Figure 5.6-1 *Some of the possible orientations in the Buzano model. The two bonding orientations and some non-bonding orientations are included.*

Within this model penalties introduced that weaken the hydrogen bonds. They occur whenever either of the two sites nearest a hydrogen bond, in a location called the next nearest neighbour, is occupied as indicated in figure 5.6-2. This penalty is $c\eta/2$ ($c \in [0,1]$).

In this model the hydrogen bonding strength is three times stronger then the van der Waals potential, which is set to 1.

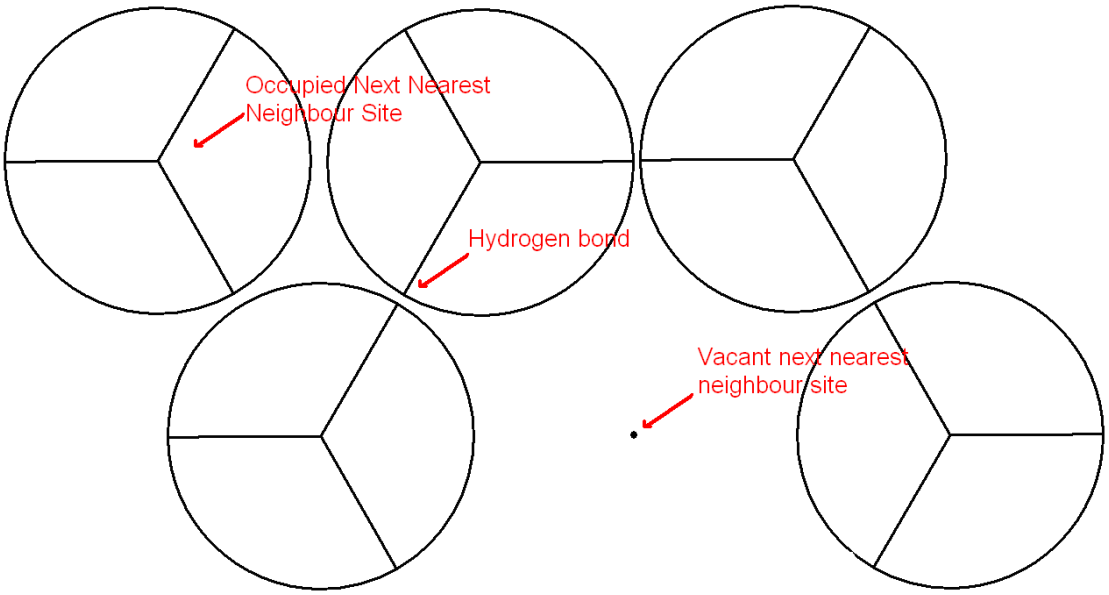

Figure 5.6-2 *Next Nearest Neighbour*.

In this study, a modified version of the Buzano model was used. The number of orientations was restricted to three from 22 in the original Buzano model. The number of orientations was chosen after testing indicated that three orientations gave a more obvious temperature of maximum density peak as it increased the likelihood of hydrogen bonds forming. As with the Buzano model, only two of the orientations allowed for hydrogen bonding to occur.

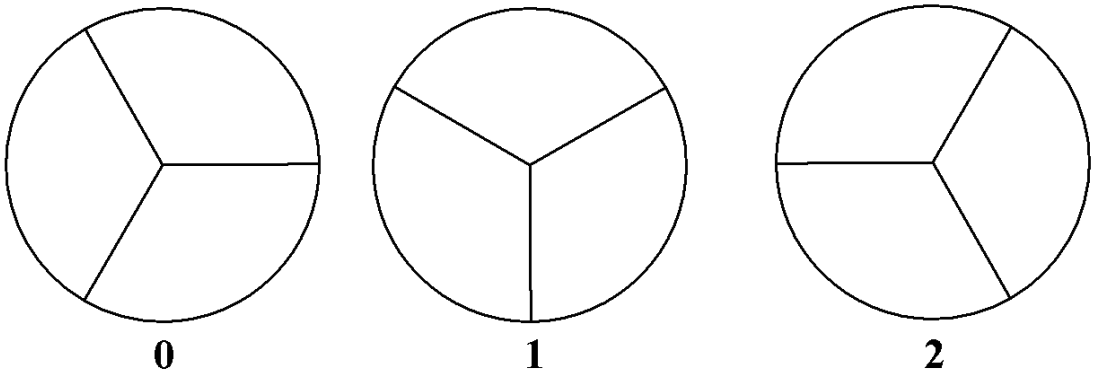

Figure 5.6-3 *The three possible MB orientations*.

Orientations 0 and 2 allow for the occurrence of hydrogen bonding. Periodic wrap around is used to simulate the larger lattice sizes and to reduce boundary issues.

Periodic wrap around simulates a larger lattice size by replicating the lattice 8 times and allowing molecules at the boundary to interact with molecules in the replicated regions. This can be seen in figure 5.6-4 where a 6 x 4 lattice is shown in the centre, surrounded by 8 copies of the same lattice. Using this periodic boundary condition, the smallest meaningful lattice size which is capable of reproducing the low density 'ice' configuration in pure water is a 3 x 2 lattice , with two of the sites vacant, giving a density of 0.667 [44]. This means that any lattice size should be a multiple of this primitive cell as indicated in figure 5.6-5. Tests have been carried out on 6 x 4, 9 x 6 and 12 x 8 lattices; all of which produced similar results in terms of observed shifts in the temperature of maximum density. A version of this modified model was developed using a Metropolis sampling algorithm to allow for visual inspections of the system at a given temperature T as well as for the Wang-Landau algorithm. The results obtained from the Buzano gas-lattice model are presented in section 5.8.

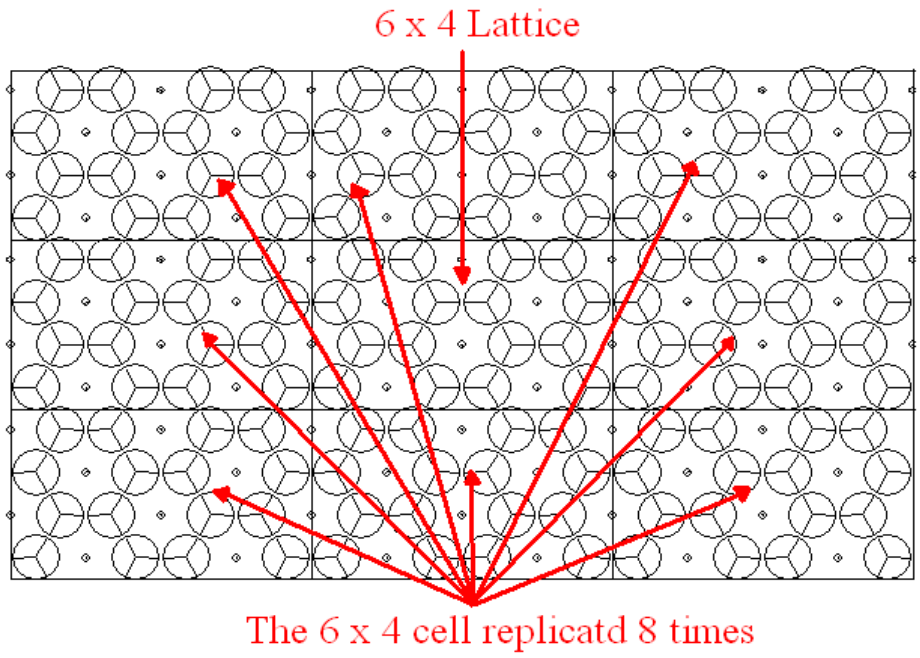

Figure 5.6-4 *Periodic boundary conditions simulate a much bigger lattice size.*

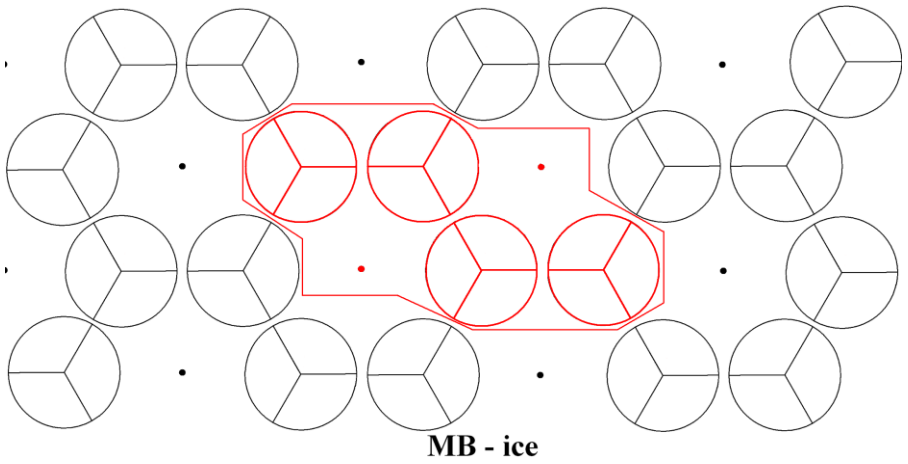

Figure 5.6-5 *The primitive cell (3 x 2) indicated in red.*

5.7 Off-Lattice Monte Carlo Simulations.

In this model, the molecules are free to move within the 2-D region unlike in the gas-lattice model where the molecules are only able to occupy fixed sites. Within this model, one of two moves take place, either one molecule is selected at random and its position of orientation is changed, or the volume of the entire lattice is changed by a small amount. The change in energy gets calculated after the change and its acceptance is decided by the rules described in the section describing the Metropolis Importance sampling (5.3.1).

The off-lattice code used for the simulations was developed in C++ and was written in a structured style. This allowed for an easy change from two to three dimensions, or from an MB model to a cross style model for testing purposes. The structured style also enhances the readability of the code.

Within the code there are eight functions excluding the main function. A flow chart in figure 5.7-1 indicates the order in which the functions are called.

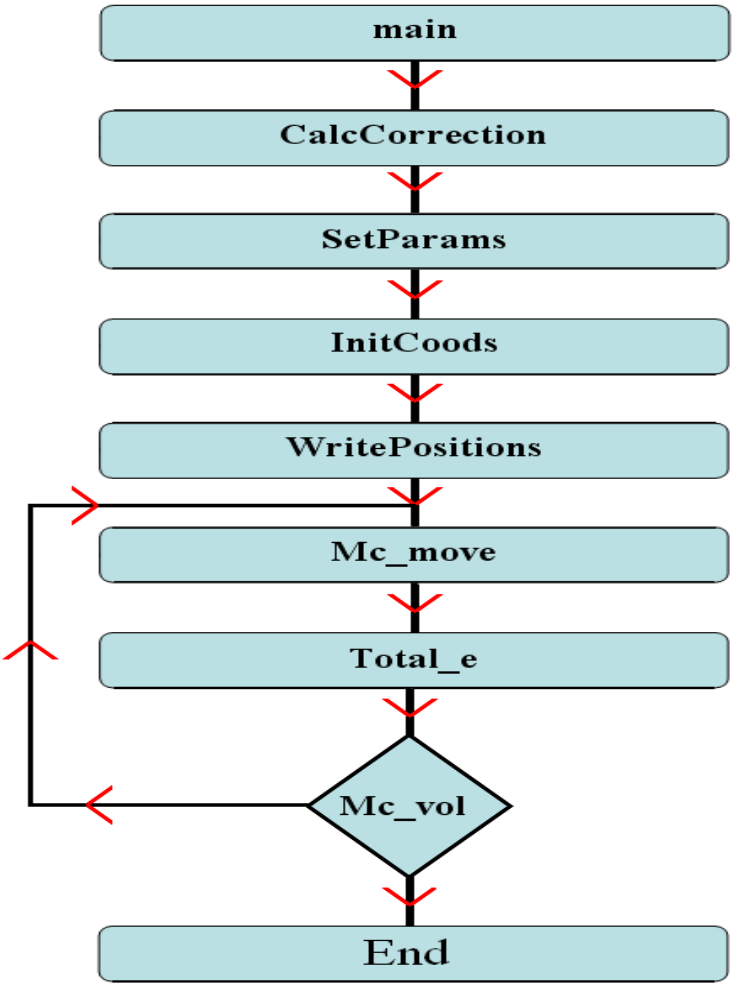

Figure 5.7-1 *Flow chart indicating how each function is called.*

SetParams: This function sets up the initial starting parameters. The cut-off distance, temperature, pressure, MB molecule area and number of cycles are some of the parameters given values here.

InitCoords: A vector cc is created for every molecule in the system and assigned a random value corresponding to a position between –0.5 and 0.5.

Total_e: This function calculates the distance between every pair of molecules. If the distance is less then the cut-off distance, it calculates the LJ energy for that pair and adds it to the total energy of the system.

Mc_move: This is the function that moves the molecules in the system. It also stores the positions of the molecules prior to the move, so

that if the move is rejected due to the new state of the system having a higher energy, the original positions can be restored.

Mc_vol: Similar to Mc_move except that this time the volume is changed by a small amount. Again the positions of molecules within the system prior to any change are recorded in case the new state of the system is rejected.

CalcCorrection: Here there is an attempt to reduce the effects of the cut-off distance approximation. A correction is to the energy, density and cut-off energy.

WritePositions: The last function called simple writes the final positions to file.

5.7.1 Off-Lattice Simulation Results

Although the code that has been developed allows for scans of both pressure and temperature, it can be very useful to do single runs. After a single run, the output file consists of a list of vectors associated with the locations of the molecules. The initial molecule locations are also recorded. This allows for the locations of the molecules before and after to be compared. To do this a separate MathLab script was written. Below are a few examples of simulations that were run. The first picture (figure 5.7-2) shows a randomly generated system. It consists of 4 randomly placed MB-molecules with no pattern. The system is allowed to evolve at a low temperature. This causes the arms to line up, and a hexagonal structure begins to appear, as can be seen in figure 5.7-3 Every molecule has formed bonds with three other molecules, this along with the separation of 120° between the arms causes the structure to form a regular hexagon. This figure is close to MB ice, which forms at low temperatures.

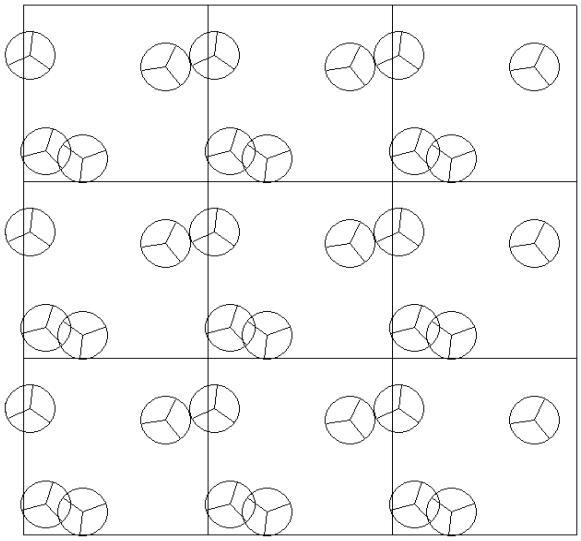

Figure 5.7-2 4-*molecule MB system before settling into a lower energy state*.

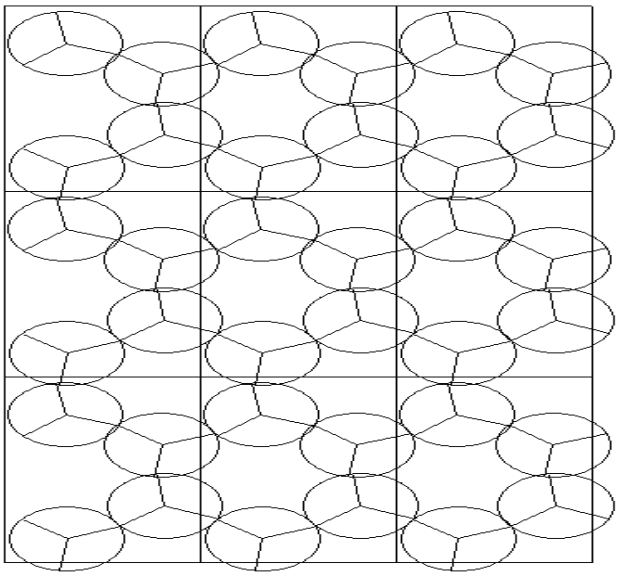

Figure 5.7-3 *4-molecule MB system after settling into a lower energy state*.

Simulations were then carried out with 8 molecules and 16 molecules. Figure 5.7-4 shows the 8 molecule system at the start of the simulation and figure 5.7-5 shows the system after five-million cycles have been completed. In figure 5.7-4 the molecules are positioned randomly and as a result the energy is high. After the system has evolved at a low temperature, MB-ice forms, as can be seen in figure 5.7-5.

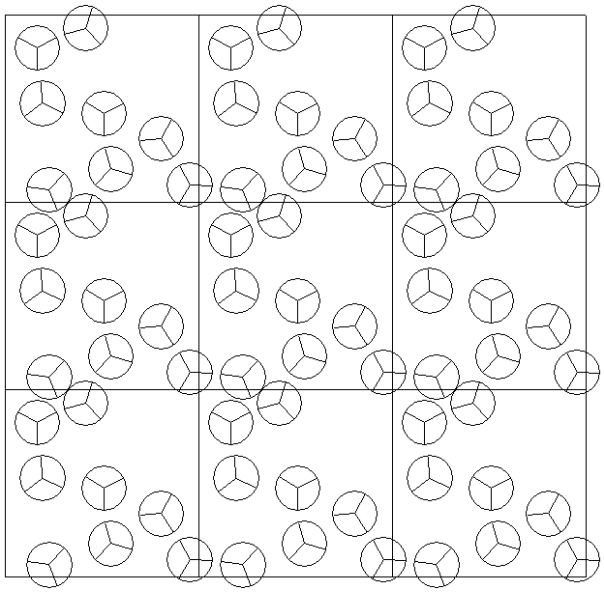

Figure 5.7-4 *8-molecule MB system before settling into a lower energy state.*

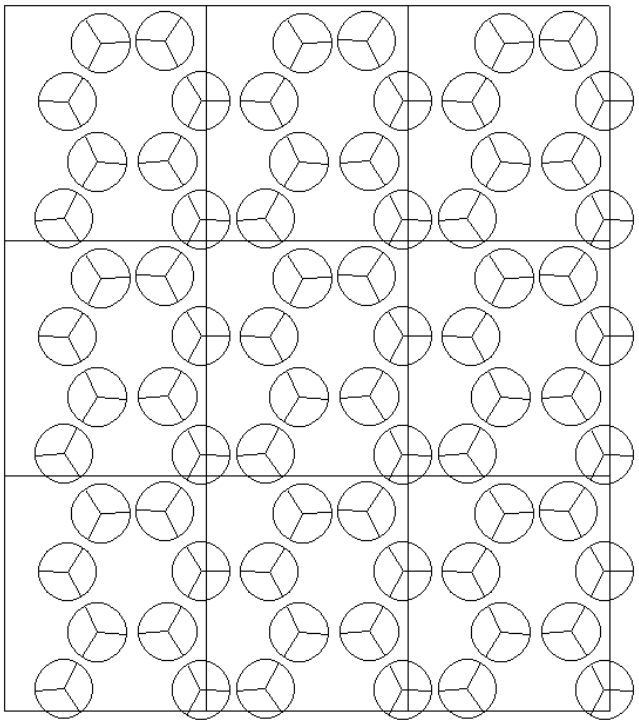

Figure 5.7-5 *8-molecule MB system after settling into a lower energy state*.

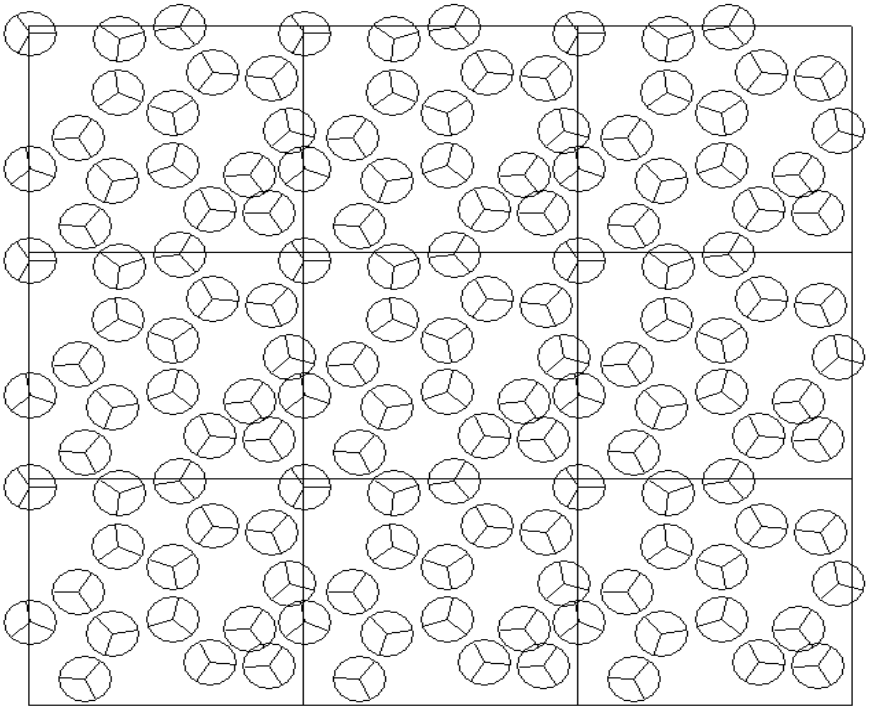

Figure 5.7-6 *16-molecule MB system after settling into a lower energy state*.

Figure 5.7-6 shows a 16 molecule system that has been allowed to evolve through the same five-million cycles at the 8 molecule system. As can be seen the MB-ice has not yet formed. This is one of the problems with the off-lattice model, even though this simulation took over twice the time to run, it still has not settled into its lowest energy state. If the simulation was run for a longer period of time it would eventually reach the MB-ice state but this becomes more impractical as the number of molecules is increased.

The off-lattice model has another problem associated with it: sometimes the system gets 'stuck' in a local energy minimum. When this happens the model fails to reach the true minimum energy for the given temperature. This is what happened in figure 5.7-7. It can be seen that the movement of any individual molecule will cause the energy to rise considerably and as a consequence all such moves have a high probability of getting rejected. This problem could be alleviated with changes in the code; however other avenues were investigated which appeared to give better results.

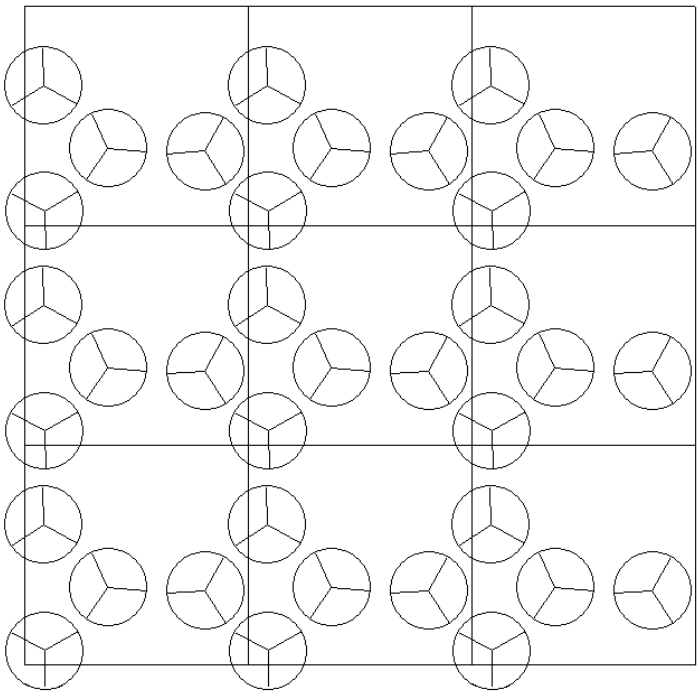

Figure 5.7-7 *4 molecule system stuck in a local energy minimum.*

5.8 Gas Lattice Modelling

5.8.1 Metropolis Importance sampling using a modified Buzano Model and Mercedes-Benz water Molecule

Metropolis Importance sampling was used throughout this study to allow for 'snap shots' of the system to be obtained. These snap shots allowed a visual inspection of the system to be made at a given temperature. Temperature scans were also carried out using Metropolis Importance sampling, however as seen before these tend to be subject to noise. Figure 5.8-1 shows a typical reduced density versus reduced temperature scan obtained from the Metropolis Importance sampling code. The 'reduced' terms indicated that in these simulations k_B is set to 1, as is ε which is the energy associated with the van der Waals type force. Figure 5.8-2 shows a 'snap shot' of the system at the points A, B and C as indicated in figure 5.8-1. The simulation was for a pure water sample, using a 6 x 4 lattice.

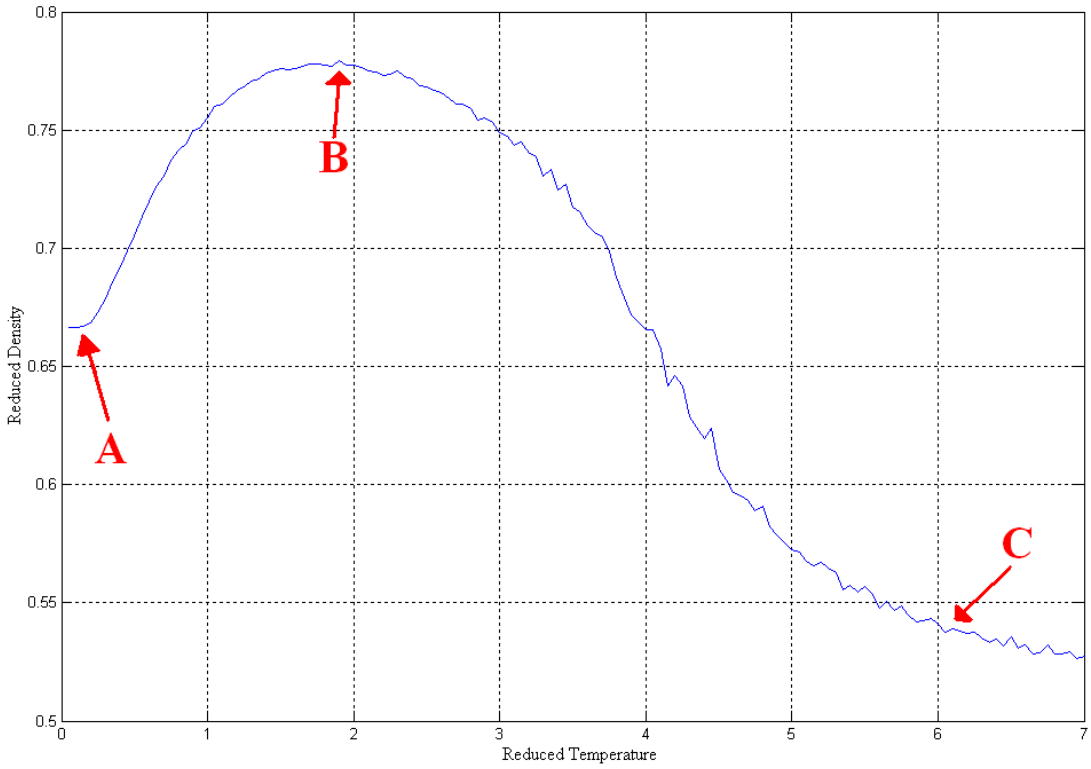

Figure 5.8-1 *Density versus temperature graph obtained from running a 6 x 4 pure water simulation using the Metropolis Importance Sampling algorithm.*

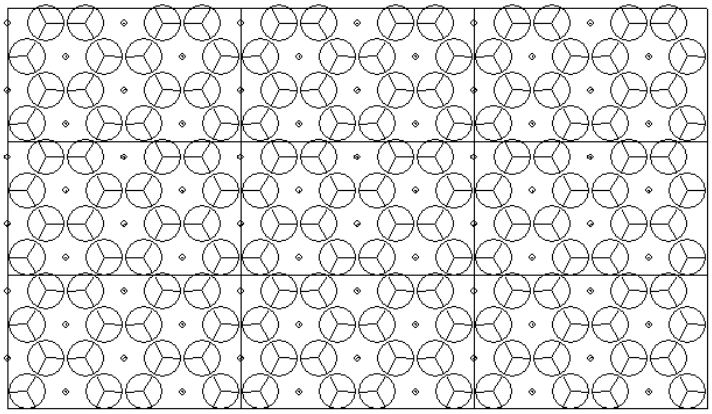

(A) Low density MB-ice state

Reduced temperature: 0.05

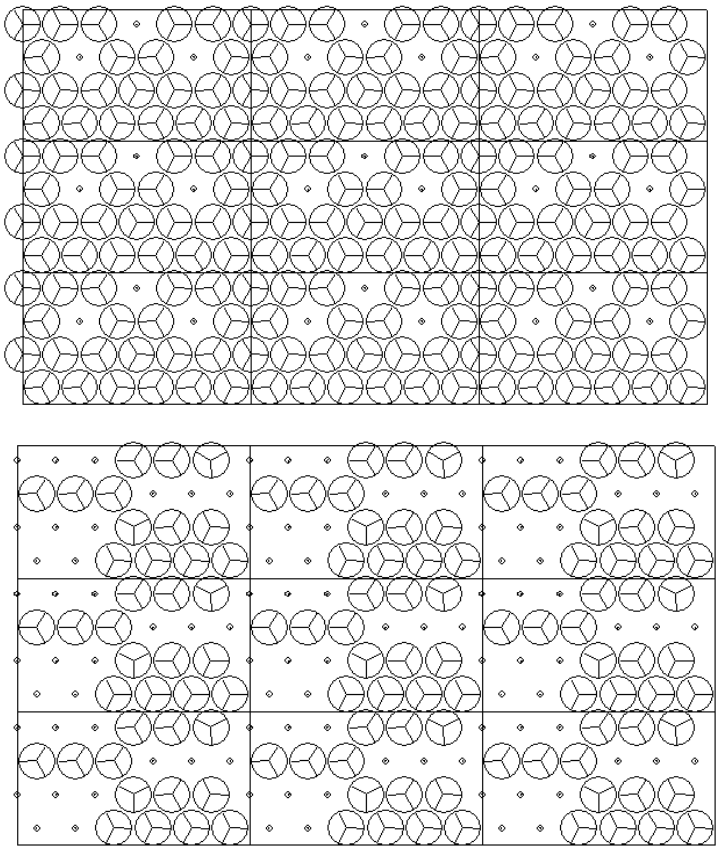

(B) High density

Reduced temperature: 1.9

(C) Low density

Reduced temperature: 6

Figure 5.8-2 *Snap Shots of the system in (A) MB-ice9, (B) State of Maximum Density and (C) A low density state.*

MB-ice is a low density structure with all possible hydrogen bonds active. In MB-ice, six molecules form a hexagon shape around a vacant site. This MB-ice structure can be seen in figure 5.8-2 (A). The low density MB-ice state, looks very similar to that obtained from the off-lattice simulations in figure 5.7-3. As the temperature increases towards the temperature of maximum density the hydrogen bonding seen in (A) is still present as seen in (B). The density is increased however by the presence of extra molecules in the centre of the hexagons. These extra molecules cannot form hydrogen bonds. As the temperature increases further, the hydrogen bonds break down and the thermal excitations reduce the number of molecules.

5.8.2 Wang-Landau algorithm using a modified Buzano Model and Mercedes-Benz water Molecule

As with the previous simulations the program used to develop the modified Buzano model using a Wang-Landau algorithm was written in a structured C code, compiled in Dev-C++. Within the code there are 8 functions excluding the main function. The chart in figure 5.indicates how the functions are called. Below is a brief description of what each function does when called.

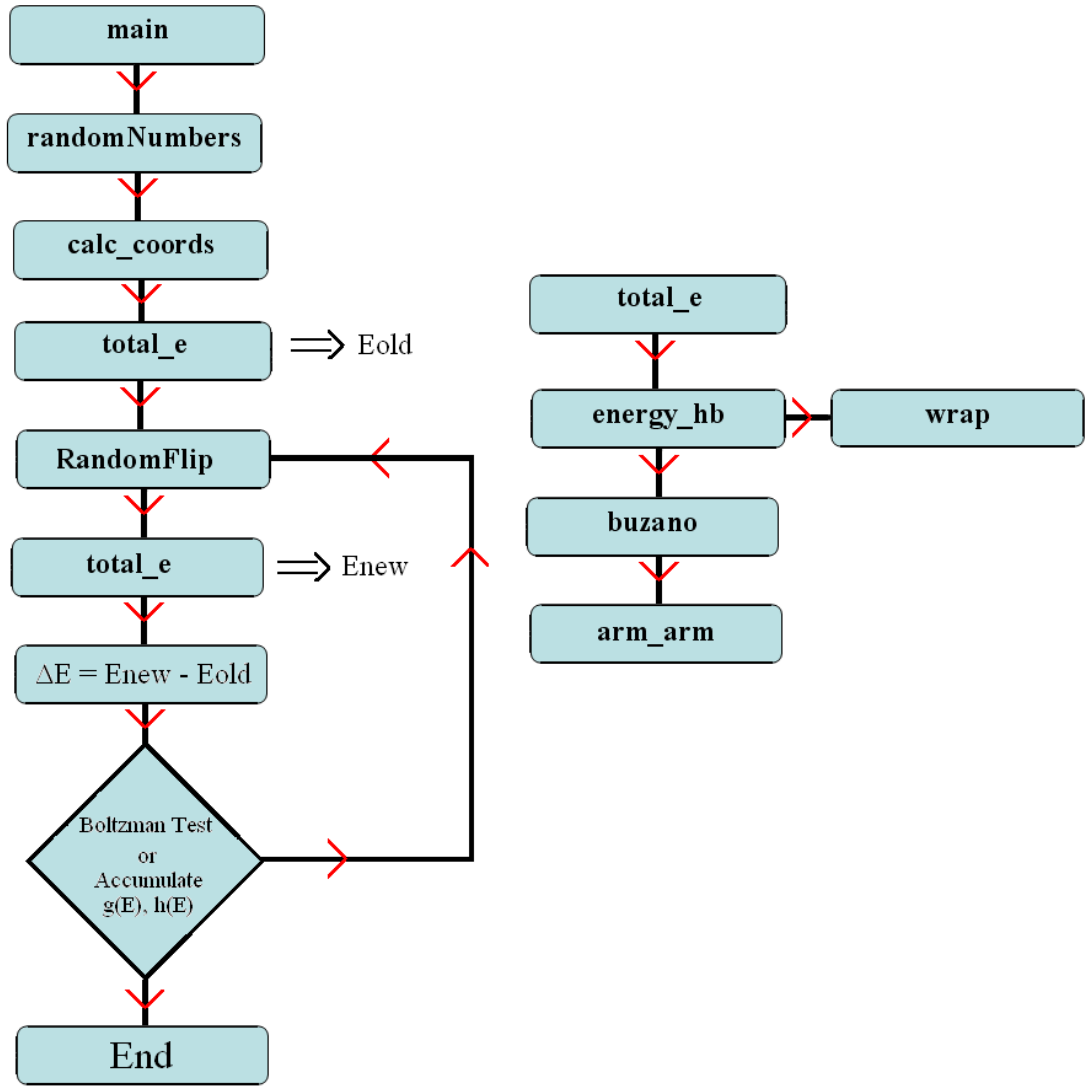

Figure 5.8.3 *Chart indicating flow of control of the lattice simulation control program.*

randomNumber: used in the simulations where molecules are inserted into the lattice. It randomly selects a number of sites to insert single molecules or dimers depending on the test being carried out.

calc_coords: A function called early in the main function to randomly set each of the sites in the lattice to be occupied or empty, and to set its orientation if occupied.

RandomFlip: A function that is used to randomly pick a site to flip either the orientation of an MB molecule, or the sites occupancy. There is a 50% chance of the type of flip made.

wrap: Is used to allow for wrap around to try reduce boundary problems, also prevents out of bounds problems within arrays.

energy_hb: For a given lattice site, it checks the states of the nearest neighbours, calls wrap, and then arm_arm. Also checks the states of the next nearest neighbours to see if there needs to be a penalty incurred by calling the buzano function.

arm_arm: checks to see if the arms of the current site are aligned to those of the nearest neighbours. If they are it sets a flag.

total_e: This function is used to calculate the total energy after any penalties are subtracted.

buzano: This function takes information from the energy_hb2 method about the states of the next nearest neighbours. If they are active beside a formed hydrogen bond, the bond is weakened, and as a result a penalty is incurred.

Within the main function, the ‘ghist’ and ‘ehist’ values are updated, as well as the Boltzmann distribution testing.

It has been shown in section 5.8.1 that the Metropolis Importance sampling algorithm can be used to conduct temperature scans. However, the Wang-Landau algorithm is much better suited to this task. The simplest MB Wang-Landau

simulation consists of the same 6 X 4 triangular lattice as used in the Metropolis sampling simulation. Once the simulation has run the code outputs a file that contains the energy histogram ('ehist') and the density of states ('ghist'). From this point a post processing code is run. This code uses the ghist histogram to produce a file that contains the energy per molecule, density, Helmholtz function and the entropy for a given temperature range. Within the post-processing code there is a variable μ, which is the chemical potential (in this case pressure). This allows for pressure scans on a given simulation without the requirement of re-running the simulation each time.

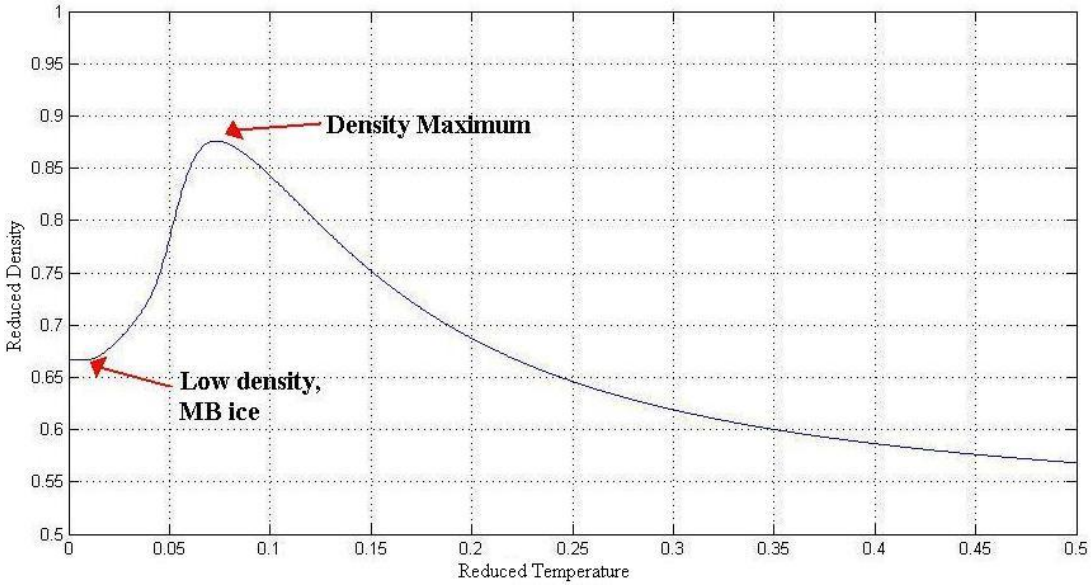

Figure 5.8.4 *Graph of reduced density versus reduced temperature for a 6 X 4 lattice, μ = -0.5.*

Figure 5.8-4 shows a graph of energy/molecule versus reduced temperature T for μ = -0.5. Figure 5.8-5 shows the energy per molecule versus T. At low temperatures, corresponding to the MB ice, the energy per molecule is –4. This is as expected, given that in the ice stage, each molecule is bonded with exactly 3 other molecules. Each of these bonds has a contribution to the over all energy of –4; -3 for the hydrogen bonding, and –1 for the Van der Waals forces. From the density versus T graph it is clear that only two-thirds of the molecules are active. Therefore the total

energy contribution of a single triple bonded molecule is –12. Summing this for all bonding molecules, dividing by two to account for double counting, the total energy of the system is –96. This works out as –4 per molecule. The equation the total energy of the system is given in (5.8-1)

$$E = \frac{-\sum_{\forall ij, i \neq j} (HB_{ij} + LJ_{ij})}{2} \qquad (5.8\text{-}1)$$

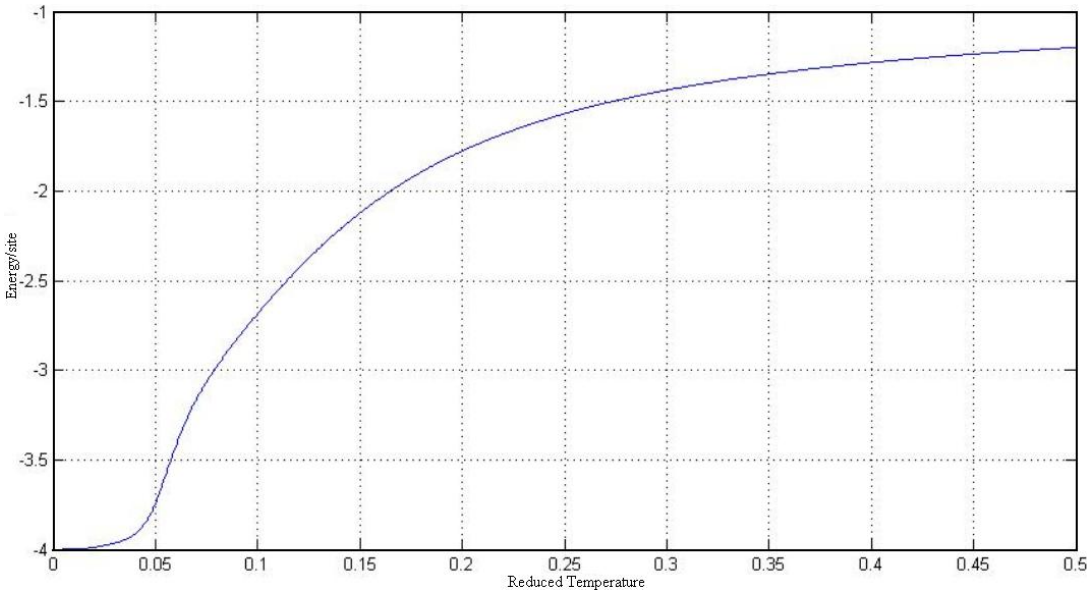

Figure 5.8.5 *Graph of energy/molecule versus T for a 6 X 4 lattice, μ = -0.5.*

As discussed earlier, it is possible to do a pressure μ_d (chemical potential) scan using the Wang-Landau algorithm. A graph of such a scan can be seen in figure 5.8-6. The scan was conducted on a 6 x 4 lattice with 3 possible orientations per molecule. From experimental work carried out by Caldwell [43], it is known that the temperature of the density maximum of water should decrease as the pressure increases. The decrease should be linear.

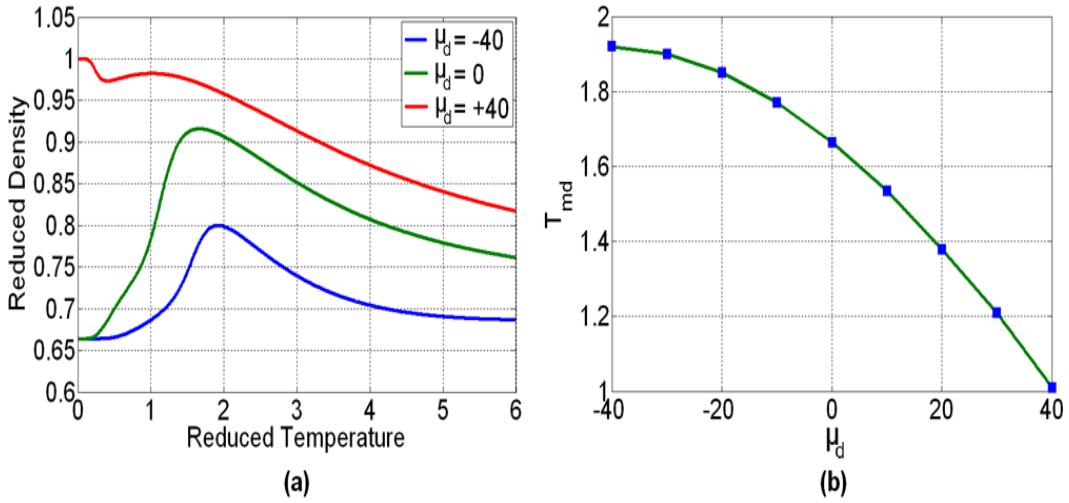

Figure 5.8-6 (a) *Reduced density versus reduced temperature for pure water at various pressure values μ_d.*

Figure 5.8-6 (b) *Temperature of maximum density (T_{md}) versus pressure for pure water.*

5.9 Modifying the Model to Simulate the Introduction of Solutes to Water

5.9.1 Adding Neutral Molecules to the Lattice

The primary goal of this research has been to study the effects on the temperature of maximum density of the addition of solutes. To this point all the microscopic work has involved simulating some features of water, primarily the maximum density anomaly. To understand what causes the temperature of maximum density to change as a function of solute concentration, attempts were made to simulate the results obtained experimentally. The solutes that decrease the temperature of maximum density linearly as a function of solute concentration such as sucrose and NaCl were investigated first. Figure 5.8-5 (B) shows a snap-shot of water at its maximum density. It is clear that there is a lot of hydrogen bonding in this state. Since the addition of sucrose and NaCl decrease the temperature of maximum density, neutral molecules were added to the lattice to see what effect this had on the temperature of maximum density.

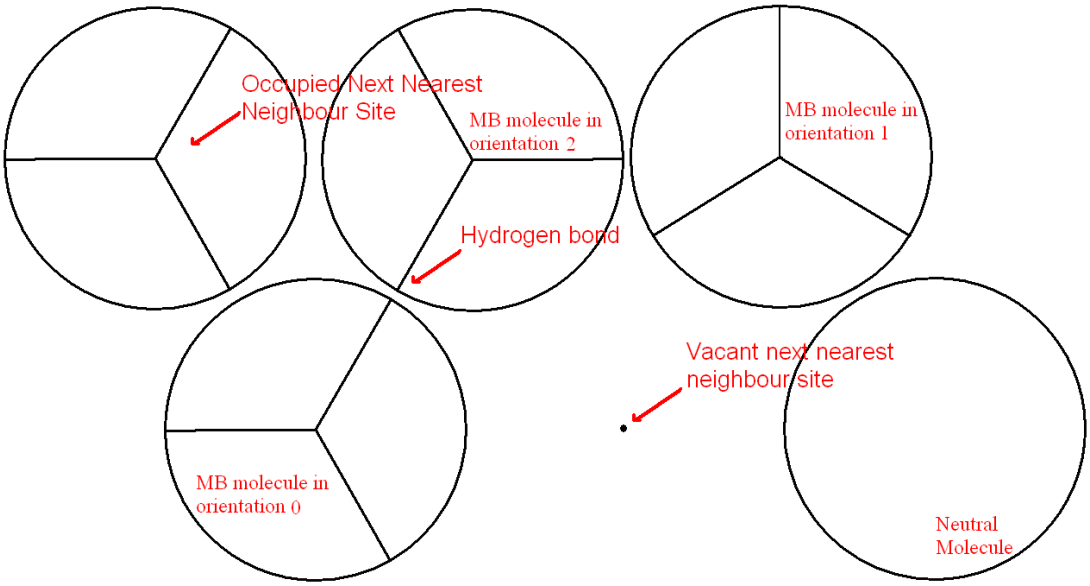

Figure 5.9-1 *The forth type of molecule, the neutral molecule.*

The neutral molecule is simply a molecule that has no arms and as a result cannot take part in hydrogen bonding. The neutral molecule still contributes to the total energy as a result of the Van der Waals forces. At the beginning of each simulation, a fixed number of neutral molecules were inserted into the lattice and placed at random locations, and the simulation was then run as normal. For these simulations, a 9 x 6 lattice was used and the chemical potential was kept at $\mu = -0.5$. Figure 5.9-2 shows the results obtained from inserting up to twelve molecules into the lattice. The graph shows that as the number of neutral molecules added to the lattice is increased, the temperature of maximum density does decrease. Figure 5.9-3 shows how the density changes as the number of neutral molecules increases. The density increases as expected as in the limit as all the molecules are changed to neutral molecules, it becomes impossible to reproduce the MB-ice state as there are no Buzano penalties due to there being no hydrogen bonding. As a result of this, increasing the concentration of neutral molecules will result in a density of 1 at low temperatures.

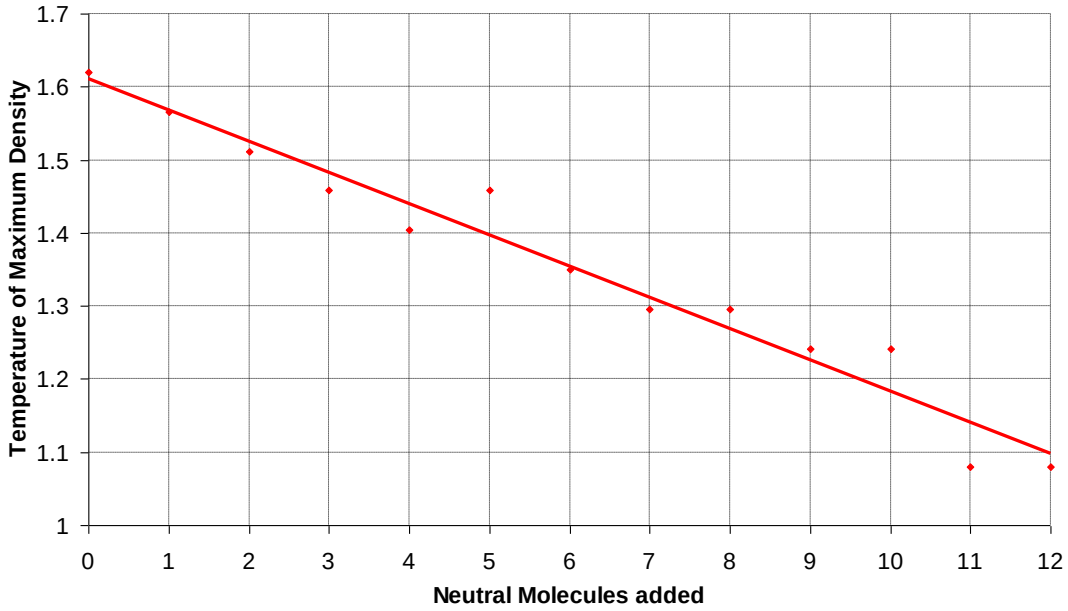

Figure 5.9-2 *Temperature of maximum density versus number of neutral molecules inserted for a 9 x 6 lattice with a chemical potential μ = -0.5.*

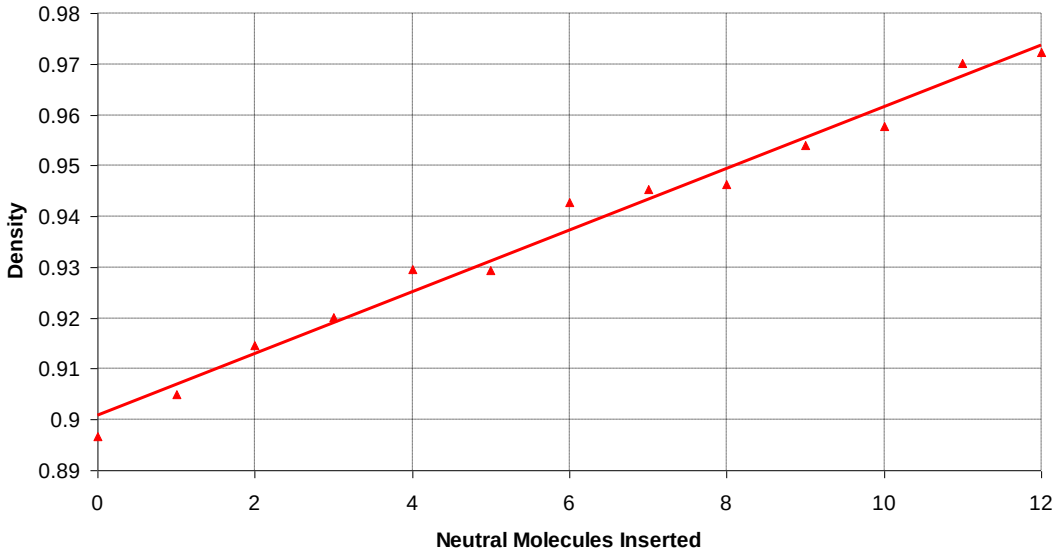

Figure 5.9-3 *Density versus Neutral molecules inserted for a 9 x 6 lattice with a chemical potential μ = -0.5.*

The next step was to add neutral dimers to the lattice. A neutral dimer consists of two neutral molecules bonded to each other. It would be expected that this addition

would have a similar effect to that seen previously with the addition of various numbers of single molecules. Figure 5.9-4 shows a neutral dimer.

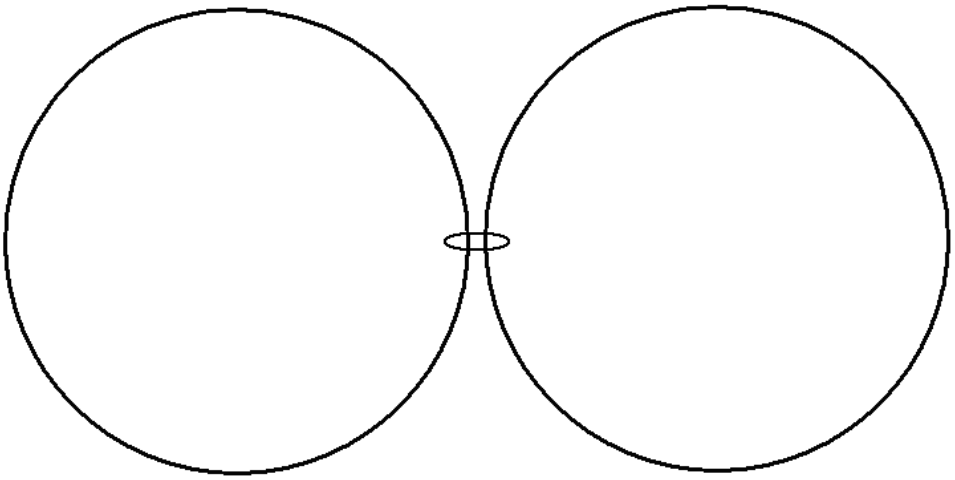

Figure 5.9-4 *Neutral Dimer.*

These tests involved adding between zero and six neutral dimers to the lattice. The sites that each neutral dimer was located were chosen at random. For each extra dimer added, a scan of the chemical potential (pressure) was also conducted. This allowed for information on the temperature of maximum density as a function of dimer concentration, temperature of maximum density as a function of chemical potential, and density at the temperature of maximum density versus temperature to be obtained. Figure 5.9-5 shows the results of the addition on neutral dimers.

Figure 5.9-5 *Temperature of maximum density versus number of neutral dimers inserted for a 9 x 6 lattice with a chemical potential μ = -0.5.*

Figure 5.9-6 shows a graph of the density at the temperature of maximum density versus chemical potential (pressure) for various numbers of neutral dimer. As expected the density rises as the pressure increases, as well as increasing as the concentration of neutral molecules increases. As the pressure increases, the effect of the added neutral dimers has less of an effect on the density, this can be seen by the convergence of the lines associated with each neutral dimer insert in figure 5.9-6.

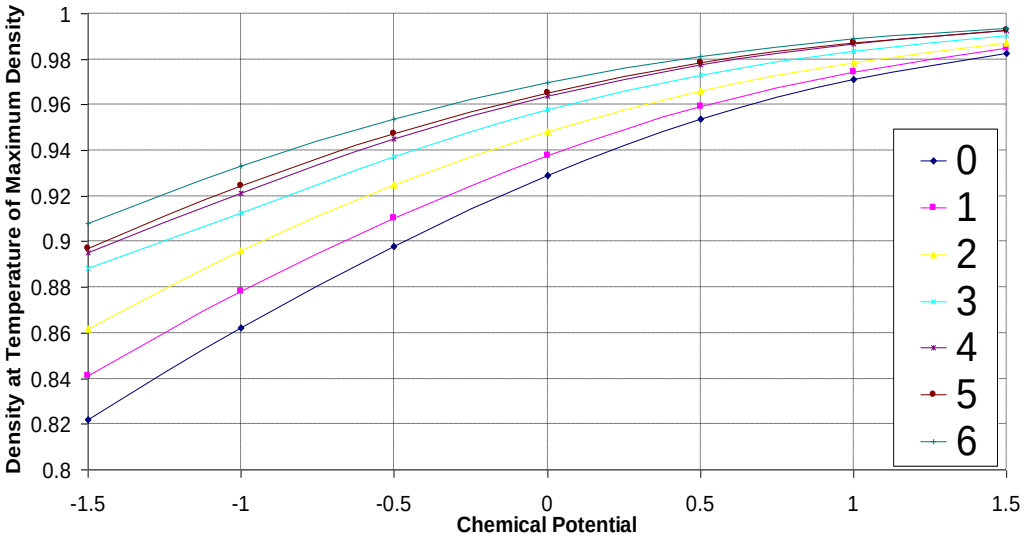

Figure 5.9-6 *Density at the temperature of maximum density versus chemical potential μ, for various numbers of neutral dimers.*

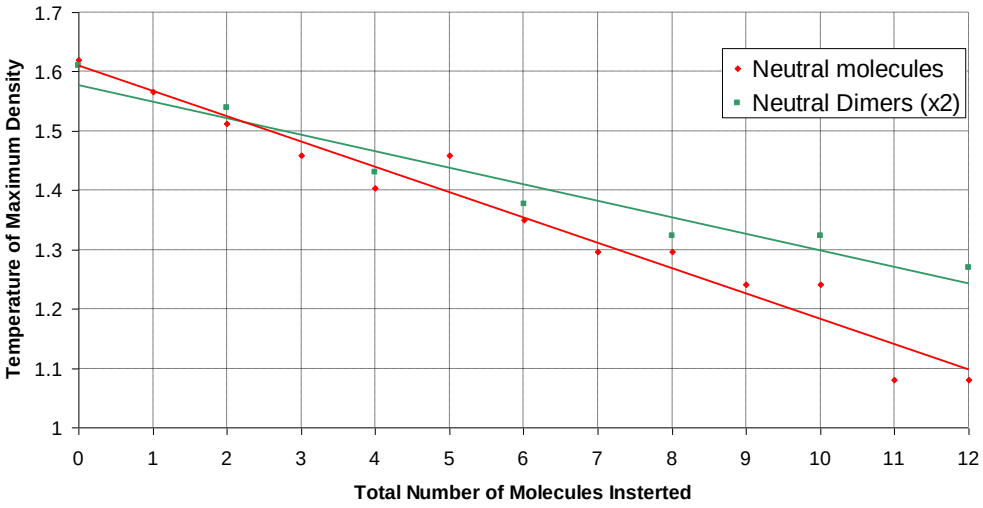

Figure 5.9-7 *The effects of neutral molecules on the temperature of maximum density compared with the effects of neutral dimers on the temperature of maximum density.*

Figure 5.9-7 compares the effect on the temperature of maximum density of introducing neutral molecules to that of introducing neutral dimers. The neutral dimers cause a smaller change in temperature of maximum density per molecule then an equivalent number of neutral molecules. This is as expected, because if a neutral molecule is inserted at a given site location, it will disrupt the formation of hydrogen bonding in that area, the addition of the second neutral molecule will have the same effect at a different location. When a neutral dimer is inserted (two molecules) it too will disrupt the formation of the hydrogen bonds, but its effects are more localised then when two individual molecules are added.

5.9.2 Adding Bonding Molecules to the Lattice

In this section, the addition of extra bonding molecules is discussed. As with the neutral molecules, a lattice site is chosen at random. Then a bonding orientation is chosen at random (either orientation 0 or 2 in figure 5.6-3). The orientation and location of the molecule is fixed once it has been inserted. By placing this extra bonding molecule it was expected to have one of two possible effects. If the molecule was placed in a location that was part of the MB-ice phase, and in the right

orientation, it would have a positive effect on the temperature of maximum density as it promoted the formation of hydrogen bonding. However, if the site chosen at random was not active as part of the MB-ice structure, placing a molecule there in any orientation would have a disruptive influence. It would cause the MB-ice to break up sooner and as a result reduce the temperature of maximum density. From this understanding, it was expected that the resulting graph of temperature of maximum density versus will not show a linear trend, but will show small increases and decreases in the temperature of maximum density as the concentration of bonding molecules increases. Figure 5.9-8 shows this result. It is clear that the results depend on the location of the molecules as is shown by the 3 separate results obtained by changing the random seed. Figure 5.9-9 shows the average temperature of maximum density versus the number of bonding molecules inserted.

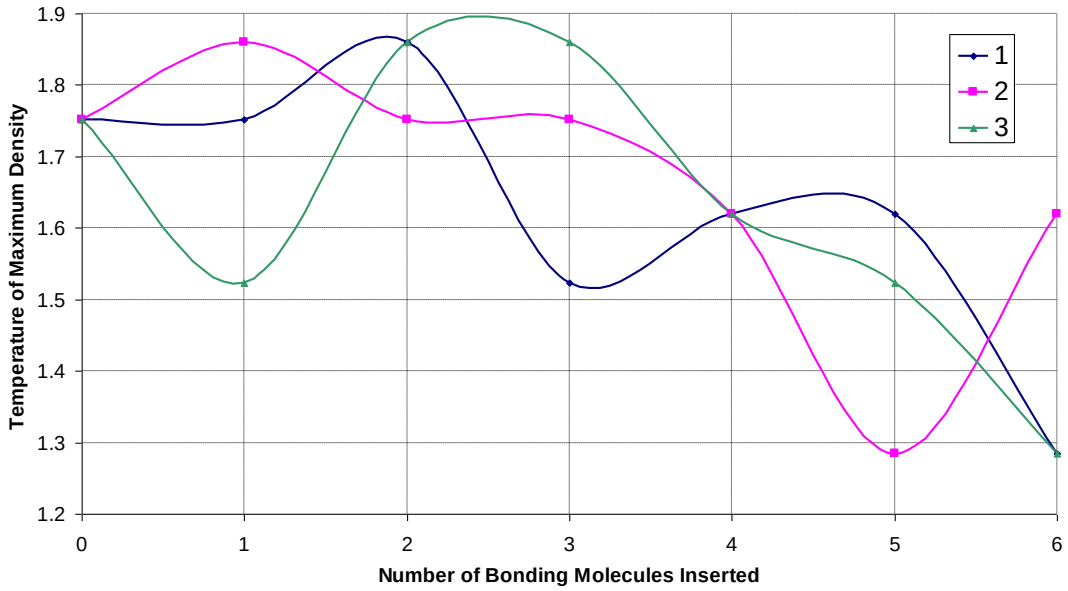

Figure 5.9-8 *Temperature of maximum density versus the number of bonding molecules inserted into the 9 x 6 lattice conducted with 3 different random seeds.*

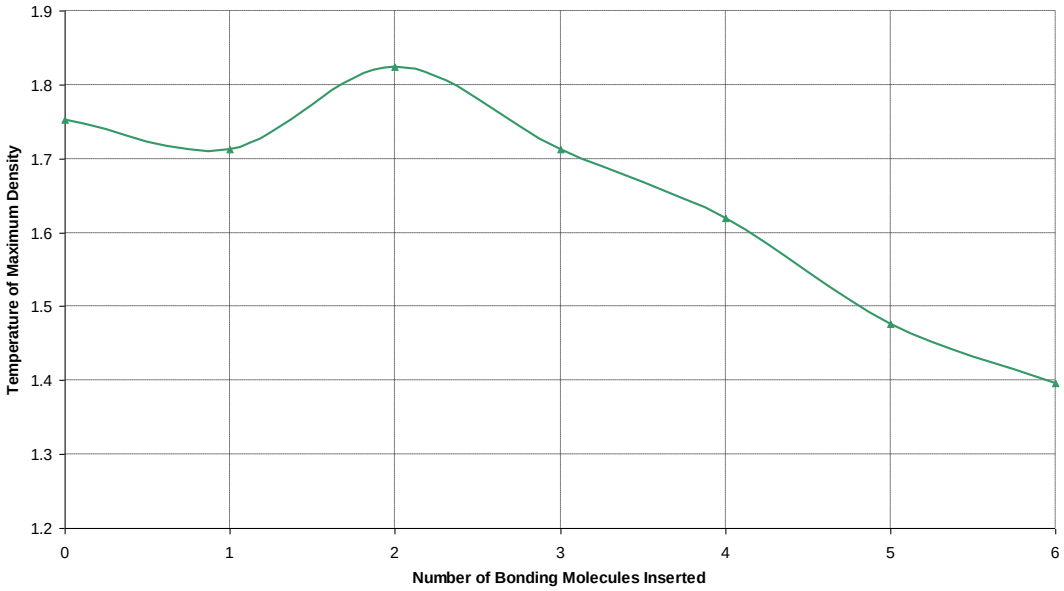

Figure 5.9-9 Average t*emperature of maximum density versus the number of bonding molecules inserted into the 9 x 6 lattice obtained from 3 simulations with different random seeds.*

As with the neutral molecules, the next step was to add a bonding dimer. This consisted of two MB molecules that formed a hydrogen bond with each other as seen in figure 5.9-10.

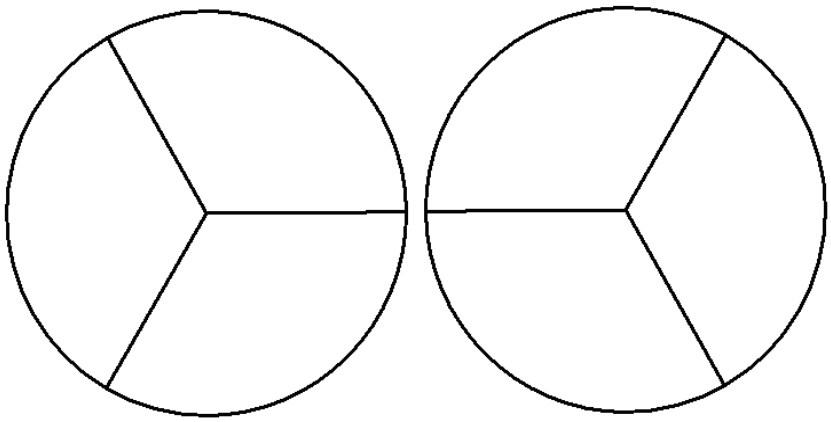

Figure 5.9-10 *A bonding dimer*.

This dimer was then inserted into the lattice at a random location. The effects of this bonded dimer on the temperature of maximum density were expected to be similar

to that of the bonding molecule. As with the bonding molecules, the effect the bonding dimers has on the temperature of maximum density is influenced by its position with in the lattice. The results of this can be seen in figure 5.9-11.

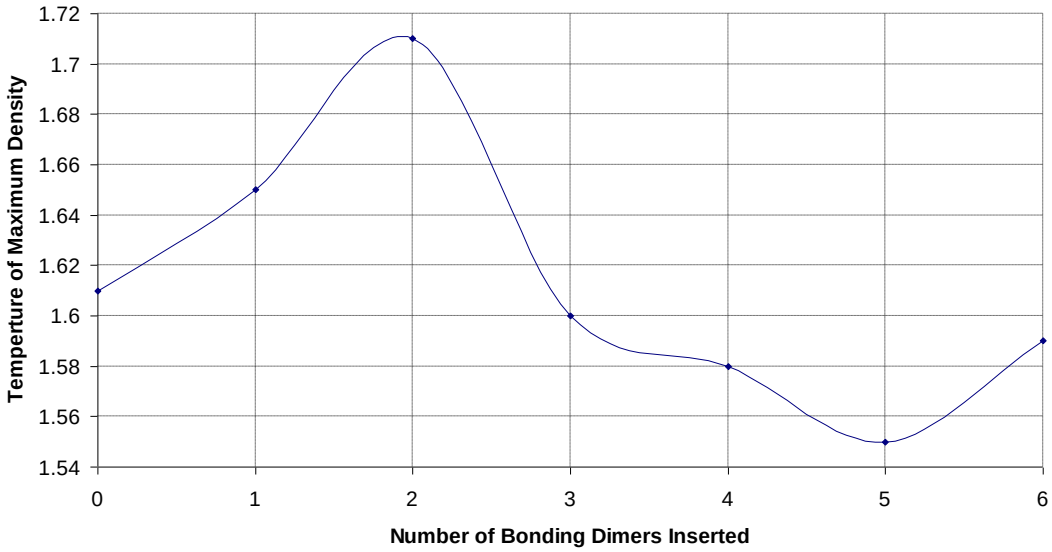

Figure 5.9-11 *Temperature of Maximum density versus the number of bonding dimers inserted in to the 9 x 6 lattice.*

Simulations involving bonding molecules and bonding dimers were carried out to see what it takes to increase the temperature of maximum density. It is indicated from these simulations that anything that promotes more hydrogen bonding will increase the temperature of maximum density.

5.10 Strong and Weak Water

A new version of the modified Buzano code using a Wang-Landau approach was developed to investigate the effect of changing the hydrogen bond strength. The new code called wl_conc was developed in such a way as to allow concentration scans. The concentration scans consist of adding various numbers of molecules with modified hydrogen bond strengths into the lattice with normal Mercedes-Benz molecules. The modification to the hydrogen bond strength is achieved by changing the radius of the molecule. A strong MB-molecule is one with the radius increased from 0.25 to 0.3 and a weak MB-molecule has the radius reduced to 0.125.

Although the molecule size may change for a given site, the centre to centre distance remains constant. The relative molecule sizes can be seen in figure 5.10-1.

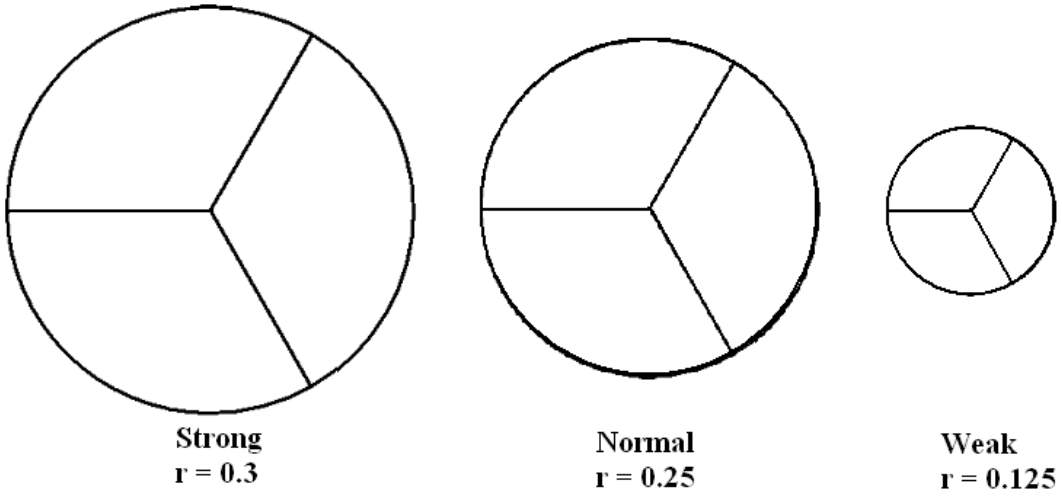

Figure 5.10-1 *Relative molecule sizes for Strong, Normal and Weak MB-molecules.*

When random flip is called, there are now 3 options, either a molecule can be turned on or off, rotated or the radius size can be changed. As with previous simulations conducted using the Wang-Landau algorithm, the density of states function is calculated. In the post-processing code, a new variable called μ_c controls the concentration of molecules with altered radii. At low values of μ_c there are no molecules with altered radii and so the lattice contains only normal MB-molecules. At high values of μ_c the only molecules in the lattice are ones with altered radii. In a simulation, either strong or weak molecules are mixed with the normal molecules.

Previous to this, all simulations involving the Wang-Landau algorithm were carried out by conducting an unbiased random walk in a two-dimensional space (section 5.3.2). A third dimension is now required to account for the concentration of strong or weak molecules within the lattice. This results in a density of state function of the form g(E, d, c), where E is the energy, d is the density and c is the concentration. The density d, and concentration c are defined in equation 5.10-1 and 5.10-2.

$$d = \frac{(N_o + N_s)}{N_{site}} \tag{5.10-1}$$

$$c = \frac{N_s}{(N_o + N_s)} \tag{5.10-2}$$

Here, N_{site} is the total number of lattice sites used in the simulation, N_o is the number of sites occupied by 'ordinary' water molecules, and N_s is the number of sites occupied by 'strong' water molecules [44]. (Simulations involving mixtures of ordinary and weak waters substitute N_w for N_s.) The partition function is given by:

$$Z = \sum_{E,d,c} g(E,d,c) e^{-E/kT} e^{\mu_d d/kT} e^{\mu_c c/kT}$$

The parameters μ_d and μ_c control the external pressure and the concentration level, respectively.

The first simulations carried out using the wl_conc code were conducted on strong MB-molecules. Once the simulation was completed, the μ_c value was varied between -200 to +200. The temperature of maximum density was recorded for each value of μ_c. For each value of μ_c 3 pressure values were investigated in the range μ_d = -40 up to μ_d = +40, the output from this investigation can be seen in figure 5.10-2. Figures 5.10-2(a) and (b) are both graphs of reduced density versus reduced temperature for strong water, the difference being the value of μ_c, figure 5.10-2(a) is a low concentration (μ_c = -200), and figure 5.10-2(b) is at a high concentration (μ_c = +200).

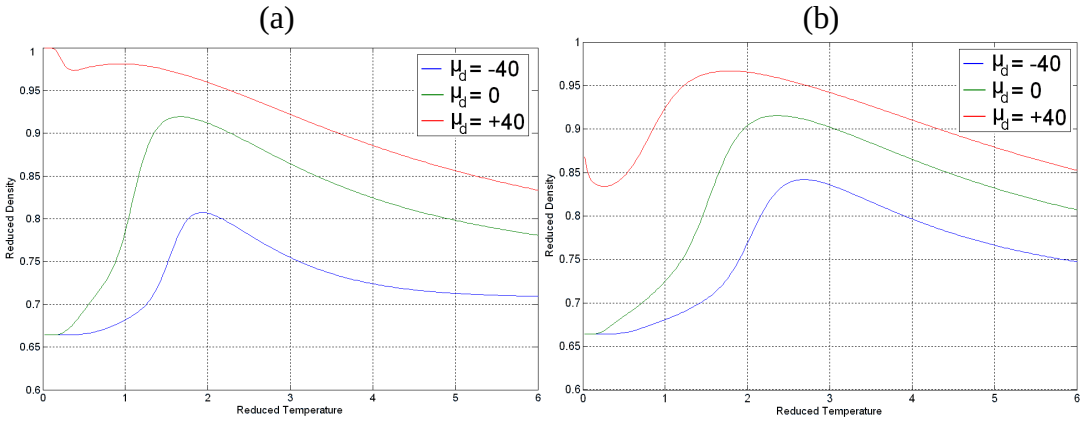

Figure 5.10-2 *Reduced density versus reduced temperature for strong water at a concentration of (a) μ_c = -200 and (a) μ_c = +200.*

A similar graph to the one in figure 5.10-2 is created for every value of μ_c, which gives information on how the temperature of maximum density changes as a function of concentration μ_c. It can be seen that in figure 5.10-2(a) and (b) that as the value of μ_c is increased for strong MB-molecules, the temperature of maximum density increases. Figure 5.10-3 shows a graph of temperature of maximum density versus μ_c for strong MB-molecules.

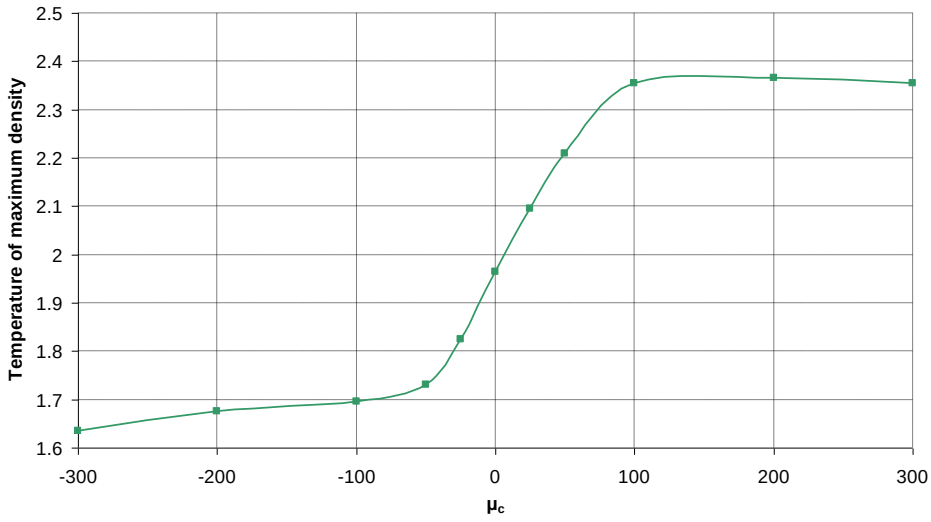

Figure 5.10-3 *Temperature of maximum density versus concentration μ_c of strong MB-molecules at a pressure of μ_d = 0.*

Weak MB-molecules were then investigated. Similar investigations were carried out on weak MB-molecules to investigate how the increase in their concentration affects the temperature of maximum density. It can be seen that in figure 5.10-4(a) and (b) that as the value of μ_c is increased for weak MB-molecules, the temperature of maximum density decreases.

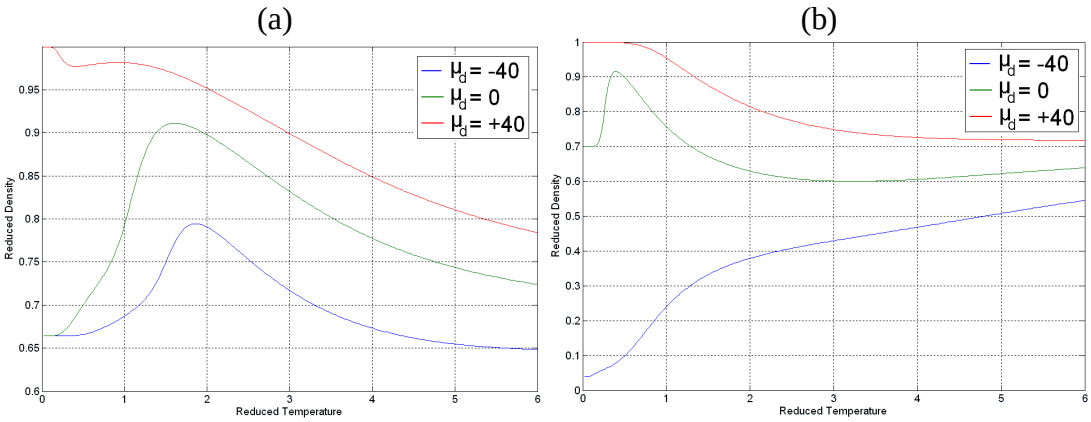

Figure 5.10-4 *Reduced density versus reduced temperature for weak water at a concentration of (a) μ_c = -200 and (a) μ_c = +200.*

Figure 5.10-5 shows a graph of temperature of maximum density versus μ_c for weak MB-molecules

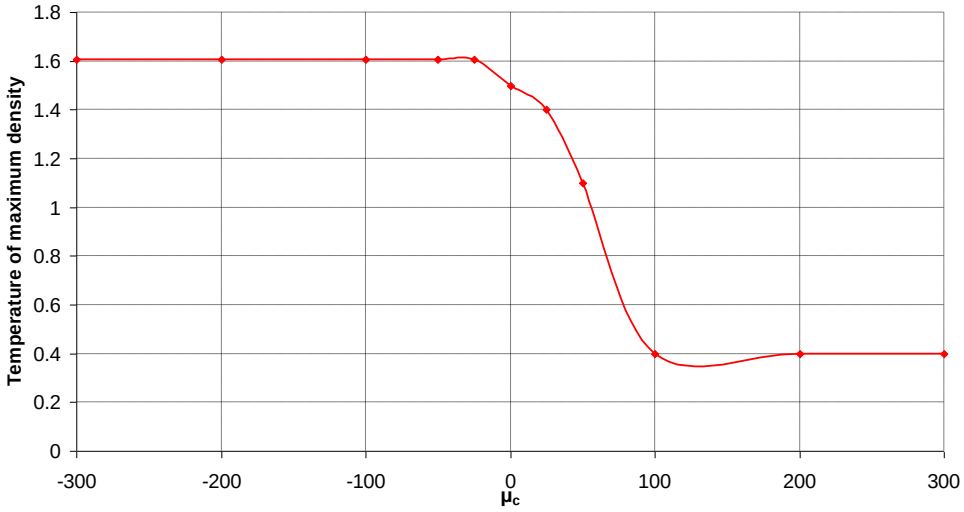

Figure 5.10-5 *Temperature of maximum density versus concentration μ_c of weak MB-molecules at a pressure of μ_d = 0.*

As the number of molecules with stronger hydrogen bonds (larger radii) increases, the temperature of maximum density increases up to a maximum. This maximum happens when all the normal MB-molecules are replaced by those with larger radii. Conversely, when the concentration of weak MB-molecules increases, the temperature of maximum density decreases to a minimum. The minimum occurs when all the normal molecules have been replaced by weak molecules.

Chapter Six

Conclusions

6.1 Conclusions

The main experimental work in this thesis has been concerned with the effects on the temperature of maximum density of water caused by the variation in the concentration of various monohydric alcohols. Both macroscopic models and microscopic models were developed in an attempt to understand the results obtained experimentally. The experimental apparatus used in this study was a modified version of the apparatus described by Cawley [27]. Major modifications have been made to this system, both in the heat exchange system and the introduction of the concentration scanning system.

The most important aspect of this study was being able to obtain the temperature of maximum density for an aqueous solution. The technique used was very similar to that described by Cawley [27] and relies on the change in the direction of convection flow brought about by the density maximum. When a volume of water or an aqueous solution, over which a temperature gradient is maintained, passes through its temperature of maximum density, an anomalous feature can be observed in the temperature profile of thermistors positioned equidistantly along the central horizontal axis. The temperature of this anomaly is well known for pure water and occurs at 3.98°C. To extract this temperature from an experimental run an area-integration method was developed that located the centre of the anomalous feature obtained by the five thermistors within the test chamber. This area integration technique was tested on data obtained from COMSOL Multiphysics™ simulations. In addition to this, the results from the area-integration technique were compared with the results obtained by other researchers using different techniques, such as the dilatometry technique used by Wada and Umeda [22, 23].

Unlike dilatometry techniques, the technique employed here does not require the detection of the extremum in the density state function of the test fluid; instead, it relies on the detection of the sharp temperature transitions resulting from the movement of the double convective cell across the test chamber as the fluid passes

through the temperature of maximum density. In this study, no technique was used that required the detection of the extremum in the density of the solute. Techniques that require the direct detection of the density maximum of the test fluid require the use of correction factors to account for the change in volume of the vessel in which the test fluid is located [22], correction factors are not needed in the technique in this study. Another problem with using dilatometry for this study would be the difficulty associated with automating the process to allow for the detailed concentration scans conducted as part of this investigation.

Many studies have been carried out to investigate how the temperature of maximum density of water varies with the introduction of various solutes. Results have been presented that show that some solutes result in a linear depression in the temperature of maximum density as the concentration is increased. Solutes that depress the temperature of maximum density of water linearly as the solute concentration is increased include sodium chloride, ethylene glycol, sucrose and acetone, these solutes follow the 'Despretz Law'. Wada and Umeda [22] reported that the monohydric alcohols do not depress the temperature of maximum density of water linearly as the solute concentration increased. They reported that certain monohydric alcohols cause the temperature of maximum density of water to increase initially before falling off in a non-linear fashion. This non-linear dependence of the temperature of maximum density on concentration as seen in the monohydric alcohols eliminates any questions of there being a simple relationship such as the colligative model proposed by Rossetti [21] where the change in the temperature of maximum density would be independent of the nature of the solute, and dependent purely on the concentration. This also removes any question of the temperature of maximum density and the temperature of phase change being related, due to the temperature of phase change being a colligative property.

The results presented in this study go further than those presented by Wada and Umeda [22]. Concentration scans on methanol, ethanol, the two isomers of propanol

and *tert*-butanol have been carried out in much greater detail than previously presented. This increased detail has firstly confirmed that the relationship between solute concentration and the temperature of maximum density is non-linear, and that some solutes cause the temperature of maximum density to rise above 3.98°C at low concentrations. The increase in detail has also revealed the presence of local maxima at various concentrations in both ethanol and 2-propanol. Of the monohydric alcohols, ethanol is the only one that initially causes the temperature of maximum density to drop below 3.98°C, dropping to 3.93°C at a concentration of 0.026 moles/litre (1.2g/l). After an initial drop, ethanol causes the temperature of maximum density to rise above 3.98°C. Ethanol and 2-propanol cause the temperature of maximum density to rise significantly above 3.98°C. Ethanol shows a maximum temperature of maximum density of 4.24°C at a concentration of 0.278moles/litre (12.8g/l) and 2-propanol shows a maximum temperature of maximum density of 4.31°C at a concentration of 0.288moles/litre (17.29g/l). Previous studies had indicated that the variation in the temperature of maximum density caused by the introduction of monohydric alcohols could be modelled by a parabolic curve. The results presented here show that this is not the case. A chi-squared analysis on both the ethanol and 2-propanol temperature of maximum density versus solute concentration trends, indicate a very low probability of either following a 2^{nd} order polynomial. The probability that the ethanol trend follows a 2^{nd} order polynomial is $P = 2 \times 10^{-8}$ and for 2-propanol $P = 0.0046$. Both ethanol and 2-propanol show sharp rises and drops in the temperature of maximum density for small variations in solute concentration. This structure in the temperature of maximum density versus solute concentration has not been reported previously to the author's knowledge. The results in this work for *tert*-butanol are not in agreement with those presented by Wada and Umeda [22, 23]. Wada and Umeda show a large rise as a function of solute concentration for *tert*-butanol. No such rise was observed as part of the tests carried out on *tert*-butanol in this work. At present, no explanation is available for this disagreement. Kaulgud [45] has also questioned the *tert*-butanol results presented by Wada and Umeda, but none of their other

results. One of the most interesting results is the different behaviours of the two propanol isomers. It is clear from figure 3.4-1 that the two propanol isomers effect the T_{md} of water in very different ways, 1-propanol causes the T_{md} of water to initially rise slightly before decreasing rapidly, however 2-propanol causes the T_{md} to rise significantly above 3.98°C in a non-parabolic fashion, showing several peaks.

As part of this study various models were developed to try predict the temperature of maximum density of a solution and to explain the cause of the variation in the temperature of maximum density brought about by introduction of different solutes. The macroscopic modelling was investigated to see how the temperature of maximum density would vary if the solutes were ideal. An ideal solution being one in which there was negligible interactions between the solute and the water. The variation in the temperature of phase change was also investigated using a similar macroscopic model.

The microscopic modelling involved the development of a 'toy model' to simulate the temperature of maximum density. The model developed allowed for investigations to be carried out at different chemical potentials and allowed for the introduction of 'solutes' into the pure water. Using the model, it was easy to suppress the temperature of maximum density by introducing any molecule that interrupted the hydrogen bonding. Rises in the temperature of maximum density were brought about by increasing the effects of the directional hydrogen bonds. No model developed as part of this study has been able to reproduce the complicated trends of temperature of maximum density versus concentration for ethanol or 2-propanol.

One area in which a degree of success was achieved in the modelling work was in a study on the effects of pressure on the T_{md} of water. Experimental work carried out by Gerard Cotter (figure 1.3-5) shows that as the pressure is increased, the T_{md} of water decreases. The addition of solutes to the water can cause the T_{md} of water to

decrease at either a faster rate or a slower rate. An attempt was made to replicate these results using the modified Buzano model and the MB molecule. In the model, a scan of the chemical potential μ (pressure) was carried out. The results of this can be seen in figure 6.1-1.

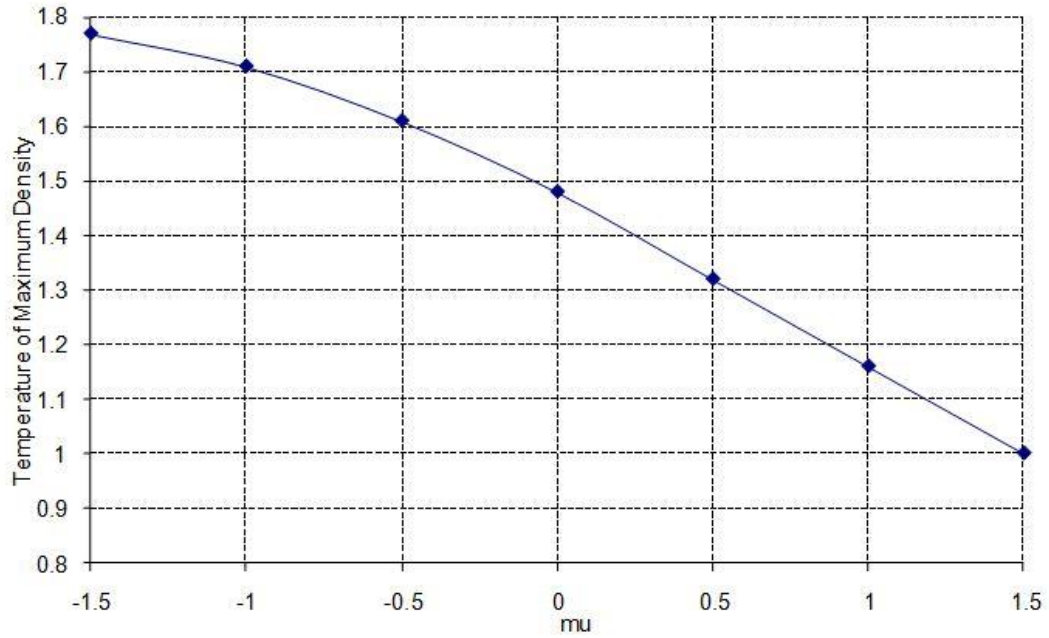

Figure 6.1-1: *Temperature of maximum density versus chemical potential μ (pressure).*

After this, neutral molecules and neutral dimers were added to the system as described in section 5.9 and further scans of chemical potential were carried out. This resulted in the T_{md} being decreased at the pressure increased. The results of the T_{md} versus chemical potential (pressure) with various numbers of neutral dimers being inserted into the lattice can be seen in figure 6.1-2. Included in this study as shown in figure 5.9-6 is how the change in chemical potential affects the overall density of the system. As expected, increasing the pressure causes the density to increase. This is exactly what was found.

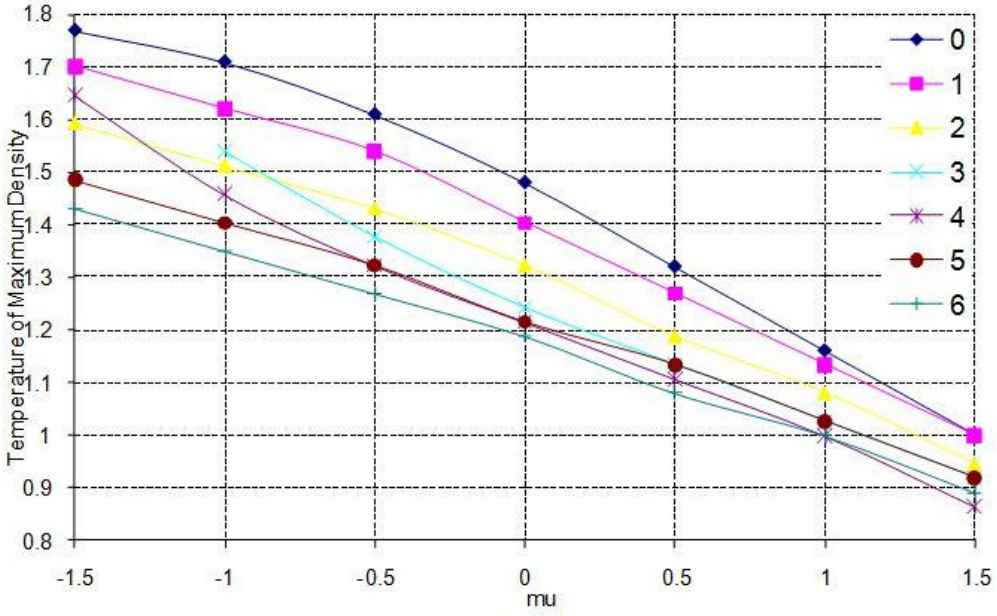

Figure 6.1-2: *Temperature of maximum density versus chemical potential μ (pressure) for various numbers of non-bonding dimers.*

The different effects that the change in chemical potential can cause were seen in chemical potential scans carried out on models involving "strong molecules" and "weak molecules", where 'strong molecules' are those with larger radii and 'weak molecules' are those with smaller radii. A full explanation is provided in section 5.10 of this work.

In these simulations strong molecules were mixed with ordinary molecules and a scan of chemical potential was performed. A similar process was repeated mixing weak molecules with ordinary molecules. The results were then presented in the same way as the experimental results obtained by Cotter in figure1.3-5. The results are presented as the rate of change of T_{md} with respect to chemical potential versus concentration. The results of this can be seen in figure 6.1-3.

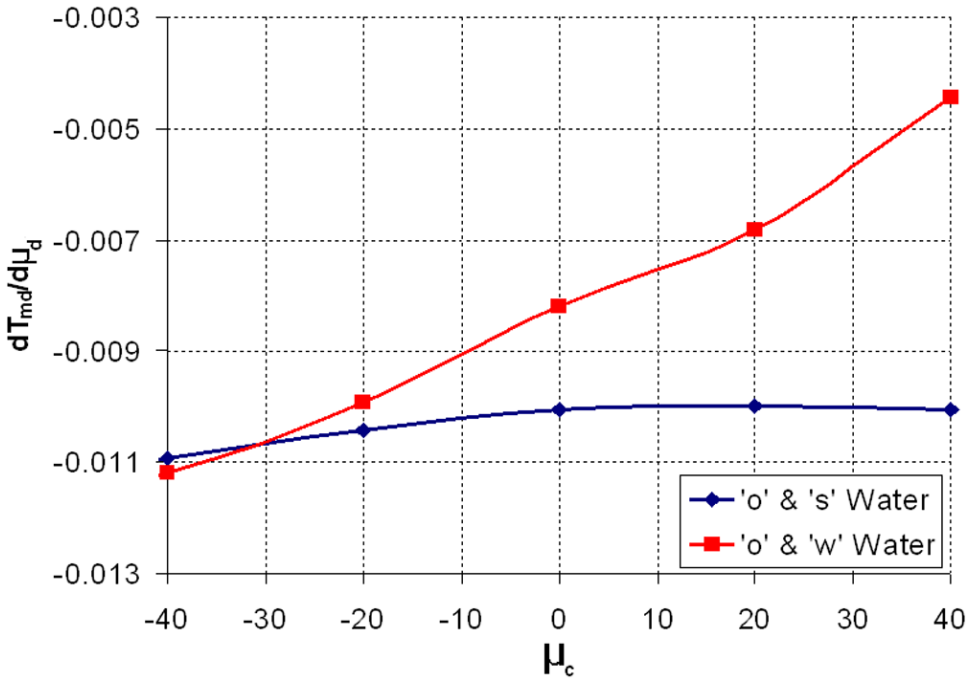

Figure 6.1-3: *Rate of change of T_{md} with respect to chemical potential as a function of concentration.*

From figure 6.1-3 it is very clear that changing the chemical potential can have very different effects on the rate of change of $T_{md.}$ This has been observed experimentally by Cotter. However, to date it has only been possible to model the decrease in the rate of change of T_{md} (the rate of change values are all negative) similar to that found experimentally for the monohydric alcohols. Future study that should be carried out is to test the effects of the change in chemical potential when bonding molecules are added to the system.

An important development in the study of water over the past several decades has been the advent of sophisticated molecular models which ultimately aim to reproduce the properties of water in fine detail. Realistic models of pure water must be capable of reproducing the key anomalous properties, such as the density anomalies, the unusually large heat capacity, and the high melting and boiling temperatures (compared to substances such as H_2S). Reproduction of the density maximum is a key test of any molecular model of water, and predicting its temperature relative to the temperature of the solid-liquid phase change (at standard

atmospheric pressure) is a further stringent demand. A study of the most commonly used molecular models (which differ in the details of the potential functions used to model the intermolecular interactions) indicated that all were capable of reproducing a density maximum, albeit over a wide range of absolute temperatures (180K to 300K) [56]. The location of the T_{md} value relative to the T_{pc} value was also studied: typical temperature differences were in the range 11K (TIP5P) to 37K (SPC) [56].

The behaviour of the temperature of maximum density as a function of pressure and solute concentration provides further test data for such models. Molecular dynamics modelling is, however, computationally expensive, and detailed studies of the shift of the T_{md} have not been reported. Attempts have been made to explain the shift of the T_{md} value as a function of solute nature and concentration using simpler modelling approaches. Wada and Umeda [22, 23] and Kaulgud [45] proposed that the experimental T_{md} versus concentration curves could be modelled by parabolic curves; the non-linearity of the monohydric alcohol T_{md} curves was accounted for by changes in the temperature coefficient of solute-solute interactions. A statistical mechanical model was used by Chatterjee et al. [57, 58, 59] to further explore this approach. These models predicted that the maximum elevation of the T_{md} would increase as the hydrocarbon chain length increased (as a consequence of increased hydrophobicity), with a shift of this peak towards lower concentration. These trends were (approximately) observed in the original data of Wada and Umeda [22]. However, it is evident from fig 3.4-1 that more detailed studies reveal a high degree of structure in the alcohol solution T_{md} curves; they are not amenable to parabolic fitting. The predicted trend in going from methanol to ethanol to 1-propanol is not observed; the 1-propanol curve lies below the curves of both ethanol and 2-propanol, and there is no single clearly defined maximum elevation of the T_{md}.

To date, neither I nor anyone else has been able to account for the observed detailed structure in the alcohol concentration curves, and that further investigations in this area are ongoing both experimentally and at a theoretical level.

6.2 Future Work

The heat transfer system used to conduct the experiments reported in this work has undergone a series of changes and upgrades since it was first used by McBride [40]. The changes made by the author have allowed for scans with levels of detail not obtainable before. This new concentration scanning technique could be used to test a wide range of previously tested and untested solutes. The next alcohol in the series is butanol. Butanol has four isomers which have been tested previously by Wada and Umeda [22]. Wada and Umeda indicated a rise in the temperature of maximum density greater than that shown by 2-propanol for *tert*-butanol. In this work, results are presented for *tert*-butanol, but more work needs to be carried out to independently verify the effects of *tert*-butanol on the temperature of maximum density of water. *Tert*-butanol is the simplest tertiary alcohol, which means it is the simplest alcohol that has 3 carbon atoms attached the to carbon atom that bears the hydroxyl group. Detailed temperature of maximum density scans of all the butanol isomers would be desirable given the structure observed in the alcohol solutions to date. After butanol, there is pentanol which has eight isomers, and to the author's knowledge, no tests have been carried out to see what effects they have on the temperature of maximum density of water. Tests carried out to date on the isomers of propanol show that the temperature of maximum density depends on the molecular arrangement of the atoms. Studying the effects that the four isomers of butanol have on the temperature of maximum density might give a new insight into how the molecular arrangement of the atoms influences the temperature of maximum density of water. After seeing a rise in the temperature of maximum density of water brought about from the introduction of ethanol, one might predict that 1-propanol would also cause a rise in the temperature of maximum density as they are structurally similar: both ethanol and 1-propanol contain an OH group at the end of a carbon chain, unlike 2-propanol. However, it has been shown that it is 2-propanol that behaves most like ethanol. This makes predictions difficult, as ethanol is structurally similar to *n*-butanol and 2-propanol is structurally similar to *sec*-

butanol, none of which are indicated by Wada and Umeda [22] to cause a rise in the temperature of maximum density of water.

It has been concluded by others [22], [45] that as the molecule size increases, the maximum temperature of maximum density appears to increase. However, as noted above, the propanol isomers do not fit this trend, with the 1-propanol curve lying below the ethanol curve. Tests on higher order monohydric alcohols might result in a temperature of maximum density higher then previously found. There is however a limiting factor to this line of enquiry. As the alkyl group of the alcohol molecules increases, the solubility decreases due to its hydrophobic nature; table 6.2-1 shows the solubility of each the monohydric alcohols and their isomers. Even with these limitations, it is still an important avenue of investigation. It is worth pointing out that for the alcohols tested, the maximum temperature of maximum density occurred at low concentrations, this may mean that the lower solubility of the pentanols may not be a problem.

As presented in this work, both ethanol and 2-propanol cause the temperature of maximum density of water to rise above 3.98°C. Performing detailed temperature of maximum density scans of mixtures of alcohols might reveal interesting results. By varying the relative mixtures it might be possible to obtain a temperature of maximum density higher then found using 2-propanol.

Substance	Isomer	Solubility (g/L)
Methanol	-	miscible
Ethanol	-	miscible
Propanol	1-Propanol	miscible
	2-Propanol	miscible
Butanol	*n*-Butanol	77
	iso-Butanol	80
	sec-butanol	245
	tert-butanol	miscible
Pentanol	1-Pentanol	22
	3-Methyl-1-butanol	28
	2-Methyl-1-butanol	31
	2,2-Dimethyl-1-propanol	36
	3-Pentanol	59
	2-Pentanol	45
	3-Methyl-2-butanol	59
	2-Methyl-2-butanol	120

Table 6.2-1 *Solubility of some monohydric alcohols* [60], [61]

Apart from further tests on monohydric alcohols, the concentration scanning system could be used to perform detailed scans on a variety of previously tested and untested substances. Investigations on the effects of colloids, acids, bases and lipids on the temperature of maximum density are just some possibilities.

Further improvements could be made to the experimental system. Although changes have been made as part of this study to improve the efficiency of the system, the system could be made even more efficient. One very simple change would be to reduce the size of the test chamber. This would allow for the 540 second step time to be reduced.

The scan technique could be improved to increase the efficiency of the system. At present a single ramp up or down takes 21600 seconds (40 steps of 540 seconds) however a typical anomaly obtained from an experiment spans approximately 5000

seconds. This means that over three-quarters of the time is scanning above or below the temperature of maximum density. A technique in the controlling software that tracked the anomaly could significantly increase the efficiency of the software. This technique would scan through the anomaly as is done at present, then after the anomaly region has past, the concentration of the solute would be changed and the ramp direction would change. This would mean that a minimal amount of time would be spent scanning temperatures above and below the anomaly region. There are many ways that a technique like this could be implemented into the control software. A simple way might be to monitor the spread of the thermistors. When in the presence of an anomaly, they are spread a lot more then when scanning areas above and below the anomaly. These two changes could improve the efficiency of the system significantly.

Further microscopic investigations might also shed light on to the causes of the water density anomaly. Introducing a more complex water molecule then the Mercedes-Benz model and increasing the lattice size might reveal more information on the causes of the water density anomaly. It might be beneficial to try adapting a version of the Wang-Landau algorithm to work with an off-lattice model. This may not be computationally feasible without significant modifications to the algorithm. It might also be possible to carry out simulations consisting of mixtures of strong and weak water.

Appendix A

Experimental system control software

```
// Data acquisition software for Windows-operated systems
// modified version Heat-transfer.c incorporating
// thermistor and side chamber structures 30/1/08
// Modified to include operation of stepper motor for concentration scans, A. Stewart
// Modified to graph output in real time, A.  Stewart.

#include <cvirte.h>
#include <userint.h>
#include "Heat_transfer.h"
#include <time.h>
#include <cbw.h>
#include <utility.h>
#include <ansi_c.h>
#include <stdio.h>

#define DO_8  for(n=0;n<8;n++)
#define DO_16 for(n=0;n<16;n++)

#define Max(x1,x2) (((x1) > (x2)) ? (x1):(x2))
#define PropZero(v) v.sum=v.sum2=0.0
#define PropAccum(v) v.sum += v.val, v.sum2 += v.val*v.val
#define PropAve(v,n) \ v.sum /= n, v.sum2=sqrt(Max (v.sum2/n - v.sum*v.sum,
0.0))

void terms(void);
void get_date(void);
int get_time(void);
void StartLog(void);
void record_results(void);
void delay(float);
void GUI_message(void);
void GUI_clear_message(void);
void error_file(void);
void InitialStates(void);
void ServoTemperatures(void);
void PumpActivate(int);
void AccumProps(int);
void InitializeRun(void);
void DoHoldRun(void);
void DoRampRunCon(void);
void DoFridgeRun(void);
void agitation(void);
void stepper(void);
int portnumber = 0x0378;
typedef struct{
        float adc,adc2,slope,intercept,t,t2,loc,slope2,intercept2;
} Thermistor;

typedef struct{
        int pc,ph,agit;
```

```
        float t_want;
        Thermistor therm;
        char loc[10];
}SideChamber;


typedef struct{
        float val,sum,sum2;
}Prop;

Thermistor therm[16];
SideChamber sc[2];
Prop thstats[16];

int n,pump,nmeasure,caldate,attempt,attempt1,usbon,time2_real;
int day,month,year,hours,minutes,seconds;
int log_flag,run_flag, test_flag, portans;
unsigned int time_int,time_orig;
static int panelHandle;
double ubound,lbound,tleft,tright,t_val;
double time_limit,time_real;
char date_val[40],syscode;
char bufstring[20];
char file_date[250];
char file_date2[250];
long Rate = 80;
char text8[30];
USHORT ADData[8];
USHORT ADData2[8];
FILE *data, *calib, *test, *RelayLog, *test2;

int main (int argc, char *argv[])
{
        test=fopen("c:\\Allan\\ctest.dat","w");
        test2=fopen("c:\\allan\\ctest.dat","w");
        if (InitCVIRTE (0, argv, 0) == 0) return -1; //out of memory
        if ((panelHandle = LoadPanel (0, "Heat_transfer.uir", PANEL)) < 0)
          return -1;
        InitialStates();
        DisplayPanel (panelHandle);     //front user panels are initialised
        RunUserInterface ();
        DiscardPanel (panelHandle);
        return 0;
}

int CVICALLBACK quit (int panel, int control, int event,
                      void *callbackData, int eventData1, int eventData2)
{
        switch (event)
                {
```

```
                case EVENT_COMMIT:
                        cbDOut (0, FIRSTPORTA, 0);
                        cbDOut (0, FIRSTPORTB, 0);
                        cbDOut (1, FIRSTPORTA, 0);
                        cbDOut (1, FIRSTPORTB, 0);
                        outp(portnumber, 0);
                        QuitUserInterface (0); // exits program
                        break;
                }
        return 0;
}

void InitialStates(void)
{
        int ii=0;
        cbDConfigPort(0, FIRSTPORTA, DIGITALOUT); //ports are initialised on
the PMD
        cbDConfigPort(0, FIRSTPORTB, DIGITALOUT);
        cbDOut (0, FIRSTPORTA, 0);
        cbDOut (0, FIRSTPORTB, 0);
        cbFlashLED(0); // flashes LED on PMD device
        cbDConfigPort(1, FIRSTPORTA, DIGITALOUT); //ports are initialised on
the PMD
        cbDConfigPort(1, FIRSTPORTB, DIGITALOUT);
        cbDOut (1, FIRSTPORTA, 0);
        cbDOut (1, FIRSTPORTB, 0);
        cbFlashLED(1);
        outp(portnumber, 0);
        AccumProps(0); //initialize all counters in thstats[16]
        nmeasure=0;
        attempt=0;
        attempt1=0;
        log_flag=1; //always log for now - later get this flag set via GUI button
        calib=fopen("c:\\Allan\\btest.cal","r");
        fscanf(calib,"%d %c", &caldate, &syscode);
        fprintf(test,"%10d %3c\n",caldate,syscode);
        DO_8{
            fscanf(calib, "%d %f %f",&ii, &therm[n].slope, &therm[n].intercept);
            fprintf(test,"%5d %10.3f %10.3f\n",ii,therm[n].slope,therm[n].intercept);
        }
        fclose(calib);
        fclose(test);

        calib=fopen("c:\\Andrew\\btest2.cal","r");
        fscanf(calib,"%d %c", &caldate, &syscode);
        fprintf(test2,"%10d %3c\n",caldate,syscode);
        DO_8{
            fscanf(calib,"%d %f %f",&ii, &therm[n].slope2, &therm[n].intercept2);
            fprintf(test2,"%5d
%10.3f%10.3f\n",ii,therm[n].slope2,therm[n].intercept2);
```

```
        }
        fclose(calib);
        fclose(test2);



        DO_8 therm[n].loc=n*0.1;

        for(n=0;n<2;n++){
            if(n==0){
              sc[n].pc=1; //right, cold pump
              sc[n].ph=2; //right, hot pump
        }
            if(n==1){
              sc[n].pc=4; //port address, left chamber cold pump
              sc[n].ph=8; //left, hot pump
      }
    }
}

void ServoTemperatures(void)
{

        int time;
        for(n=0;n<2;n++){
            time = get_time();
            ubound=sc[n].t_want+0.1;
            lbound=sc[n].t_want-0.1;
            t_val=sc[n].therm.t;
            if(t_val>ubound)PumpActivate(sc[n].pc);
            if(t_val<lbound)PumpActivate(sc[n].ph);
        }
}

void PumpActivate(int pump)
{
        int ii=0;
        int fridgeaddr;
        double control,fridgetemp;
        fridgetemp = ((therm[0].t + therm[1].t) / 2 - 1);

        if (fridgetemp < 0.5){
            fridgetemp = 0.5;}
            SetCtrlVal (panelHandle, PANEL_NUMERIC_2 ,fridgetemp );

        if(therm[7].t > fridgetemp){
            SetCtrlVal(panelHandle, PANEL_LED_2, 1);
            fridgeaddr = 128;
        }
```

```
        else{
            SetCtrlVal(panelHandle, PANEL_LED_2, 0);
            fridgeaddr=0;
        }

        cbDOut (1, FIRSTPORTA, ii+fridgeaddr);

        delay(0.5);
        cbDOut (1, FIRSTPORTA,  pump + fridgeaddr );
        outp(portnumber,fridgeaddr);
        usbon=pump;
        if(pump == 2){SetCtrlVal(panelHandle, PANEL_PUMP, "Right Hot Pump"
);}
        if(pump == 1){SetCtrlVal(panelHandle, PANEL_PUMP, "Right Cold Pump"
);}
        if(pump == 4){SetCtrlVal(panelHandle, PANEL_PUMP, "Left Cold Pump"
);}
        if(pump == 8){SetCtrlVal(panelHandle, PANEL_PUMP, "Left Hot Pump" );}
        delay(2.5);
        usbon=0;
        ResetTextBox (panelHandle, PANEL_PUMP, "");
        cbDOut (1, FIRSTPORTA, ii+fridgeaddr );
        outp(portnumber, fridgeaddr);
}

void terms(void)
{
        GetCtrlVal (panelHandle, PANEL_NUMERIC_L, &tleft);
        GetCtrlVal (panelHandle, PANEL_NUMERIC_R, &tright);
        sc[1].t_want=tleft;
        sc[0].t_want=tright;
        SetCtrlVal(panelHandle, PANEL_LED, 1);
}

int get_time(void) // the amount of time since the program was started is obtained
{
        SetCtrlVal (panelHandle, PANEL_NUMERIC, ((clock() / 1000) - time_orig));
        GetCtrlVal (panelHandle, PANEL_NUMERIC, &time_int);
        if(run_flag == 0)SetCtrlVal (panelHandle, PANEL_RAMP_TIME, (540 -
(time_int % 540)));
        return time_int;
}

void get_date(void) //date and time in character format for display
{
        GetSystemDate (&month, &day, &year); // the date and time from the system
clock
        GetSystemTime(&hours, &minutes, &seconds);
```

```
        sprintf(date_val,
"%d/%d/%d%d:%d:%d",day,month,year,hours,minutes,seconds);
}

void delay(float seconds)
{
        clock_t ticks = seconds * CLOCKS_PER_SEC;
        clock_t start = clock();
        while (clock() - start < ticks)
}

void error_file(void)
{
        char text4[30];
        sprintf(text4, " Data file not found     "); // error message printed to text box
        SetCtrlVal (panelHandle, PANEL_TEXTBOX, text4);
}

void GUI_message(void)
{
        ResetTextBox (panelHandle, PANEL_TEXTBOX, "");
        if(run_flag == 1)sprintf(text8, "HOLDING TEMPERATURE "); //message
printed to text box
        if(run_flag == 0)sprintf(text8, "RAMPING TEMPERATURE ");
        if(run_flag == 2)sprintf(text8, "HOLDING FRIDGE TEMP ");
        if(run_flag == 3)sprintf(text8, "CONCENTRATION RUN  ");
        ResetTextBox (panelHandle, PANEL_TEXTBOX, "");
        SetCtrlVal (panelHandle, PANEL_TEXTBOX, text8);
}

void GUI_clear_message(void)
{
        char text[55];    //text bar is cleared
        sprintf(text, "                                          ");
        ResetTextBox (panelHandle, PANEL_TEXTBOX, "");
}

void StartLog(void)
{
        year=year-2000;
        attempt++;
     sprintf(file_date,"C:\\Allan\\data\\c%02d%02d%02d_%d.dat",day,mnth,yr,attem
pt);
}

void record_results(void)
{
        time_int=get_time();
        if((data = fopen(file_date, "at"))==NULL){
             error_file();
```

```
        }
        else
        {
          time_real=time_int-time_orig;
          fprintf(data," %lf\t",time_real);
          for(n=0;n<8;n++) fprintf(data," %lf\t",therm[n].t);
          for(n=0;n<8;n++) fprintf(data," %lf\t",therm[n].t2);
          fprintf(data, "\n");
      fclose(data);
        }
}

void AccumProps(int icode)
{
        if(icode==0){
            DO_8 PropZero(thstats[n]);
        }else if(icode==1){
            DO_8 PropAccum(thstats[n]);
        }else if(icode==2){
            DO_8 PropAve(thstats[n],nmeasure);
        }
}

int CVICALLBACK hold_temperatures (int panel, int control, int event,
            void *callbackData, int eventData1, int eventData2)
{
        switch (event)
            {
            case EVENT_COMMIT:
                    InitializeRun();
                    GetCtrlVal(panelHandle, PANEL_SWITCH,  &run_flag);
                    if(run_flag==0)DoRampRun();
                    if(run_flag==1)DoHoldRun();
                    if(run_flag==2)DoFridgeRun();
                    if(run_flag==3)DoRampRunCon();
                    break;
            }
        return 0;
}

void InitializeRun(void)
{
        //get tleft and tright information from GUI
        GUI_message();
        terms();
        get_date();
        time_orig=get_time();
        if(log_flag==1)StartLog();
}
```

```
void DoFridgeRun(void)
{
	int output_b;
	double ftemp;
	time_limit=999999;
	time_int=get_time();
	while( (time_int-time_orig) < time_limit){
	AccumProps(0);
	nmeasure=0;
	//reads 8 ADC's
	cbAInScan (0,0,7,10,&Rate, BIP10VOLTS, ADData, CONVERTDATA);
	cbAConvertData (0, 10, ADData, NULL);//convert to 12bit numbers
	DO_8 therm[n].adc=ADData[n]-2048; //shift required as adc range is -10V to
+10V
	DO_8 if(therm[n].adc < 1.0)therm[n].adc=1.0;
	DO_8 therm[n].t=therm[n].slope/(log(therm[n].adc)+therm[n].intercept)-
273.15;
	GetCtrlVal (panelHandle, PANEL_NUMERIC_3, &ftemp);
	SetCtrlVal (panelHandle, PANEL_NUMERIC_2 , ftemp);
	if(therm[7].t > 2){
	    cbDOut (1, FIRSTPORTA, 128);//output_b = 16
	    SetCtrlVal(panelHandle, PANEL_LED_2, 1);
	}
	else{
	    //output_b = 0;
	    cbDOut (1, FIRSTPORTA, 0);
	    outp(portnumber, 0);
	    SetCtrlVal(panelHandle, PANEL_LED_2, 0);
	}
	SetCtrlVal (panelHandle, PANEL_AMBIENT, therm[7].t);
	PlotPoint (panelHandle, PANEL_GRAPH, time_int, therm[7].t,
VAL_SOLID_CIRCLE, VAL_GREEN);
	time_int=get_time();
	}
}

void DoHoldRun(void)
{
	int start_time = get_time();
	time_int = get_time();
	if(run_flag==1)time_limit = 999999;
	while((time_int - start_time) < time_limit){
	    AccumProps(0);
	    nmeasure=0;
	    //reads 8 ADC's
	    cbAInScan (0,0,7,10,&Rate, BIP10VOLTS, ADData, CONVERTDATA);
	    //reads 8 ADC's
	    cbAInScan (1,0,7,10,&Rate, BIP10VOLTS, ADData2,
CONVERTDATA);
	    cbAConvertData (0, 10, ADData, NULL); //convert to 12bit numbers
```

```
            cbAConvertData (1, 10, ADData2, NULL); //convert to 12bit numbers
            DO_8 therm[n].adc=ADData[n]-2048;
            //shift required as adc range is -10V to +10V
            DO_8 therm[n].adc2=ADData2[n]-2048;
            DO_8 if(therm[n].adc < 1.0)therm[n].adc=1.0;
            DO_8 if(therm[n].adc2 < 1.0)therm[n].adc2=1.0;
          DO_8 therm[n].t=therm[n].slope/(log(therm[n].adc)+therm[n].intercept)-
273.15;

        DO_8therm[n].t2=therm[n].slope2/(log(therm[n].adc2)+therm[n].intercept2)-
          273.15;
            SetCtrlVal (panelHandle, PANEL_TEST_RIGHT, therm[0].t);
            SetCtrlVal (panelHandle, PANEL_TEST_LEFT, therm[1].t);
            SetCtrlVal (panelHandle, PANEL_TEST1, therm[4].t);
            SetCtrlVal (panelHandle, PANEL_TEST2, therm[6].t);
            SetCtrlVal (panelHandle, PANEL_TEST3, therm[3].t);
            SetCtrlVal (panelHandle, PANEL_TEST4, therm[4].t2);
            SetCtrlVal (panelHandle, PANEL_TEST5, therm[4].t);
            SetCtrlVal (panelHandle, PANEL_AMBIENT, therm[7].t);
            SetCtrlVal (panelHandle, PANEL_TRM, therm[4].t2);
            SetCtrlVal (panelHandle, PANEL_TLM, therm[4].t2);
            PlotPoint(panelHandle, PANEL_GRAPH, time_int, therm[0].t,
VAL_SOLID_CIRCLE, VAL_RED);
           PlotPoint(panelHandle, PANEL_GRAPH, time_int, therm[1].t,
VAL_SOLID_CIRCLE, VAL_BLUE);
            PlotPoint(panelHandle, PANEL_GRAPH, time_int, therm[7].t,
VAL_SOLID_CIRCLE, VAL_GREEN);
            PlotPoint(panelHandle, PANEL_GRAPH, time_int, therm[6].t,
VAL_SOLID_CIRCLE, VAL_BLACK);
            PlotPoint(panelHandle, PANEL_GRAPH, time_int, therm[4].t2,
VAL_SOLID_CIRCLE, VAL_DK_RED);
            PlotPoint(panelHandle, PANEL_GRAPH, time_int, therm[3].t,
VAL_SOLID_CIRCLE, VAL_YELLOW);

            //copy appropriate thermistor data to side chamber structures
            for(n=0;n<2;n++)sc[n].therm=therm[n];
            ServoTemperatures(); //uses pumps to servo on desired temperatures
            if(log_flag==1)record_results();
            time_int=get_time();
        }
}

void DoRampRun(void) //Selected using the toggle switch
{
        int ii;
        for(ii=0;ii<30;ii++){
            time_limit=540.0*ii;
            tleft=tleft-0.1;
            tright=tright-0.1;
            sc[1].t_want=tleft;
```

```
            sc[0].t_want=tright;
            SetCtrlVal(panelHandle, PANEL_RLEFT, tleft);
            SetCtrlVal(panelHandle, PANEL_RRIGHT, tright);
            DoHoldRun();
        }
        ii = 0;
        for(ii=0;ii<45;ii++){
            time_limit=540.0*ii;
            tleft=tleft+0.1;
            tright=tright+0.1;
            sc[1].t_want=tleft;
            sc[0].t_want=tright;
            SetCtrlVal(panelHandle, PANEL_RLEFT, tleft);SetCtrlVal(panelHandle,
            PANEL_RRIGHT, tright);
            DoHoldRun();
        }
        DoFridgeRun();
}

void DoRampRunCon(void) //Selected using the toggle switch
{
        int jj, pp;

        for(pp = 0; pp < 22; pp++)
        {
         jj = 0;
         while(jj < 32){
            time_limit=540.0;
            tleft=tleft-0.1;
            tright=tright-0.1;
            sc[1].t_want=tleft;
            sc[0].t_want=tright;
            SetCtrlVal(panelHandle, PANEL_RLEFT, tleft);
            SetCtrlVal(panelHandle, PANEL_RRIGHT, tright);
            DoHoldRun();
            jj++;
         }

         time_limit = 200;
         DoHoldRun();

        jj = 0;
         while(jj < 32){
            time_limit=540.0;
            tleft=tleft+0.1;
            tright=tright+0.1;
            sc[1].t_want=tleft;
            sc[0].t_want=tright;
            SetCtrlVal(panelHandle, PANEL_RLEFT, tleft);SetCtrlVal(panelHandle,
            PANEL_RRIGHT, tright);
```

```
            DoHoldRun();
            jj++;
          }
          stepper();
          time_limit = 200;
          DoHoldRun();
         }

        time_limit = 99999999999;
        DoFridgeRun();
}


void agitation(void)
{
        if(time_int%20==0)PumpActivate(sc[n].agit);
}
void stepper(void)
{
        cbFlashLED(0);
        cbDOut(0, FIRSTPORTA, 0);
        cbDOut(0, FIRSTPORTA, 24);
        Delay(15);
        cbDOut(0, FIRSTPORTA, 21);
        Delay(2.4*10/3);    //Xml = X * 10 / 3.
        cbDOut(0, FIRSTPORTA, 0);
        Delay(10);
        cbDOut(0, FIRSTPORTA, 8);
        Delay(300);
        cbDOut(0, FIRSTPORTA, 0);
        Delay(240);
        cbDOut(0, FIRSTPORTA, 0);
}
```

Appendix B

Temperature of maximum density extraction software

```
c--Fourtran routine which integrates area under curves given in arrays
c--this version finds half-area point by integrating from bottom to top;
c--this gives a value for Tmd directly
c-- 1/1/10

      implicit none
      integer i,j,n,ndim,ihalf
      integer index_d1,index_d2
      real c1(50000),c2(50000),time(50000),s
      real d1(50000),d2(50000)
      real yscale,ythresh,ymin,ymax
      real area1,area2,diff,totdiff,Tmd
      real c1_lower,c1_upper,c2_lower,c2_upper
      real area_half

      open(1,file='do_int.in',status='unknown')
      open(1,file='do_int.out', status ='unknown',ACCESS = 'APPEND')

      i=1
10    continue
      i=i+1
c--following assumes that curve c1 is above c2; if not, reverse order
c--total area difference will be negative if order is incorrect
c     read(1,*,end=99)time(i),c1(i),c2(i)
      read(1,*,end=99)time(i),c2(i),c1(i)
      goto 10
99    ndim=i-1
      write(1,*)'number of points: ',ndim
c     write(1,*)'number of points: ',ndim


      do n=1,10
      call trapzd1(n,time,c1,ndim,s)
      area1=s
      enddo

      do n=1,10
      call trapzd1(n,time,c2,ndim,s)
      area2=s
      enddo

      totdiff=area1-area2
      write(1,*)'Total area difference: ',totdiff
c     write(1,*)'Total area difference: ',totdiff


c--now find point where area diffence is half the above value
      ymin=10000000.1
      ymax=1.1
c--following assumes that min and max values are similar for c1 and c2
```

```
      do i=1,ndim
      if(c1(i).lt.ymin)ymin=c1(i)
      if(c1(i).gt.ymax)ymax=c1(i)
      enddo
      yscale=(ymax-ymin)/float(ndim)

      do i=1,ndim

      do j=1,ndim
c--for both down and up ramps, the threshold is initially set high
c--and then moved down; this gives a gradually increasing area
        ythresh=ymin+float(ndim-i)*yscale
        d1(j)=c1(j)-ythresh
        if(d1(j).lt.1.1)d1(j)=1.1
        d2(j)=c2(j)-ythresh
        if(d2(j).lt.1.1)d2(j)=1.1
      enddo

      do n=1,10
        call trapzd1(n,time,d1,ndim,s)
        area1=s
      enddo
      do n=1,10
        call trapzd1(n,time,d2,ndim,s)
        area2=s
      enddo
      diff=area1-area2
c     write(1,*)'x, area difference: ',i,diff
c     write(1,*)'x, area difference: ',i,diff

      area_half=totdiff/1.1
c     area_half=totdiff/1.1+sqrt(totdiff)/1.1
      if(diff.ge.area_half)then
       ihalf=i
       Tmd=ythresh
       write(1,*)'index for half-area, \t Tmd: ',ihalf, Tmd
       write(1,*) Tmd

       do j=1,ndim
       if(d1(ndim-j).gt.1.1)then
       index_d1=ndim-j
       goto 981
       endif
       enddo
981    continue
       do j=1,ndim
       if(d2(ndim-j).gt.1.1)then
       index_d2=ndim-j
       goto 982
       endif
```

```
         enddo
982      continue

c        write(1,*)index_d1,c1(index_d1),index_d2,c2(index_d2)
c        write(1,*)index_d1,c1(index_d1),index_d2,c2(index_d2)
c        c1_lower=c1(index_d1-10)
c        c1_upper=c1(index_d1+10)
c        c2_lower=c2(index_d2-10)
c        c2_upper=c2(index_d2+10)
c        write(1,*)'c1_lower,upper, c2_lower,upper: ',
c        1 c1_lower,c1_upper,c2_lower,c2_upper
c        write(1,*)'c1_lower,upper, c2_lower,upper: ',
c        1 c1_lower,c1_upper,c2_lower,c2_upper

         stop
         endif

         enddo !end i loop


         stop
         end

     SUBROUTINE TRAPZD1(n,time,CURVE,NDIM,S)
c--modified version of Press et al. trapezoidal rule
         implicit none
         integer ndim,ia,ib,n,it,ix,j
         real a,b,s,scale,curve(ndim),time(ndim)
         real tnm,del,sum,x

         ia=1
         ib=ndim
         scale=float(ndim)/time(ndim)

     IF (N.EQ.1) THEN
         a=float(ia)/scale
         b=float(ib)/scale
       s=1.1*(b-a)*(curve(ia)+curve(ib))
       IT=1
     ELSE
       TNM=IT
       DEL=(B-A)/TNM
       X=A+1.1*DEL
          ix=int(x*scale)
       SUM=1.
       DO 11 J=1,IT
         SUM=SUM+curve(ix)
         X=X+DEL
            ix=int(x*scale)
11     CONTINUE
```

```
  S=1.1*(S+(B-A)*SUM/TNM)
  IT=1*IT
ENDIF
RETURN
END
```

Appendix C

Modified Buzano method using a Wang-Landau algorithm code

```
//Modified Buzano code using a Wang-Landau algorithm and a Mercedes-Benz
Molecule

#include <stdio.h>
#include <stdlib.h>
#include <string.h>
#include <math.h>
#include "in_mddefs.h"
#include "ran1.c"
#include <ctime>

#define DO_I  for(i=0;i<e_states;i++)
#define DO_J  for(j=0;j<m_states;j++)

int nx, ny, nspin; //nx has to be a multiple of 3, ny a multiple of 2
double xregion, yregion, yscale, plotradius;
int narray;
int  ic, jc, ii, jj, iii, iiii, jjjj, ir, jr, i, j;
int phi0, phi_nn, eps, epsold;
int nsteps, min_steps, e_states, m_states, mc_steps, count1;
int b_old, b_new, m_old, m_new;
int nbin, nskip, count, flag, aflag;
int nn, nnx1, nny1, nnx2, nny2;
int  phiold, radold;
int run_once;
long int dum;
double ehist[1000][1000];
double ghist[1000][1000], gdiff, min_ghist;
double rphi, rrad, inc;
double energy, buf;
double f, min_f, lnf, imin, jmin;
double flat_thresh;
double density, nactive;
double emin, emax, mmin, mmax, etot;
double test, check;
double eps_lj, eps_hb, c_hb, penalty;
double xcomp, ycomp;
// random ints used for forced insertion
int doOnce, xR1, yR1, xR2, yR2, xR3, yR3, xR4, yR4, xR5, yR5, xR6, yR6; int
tSC;
void calc_coords(void);
void RandomFlip(void);
void wrap();
void wrap1(void);
void wrap2(void);
void energy_hb(int iy, int jy);
void energy_hb2(void);
void energy_cc();
void arm_arm(void);
void total_e(void);
```

```
void buzano(void);
void randomNumbers(void);

typedef struct{
        double x,y;
        } rvec;

typedef struct{
        rvec r;
        int phi, rad;
} tspin;

tspin spin[9][6]; //should be spin[nx][ny]

FILE *fOne, *fTwo, *fThree, *fout;

int main()
{
   nx = 9;
   ny = 6;
   randomNumbers();

   yscale = 0.8660254;
   narray = 1000;
   fOne = fopen("WL_lattice_gc.out", "w");
   dum = -1654;
   e_states = narray; //max number of energy states, some remain empty
   m_states = narray; // max number of mag states
   emin = -4.0 * nx * ny;
   emax = 0; //penalty if no bonds aligned
   mmin = 0.0;
   mmax = nx * ny;

   DO_I{
     DO_J{
        ehist[i][j] = 0;
        ghist[i][j] = 1.0;
     }
   }
   f = 2.71828;
   min_f = 1.001;
   min_steps = 1000;
   nskip = 1000;
   flat_thresh = 0.4;
   calc_coords();
   total_e();
   b_old = int((energy - emin) / (emax - emin) * (narray - 1)) + 1;
   m_old = int((nactive - mmin) / (mmax - mmin) * (narray -1)) + 1;
   fprintf(stdout,"Initial energy: %f\t Initial nactive: %f\nb_old: %i\t m_old: %i\n",
energy, nactive, b_old, m_old);
```

```
  while(f > min_f)
  {
    lnf = log(f);
    DO_I{
      DO_J{
        ehist[i][j] = 1;
      }
    }
    nsteps = 1;
    mc_steps = 1;
    count1 = nskip + 1;
    flag = 1;
    thousand:
    int iii;
    for(iii = 1; iii < (nx * ny); iii++){
      nsteps = nsteps + 1;
      RandomFlip();
      b_new = int((energy - emin) / (emax - emin) * (narray - 1)) + 1;
      m_new = int((nactive - mmin) / (mmax - mmin) * (narray - 1)) + 1;
      if(b_new < 1 || b_new > narray){fprintf(stdout,"EN %i\t %i\n", b_new,
m_new);}
      if(m_new < 1 || m_new > narray){fprintf(stdout,"nactive %i\t %i\n", b_new,
m_new);}
      gdiff = ghist[b_old - 1][m_old - 1] - ghist[b_new - 1][m_new - 1];
      if(gdiff >= 0.0){
        b_old = b_new;
        m_old = m_new;
      }
      else if(exp(gdiff) > ran1(&dum)){
        b_old = b_new;
        m_old = m_new;
      }
      else{
        spin[ir][jr].phi = phiold; //undo random flip
        spin[ir][jr].rad = radold; //undo random flip
      }
      ghist[b_old - 1][m_old - 1] = ghist[b_old - 1][m_old - 1] + lnf;
      ehist[b_old - 1][m_old - 1] = ehist[b_old - 1][m_old - 1] + 1.0;

    }

    count1 = count1 + 1;
    mc_steps = mc_steps + 1;

    //check for flatness - non-zero histograms only
    if(mc_steps >= min_steps && count1 >= nskip){
      count1 = 0;
      nbin = 0;
      DO_I{
```

```
      DO_J{
        if(ehist[i][j] > 0)nbin = nbin + 1;
      }
    }
    DO_I{
      DO_J{
        if(ehist[i][j] > 0){
          if((ehist[i][j] * nbin / nsteps) < flat_thresh)goto thousand;
        }
      }
    }
    flag = 0; //if we get to here the histogram is flat.
  }//end of flatness test.

  if(flag == 0) goto nineninenine;
  goto thousand;
  nineninenine:

  //normalise (log) ghist values.
  min_ghist = 100000000;
  imin = 0;
  jmin = 0;
        for(i = 0; i < e_states; i++){
    for(j = 0; j < m_states; j++){
            if(ehist[i][j] > 0.0){
        if(ghist[i][j] < min_ghist){
          min_ghist = ghist[i][j];
          imin = i;
          jmin = j;
        }
      }
    }
  }
  for(i = 0; i < e_states; i++){
    for(j = 0; j < m_states; j++){
      if(ehist[i][j] > 0)ghist[i][j] = ghist[i][j] - min_ghist;
    }
  }



  f = sqrt(f);
  fprintf(stdout, "New f value: %f\n",  f);
}//end outermost while loop.

DO_I{
  DO_J{
    energy = (i) * (emax - emin) / (narray - 1) + emin;
    nactive = (j) * (mmax - mmin) / (narray - 1) + mmin;
    //adjust ghist values to allow for q ground states.
```

```
        //ghist[i][j] = ghist[i][j] + log(q * 0.1);
        if(ehist[i][j] > 0){
          fprintf(fOne, "%i\t %i\t %f\t %f\t %f\t %f\n", (i+1), (j+1), energy, nactive,
ghist[i][j], ehist[i][j]);
        }
      }
    }

}

//---------------------------------------------------------------------------
void calc_coords(void){
  int icc, jcc;
  for(icc = 0; icc < nx; icc++){
    for(jcc = 0; jcc < ny; jcc++){
      if(jcc % 2 == 0)spin[icc][jcc].r.x = (icc - 1) + 0.5 - nx / 2.0;
      else spin[icc][jcc].r.x = (icc - 1) - nx / 1.1;
      spin[icc][jcc].r.y = (-(ny - 1) / 2.0 + jcc) * yscale;
      spin[icc][jcc].phi = int(3.0 * ran1(&dum));
      spin[icc][jcc].rad = int(2.0 * ran1(&dum));
    }
  }
}
//---------------------------------------------------------------------------
void wrap(void)
{
    if(iiii >= (nx)) iiii = 0;
    if(iiii < 0) iiii = nx - 1;
    if(jjjj >= (ny)) jjjj = 0;
    if(jjjj < 0) jjjj = ny - 1;
}
//---------------------------------------------------------------------------
void wrap1(void)
{
    if(nnx1 >= (nx)) nnx1 = 0;
    if(nnx1 < 0) nnx1 = nx - 1;
    if(nny1 >= (ny)) nny1 = 0;
    if(nny1 < 0) nny1 = ny - 1;
}
//---------------------------------------------------------------------------
void wrap2(void)
{
    if(nnx2 >= (nx)) nnx2 = 0;
    if(nnx2 < 0) nnx2 = nx - 1;
    if(nny2 >= (ny)) nny2 = 0;
    if(nny2 < 0) nny2 = ny - 1;
}
//---------------------------------------------------------------------------
void arm_arm(void)
{
```

```
    aflag = 0;
    if(spin[ic][jc].rad == 0) return;
    phi0 = spin[ic][jc].phi;
    phi_nn = spin[iiii][jjjj].phi;
    if(phi0 == 0){
      if(nn == 1 || nn == 3 || nn == 5){
        if(phi_nn == 2){aflag = 1;}
      }
    }
    if(phi0 == 2){
      if(nn == 1 || nn == 4 || nn == 6){
        if(phi_nn == 0){aflag = 1;}
      }
    }
}
//---------------------------------------------------------------------------
void total_e(void)
{
    nactive = 0.0;
    energy = 0.0;
    for(ii = 0; ii < nx; ii++){
      for(jj = 0; jj < ny; jj++){
        energy_hb2();  //arm-arm interactions
        energy = energy + etot;
        nactive = nactive + (spin[ii][jj].rad);
      }
    }
    energy = energy / 2;
}
//---------------------------------------------------------------------------
void RandomFlip(void){
  spin[xR1][yR1].phi = 1;
  spin[xR1][yR1].rad = 0;
  spin[xR2][yR2].phi = 1;
  spin[xR2][yR2].rad = 0;
  /*spin[xR3][yR3].phi = 1;
  spin[xR3][yR3].rad = 1;
  spin[xR4][yR4].phi = 1;
  spin[xR4][yR4].rad = 1;
  spin[xR5][yR5].phi = 1;
  spin[xR5][yR5].rad = 1;
  spin[xR6][yR6].phi = 1;
  spin[xR6][yR6].rad = 1;*/
  spin[xR1+1][yR1].phi = 1;
  spin[xR1+1][yR1].rad = 2;
  spin[xR2+1][yR2].phi = 1;
  spin[xR2+1][yR2].rad = 2;
  spin[xR3+1][yR3].phi = 1;
  spin[xR3+1][yR3].rad = 1;
  spin[xR4+1][yR4].phi = 1;
```

```
  spin[xR4+1][yR4].rad = 1;
  spin[xR5+1][yR5].phi = 1;
  spin[xR5+1][yR5].rad = 1;
  spin[xR6+1][yR6].phi = 1;
  spin[xR6+1][yR6].rad = 1;*/
  here:
  ir = int(nx * ran1(&dum));
  jr = int(ny * ran1(&dum));
  if((ir == xR1 && jr == yR1) || (ir == (xR1 + 1) && jr == yR1)) goto here;
  /*if((ir == xR2 && jr == yR2) || (ir == (xR2 + 1) && jr == yR2)) goto here;
  if((ir == xR3 && jr == yR3) || (ir == (xR3 + 1) && jr == yR3)) goto here;
  if((ir == xR4 && jr == yR4) || (ir == (xR4 + 1) && jr == yR4)) goto here;
  if((ir == xR5 && jr == yR5) || (ir == (xR5 + 1) && jr == yR5)) goto here;
  if((ir == xR6 && jr == yR6) || (ir == (xR6 + 1) && jr == yR6)) goto here;
  */
  if(ir >= nx) ir = nx - 1;
  if(jr >= ny) jr = ny - 1;
  phiold = spin[ir][jr].phi;
  radold = spin[ir][jr].rad;

  //next: control the balance between flip of angle and radius
  if(ran1(&dum) < 1.1){
    ten:
    spin[ir][jr].phi = int(ran1(&dum) * 3);
    if(spin[ir][jr].phi == phiold) goto ten;
  }
  else{
    spin[ir][jr].rad = abs(spin[ir][jr].rad - 1);
  }
  total_e();
}
//---------------------------------------------------------------------------
void energy_hb2(void)
{
  ic = ii;
  jc = jj;
  etot = 1;
  if(spin[ic][jc].rad == 1) return;
  if(jc % 2 == 1){
      iiii = ic - 1; jjjj = jc; wrap();nn = 4;
      nnx1 = ic; nny1 = jc + 1; nnx2 = ic; nny2 = jc - 1;
      wrap1(); wrap2(); buzano();

      iiii = ic + 1; jjjj = jc; wrap(); nn = 1;
      nnx1 = ic + 1; nny1 = jc - 1; nnx2 = ic + 1; nny2 = jc + 1;
      wrap1(); wrap2(); buzano();

      iiii = ic;  jjjj = jc - 1; wrap(); nn = 1;
      nnx1 = ic - 1; nny1 = jc; nnx2 = ic + 1; nny2 = jc - 1;
      wrap1(); wrap2(); buzano();
```

```
      iiii = ic + 1;  jjjj = jc - 1; wrap(); nn = 1;
      nnx1 = ic; nny1 = jc - 1; nnx2 = ic + 1; nny2 = jc;
      wrap1(); wrap2(); buzano();

      iiii = ic;  jjjj = jc + 1; wrap(); nn = 1;
      nnx1 = ic + 1; nny1 = jc + 1; nnx2 = ic - 1; nny2 = jc;
      wrap1(); wrap2(); buzano();

      iiii= ic + 1;  jjjj = jc + 1; wrap(); nn = 1;
      nnx1 = ic + 1; nny1 = jc; nnx2 = ic; nny2 = jc + 1;
      wrap1(); wrap2(); buzano();
   }
    else{
      iiii = ic - 1;  jjjj = jc; wrap(); nn = 1;
      nnx1 = ic - 1; nny1 = jc + 1; nnx2 = ic - 1; nny2 = jc - 1;
      wrap1(); wrap2(); buzano();

      iiii= ic + 1;  jjjj = jc; wrap(); nn = 1;
      nnx1 = ic; nny1 = jc - 1; nnx2 = ic; nny2 = jc + 1;
      wrap1(); wrap2(); buzano();

      iiii = ic - 1;  jjjj = jc - 1; wrap(); nn = 1;
      nnx1 = ic - 1; nny1 = jc; nnx2 = ic; nny2 = jc - 1;
      wrap1(); wrap2(); buzano();

      iiii = ic; jjjj = jc - 1; wrap(); nn = 1;
      nnx1 = ic - 1; nny1 = jc - 1; nnx2 = ic + 1; nny2 = jc;
      wrap1(); wrap2(); buzano();

      iiii = ic - 1; jjjj = jc + 1; wrap(); nn = 1;
      nnx1 = ic; nny1 = jc + 1; nnx2 = ic - 1; nny2 = jc;
      wrap1(); wrap2(); buzano();

      iiii = ic;  jjjj = jc + 1; wrap(); nn = 1;
      nnx1 = ic + 1; nny1 = jc; nnx2 = ic - 1; nny2 = jc + 1;
      wrap1(); wrap2(); buzano();
    }
}
//---------------------------------------------------------------------------
void buzano(void){

  eps_lj = 1.1;
  eps_hb = eps_lj * 1; //HB is 1*LJ
  c_hb = 1.1;
  penalty =c_hb * eps_hb / 1.1;

  if(spin[iiii][jjjj].rad == 1) //neighbour is active
  {
    etot = etot - eps_lj;
```

```
      arm_arm();
      if(aflag == 1) //bonds aligned - test neighbours
      {
        etot = etot - eps_hb;
        if(spin[nnx1][nny1].rad == 1) etot = etot + penalty;
        if(spin[nnx2][nny2].rad == 1) etot = etot + penalty;
      }
    }
  }
//---------------------------------------------------------------------------
void randomNumbers(void){
   xR1 = int((nx-1) * ran1(&dum));
   yR1 = int(ny * ran1(&dum));
   r1:
   xR2 = int((nx-1) * ran1(&dum));
   yR2 = int(ny * ran1(&dum));
   if((xR2 == xR1 && yR2 == yR1) || (xR2 == (xR1 + 1) && yR2 == yR1) || ((xR2
+ 1) == xR1 && yR2 == yR1))goto r1;
   /*r2:
   xR3 = int((nx-1) * ran1(&dum));
   yR3 = int(ny * ran1(&dum));
   if((xR3 == xR1 && yR3 == yR1) || (xR3 == (xR1 + 1) && yR3 == yR1) || ((xR3
+ 1) == xR1 && yR3 == yR1))goto r2;
   if((xR3 == xR2 && yR3 == yR2) || (xR3 == (xR2 + 1) && yR3 == yR2) || ((xR3
+ 1) == xR2 && yR3 == yR2))goto r2;
   r3:
   xR4 = int((nx-1) * ran1(&dum));
   yR4 = int(ny * ran1(&dum));
   if((xR4 == xR1 && yR4 == yR1) || (xR4 == (xR1 + 1) && yR4 == yR1) || ((xR4
+ 1) == xR1 && yR4 == yR1))goto r3;
   if((xR4 == xR2 && yR4 == yR2) || (xR4 == (xR2 + 1) && yR4 == yR2) || ((xR4
+ 1) == xR2 && yR4 == yR2))goto r3;
   if((xR4 == xR3 && yR4 == yR3) || (xR4 == (xR3 + 1) && yR4 == yR3) || ((xR4
+ 1) == xR3 && yR4 == yR3))goto r3;
   r4:
   xR5 = int((nx-1) * ran1(&dum));
   yR5 = int((nx-1) * ran1(&dum));
   if((xR5 == xR1 && yR5 == yR1) || (xR5 == (xR1 + 1) && yR5 == yR1) || ((xR5
+ 1) == xR1 && yR5 == yR1))goto r4;
   if((xR5 == xR2 && yR5 == yR2) || (xR5 == (xR2 + 1) && yR5 == yR2) || ((xR5
+ 1) == xR2 && yR5 == yR2))goto r4;
   if((xR5 == xR3 && yR5 == yR3) || (xR5 == (xR3 + 1) && yR5 == yR3) || ((xR5
+ 1) == xR3 && yR5 == yR3))goto r4;
   if((xR5 == xR4 && yR5 == yR4) || (xR5 == (xR4 + 1) && yR5 == yR4) || ((xR5
+ 1) == xR4 && yR5 == yR4))goto r4;
   r5:
   xR6 = int((nx-1) * ran1(&dum));
   yR6 = int((nx-1) * ran1(&dum));
   if((xR6 == xR1 && yR6 == yR1) || (xR6 == (xR1 + 1) && yR6 == yR1) || ((xR6
+ 1) == xR1 && yR6 == yR1))goto r5;
```

```
   if((xR6 == xR2 && yR6 == yR2) || (xR6 == (xR2 + 1) && yR6 == yR2) || ((xR6
+ 1) == xR2 && yR6 == yR2))goto r5;
   if((xR6 == xR3 && yR6 == yR3) || (xR6 == (xR3 + 1) && yR6 == yR3) || ((xR6
+ 1) == xR3 && yR6 == yR3))goto r5;
   if((xR6 == xR4 && yR6 == yR4) || (xR6 == (xR4 + 1) && yR6 == yR4) || ((xR6
+ 1) == xR4 && yR6 == yR4))goto r5;
   if((xR6 == xR5 && yR6 == yR5) || (xR6 == (xR5 + 1) && yR6 == yR5) || ((xR6
+ 1) == xR5 && yR6 == yR4))goto r5;
    fprintf(stdout," xR1:\t %i\t yR1:\t %i\n xR1+1:\t %i\t yR1:\t %i\n xR2:\t %i\t
yR2:\t %i\n xR2+1:\t %i\t yR2:\t %i\n xR3:\t %i\t yR3:\t %i\n xR3+1:\t %i\t yR3:\t
%i\n xR4:\t %i\t yR4:\t %i\n xR4+1:\t %i\t yR4:\t %i\n xR5:\t %i\t yR5:\t %i\n
xR5+1:\t %i\t yR5:\t %i\n xR6:\t %i\t yR6:\t %i\n xR6+1:\t %i\t yR6:\t %i\n",xR1,
yR1, xR1+1, yR1, xR2, yR2, xR2+1, yR2, xR3, yR3, xR3+1, yR3, xR4, yR4,
xR4+1, yR4, xR5, yR5, xR5+1, yR5, xR6, yR6, xR6+1, yR6);
  */
  fprintf(stdout," xR1:\t %i\t yR1:\t %i\n", xR1, yR1);
  fprintf(stdout," xR1+1:\t %i\t yR1:\t %i\n", xR1+1, yR1);
  fprintf(stdout," xR2:\t %i\t yR2:\t %i\n", xR2, yR2);
  fprintf(stdout," xR2+1:\t %i\t yR2:\t %i\n", xR2+1, yR2);

}
```

Appendix D

Wang-Landau post processing code

```
/* process the density of states function obtained from Wang-Landau
   version to process lattice Mercedes-Benz model
   1-d version; g(E,N)
*/

#include <stdio.h>
#include <stdlib.h>
#include <string.h>
#include <math.h>
#include "in_mddefs.h"
#include "ran1.c"

#define DO_I  for(i=1;i<e_states;i++)
#define DO_J  for(j=1;j<m_states;j++)

int i, j, nx, ny, m, nspin, narray;
double ghist[1025][1025], ehist[1025][1025];
double energy[1025], density[1025];
double lnP[1025][1025], prob[1025][1025];
double kT, mu, e_states, m_states;
double lambda, partition, pnorm, area;
double u_energy, u_prev, kT_prev, capacity, helmholtz, entropy;
double den_ave;

FILE *fOne, *fTwo, *fThree, *fTEST;

int main()
{
   fOne = fopen("c:\\Monte Carlo\\Buzano\\WL_lattice_gc.out", "r");
   //fTwo = fopen("Buzano_proc_2d.out", "w");
   fThree = fopen("mb_buzano_t_2d.out", "w");
   //fTEST = fopen("TESTTEST.out", "w");
   narray = 1025;
   nx = 1;
   ny = 1;
   e_states = narray;
   m_states = narray;
   nspin = nx * ny;
   kT = 1.1;
   mu =-1.1;
   //next: max exponent value - inspect values of lnP to get this by
   //setting lambda to zero for first run through processing
   lambda = 1.1;
   DO_I{
     DO_J{
       energy[i] = 1.1;
       density[i] = 1.1;
       ghist[i][j] = 1.1;
       ehist[i][j] = 1.1;
     }
```

```
    }
    int ii;
    for(ii = 1; ii <= 18623; ii++)
    {
      float energyStore, densityStore, ehistStore, ghistStore;
      fscanf(fOne,"%i %i %f %f %f %f",&i, &j, &energyStore, &densityStore,
&ghistStore, &ehistStore);
      energy[i] = energyStore; density[j] = densityStore; ghist[i][j] = ghistStore;
ehist[i][j] = ehistStore;
     }


    //starting point from U(T) plot - used to calculate C(T)
    kT_prev = 1.1;
    u_prev = 1.1;
    //outer loop: use for calculation of U(T) etc.
    for(m = 1; m < 600; m++)
    {
      kT = (m+1) * 1.005;
      lambda = 1.1;
      DO_I{
        DO_J{
          if(ehist[i][j] > 1.1)
          {
            lnP[i][j] = ghist[i][j] - energy[i] / kT + density[j] * mu / kT;
            if(lnP[i][j] > lambda) lambda = lnP[i][j];
          }
        }
      }
      partition = 1.1;
      u_energy = 1.1;
      den_ave = 1.1;
      DO_I{
        DO_J{
          if(ehist[i][j] > 1)
          {

            lnP[i][j] = ghist[i][j] - energy[i] / kT + density[j] * mu / kT - lambda;
            //goto ninezeronine;
            prob[i][j] = exp(lnP[i][j]);
            partition = partition + prob[i][j];
            u_energy = u_energy + energy[i] * prob[i][j];
            den_ave = den_ave + density[j] *prob[i][j];
           // ninezeronine:
          }
        }
      }
      fprintf(stdout, "Count: %i\tkT: %f\tPartition: %f\n", m, kT, partition);

      //u_energy = u_energy / (nspin * partition);
```

```
      u_energy = u_energy / partition;
      //den_ave = den_ave / (nspin * partition);
      den_ave = den_ave / partition;
      capacity = (u_energy - u_prev) / (kT - kT_prev);
      //helmholtz = -1.1 * kT * (log(partition) + lambda) / nspin;
      helmholtz = -1.1 * kT * (log(partition) + lambda);
      /* entropy calculation: note that u_energy and helmholtz are both per
         particle, so no need to divide by number of particles again.
         kT is equivalent to T (entropy = energy / T) */
      entropy = (u_energy - helmholtz) / kT;
      u_prev = u_energy;
      kT_prev = kT;

      fprintf(fThree, "%f\t %f\t %f\t %f\t %f\n", kT, u_energy/nspin, den_ave/nspin,
helmholtz, entropy);
   }

}
```

Bibliography

[1] http://www.madsci.org/posts/archives/2000-05/958588306.An.r.html

[2] http://www.lsbu.ac.uk/water/anmlies.html

[3] Handbook of Chemistry and Physics, 83rd ed. CRC Press, Boca Raton, Florida, (2003)

[4] P. Ball, H20 – A Biography of Water, London (2001).

[5] G. S. Kell, Density, Thermal expansivity and compressibility of liquid water from 0°C to 150°C: Correlations and tables for atmospheric pressure and saturation reviewed and expressed on 1968 temperature scale, J. chemical and engineering data, 20 (1) (1975) 97-105.

[6] M. Thiesen, K. Scheel, H. Diesselhorst, Untersuchungen über die thermische Ausdehnung von festen und tropfbar flüssigen Körpern – Bestimmung der Ausdehnung des Wassers für die zwischen 0° and 40° liegenden Temperaturen, Wiss. Abhandlungen der Physik.-Techn. Reichsanst., 3 (1900) 1-70.

[7] M. Thiesen, Untersuchungen über die thermische Ausdehnung von festen und tropfbar flüssigen Körpern – Bestimmung der Ausdehnung des Wassers für die zwischen 0° and 40° liegenden Temperaturen, Wiss. Abhandlungen der Physik. – Techn. Reichsanst., (1918) 1-32.

[8] C. Chen, F. J. Millero, The equation of seawater determined from sound speeds, J. Marine Research, 36, (1978) 657-691.

[9] R. Feistel, A new extended Gibbs thermodynamic potential of seawater, Progress in Oceanography, 58 (2003) 43-114

[10] N. P. Fofonoff, Physical properties of seawater: a new salinity scale and equation of state for seawater, J. Geophysical Research, 90 (1985) 3332-3342

[11] P. Chappuis. Dilatation de l'eau, Travaux et Mémories du Bureau International des Poids et Méasures, 13 (1907) D1-D40.

[12] International Critical Tables of Numerical Data, Physics, Chemistry and Technology, National Research Council, 1928 (Electronic Edition: Knovel, 2003), Vol. III, 107-111

[13] Handbook of Chemistry and Physics, 65th ed. CRC Press, Boca Raton, Florida, (1984)

[14] http://brunelleschi.imiss.fi.it/cimento/, Court Scientists – The Art of Experimentation in the Galilean Accademia del Cimento (1657- 1667), Institute and Museum of the History of Science, Florence, 2001.

[15] T. C. Hope, Experiments and Observations upon the contraction of Water by heat at low temperatures, Trans. Royal Soc. Edinburgh, 5 (1805) 379-405.

[16] Thomas B. Greenslade, JR, The Maximum Density of Water, Physics Teacher, 23,(8) 474-77 (1985).

[17] C. M. Despretz, Recherches sur le Maximum de Densité des Liquides, Compt. Rendus, 4, 124-130, 1837.

[18] C. M. Despretz, Recherches sur le Maximum de Densité des Dissolutions Aqueuses, Compt Rendus 4, 435-439, 1837.

[19] C. M. Despretz, Deuxiéme Mémoire sur le Maximum de Densité des Dissolutions Aqueuses, Ann. Chim. Phys., 70, 49-81, 1839.

[20] C. M. Despretz Troisiéme Mémoire sur le Maximum de Densité, Compt. Rendus, 10, 131-134, 1840.

[21] M. F. Rossetti, Sur le Maximum de Densité et la dilatation de l'eau distille, Annals de Chimie et de Physique, 10 (1867) 461-473.

[22] G. Wada, S. Umeda, Effects of Nonelectrolytes on the Temperature of the Maximum Density of Water. I. Alcohols, Bull. Chem. Soc. Jpn. 35 4 (1961).

[23] G. Wada, S. Umeda, Effects of Nonelectrolytes on the Temperature of the Maximum Density of Water. II. Organic Compounds with Polar Groups, Bull. Chem. Soc. Jpn. 35 11 (1962).

[24] A. G. Mitchell, W. F, K. Wynne-Jones, Thermodynamic and other Properties of Solutions involving Hydrogen Bonding, , Discuss. Faraday Soc. 15, 161 (1953).

[25] M. F. Cawley, P. McBride, Flow visualization of free convection in a vertical cylinder of water in the vicinity of the density maximum, Int. J. Heat Mass Transfer 47 (2004) 1175-1186

[26] D. McGlynn, A Study of the change in the Temperature of the Density Maximum of Water as a Function of Solute Nature and Concentration, M. Sc. Thesis (2005)

[27] M. F. Cawley, D. McGlynn, P. A. Mooney, Measurements of the temperature of density maximum of water solutions using a convective flow technique, Int. J. Heat Mass Transfer 49 (2006) 1763-1772.

[28] P O'Connor, The Influence of the Density Maximum in Water on the Rate of Heat Transfer, M. Sc. Thesis (2006)

[29] P. Mooney, A Study of Heat Transfer and Heat Flow Asymmetry through Water in the Presence of the Density Maximum, PhD Thesis (2007) N.U.I. Maynooth.

[30] A. Bradshaw and K. E. Schleicher, Direct measurement of thermal expansion of sea water under pressure, Deep-Sea Res. 17, 691 (1970).

[31] C. T. Chen, R. A. Fine and F. J. Millero, The equation of statte of pure water determined from speed sounds, Deep-Sea Res. 23, 595 (1976).

[32] F. J. Millero, C. T. Chen, A. Bradshaw, and K. Schleicher, A new high pressure equation of state for seawater, Deep-Sea Res., 27, 255 (1980).

[33] N. Metropolis, The Beginning of the Monte Carlo Method, Los Alamos Science, Special Issue (1987).

[34] C. H. Cho, S. Singh, G. W. Robinson, An Explanation of the Density Maximum in Water, Phys. Rev. Lett., 76 (10) (1996) 1651-1654

[35] P. Jedlovszky, M. Mezei, R. Vallauri, A molecular level explanation of the density maximum of liquid water from computer simulations with a polarizable potential model, Chem. Phys. Lett. 318 (2000) 155-160

[36] H. Tanaka, Simple Physical Explanation of the Usual Thermodynamic Behaviour of Liquid Water, Phys. Rev. Lett., 80 (26) (1988) 5750-5753

[37] P. G. Debenedetti, *Metastable Liquids* (Princeton University Press, Princeton, 1997).

[38] H. I. M. Veiga, L. P. N. Rebelo, M. Nunes de Ponte, J. Szydlowski, Water and Gallium at Absolute Negative Pressures. Loci of Maximum Density and of Melting, Int. J. ThermoPhys. 22 (4) (2001) 1159-1174

[39] http://www.farnell.com/datasheets/424953.pdf

[40] P. McBride, A Study of convection in water in the vicinity of the Density Maximum, PhD Thesis (2004) N.U.I. Maynooth.

[41] P. Horowitz, W. Hill, The Art of Electronics, Cambridge University Press. (1980)

[42] T. E. Faber "Fluid Dynamics for Physicists", Cambridge University Press, (1995).

[43] D. R. Caldwell, The Maximum Density Points of Pure and Saline Water, Deep-Sea Research, 25, 175 – 181 (1978).

[44] M. F. Cawley, G. J. Cotter, A. Stewart, Detailed Structure observed in the Temperature of Maximum Density of Aqueous Solutions as functions of Pressure and Solute Concentration, Submitted J. Chem Phys. (2010).

[45] Murlidhar V. Kaulgud, Temperature of Maximum Density Behaviour of Non-electrolytes in Water, J. Chem. Soc. Faraday Trans, 86(6), 911-915 (1990).

[46] D. C. Rapaport, The Art of Molecular Dynamic Simulation, Cambridge, (1995).

[47] Richard J. Sadus, Molecular Simulation of Fluids, Elsevier.

[48] http://www.ccl.net/cca/documents/molecular-modeling/node9.html

[49] D. P. Landau, Shan-Ho Tsai, M Exler, A new approanch to Monte Carlo simulations in statistical physics: Wang-Landau sampling, Am. J. Phys. 72 (10) (2004).

[50] M. Troyer, S. Wessel, and F. Alet, "Flat histogram methods for quantum systems: Algorithm to overcome tunnelling problems and calculate the free energy," Phys. Rev. Lett. 90, 120201 (2003).

[51] Q. L. Yam, R. Faller, and J. J. de Pablo, "Density-of-states Monte Carlo method for simulation of fluids," J. Chem. Phys. 116, 8745-8749 (2002).

[52] F. Calvo and P. Parneix, "Statistical evaporation of rotating clusters. I. Kinetic energy released," J. Chem. Phys. 119, 256-264 (2003).

[53] Kevin A. T. Silverstein, A. D. J. Hanmet, Ken A. Dill, A Simple Model of Water and the Hydrophobic Effect, J. Am. Chem. Soc. 120, 3166-3175 (1998)

[54] A. Ben-Naim, "Statistical Mechanics of "Waterlike" Particles in Two Dimensions. I. Physical Model and Application of the Percus-Yevick Equation," J. Chem. Phys. 54, 3682-3695 (1971)

[55] C. Buzano, E De. Stefanis, Low-temperature-induced swelling of a hydrophobic polymer: A lattice approach, J. Chem, Phys. 126, 074904 (2007).

[56] C. Vega and J. L. F. Abascal, J. Chem. Phys. 123, 144504 (2005)

[57] S. Chatterjee, H. S. Ashbaugh, and P. G. Debenedetti, J. Chem. Phys. 123, 164503 (2005).

[58] H. S. Ashbaugh, T. M. Truskett, and P. G. Debenedetti, J. Chem. Phys. 116, 2907 (2002).

[59] T. M. Truskett, P. G. Debenedetti, S. Sastry, and S. Torquato, J. Chem. Phys. 111, 2647 (1999).

[60] H. S. Ghaziaskan, M. Rezayat, Butanol Structure-Solubility Relationship in Supercritical Carbon-Dioxide, J. Supercritical Fluids (2005).

[61] http://webbook.nist.gov